Molecular Design of Functional Polyesters via Ring-opening Alternating Copolymerization using Simple Organocatalysts

A Dissertation for the Degree of Doctor of Philosophy

Ryota Suzuki

Hokkaido University

December, 2024

Acknowledgments

The study presented in this dissertation has been performed under the direction of Professor Toshifumi Satoh, Division of Applied Chemistry, Faculty of Engineering, Hokkaido University, from 2020 to 2024. The author wishes to express his sincere gratitude to Professor Toshifumi Satoh for his kind instruction, helpful advice, and unstinting encouragement throughout the course of this work.

The author is also deeply grateful to Associate Professor Takuya Isono, Associate Professor Kenji Tajima, Associate Professor Takuya Yamamoto, Assistant Professor Feng Li, and Specially Appointed Assistant Professor Tianle Gao. Division of Applied Chemistry, Faculty of Engineering, Hokkaido University, for their helpful and valuable suggestion with continuous encouragement throughout this work.

The author wishes to express sincere gratitude to Prof. Xiaochao Xia, Prof. Brian J. Ree, Dr. Dai-Hua Jiang, and Mr. Chun-Yao Ke. This research would not have been possible without his invaluable support and guidance. The author also thanks Mr. Yoji Horie, Mr. Masaru Ando, Mr. Katsuaki Takahashi, and Mr. Yusuke Takagi, Toagosei Co., Ltd. The author is grateful for their cooperation in various aspects, from material characterization to data analysis and discussion.

The author is further indebted to Drs. Yoshinobu Mato, Saburo Kobayashi, Satoshi Katsuhara for their patient teaching and fruitful daily discussion. The author thanks all of the member of Professor Satoh's group.

The author is very grateful to the Research Fellowships of the Japan Society for the Promotion of Science (JSPS) for Young Scientists during 2023-2024.

Finally, the author would like to express his utmost gratitude to family for their understanding, support, and continuous encouragement throughout his research and daily life.

December, 2024

Ryota Suzuki

Contents

Chapter 1

General Introduction

1.1 Applications of functional polyesters

Polyesters, including poly(ethylene terephthalate) (PET), polylactide (PLA), poly(ε-caprolactone) (PCL), poly(butylene succinate) (PBS), and polyhydroxyalkanoate (PHA), represent a significant class of polymer material widely used in various industries for producing fibers, plastic bottles, adhesives, plasticizer, and elastomers (**Figure 1.1**). Certain polyesters have been developed for specialized applications, including as biodegradable sheets, biomedical materials, bioabsorbable sutures, and nanocarriers for drug delivery, based on their inherent biocompatibilities and biodegradabilities.[1,2] Strategies that modify and functionalize polyesters are crucial for delivering the abovementioned functional requirements (**Figure 1.2**). For instance, introducing specific functional groups can enhance the degradation behavior or control the drug-releasing properties of polyesters.[3–7] Similarly, topological modifications, such as cyclization, grafting, and branching, can significantly influence the physical properties of conventional linear polyesters (**Figure 1.2**).[8–10] Furthermore, copolymerization has also been used to improve the properties of polyesters, which has led to the synthesis of various copolyesters with different sequences, including random, gradient, and block (**Figure 1.2**).[11–13] As a result, a wide variety of functional polyesters have been synthesized. Nevertheless, the successful applications of these materials require precise designs that are tailored for specific uses, which involves carefully controlling parameters such as the melting point, glass-transition

temperature, thermal stability, and degree of crystallinity. Beyond these physical properties, the chemical architecture, including both main- and side-chain structures, must be finely designed to optimize functionality for the intended use.

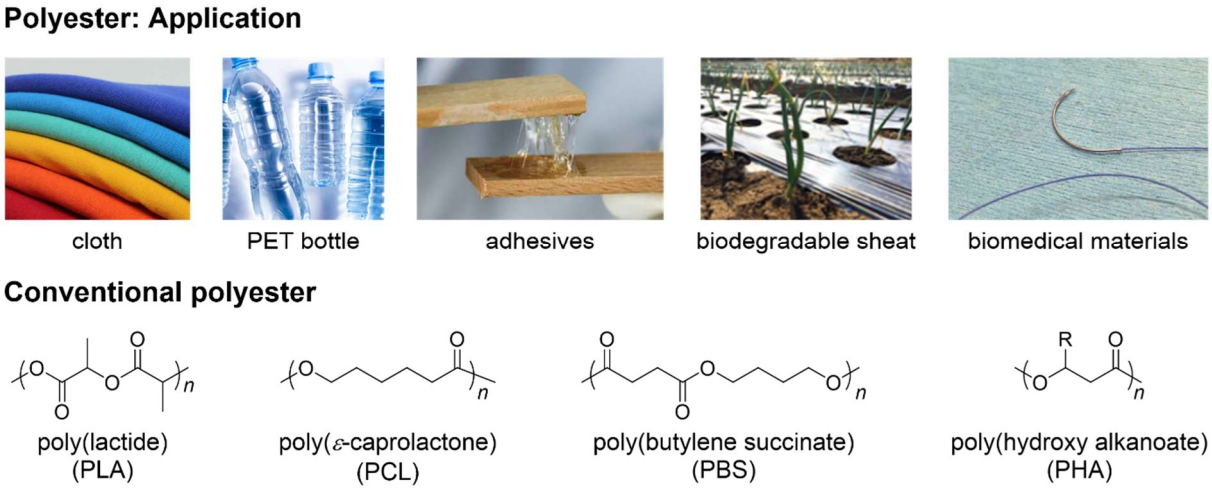

Figure 1.1. Representative polyesters and their uses.

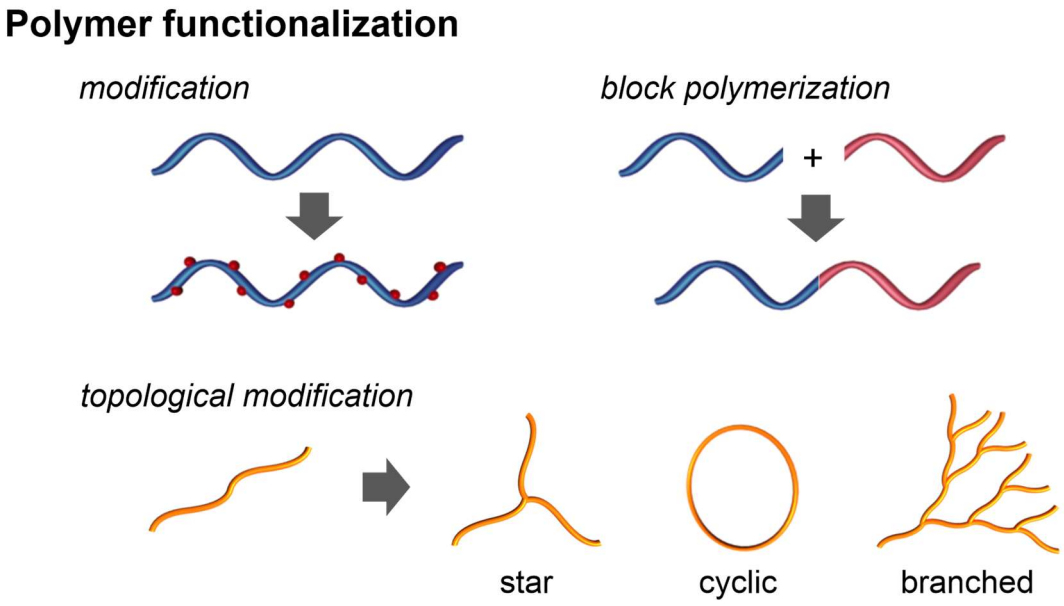

Figure 1.2. General strategies for functionalizing polymers.

The development of functional polyesters is a time- and resource-intensive process owing to the complexity of balancing aforementioned various factors. Therefore, there is a growing need for a simple, yet versatile, precision-polymerization approach for synthesizing a broad array of functional polyesters; such a framework is significantly promising for accelerating advances in materials science and polymer chemistry, particularly toward the development of next-generation functional materials.

1.2 Conventional methods for synthesizing polyesters

1.2.1 Polycondensation

Polycondensation is among the most widely used methods for synthesizing polyesters in industry.[14] The polycondensation of (a) diol and dicarboxylic acid, or (b) hydroxylic acid, yields a variety of polyesters (**Figure 1.3**), including PET and PBS as examples. Although this approach provides access to a wide array of polyester structures, it faces several challenges, including harsh polymerization conditions that involve high temperatures and vacuums, the requirement to remove low-molecular-weight byproducts, and the inherent difficulties associated with achieving high molecular weights. Despite these limitations, a wide variety of available monomers, particularly in polycondensation from diol and dicarboxylic acid, allows for the synthesis of polyesters with diverse structures and properties through judicious monomer selection.

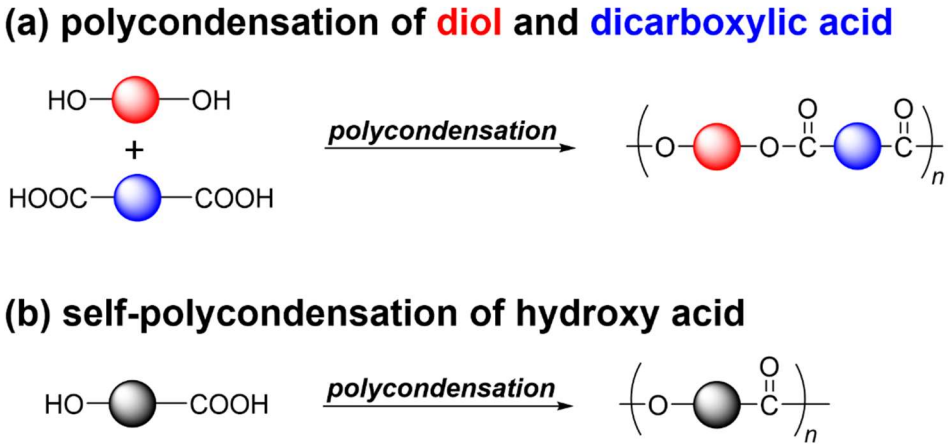

Figure 1.3. Polycondensation of (a) diol and dicarboxylic acid and (b) hydroxylic acid.

For instance, with the aim of developing polyester materials as potential alternatives to polyolefins, Mecking et al. reported the synthesis of highly crystalline polyesters via polycondensation of monomers containing long alkyl chain (**Figure 1.4**).[15,16] Sheares et al. reported the preparation of polyesters with alkenes incorporated in the main chain; thermal cross-linking subsequently, resulted in amorphous thermosetting elastomers that are potentially applicable to biodegradable devices (**Figure 1.5**).[17,18] Additionally, hyperbranched polyesters have been synthesized by polycondensation of A_2+B_3-type monomer combinations, such as "sebacic acid and glycerol" or "1,8-octanediol and citric acid", with the resulting polymers exhibiting properties suitable for degradable elastomers (**Figure 1.6**).[19,20] Furthermore, polyesters with functionalized side chains such as alkenes, alkynes, amino groups, and thiol groups have been synthesized by polycondensation from monomers containing the respective functional groups (**Figure 1.7**).[21,22]

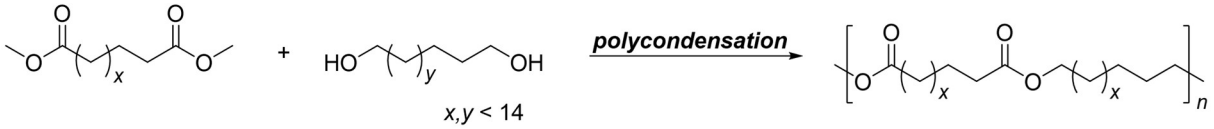

Figure 1.4. Polycondensation of long-chain monomers to afford long-chain aliphatic polyesters.[15,16]

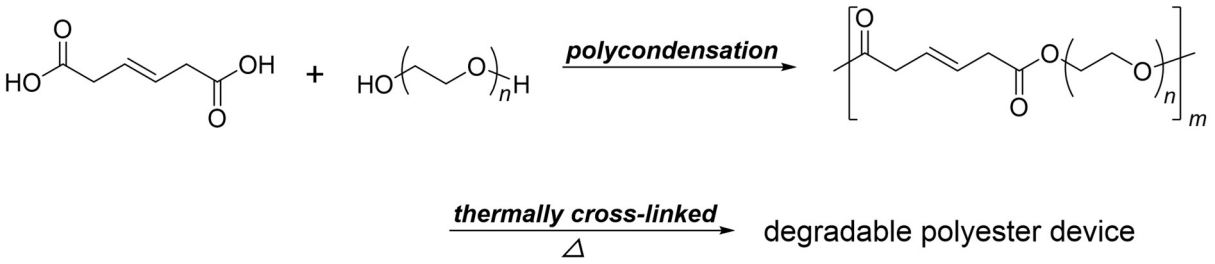

Figure 1.5. Synthesis of network polyester for degradable device via polycondensation of unsaturated dicarboxylic acid and poly(ethylene glycol), followed by thermal cross-linking.[17,18]

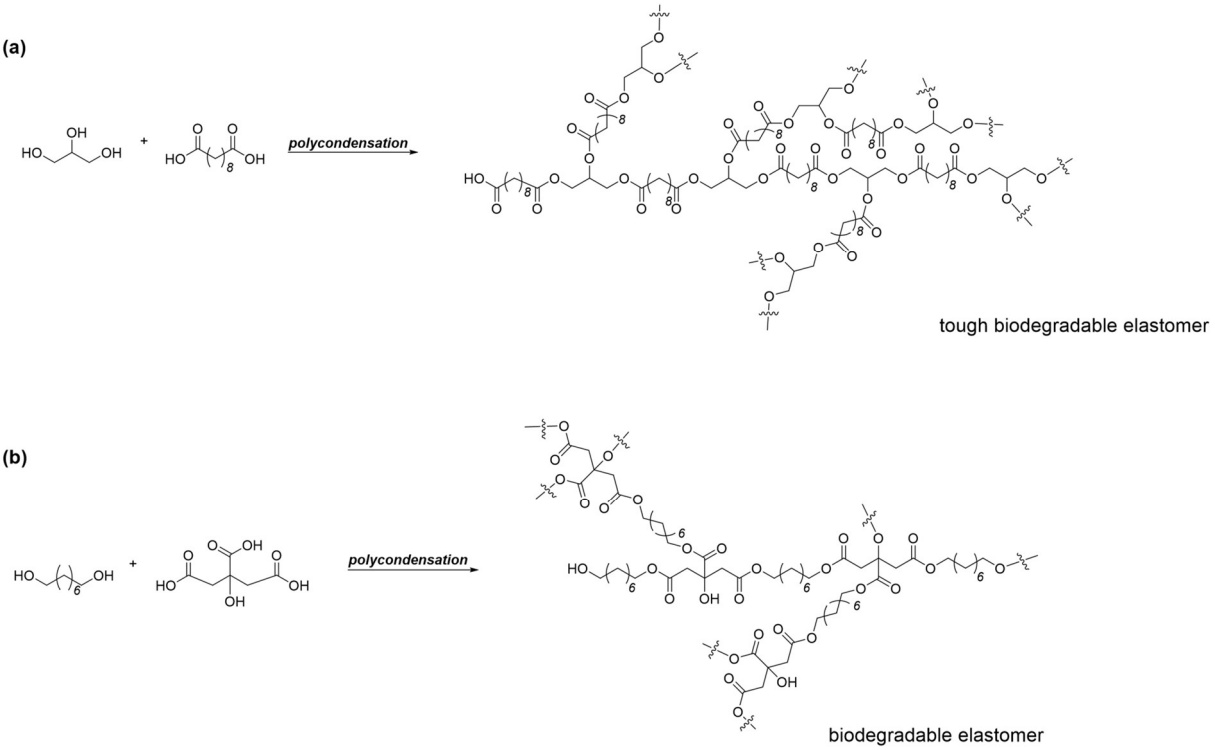

Figure 1.6. Conventional synthetic strategies for the formation of hyperbranched polyesters: polycondensation of (a) glycerol and sebacic acid and (b) 1,8-octanediol and citric acid.[19,20]

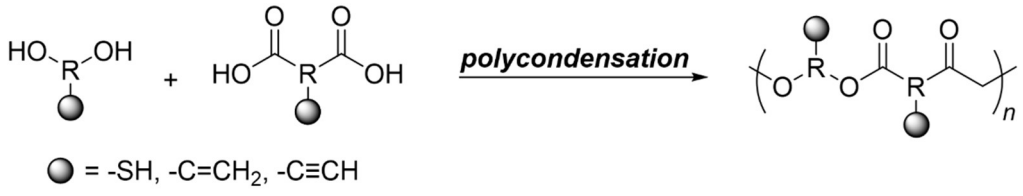

Figure 1.7. Polycondensation of functionalized monomers.[21,22]

The ability to synthesize functional polyesters with a wide variety of structures by simply altering the monomer is a notable advantage of the polycondensation method. However, precisely controlling key parameters, such as molecular weight, polydispersity, and end-group functionality, is challenging owing to the step-growth mechanism associated with polycondensation. In addition, stringent polymerization conditions and difficulties in achieving high molecular weights remain significant obstacles for the development of advanced functional materials. Additionally, side reactions such as cyclization can lead to the formation of cyclic by-products that further complicate the polymerization process and hinder the formation of well-defined polymer architectures.

1.2.2 Ring-opening polymerization

The ring-opening polymerization (ROP) of a cyclic ester is a polymerization approach known for providing excellent control over polymerization precision, in contrast to polycondensation that suffers from polymerization-control difficulties (**Figure 1.8**).[23] For example, poly(L-lactide) (PLLA) and PCL, common biodegradable polyesters that are widely used in surgical sutures, agricultural films, and 3D printing tracheal scaffolds, are synthesized via the ROP of L-lactide (LLA) and ε-caprolactone (CL).[24–26] Functional groups can be easily introduced at the chain ends owing to the chain-growth nature of ROP; this advantage facilitates the synthesis of end-functionalized polyesters via ROP using functional initiators (**Figure 1.9**). Satoh et al. successfully synthesized poly(δ-valerolactone) (PVL) with an azido α chain-end and a hydroxyl ω chain-end via ROP using an azido-functionalized initiator.[27] Notably, cyclic PVL was created via the azido–alkyne click reaction of the synthesized PVL, thereby highlighting the versatility of this functionalization strategy. Grayson et al. reported a comparable approach for the synthesis of macrocyclic PCL.[28] Furthermore, star-shaped polyesters have been synthesized using multi-functional alcohols as initiators, and block copolymers can be prepared in a similar fashion by employing hydroxyl-terminated polymers as macroinitiators.[29,30]

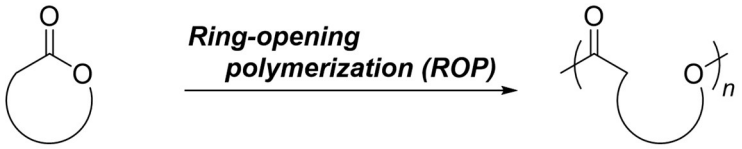

Figure 1.8. Ring-opening polymerizations of cyclic esters.

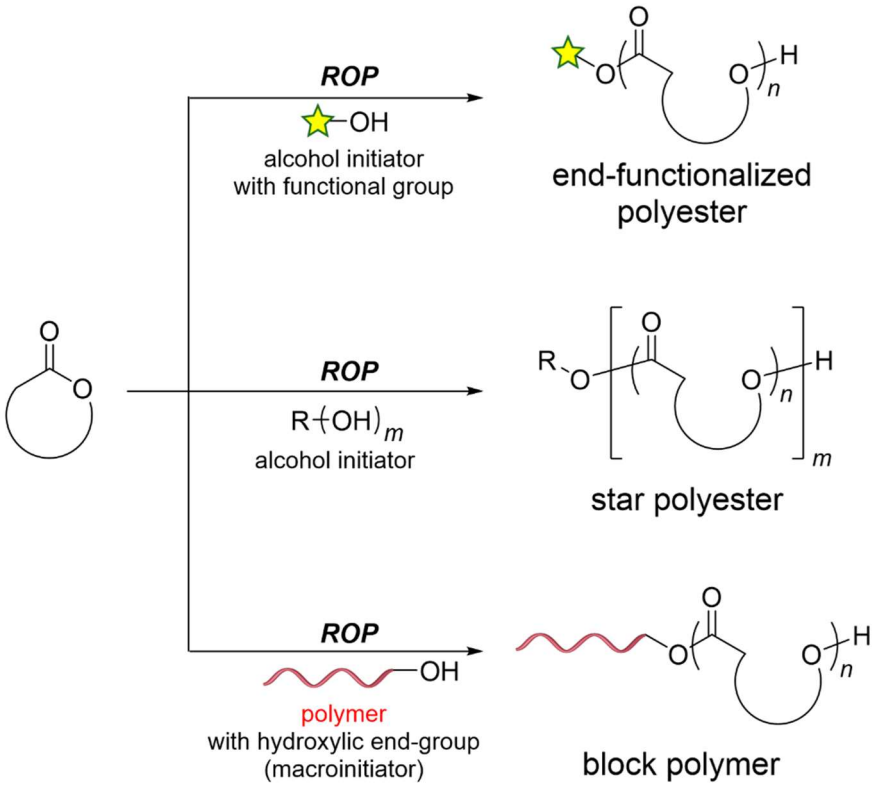

Figure 1.9. Synthesis of functional polyesters via ROP using functional initiators.

Compared to polycondensation, ROP facilitates the synthesis of high-molecular-weight polyesters with narrow polydispersities under mild conditions.[31,32] Polyester functionality can be extended using ROP by employing various judiciously designed cyclic ester monomers (**Figure 1.10**).[1] Although synthesizing and purifying these monomers can be time-consuming and labor-intensive, this approach remains an effective route for producing functional polyesters. For instance, Fréchet et al. reported the precise syntheses of hyperbranched polyesters via the ROP of 4-(2-hydroxyethyl)-ε-caprolactone.[33] Thus, various functional lactones have become attractive to many researchers.

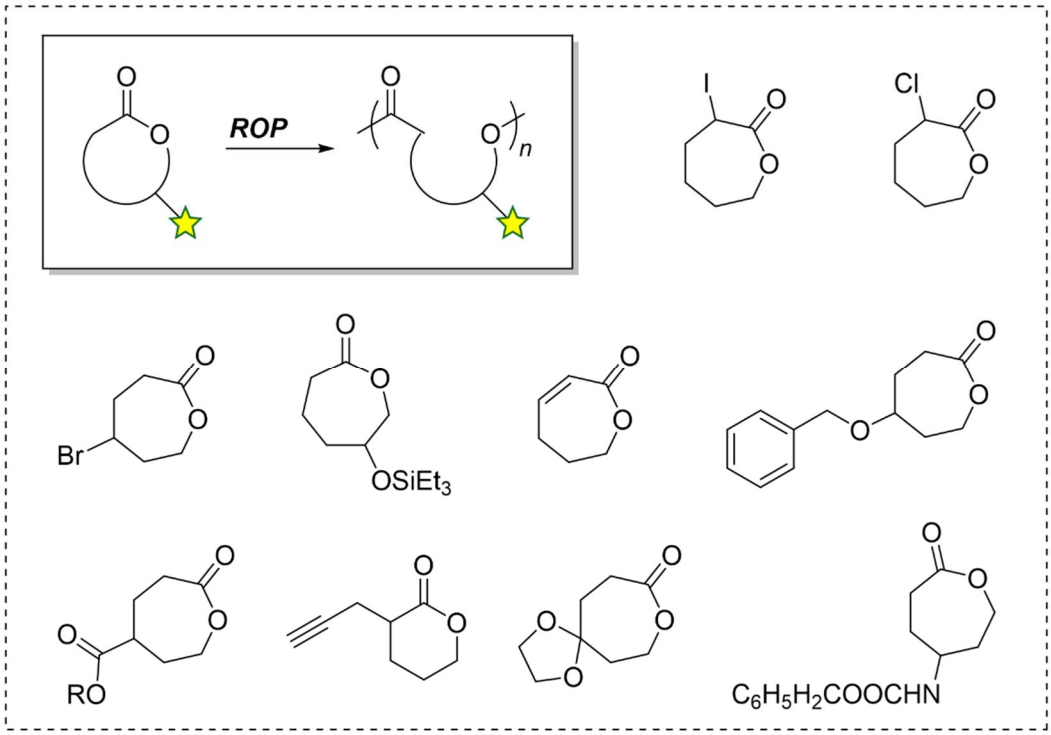

Figure 1.10. Functional polyesters synthesized by ROP using functional lactones.[1]

Functionalized lactides have also been studied extensively, and polyesters with polar functional groups (i.e., hydroxy or amino groups) on their side chains have been synthesized via polymerization followed by deprotection (**Figure 1.11**).[34] However, this approach is restricted by the limited range of available monomers.

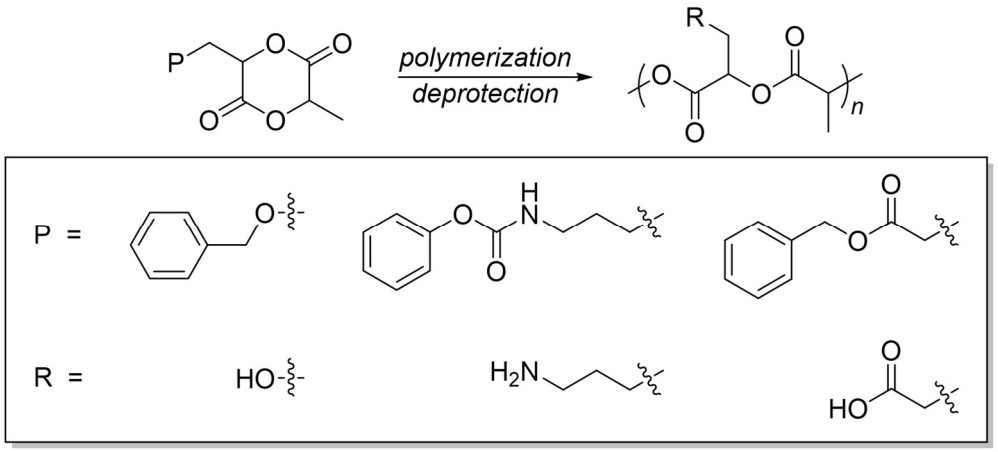

Figure 1.11. Synthesizing various polyesters with highly polar functional groups from functional lactides via ROP following deprotection.[34]

In summary, although ROP offers precise polymerization control and chain-end/side-chain functionality, it is constrained by the narrow range of accessible cyclic ester monomers.

1.2.3 Ring-opening alternating copolymerization

Traditional methods for synthesizing polyesters, such as polycondensation and ROP, often involve trade-offs between polymerization controllability and polymer structural diversity. Therefore, the development of synthetic approaches that satisfy both of these criteria remains a significant challenge. To address this issue, ring-opening alternating copolymerization (ROAC) of cyclic anhydrides and epoxides has garnered attention over the past decade.[35,36] The alternating ring-opening reactions of cyclic anhydrides and epoxides result in the formation of copolyesters composed of two distinct monomers (**Figure 1.12**). In addition, this method offers several advantages owing to its chain-growth nature, including the ability to introduce end functionality, achieve precise molecular weight control, and produce high-molecular-weight polymers. Moreover, cyclic anhydrides and epoxides are widely available and commercially accessible, which facilitates the syntheses of a diverse range of polyesters by simply altering monomer combinations.

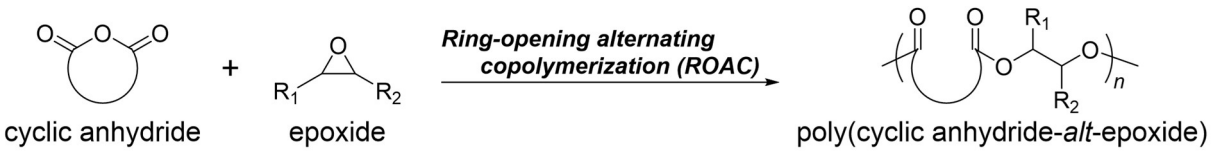

Figure 1.12. Ring-opening alternating copolymerization of cyclic anhydride and epoxide.

For instance, Coates et al. synthesized enantiopure polyesters via chiral metal complex-catalyzed ROAC from succinic anhydride and optically pure propylene oxide via the formation of a stereocomplex (**Figure 1.13**).[37] Additionally, Hao et al. reported the synthesis of thermally responsive biodegradable polyesters using epoxide-bearing oligo-ethylene glycol side chains (**Figure 1.14**).[38] Furthermore, the ROAC has been successfully used to synthesize functional polyesters for a variety of applications, with energy storage materials, polyurethane precursors, and luminescent materials as examples.[39–41]

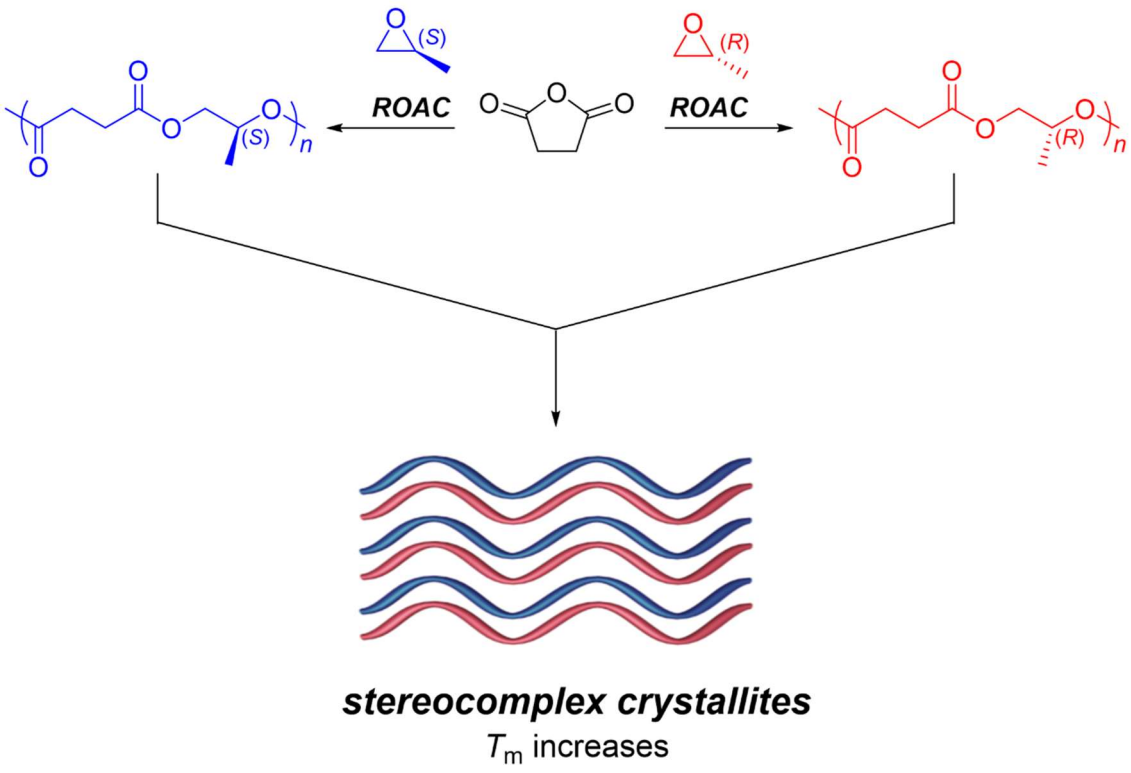

Figure 1.13. Regioselectively polymerizing cyclic anhydride and epoxide, and stereocomplex formation via the crystallization of enantiomeric polymer chains.[37]

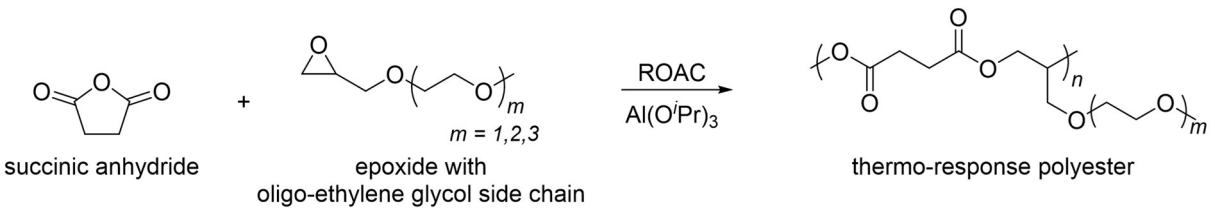

Figure 1.14. Synthesizing thermally responsive polyesters via the ROAC of succinic anhydride and epoxide bearing oligo(ethylene glycol) side chain.[38]

Moreover, the terpolymerization of a cyclic ester alongside a cyclic anhydride and an epoxide has demonstrated the ability to undergo self-switchable polymerization (**Figure 1.15**),[42] in which, the reaction automatically switches from cyclic anhydride and epoxide ROAC to cyclic ester ROP owing to differences in monomer reactivities, thereby enabling the one-pot, one-step syntheses of block copolymers that normally require multiple synthesis steps.

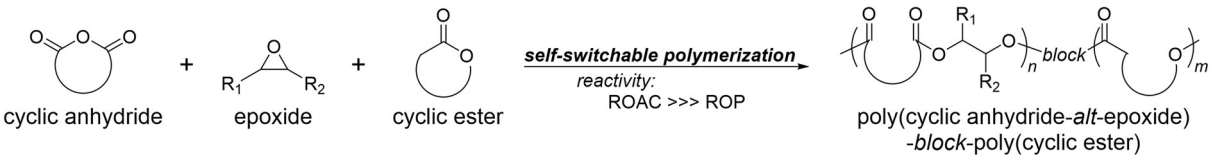

Figure 1.15. Self-switchable polymerization of cyclic anhydride, epoxide, and cyclic ester to form block polyester in a one-pot, one-step manner.

ROAC is a highly versatile and effective synthetic approach for producing functional polyesters as it provides the precision and diversity required for advanced material applications. However, previous research has largely been confined to relatively simple ROAC processes and has not fully explored the key advantages of this approach, including its (1) potential for

structural diversity, (2) controlled/living nature, and (3) ability to create materials through block copolymerization. Moreover, functional polyester synthesis via the ROAC remains largely unexplored, thereby presenting significant opportunities for innovation. In addition, catalyst safety is a critical ROAC challenge, particularly when considering the practical applications of these functional polyesters. These issues are addressed in greater detail in Section 1.3.

1.3 Conventional ROAC catalysts

Although the ROAC is an excellent polymerization method, catalyst safety must be considered when synthesizing functional polyesters, particularly when intended for biomedical and environmental applications. The first studies on the ROACs of cyclic anhydrides and epoxides were reported by Inoue's group, who used porphyrin-based catalysts (**Figure 1.16a**).[43] More recently, significant progress in the development of transition-metal-based catalyst systems has been reported, particularly by Coates, Nozaki, and Lu; these catalysts include metal-salen-type catalysts for epoxide/cyclic anhydride ROACs.[35,44,45] While these metal complex catalysts are highly catalytically efficient, they are costly and prepared using labor-intensive procedures. Additionally, residual metals are concerned for biomedical and environmental applications, where metal toxicity poses a major issue.

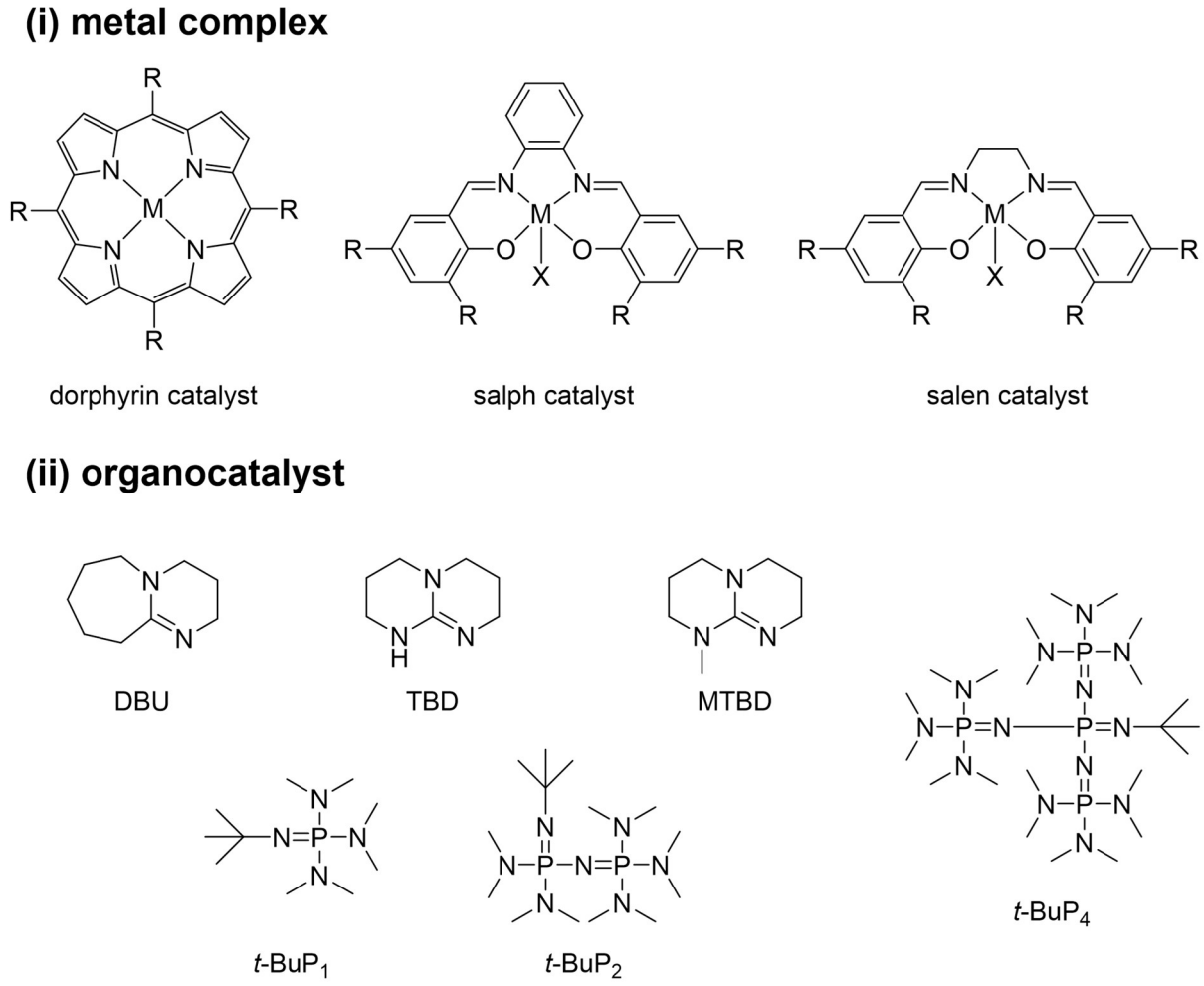

Figure 1.16. Common ROAC catalysts: (a) metal complexes and (b) organobase catalysts.

On the other hand, organobase catalysts have also emerged as pivotal ROAC players (**Figure 1.16.b**). Commonly used organobase catalysts, such as phosphazene bases, 1,8-diazabicyclo[5.4.0]undec-7-ene (DBU), 4-dimethylaminopyridine (DMAP), and triazabicyclodecene (TBD), are efficient in the ROAC systems.[46] Compared to metal-complex catalysts, organobase catalysts are advantageous because they enable end-functionalization through the use of various types of initiator, such as alcohols, carboxylates, and halide ions.

Satoh's group also developed several ROAC catalysts and showed that alkali metal carboxylates (AMCs) are effective (**Figure 1.17**),[47–49] with the most prominent examples including sodium acetate and potassium acetate, both of which are commonly used as food additives. From an industrial perspective, AMCs are particularly valuable because they are inexpensive, easy to handle, essentially non-toxic, and highly stable.[47] Additionally, the basicity of an alkali metal carboxylate can be fine-tuned by choosing appropriate carboxylate moieties and countercations, which enables further customization of catalytic activity. Consequently, recent advancements in ROAC catalyst discovery and development have led to a shift in focus towards safer and more environmentally friendly methods for synthesizing polyesters, and addressing concerns regarding potential metal toxicity.

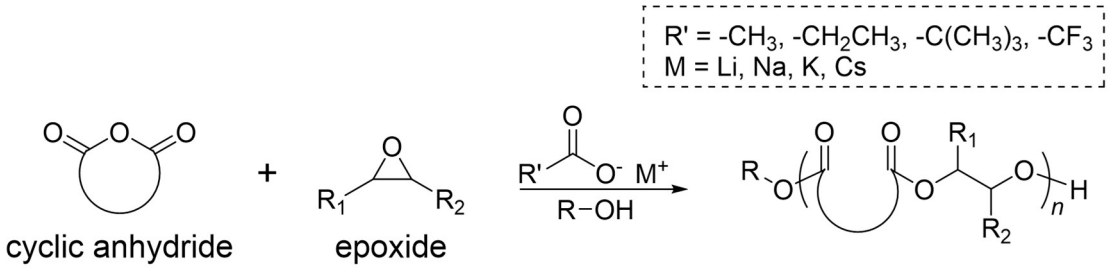

Figure 1.17. AMC-catalyzed ROAC. Selecting the carboxylate and cation parts of the AMC catalyst facilitates control over catalytic activity.[47]

The discovery of ROAC reactions involving cyclic anhydrides and epoxides, along with organocatalyst advancements, has significantly accelerated the syntheses of polyesters with precise and diverse structures. However, current organocatalytic ROAC research primarily focuses on exploring novel monomers and catalysts, which limits scope to the control of main-chain structures and evaluating polymerization behavior. Therefore, fully exploiting the potential of ROAC by introducing functional groups into the side and terminal chains and controlling polymer topology is essential for promoting the development of new functional polyesters.

1.4 Objective and outline of this thesis

Polyesters are widely used in a wide variety of applications that range from commodity plastics to advanced functional materials. The properties of functional polyesters depend highly on a number of factors, including the main- and side-chain structures of the polymer, its end-group functionalities, molecular weight, polydispersity, and topology, all of which require precise control. The ROACs of cyclic anhydrides and epoxides offer unique advantages in this regard because they provide excellent polymerization controllability owing to the associated chain-growth mechanism, which facilitates the synthesis of polyesters with diverse repeating structures that depend on the specific monomer combination. However, previous ROAC studies have been confined to exploring applicable monomers and developing novel catalysts, with little focus on harnessing the exceptional polymerization controllability offered by ROAC for the synthesis of functional polyesters with advanced structural properties. Moreover, the use of environmentally and biologically safe catalysts is critical for practical applications of polyesters. Although metal-based catalysts have traditionally been employed, recent organocatalysis advancements, particularly the discovery of organobase catalysts, have provided safer alternatives that effectively address these concerns.

Therefore, the development of a simple and efficient method for synthesizing functional polyesters with controllable architectures by exploiting the inherent advantages of

organocatalyzed ROAC is the objective of this study. Specifically, this study focused on the synthesis of several key functional polyester types, including side-chain/chain-end-functionalized polyesters, polyesters with highly branched architectures, and block polyesters. Furthermore, applications of the synthesized block copolymers were explored in detail.

As outline of the thesis is described in bellow:

Chapter 2 describes the ROACs of cyclic anhydrides and glicidylamines for producing amino-functionalized polyesters (APEs), as shown in **Figure 1.18**. Catalyst screening revealed that these ROACs proceeded smoothly with AMCs and phosphazene bases as catalysts, and even without catalyst. APEs with adjustable molecular weights and functional end groups can be produced owing to the controlled nature of this ROAC. Moreover, the ROAC system enabled the synthesis of APEs with different main/side-chain structures by simply changing the combination of the two monomers. Considering the advantages of the chain-growth mechanism and wide monomer scope, the established ROAC system may accelerate the exploration of a novel class of APE for use in various applications, such as gene delivery carriers, antibacterial coatings, and biodegradable materials.

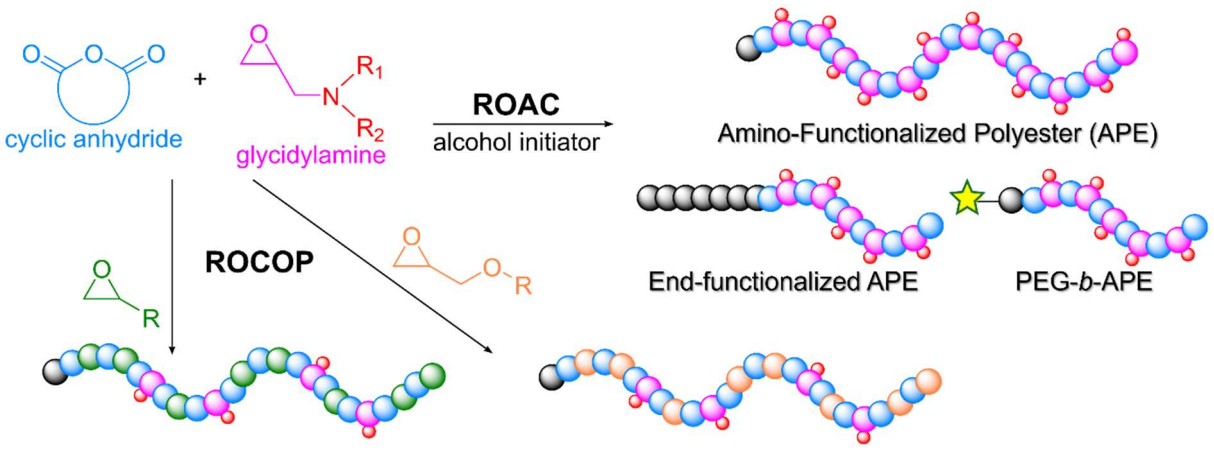

Figure 1.18. Illustration of the Chapter 2 outline.

Chapter 3 describes the ROACs of trimellitic anhydride (TA) with epoxides to afford hyperbranched polyesters (HBPEs), as shown in **Figure 1.19**. Cesium pivalate-catalyzed ROACs of TA and epoxides were performed in the presence of an alcohol initiator under bulk conditions. The hyperbranched structures of the obtained products were confirmed by NMR spectroscopy, viscometry, and light-scattering experiments. The versatility of the developed HBPE synthesis method was demonstrated through the use of a range of alcohol initiators and epoxides, resulting in several HBPEs with structures and properties depended on the resulting backbone structure of the polymer. Furthermore, the terpolymerization of TA, epoxide, and L-lactide (LLA) exhibited self-switching behavior, from the ROAC of the cyclic anhydride to the ROP of LLA, resulting in the successful synthesis of a core-shell block polyester, with a poly(TA-*alt*-epoxide) inner core and a PLLA outer shell.

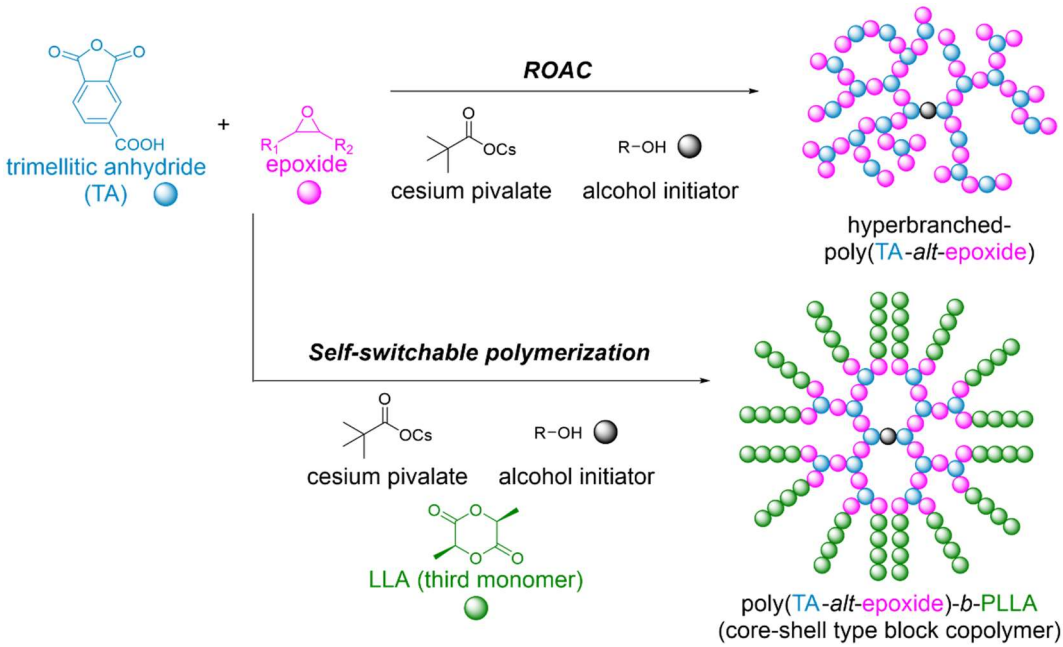

Figure 1.19. Illustration of the Chapter 3 outline.

Chapter 4 describes the one-pot, one-step synthesis of ABA-triblock copolyesters in a terpolymerization system (i.e., self-switchable polymerization that combines the ROAC and ring-opening polymerization of LLA) and evaluates their performance as hot-melt adhesives, as shown in **Figure 1.20**. PLLA-*tapered block*-poly(GA-*alt*-BO)-*tapered block*-PLLA was synthesized in a one-pot/one-step manner via cesium pivalate-catalyzed ring-opening copolymerization of GA, BO, and LLA in the presence of a diol initiator. Additionally, a series of tapered-block or real-block copolyesters ccomposed of poly(anhydride-*alt*-epoxide) (B segment) and PLLA (A segment), with AB-, BAB-, $(AB)_3$-, and $(AB)_4$-type architectures were synthesized by varying the monomer combinations, alcohol initiator, and initial feed ratios. The lap-shear tests of these copolyesters revealed a good relationship between adhesive strengths

and polymer structures (i.e., segment ratio, molecular weight, repeating unit structure, and macromolecular architecture). Among the samples tested, the $(AB)_4$-type copolyester (i.e., poly(GA-*alt*-BO)-*tb*-PLLA)$_4$) exhibited the best adhesive strength, with the value of 6.74 ± 0.64 MPa comparable to those of commercial products such as polyester-based and poly(vinyl acetate)-based hot-melt adhesives.

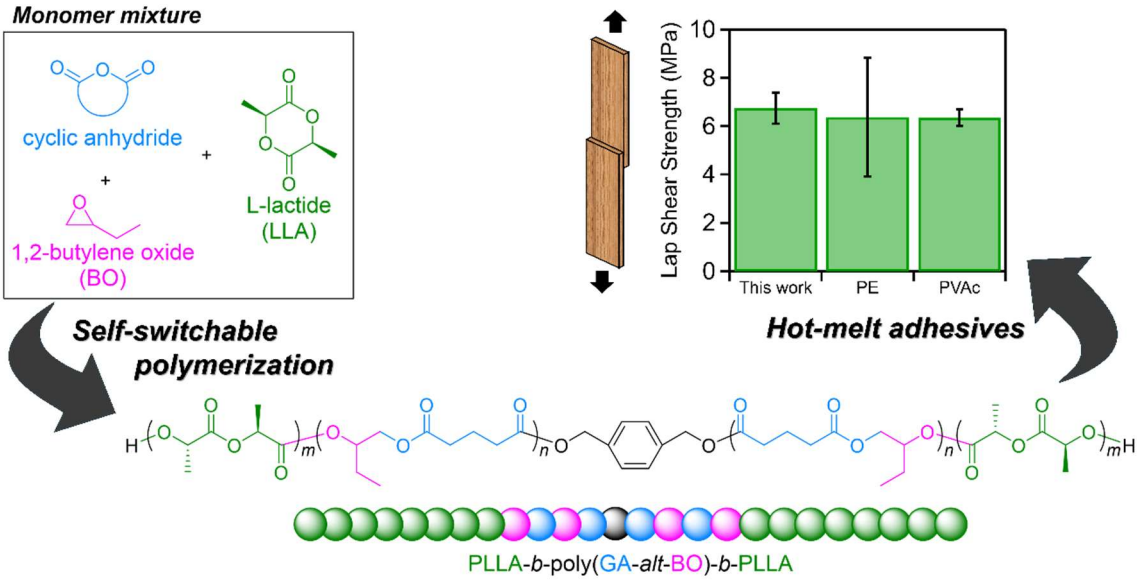

Figure 1.20. Illustration of the Chapter 4 outline.

Chapter 5 summarizes the molecular design of functional polyesters via ROAC established in this research as the overall conclusions of this thesis.

1.5 References

1. H. Seyednejad, A. H. Ghassemi, C. F. van Nostrum, T. Vermonden, W. E. Hennink Functional aliphatic polyesters for biomedical and pharmaceutical applications. *Journal of Controlled Release* **2011**, *152*, 168–176.

2. C. Shi, E. C. Quinn, W. T. Diment, E. Y.-X. Chen Recyclable and (Bio)degradable Polyesters in a Circular Plastics Economy. *Chem. Rev.* **2024**, *124*, 4393–4478.

3. Y. Wang, R.-J. van Putten, A. Tietema, J. R. Parsons, G.-J. M. Gruter Polyester biodegradability: importance and potential for optimization. *Green Chem.* **2024**, *26*, 3698–3716.

4. A. Lv, Z.-L. Li, F.-S. Du, Z.-C. Li Synthesis, Functionalization, and controlled degradation of high molecular weight polyester from itaconic acid via ADMET polymerization. *Macromolecules* **2014**, *47*, 7707–7716.

5. T. Fuoco, M. Cuartero, M. Parrilla, J. J. G.-Guzman, G. A. Crespo, A. F.-Wistrand Capturing the real-time hydrolytic degradation of a library of biomedical polymers by combining traditional assessment and electrochemical sensors. *Biomacromolecules* **2021**, *22*, 949–960.

6. S. Suliman, Y. Sun, T. O. Pedersen, Y. Xue, J. Nickel, T. Waag, A. F.-Wistrand, D. S.-Nethl, A. Krueger, D. E. Costea, K. Mustafa In Vivo Host Response and Degradation of Copolymer Scaffolds Functionalized with Nanodiamonds and Bone Morphogenetic Protein 2. *Adv. Healthcare Mater.* **2016**, *5*, 730–742.

7. H. Seyednejad, D. Gawlitta, R. V. Kuiper, A. Bruin, C. F. Nostrum, T. Vermonden, W. J. A. Dhert, W. E. Hennink *In vivo* biocompatibility and biodegradation of 3D-printed porous scaffolds based on a hydroxyl-functionalized poly(ε-caprolactone). *Biomaterials* **2012**, *33*, 4309–4318.

8. Y. Mato, M. Sudo, H. Marubayashi, B. J. Ree, K. Tajima, T. Yamamoto, H. Jinnai, T. Isono, T. Satoh Densely Arrayed Cage-Shaped Polymer Topologies Synthesized via Cyclopolymerization of Star-Shaped Macromonomers. *Macromolecules* **2021**, *54*, 9079–9090.

9. D. J. A. Cameron, M. P. Shaver Aliphatic polyester polymer stars: synthesis, properties, and

applications in biomedicine and nanotechnology. *Chem. Soc. Rev.* **2011**, *40*, 1761–1776.

10. J. N. Hoskins, S. M. Grayson Cyclic polyesters: synthetic approaches and potential applications. *Polym. Chem.* **2011**, *2*, 289–299.

11. D. K. Schneiderman, M. A. Hillmyer Aliphatic Polyester Block Polymer Design. *Macromolecules* **2016**, *49*, 2419–2428.

12. C. Diaz, P. Mehrkhodavandi Strategies for the synthesis of block copolymers with biodegradable polyester segments. *Polym. Chem.* **2021**, *12*, 783–806.

13. S. Liu, J. Yu, H. Li, K. Wang, G. Wu, B. Wang, M. Liu, Y. Zhang, P. Wang, J. Zhang, J. Wu, Y. Jing, F. Li, M. Zhang Controllable Drug Release Behavior of Polylactic Acid (PLA) Surgical Suture Coating with Ciprofloxacin (CPFX)—Polycaprolactone (PCL)/Polyglycolide (PGA). *Polymers* **2020**, *12*, 288.

14. P. Blondel, T. Briffaud, M. R. G. Werth Kinetics of polycondensation in an industrial environment. *Macromol. Symp.* **1997**, *122*, 243–248.

15. F. Stempfile, P. Ortmann, S. Mecking Long-Chain Aliphatic Polymers To Bridge the Gap Between Semicrystalline Polyolefins and Traditional Polycondensates. *Chem. Rev.* **2016**, *116*, 4597–4641.

16. S. T. Schwab, M. Baur, T. F. Nelson, S. Mecking Synthesis and Deconstruction of Polyethylene-type Materials. *Chem. Rev.* **2024**, *124*, 2327–2351.

17. D. A. Olson, S. E. A. Gratton, J. M. DeSimone, V. V. Sheares Amorphous Linear Aliphatic Polyesters for the Facile Preparation of Tunable Rapidly Degrading Elastomeric Devices and Delivery Vectors. *J. Am. Chem. Soc.* **2006**, *128*, 13625–13633.

18. A. H. Brown, V. V. Sheares Amorphous Unsaturated Aliphatic Polyesters Derived from Dicarboxylic Monomers Synthesized by Diels−Alder Chemistry. *Macromolecules* **2007**, *40*, 4848–4853.

19. Y. Wang, G. A. Ameer, B. J. Sheppard, R. Langer A tough biodegradable elastomer. *Nature Biotechnology* **2002**, *20*, 602–606.

20. J. Yang, A. R. Webb, G. A. Ameer Novel Citric Acid-Based Biodegradable Elastomers for Tissue Engineering. *Adv. Mater.* **2004**, *16*, 511–516.

21. Y. Yu, H. Liu, Z. Wei Synthesis, physical properties, and functionalization of biobased unsaturated polyesters derived from Cis-2-butene-1,4-diol. *Polymer Degradation and Stability* **2022**, *206*, 110203.

22. H. Han, J. Zhu, F.-F. Zhang, F.-X. Li, X.-L. Wang, J.-Y. Yu, X. H. Qin, D.-Q. Wu Hydrophilic and degradable polyesters based on l-aspartic acid with antibacterial properties for potential application in hernia repair. *Biomater. Sci.* **2019**, *7*, 5404–5413.

23. C. Jérôme, P. Lecomte Recent advances in the synthesis of aliphatic polyesters by ring-opening polymerization. *Advanced Drug Delivery Reviews* **2008**, *60*, 1056–1076.

24. P. Feng, R. Zhao, W. Tang, F. Yang, H. Tian, S. Peng, H. Pan, C. Shuai Structural and Functional Adaptive Artificial Bone; Materials, Fabrications, and Properties. *Adv. Funct. Mater.* **2023**, *33*, 2214726.

25. V. G. Rahul, J. Wilson, L. V. Thomas, P. D. Nair Assessing the 3D Printability of an Elastomeric Poly(caprolactone-*co*-lactide) Copolymer as a Potential Material for 3D Printing Tracheal Scaffolds. *ACS Omega* **2022**, *7*, 7002–7011.

26. S. W. Kennedy, N. R. Choudhury, R. Parthasarathy 3D printing soft tissue scaffolds using Poly(caprolactone). *Bioprinting* **2023**, *30*, e00259.

27. H. Misaka, R. Kakuchi, C. Zhang, R. Sakai, T. Satoh, T. Kakuchi Synthesis of Well-Defined Macrocyclic Poly(*δ*-valerolactone) by "Click Cyclization". *Macromolecules* **2009**, *42*, 5091−5096.

28. J. N. Hoskins, S. M. Grayson Synthesis and Degradation Behavior of Cyclic Poly(*ε*-caprolactone). *Macromolecules* **2009**, *42*, 6406–6413.

29. H. Li, N. Zhao, C. Ren, S. Liu, Z. Li Synthesis of linear and star poly(*ε*-caprolactone) with controlled and high molecular weights via cyclic trimeric phosphazene base catalyzed ring-opening polymerization. *Polym. Chem.* **2017**, *8*, 7369–7374.

30. T. Saito, Y. Aizawa, K. Tajima, T. Isono, T. Satoh Organophosphate-catalyzed bulk ring-

opening polymerization as an environmentally benign route leading to block copolyesters, end-functionalized polyesters, and polyester-based polyurethane. *Polym. Chem.* **2015**, *6*, 4374–4384.

31. A. P. Dove Organic Catalysis for Ring-Opening Polymerization. *ACS Macro. Lett.* **2012**, *1*, 1409–1412.

32. N. E. Kamber, W. Jeong, R. M. Waymouth, R. C. Pratt, B. G. G. Lohmeijer, J. L. Hedrick Organocatalytic Ring-Opening Polymerization. *Chem. Rev.* **2007**, *107*, 5813–5840.

33. M. Liu, N. Vladimirov, J. M. Fréchet A New Approach to Hyperbranched Polymers by Ring-Opening Polymerization of an AB Monomer: 4-(2-Hydroxyethyl)-ε-caprolactone. *Macromolecules* **1999**, *32*, 6881–6884.

34. W. W. Gerhardt, D. E. Noga, K. I. Hardcastle, A. J. Garcia, D. M. Collard, M. Weck Functional Lactide Monomers: Methodology and Polymerization. *Biomacromolecules* **2006**, *7*, 1735–1742.

35. J. M. Longo, M. J. Sanford, G. W. Coates Ring-Opening Copolymerization of Epoxides and Cyclic Anhydrides with Discrete Metal Complexes: Structure–Property Relationships. *Chem. Rev.* **2016**, *116*, 15167–15197.

36. C. A. L. Lidston, S. M. Severson, B. A. Abel, G. W. Coates Multifunctional Catalysts for Ring-Opening Copolymerizations. *ACS Catal.* **2022**, *12*, 11037–11070.

37. J. M. Longo, A. M. DiCiccio, G. W. Coates Poly(propylene succinate): A New Polymer Stereocomplex. *J. Am. Chem. Soc.* **2014**, *136*, 15897–15900.

38. L. Feng, Y. Liu, J. Hao, X. Li, C. Xiong, X. Deng Synthesis and Properties of Novel Thermoresponsive Polyesters with Oligo(ethylene glycol) Pendent Chains. *Macromol. Chem. Phys.* **2011**, *212*, 2626–2632.

39. I. Nishimura, A. Kameyama, T. Sakurai, T. Nishikubo Synthesis of Polyesters Carrying Norbornadiene (NBD) Moieties by the Ring-Opening Copolymerization of Glycidyl Esters Containing NBD Moieties with Carboxylic Anhydrides and Their Photochemical Reactions. *Macromolecules* **1996**, *29*, 3818–3825.

40. D. Wang, G. Zhang, Y. Zhang, Y. Gao, Y. Zhao, C. Zhou, Q. Zhang, X. Wang Synthesis, characterization, and properties of novel polyetherester polyols and developed polyurethanes. *Journal of Applied Polymer Science* **2007**, *103*, 417–424.

41. B. Chu, X. Liu, X. Li, Z. Zhang, J. Z. Sun, Q. Yang, B. Liu, H. Zhang, X.-H. Zhang Phosphine-Capped Effects Enable Full-Color Clusteroluminescence in Nonconjugated Polyesters. *J. Am. Chem. Soc.* **2024**, *146*, 10889–10898.

42. X. Liang, W. Wang, D. Zhao, H. Liu, Y. Zhu Self-switchable polymerization catalysis with monomer mixtures: using a metal-free commercial thiourea catalyst to deliver block polyesters. *Polym. Chem.* **2023**, *14*, 4918–4926.

43. T. Aida, S. Inoue Catalytic reaction on both sides of a metalloporphyrin plane. Alternating copolymerization of phthalic anhydride and epoxypropane with an aluminum porphyrin-quaternary salt system. *J. Am. Chem. Soc.* 1985, 107, 1358–1364.

44. W. T. Diment, W. Lindeboom, F. Fiorentini, A. C. Deacy, C. K. Williams Synergic heterodinuclear catalysts for the ring-opening copolymerization (ROCOP) of epoxides, carbon dioxide, and anhydrides. *Acc. Chem. Res.* **2022**, *55*, 1997−2010.

45. E. J. K. Shellard, W. T. Diment, D. A. R.-Lara, F. Fiorentini, G. L. Gregory, C. K. Williams Al(III)/K(I) Heterodinuclear Polymerization Catalysts Showing Fast Rates and High Selectivity for Polyester Polyols. *ACS Catal.* **2024**, *14*, 1363−1374.

46. S. Pappuru, D. Chakraborty Progress in metal-free cooperative catalysis for the ring-opening copolymerization of cyclic anhydrides and epoxides. *European Polymer Journal* **2019**, *121*, 109276.

47. X. Xia, R. Suzuki, K. Takojima, D.-H. Jiang, T. Isono, T. Satoh Smart Access to Sequentially and Architecturally Controlled Block Polymers via a Simple Catalytic Polymerization System. *ACS Catal.* **2021**, *11*, 5999−6009.

48. X. Xia, T. Gao, F. Li, R. Suzuki, T. Isono, T. Satoh Multidimensional Control of Repeating Unit/Sequence/Topology for One-Step Synthesis of Block Polymers from Monomer Mixtures. *J. Am. Chem. Soc.* **2022**, *144*, 17905−17915.

49. X. Xia, T. Gao, F. Li, R. Suzuki, T. Isono, T. Satoh Sequential Polymerization from Complex

Monomer Mixtures: Access to Multiblock Copolymers with Adjustable Sequence, Topology, and Gradient Strength. *Macromolecules* **2023**, *56*, 92−103.

Chapter 2

Organobase-catalyzed ROAC of Glycidylamine with Cyclic Anhydride for Synthesizing Amino-Functionalized Polyester

2.1 Introduction

Amino-functionalized polymers, which contain amino groups on their main- or side-chains, are critical functionalized polymers because of their widespread application as surface modifiers,[1] adhesives,[2–4] heavy metal-ion scavengers,[5] antibacterial materials,[6,7] and gene delivery carriers.[8,9] Poly(ethylene imine) is the most well-known amino-functionalized polymer, and numerous other types, including polystyrenes,[10,11] polyethers,[12–17] polyesters,[8,9,18–20] poly(ester amide),[21] and poly(acryl amide),[22–24] have been reported. Of these, amino-functionalized polyesters (APEs) garner particular attention because of their intriguing properties and functionalities derived from their amino groups, in addition to their inherent degradability via chemical and biological processes. APEs have been used as gene delivery carriers, antibacterial coatings, and biodegradable materials. However, owing to synthetic challenges and the potential incompatibilities of basic amines and esters, the methods of synthesizing APEs are limited.[25]

Existing APEs syntheses can be classified into two categories based on the polymerization mechanism: (a) chain-growth polymerization and (b) step-growth polymerization. The former can be further classified into three categories: the (a-1) ring-opening polymerization (ROP) of lactone monomers with unprotected tertiary amine functionalities,[9] (a-2) ROP of protected amine monomers, followed by deprotection,[20,26–31] and (a-3) ROP of functionalized monomers,

followed by post-modification (**Figure 2.1**).[32–34] The example of (a-1) is the ROP of tertiary amine-bearing valerolactone.[9] Unlike tertiary amine, primary and secondary amines can initiate ROP of cyclic esters, so that the protection and deprotection steps are necessary for the synthesis of APEs with primary and secondary amines. As for example of the (a-2) approach, Tao and Wang et al. performed the living ROP of *O*-carboxyanhydride monomer derived from bio-sourced lysine under mild conditions, and the subsequent deprotection yielded a polyester with primary amines on the side chains.[30] Nottelet et al. also reported an APE synthesis based on the ROP of protected amine-containing lactone, followed by deprotection, where the copolymerization of benzyloxycarbonyl-protected 5-amino-δ-valerolactone with ε-caprolactone successfully produced APEs with amine contents of 10–100%.[35] Waymouth et al. succeeded in synthesizing polyesters with amino groups in their main chains via the organo-catalytic ROP of *N*-acyl-substituted morpholin-2-ones, followed by deprotection.[31] As a third approach, Cheng et al. synthesized APEs by ROP of alkyne subsutited *O*-carboxyanhydride, followed by thiol-yne click reaction (a-3).[33] As mentioned in Chapter 1, ROP are known many advantages e.g., precise control over the molecular weight, monomer sequence, and chain end. However, a major drawback of the ROP approach is the limited versatility in the design of applicable monomers, which renders the production of various APEs with different main- and side-chain structures challenging. Moreover, most of these monomers require multistep

syntheses and deprotection after ROP.

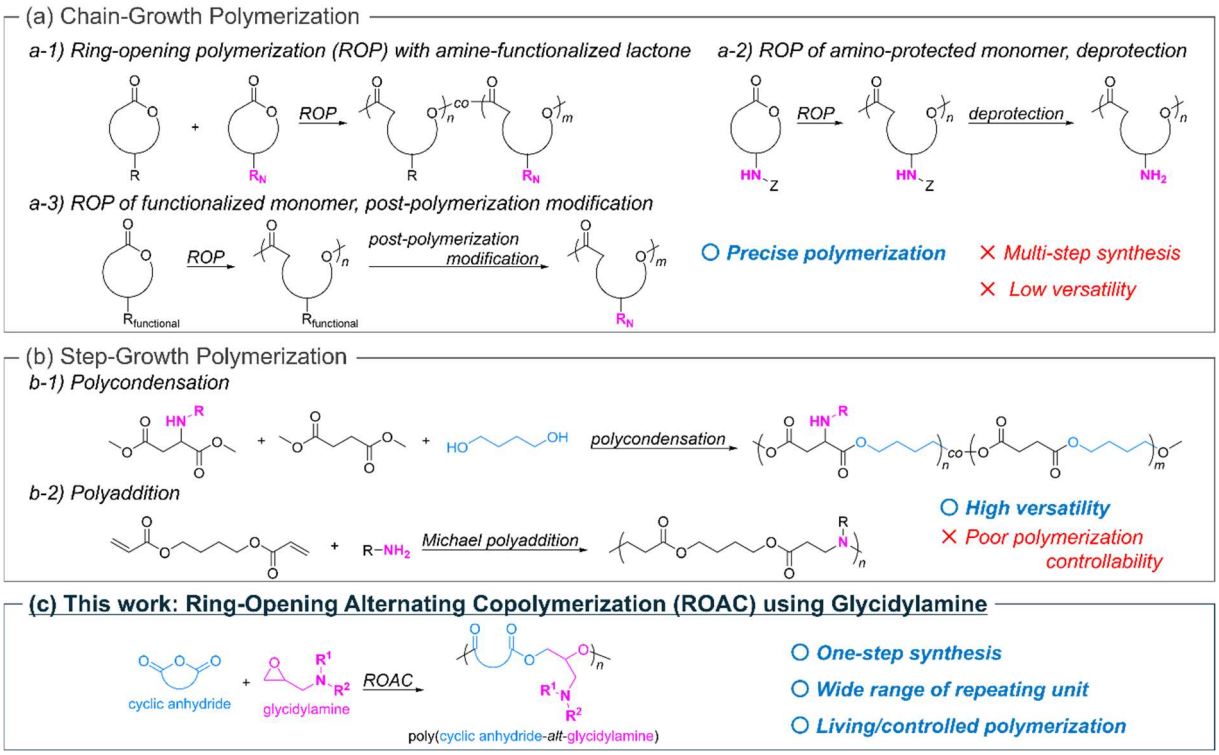

Figure 2.1. Methods of synthesizing APEs: (a) Chain-growth polymerization, (b) step-growth polymerization, and (c) ring-opening alternating polymerization using glycidylamine.

Another major approach used in synthesizing APEs is step-growth polymerization involving polycondensation (b-1) and polyaddition (b-2), as shown in **Figure 2.1**.[36–40] Wu et al. synthesized an APE via the polycondensation of diols and diesters with amino-substituted diesters.[36] Michael addition polymerization was also used in APE synthesis, e.g. Anderson et al. reported the Michael polyaddition of bis(acrylate esters) with primary or secondary amines to yield APEs.[37,38] APEs can be synthesized by converting unsaturated polyesters via aza- or thiol-Michael reactions, utilizing primary amines and amino thiols, respectively.[39,40] The

advantage of step-growth polymerization lies in the generation of the polymer main chain using two different types of monomers (e.g. diol and dicarboxylic acid), enabling the facile syntheses of polyesters with diverse main-chain structures. However, the challenge in controlling polymerization, e.g. the molecular weight, dispersity, and chain-end structures, is a major drawback of step-growth polymerization. Therefore, developing a simple, versatile method of synthesizing APEs to explore the structure-property relationships and expand the range of applications is still challenging.

Herein, the author proposes the use of ring-opening alternating copolymerization (ROAC) in the efficient syntheses of APEs. The ROAC of cyclic anhydrides and epoxides recently attracted intense attention as a novel approach for use in producing functional polyesters. The remarkable advantages of ROAC lie in the precise control over polymerization based on its controlled/living chain-growth polymerization nature and the structural diversity of the resulting polyesters derived from the two different types of monomers, i.e. ROAC simultaneously combines the advantages of the ROP and step-growth approaches in APE synthesis. A recent report by Wu clearly demonstrates that ROAC can serve as a complementary polymerization process to polycondensation, particularly in the synthesis of high value-added products.[41] Thus, the ROAC of cyclic anhydrides with amino-functionalized epoxides may be an excellent synthetic platform for APEs with diverse main- and side-chain structures,

controlled monomer sequences, and desirable chain-end structures (**Figure 2.1c**).

Glycidylamines are amino-functionalized epoxides that can be readily prepared in a single step using epichlorohydrin and secondary amines. Frey et al. pioneered the ROP of glycidyl amines bearing different side chains, where cesium alkoxide-mediated anionic ROP with an ethylene oxide co-monomer afforded amino-functionalized polyethers.[13,42–44] However, the conventional anionic ROP method, i.e., alkali-metal-mediated anionic ROP at high temperature, revealed that the chain transfer reaction to the monomer had occurred, resulting in less control over the molecular weight, molecular weight distribution, and chain-end functionality of the resultant polymers.[44] In contrast, the Satoh's group reported the homopolymerization of glycidylamines using the phosphazene base catalyst under mild conditions.[17] The approach achieved high molecular weight polymers with suppressing chain transfer reactions. This result strongly suggests ROAC of glycidylamines and cyclic acid anhydrides can be established by using a phosphazene base as a catalyst. However, despite the rapid growth in ROAC research, no studies regarding APE synthesis via ROAC have been reported.

In this chapter, the author reports a systematic study regarding the ROAC of glycidylamine with cyclic anhydrides to produce diverse APEs. The author employed several alkali metal carboxylates and phosphazene bases as a catalyst for the ROAC system. Utilizing the optimized conditions, the author successfully synthesized APEs with controlled molecular weights based

on the initial monomer-to-initiator ratio. APEs with different main and side chains and chain-end structures were also synthesized using different glycidylamine and cyclic anhydride monomers, in addition to an alcohol initiator. Moreover, the author examined a glycidylamine/non-amino functionalized epoxide/cyclic anhydride ternary monomer system to maximize the accessible molecular design of the APE.

2.2 Experimental Section

2.2.1 Materials

Phthalic anhydride (PA; >98.0%, Tokyo Chemical Industry Co. Ltd. (TCI)), succinic anhydride (SA; >95.0%, TCI), glutaric anhydride (GA; >98.0%, TCI), and diglycolic anhydride (DGA; >98.0%, TCI) were purified by sublimation before use. Epichlorohydrin (>99.0%, TCI), dibenzylamine (>97.0%, TCI), diallylamine (>98.0%, TCI), *N*-methylbenzylamine (>98.0%, TCI), phosphazene base P_2-*t*-Bu solution (*t*-BuP_2; 2.0 M solution in THF, Sigma-Aldrich), phosphazene base P_1-*t*-Bu (*t*-BuP_1; >97.0%, Sigma-Aldrich), phosphazene base P_4-*t*-Bu solution (*t*-BuP_4; 0.8 M solution in *n*-hexane, Sigma-Aldrich), 1,4-benzene dimethanol (BDM; >99.0%, TCI), tetra-*n*-butylammonium hydrogen sulfate (TBAHS; >98.0%, TCI), and sodium hydroxide (NaOH; >97.0%, FUJIFILM Wako Pure Chemical Corp. (WAKO)) were purchased from commercial sources and used as received. 3-phenyl-1-propanol (PPA; >98%, TCI), butanol (>99.0%, TCI), triethylamine (>99.0%, Kanto Chemical Co. Inc. (KANTO)), butylene oxide (BO; >99.0%, TCI), ethyl glycidyl ether (EGE; >98.0%, TCI), 5-hexen-1-ol (>97.0%, TCI), and propargyl alcohol (>95%) were purified by distillation over CaH_2 under vacuum, which were then stored under an argon atmosphere. Cesium pivalate (CsOPiv; >97.0%, TCI) and sodium acetate (NaOAc; >99%, Sigma-Aldrich) were dried by heating at 100 °C for 3 days. Poly(ethylene glycol) monomethyl ether (MeO-PEG-OH; typical M_n = 400, $M_{n,SEC}$ = 440, $Đ$ =

1.33, TCI) was dried by azeotropic distillation in benzene. *N*,*N*-Dibenzylglycidylamine (DBGA), *N*-benzyl-*N*-methylglycidylamine (BMGA), and *N*,*N*-diallylglycidylamine (DAGA) were prepared according to reported methods and then purified by distillation.[17] Chloroform-*d* ($CDCl_3$; >99.8%, KANTO), acetone (>99.0%, KANTO), hexane (>95.0%, KANTO), dry-tetrahydrofuran (dry-THF; >99.5%, KANTO), methanol (>99.8%, Sigma-Aldrich), and pyridine (>99.5%, KANTO) were used as received.

2.2.2 Instruments

Polymerizations were carried out in an MBRAUN stainless steel glovebox equipped with a gas purification system (molecular sieves and copper catalyst) in a dry argon atmosphere (H_2O, O_2 <0.1 ppm). The moisture and oxygen contents in the glovebox were monitored by a MB-MO-SE-1 and MB-OX-SE-1, respectively.

Nuclear magnetic resonance (NMR) spectra were recorded at 25 °C on a JEOL JNM-ECS400 instrument (400 MHz) or a JEOL JNM-ECZ600R (600 MHz) using $CDCl_3$ as the solvent and chemical shifts were referenced to an internal standard (TMS). The diffusion-ordered NMR (DOSY) analyses were carried out at 30 °C using the ledbpgp2s sequence with at least 15 gradient increments.

Size exclusion chromatography (SEC) was conducted in DMF at 40 °C and a flow rate of 0.6 mL min^{-1} using a Jasco high performance liquid chromatography system (PU-980 Intelligent HPLC pump, CO-965 Column oven, RI-930 Intelligent RI detector, and Shodex DEGAS KT-16) equipped with a Shodex KD-G guard column, Shodex Asahipak GF-310-HQ (7.6 mm ID × 300 mm L), and Shodex Asahipak GF-7M-HQ (7.6 mm ID × 300 mm L). The polystyrene standard curve ranging from 2,170 to 1,320,000 was used for calibration to achieve

the molecular weight ($M_{n,SEC}$) and polydispersity index ($Đ$) of the polymers.

Thermogravimetric analysis (TGA) experiments were performed using a Hitachi High-Tech Science STA200RV under nitrogen atmosphere. The sample was preheated to 100 °C for 30 min to remove water. Then, the sample was cooled to room temperature and heated to 550 °C at the heating rate of 10 °C min^{-1}.

Differential scanning calorimetry (DSC) was conducted using a Hitachi DSC 7000X. The sample was heated from 20 °C to 150 at a rate of 10 °C min^{-1} and held at 100 °C for 10 min to erase thermal history. Then, the sample was cooled to −100 °C at a rate of 10 °C min^{-1} and holed at −100 °C for 10 min. Finally, the sample was heated to 150 °C at a rate of 10 °C min^{-1}. The second heating DSC curve was used to evaluate the glass transition temperature (T_g).

Matrix-assisted desorption ionization time-of-flight mass spectrometry (MALDI-TOF MS) experiment of the polymer was performed in linear mode using a Bruker Daltonics (Germany) Ultraflex MALDI-TOF/TOF mass spectrometer equipped with a 355 nm Nd:YAG laser. The sample for the measurement was prepared by mixing the polymer (10 μL, 10 g L^{-1} in THF), matrix (2-(4-hydroxyphenylazo)benzoic acid; 50 μL, 100 g L^{-1} in THF).

2.2.3 Synthesis detail

2.2.3.1 ROAC of PA and DBGA

A typical procedure for the ROAC is as follows (method A): In an argon-filled glovebox, *t*-BuP$_1$ (40 μmol, 9.4 μL, 1.0 equiv.), PPA (40 μmol, 5.4 μL, 1.0 equiv.), PA (1.0 mmol, 148 mg, 25 equiv.), and DBGA (3.0 mmol, 760 mg, 75 equiv.) were placed in an oven-dried reaction vessel with a magnetic stir. To keep the argon atmosphere, the vessel was sealed with a greaseless valve. After removing the vessel from the glovebox, the reaction mixture was stirred at 80 °C in an oil bath. During the polymerization, a crude aliquot was time-regularly obtained from the system by a syringe in an argon flow and monitored by ^{1}H NMR spectroscopy and SEC to determine monomer conversion and molecular weight, respectively. After the defined time, the polymerization was terminated by diluting the reaction mixture with acetone. The reaction mixture was purified by reprecipitation from an acetone solution into *n*-hexane/acetone = 4/1 (vol/vol). The purified product was dried under vacuum at 40 °C to give poly(PA-*alt*-DBGA) as a colorless solid ($M_{n,NMR}$ = 8,000; $M_{n,SEC}$ = 3,760, $Đ$ = 1.10; yield: 206 mg, 74.3%).

Synthesis of poly(PA-*alt*-DBGA) using Me-PEG-OH as an initiator: The method A was used for the reaction of *t*-BuP$_1$ (40 μmol, 9.4 μL, 1.0 equiv.), Me-PEG-OH (40 μmol, 16 μL, 1.0 equiv.), PA (1.0 mmol, 148 mg, 25 equiv.), and DBGA (3.0 mmol, 760 mg, 75 equiv.) to

give PEG-*b*-poly(PA-*alt*-DBGA) as a colorless viscous liquid ($M_{n,NMR}$ = 6,700; $M_{n,SEC}$ = 4,830, $Đ$ = 1.22; yield: 138 mg, 94.0%).

Synthesis of poly(PA-*alt*-DBGA) using 5-hexen-1-ol as an initiator: The method A was used for the reaction of *t*-BuP_1 (40 μmol, 9.4 μL, 1.0 equiv.), 5-hexen-1-ol (40 μmol, 4.0 μL, 1.0 equiv.), PA (1.0 mmol, 148 mg, 25 equiv.), and DBGA (3.0 mmol, 760 mg, 75 equiv.) to give poly(PA-*alt*-DBGA) as a colorless viscous liquid ($M_{n,NMR}$ = 7,200; $M_{n,SEC}$ = 5,240, $Đ$ = 1.16; yield: 164 mg, 79.1%).

Synthesis of poly(PA-*alt*-DBGA) using propargyl alcohol as an initiator: The method A was used for the reaction of *t*-BuP_1 (40 μmol, 9.4 μL, 1.0 equiv.), propargyl alcohol (40 μmol, 2.4 μL, 1.0 equiv.), PA (1.0 mmol, 148 mg, 25 equiv.), and DBGA (3.0 mmol, 760 mg, 75 equiv.) to give poly(PA-*alt*-DBGA) as a colorless viscous liquid ($M_{n,NMR}$ = 9,000; $M_{n,SEC}$ = 5,240, $Đ$ = 1.20; yield: 178 mg, 49.1%).

Synthesis of poly(PA-*alt*-DBGA) using BDM as an initiator: The method A was used for the reaction of *t*-BuP_1 (40 μmol, 9.4 μL, 1.0 equiv.), BDM (40 μmol, 5.5 mg, 1.0 equiv.), PA (1.0 mmol, 148 mg, 25 equiv.), and DBGA (3.0 mmol, 760 mg, 75 equiv.) to give poly(PA-*alt*-

DBGA) as a colorless viscous liquid ($M_{n,NMR}$ = 7,900; $M_{n,SEC}$ = 4,150, $Đ$ = 1.21; yield: 255 mg, 79.1%).

Synthesis of poly(PA-*alt*-DBGA) without alcohol initiator: The method A was used for the reaction of *t*-BuP_1 (40 μmol, 9.4 μL, 1.0 equiv.), PA (1.0 mmol, 148 mg, 25 equiv.), and DBGA (3.0 mmol, 760 mg, 75 equiv.) to give poly(PA-*alt*-DBGA) as a colorless liquid ($M_{n,SEC}$ = 44,500, $Đ$ = 1.43; yield: 164 mg, 82.3%).

2.2.3.2 ROAC of PA and BO catalyzed by TEA

In an argon-filled glovebox, PPA (50 μmol, 6.8 μL, 1.0 equiv.), PA (1.3 mmol, 185 mg, 25 equiv.), BO (3.8 mmol, 270 mg, 75 equiv.), and TEA (3.8 mmol, 380 mg, 75 equiv.) were placed in an oven-dried reaction vessel with a magnetic stir. To keep the argon atmosphere, the vessel was sealed with a greaseless valve. After removing the vessel from the glovebox, the reaction mixture was stirred at 80 °C in an oil bath. After 6.5 h, a crude aliquot was monitored by ^{1}H NMR spectroscopy to determine monomer conversion.

2.2.3.3 Synthesis of poly(cyclic anhydride-*alt*-glycidylamine) catalyzed by *t*-BuP$_1$

A typical procedure for the ROAC is as follows (method B): In an argon-filled glovebox, *t*-BuP$_1$ (40 μmol, 9.4 μL, 1.0 equiv.), PPA (40 μmol, 5.4 μL, 1.0 equiv.), PA (1.0 mmol, 148 mg, 25 equiv.), and BMGA (3.0 mmol, 532 mg, 75 equiv.) were placed in an oven-dried reaction vessel with a magnetic stir. To keep the argon atmosphere, the vessel was sealed with a greaseless valve. After removing the vessel from the glovebox, the reaction mixture was stirred at 80 °C under an argon atmosphere in an oil bath. During the polymerization, a crude aliquot was time-regularly obtained from the system by a syringe in an argon flow and monitored by ^{1}H NMR spectroscopy and SEC to determine monomer conversion and molar mass. After the defined time, the polymerization was terminated by diluting the reaction mixture with acetone. The reaction mixture was purified by reprecipitation from an acetone solution into *n*-hexane/acetone = 4/1 (vol%). The purified product was dried under vacuum at 40 °C to give poly(PA-*alt*-BMGA) as a light yellow solid ($M_{n,NMR}$ = 4,600; $M_{n,SEC}$ = 1,790, $Đ$ = 1.23; yield: 118 mg, 48.2%).

Synthesis of poly(PA-*alt*-DAGA): The method B was used for the reaction of *t*-BuP$_1$ (40 μmol, 9.4 μL, 1.0 equiv.), PPA (40 μmol, 5.4 μL, 1.0 equiv.), PA (1.0 mmol, 148 mg, 25 equiv.), and DAGA (3.0 mmol, 460 mg, 75 equiv.) to give poly(PA-*alt*-DAGA) as a light yellow solid

($M_{n,NMR}$ = 5,300; $M_{n,SEC}$ = 2,480, $Đ$ = 1.30; yield: 216 mg, 70.5%).

Synthesis of poly(GA-*alt*-DBGA): The method B was used for the reaction of *t*-BuP_1 (40 μmol, 9.4 μL, 1.0 equiv.), PPA (40 μmol, 5.4 μL, 1.0 equiv.), PA (1.0 mmol, 114 mg, 25 equiv.), and DBGA (3.0 mmol, 760 mg, 75 equiv.) to give poly(GA-*alt*-DBGA) as a colorless viscous solid ($M_{n,NMR}$ = 2,000; $M_{n,SEC}$ = 4,390, $Đ$ = 1.50; yield: 105 mg, 75.8%).

Synthesis of poly(DGA-*alt*-DBGA): The method B was used for the reaction of *t*-BuP_1 (40 μmol, 9.4 μL, 1.0 equiv.), PPA (40 μmol, 5.4 μL, 1.0 equiv.), DGA (1.0 mmol, 116 mg, 25 equiv.), and DBGA (3.0 mmol, 760 mg, 75 equiv.) to give poly(DGA-*alt*-DBGA) as a light yellow viscous solid ($M_{n,NMR}$: N.D.; $M_{n,SEC}$ = 5,000, $Đ$ = 1.86; yield: 338 mg, 90.2%).

Synthesis of poly(SA-*alt*-DBGA): The method B was used for the reaction of *t*-BuP_1 (40 μmol, 9.4 μL, 1.0 equiv.), PPA (40 μmol, 5.4 μL, 1.0 equiv.), SA (1.0 mmol, 100 mg, 25 equiv.), and DBGA (3.0 mmol, 760 mg, 75 equiv.) to give poly(SA-*alt*-DBGA) as a black solid ($M_{n,NMR}$ = 4,900; $M_{n,SEC}$ = 6,800, $Đ$ = 2.22; yield: 150 mg, 62.1%).

2.2.3.4 Terpolymerization of cyclic anhydride, glycidylamine, and non amino-functionalized epoxide

Terpolymerization of PA, BMGA, and BO: The method B was used for the reaction of *t*-BuP$_1$ (40 μmol, 9.4 μL, 1.0 equiv.), *n*-butanol (40 μmol, 3.7 μL, 1.0 equiv.), PA (4.0 mmol, 593 mg, 100 equiv.), BMGA (6.0 mmol, 1.06 g, 150 equiv.), and BO (6.0 mmol, 433 mg, 150 equiv.) to give poly(PA-*alt*-BMGA)-*co*-poly(PA-*alt*-BO) as a light yellow viscous solid ($M_{n,NMR}$ = 6,200; $M_{n,SEC}$ = 3,120, $Đ$ = 2.23; yield: 980 mg, 89.6%).

Terpolymerization of PA, DBGA, and EGE: The method B was used for the reaction of *t*-BuP$_1$ (40 μmol, 9.4 μL, 1.0 equiv.), PPA (40 μmol, 6.7 μL, 1.0 equiv.), PA (4.0 mmol, 593 mg, 100 equiv.), DBGA (6.0 mmol, 1.46 g, 150 equiv.), and EGE (6.0 mmol, 613 mg, 150 equiv.) to give poly(PA-*alt*-DBGA)-*co*-poly(PA-*alt*-EGE) as a light yellow viscous solid ($M_{n,NMR}$ = 14,700; $M_{n,SEC}$ = 6,350, $Đ$ = 1.39; yield: 1.03 g, 79.5%).

2.3 Results and Discussion

2.3.1 Ring-opening alternating copolymerization of phthalic anhydride and *N*,*N*-dibenzylglycidylamine

To optimize the polymerization conditions for the ring-opening alternating copolymerization (ROAC) of glycidylamines and cyclic anhydrides, the author evaluated several base catalysts that have been used in ROAC. The evaluated catalysts include alkali metal carboxylates, such as cesium pivalate (CsOPiv) and sodium acetate (NaOAc),[45–50] and phosphazene bases,[51] such as *t*-BuP_1, *t*-BuP_2, and *t*-BuP_4 (runs 1–5 in **Table 2.1**). In catalyst screening, *N*,*N*-dibenzylglycidylamine (DBGA) and phthalic anhydride (PA) are used as the glycidylamine and cyclic anhydride monomers, respectively (**Scheme 2.1**).

Table 2.1. Ring-opening alternating copolymerization of PA and DBGA using different catalysts [a]

run	catalyst	time (h)	conv.$_{PA}$ (%) [b]	$M_{n,theo.}$ (g mol^{-1}) [c]	$M_{n,NMR}$ (g mol^{-1}) [b]	$M_{n,SEC}$ (g mol^{-1}) [d]	$Đ$ [d]
1	CsOPiv	9.0	77	7,800	7,100	2,670	1.62
2	NaOAc	6.5	68	6,900	11,700	3,380	1.19
3	*t*-BuP$_1$	2.5	80	6,900	8,000	3,760	1.10
4	*t*-BuP$_2$	1.5	86	8,700	8,000	2,560	1.20
5	*t*-BuP$_4$	0.8	88	9,000	8,300	3,330	1.35
6	none	6.5	69	7,100	5,500	3,510	1.18
7 [e]	*t*-BuP$_1$	5.0	61	12,000	14,300	4,130	1.16
8 [f]	*t*-BuP$_1$	6.0	59	24,000	21,000	4,370	1.19

[a] Polymerization conditions: temp., 80 °C; atmosphere, Ar; initiator, 3-phenyl-1-propanol (PPA); monomers, PA and DBGA; [catalyst]/[PPA]$_0$/[PA]$_0$/[DBGA]$_0$ = 1/1/25/75. [b] Determined via ^{1}H NMR spectroscopy in $CDCl_3$. [c] Calculated via (molecular weight (M.W.) of PPA) + [PA]$_0$/[PPA]$_0$ × conv.$_{PA}$ × (M.W. of PA + M.W. of DBGA). [d] Determined via SEC in dimethylformamide (DMF) containing 0.01 mol L^{-1} LiCl using a polystyrene (PSt.) standard. [e] [*t*-BuP$_1$]/[PPA]$_0$/[PA]$_0$/ [DBGA]$_0$ = 1/1/50/150. [f] [*t*-BuP$_1$]/[PPA]$_0$/[PA]$_0$/[DBGA]$_0$ = 1/1/100/300.

Scheme 2.1. Ring-opening alternating copolymerization of PA and DBGA

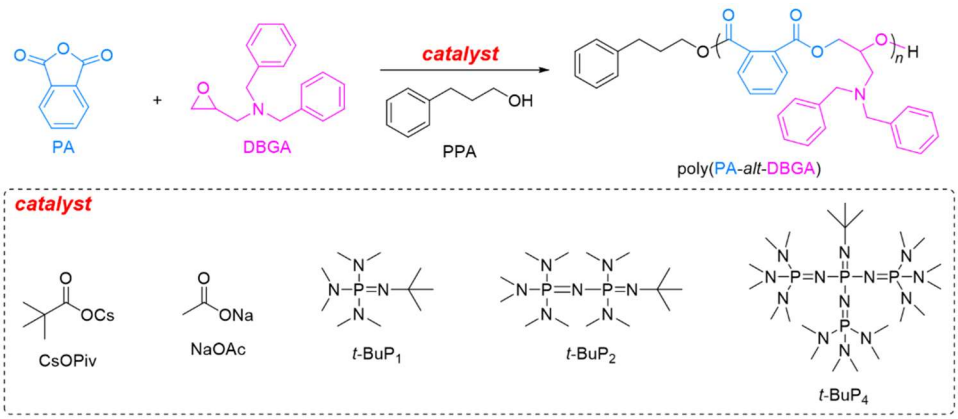

Initially, the author examined ROAC using 3-phenyl-1-propanol (PPA) and CsOPiv as the initiator and catalyst, respectively, at an initial $[CsOPiv]/[PPA]_0/[PA]_0/[DBGA]_0$ ratio of 1/1/25/75 at 80 °C in bulk (run 1 in **Table 2.1**). After 9 h, ^{1}H nuclear magnetic resonance (NMR) spectroscopy of the reaction mixture reveals a PA conversion ($conv._{PA}$) of 77%, it suggests the ROAC was successfully progressed. The ^{1}H NMR spectrum displays the characteristic signals representing the main (benzene ring of PA (*a*), 7.03–7.75 ppm; –C*H*$_2$CH– (*b*), 4.27–4.72 ppm; –CH$_2$C*H*– (*c*), 5.42–5.68 ppm) and DBGA side chains (–CHC*H*$_2$O– (*d*), 2.69–3.04 ppm; –N(C*H*$_2$C$_6$H$_5$)$_2$ (*e*), 3.44– 3.77 ppm; –C$_6$*H*$_5$ (*f*), 7.03–7.75 ppm), in addition to the terminal initiator group (C$_6$H$_5$C*H*$_2$– (*B*), 2.65 ppm; C$_6$H$_5$CH$_2$C*H*$_2$– (*C*), 1.98 ppm; C$_6$H$_5$CH$_2$CH$_2$C*H*$_2$– (*D*), 4.22 ppm) (**Figure 2.2**). Size exclusion chromatography (SEC) reveals a monomodal size distribution, which is used to calculate the number-average molecular weight ($M_{n,SEC}$) and dispersity (*Đ*) of 2,670 g mol^{-1} and 1.62, respectively, based on polystyrene calibration (**Figure 2.3**). These results confirm the success of the ROAC of the cyclic anhydride and glycidylamine in producing an alternating copolyester with amino-functionalized side chains.

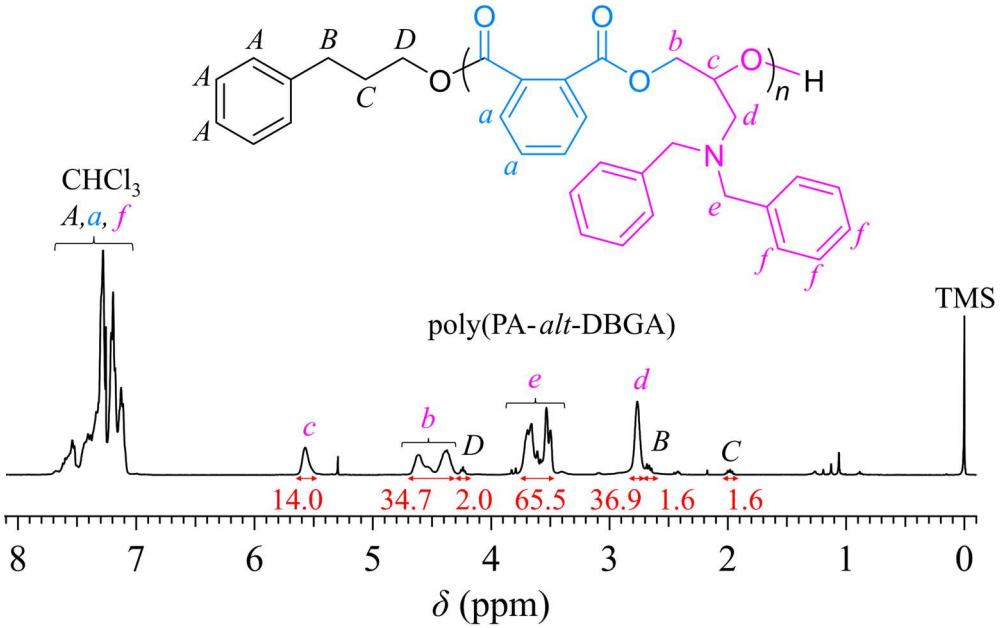

Figure 2.2. ^{1}H NMR spectrum of poly(PA-*alt*-DBGA) obtained via run 1 in Table 2.1 ($CDCl_3$, 400 MHz).

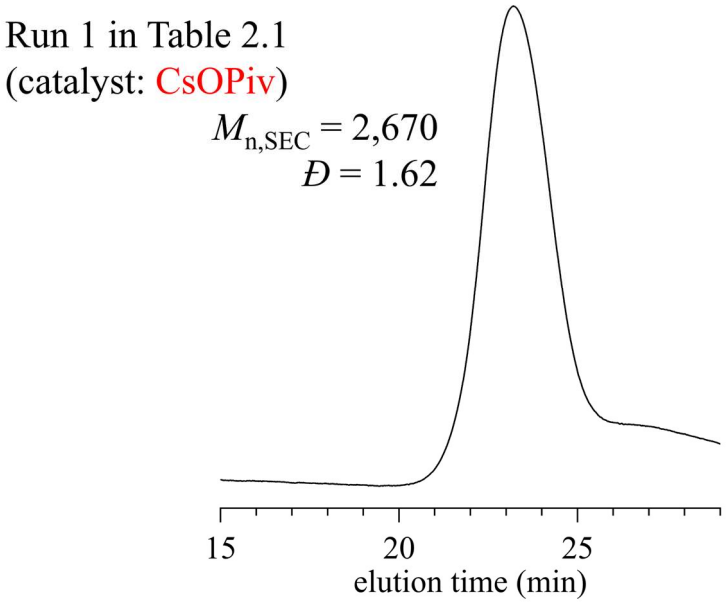

Figure 2.3. SEC trace of poly(PA-*alt*-DBGA) obtained via run 1 in Table 2.1 (eluent, DMF containing 0.01 mol L^{-1} LiCl; flow rate, 0.6 mL min^{-1}).

Under similar conditions, ROAC was performed using NaOAc as the catalyst (run 2 in **Table 2.1**). NaOAc is used as a food additive to ensure a high safety. The conv.$_{PA}$ reaches 68% after 6.5 h, affording the desired poly(PA-*alt*-DBGA) with an even narrower *Đ* of 1.19. This suggests that the control over polymerization can be further improved via careful catalyst selection.

To obtain a polymer with a narrower *Đ*, the author then examined phosphazene bases as catalysts. Notably, the use of these catalysts leads to higher levels of conv.$_{PA}$ in shorter times compared to those observed using the alkali metal carboxylate catalysts (runs 3–5 in **Table 2.1**). Furthermore, as the basicity of the phosphazene base increases (*t*-BuP$_1$, pK_{BH^+} = 26.9; *t*-BuP$_2$, pK_{BH^+} = 33.5; *t*-BuP$_4$, pK_{BH^+} = 42.7),[51] the polymerization rate increases. Moreover, the $M_{n,NMR}$ values of the poly(PA-*alt*-DBGA) obtained using the phosphazene bases closely match the theoretical molecular weights ($M_{n,theo.}$). Slight increases in *Đ* are observed when utilizing *t*-BuP$_2$ and *t*-BuP$_4$ (*Đ* = 1.20 and 1.35, respectively), which may be due to side reactions, such as transesterification, promoted by their exceedingly strong basicities (**Figure 2.4**). In general, basic and acidic catalysts are indispensable in the ROAC of cyclic anhydrides and epoxides. Remarkably, the ROAC of PA and DBGA proceeds even without a catalyst (run 6 in **Table 2.1**). As ROAC proceeds via an anionic polymerization mechanism when a basic catalyst is used, the ROAC of DBGA may be catalyzed by its tertiary amine moiety. To evaluate this hypothesis,

the author examined the ROAC of PA and butylene oxide (BO) in the presence of a large quantity of a tertiary amine (triethylamine; TEA) at an initial $[PPA]_0/[PA]_0/[BO]_0/[TEA]$ ratio of 1/25/75/75 (**Table 2.2**). Expectedly, ^{1}H NMR spectroscopy reveals a $conv._{PA}$ of >99% after 6.5 h and the formation of the corresponding alternating copolymer poly(PA-*alt*-BO) (**Figure 2.5**). Therefore, the tertiary amine moiety of the glycidylamine monomer acts as a catalyst in ROAC. Nevertheless, considering the molecular weight controllability and lowest $Đ$, *t*-BuP_1 is the optimal catalyst for use in this ROAC system.

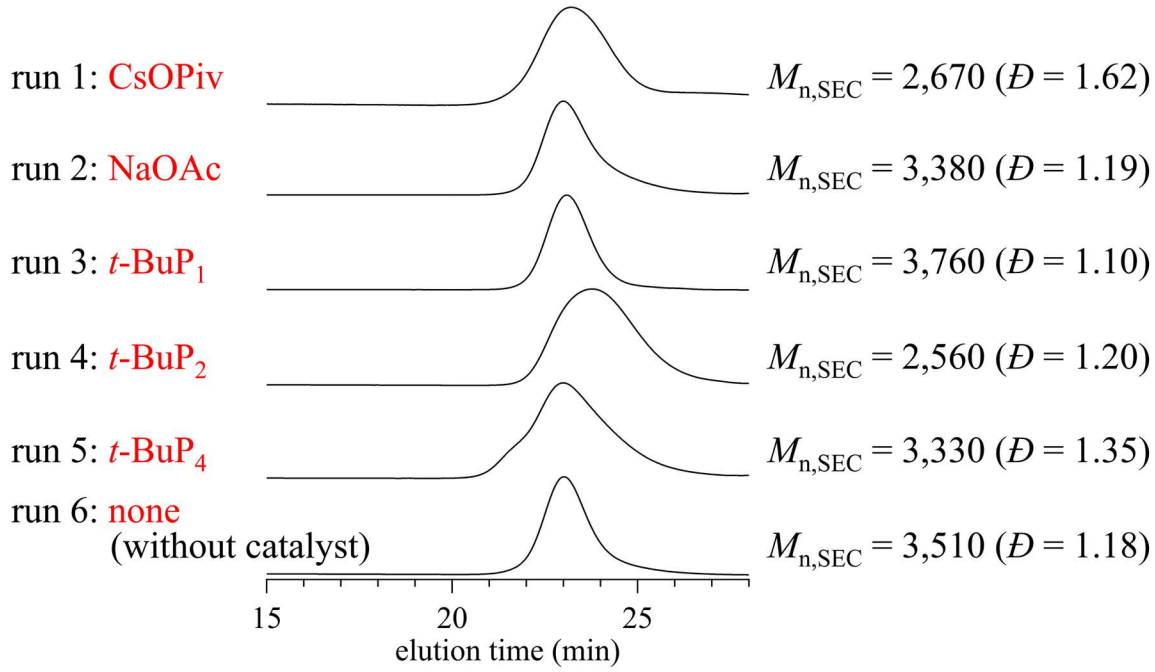

Figure 2.4. SEC traces of poly(PA-*alt*-DBGA) obtained via runs 1–6 in Table 2.1 (eluent, DMF containing 0.01 mol L^{-1} LiCl; flow rate, 0.6 mL min^{-1}).

Table 2.2. ROAC of PA and BO with excess amount of tertiary amine as a catalyst [a]

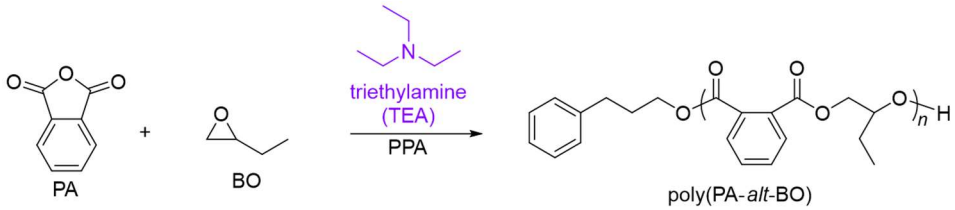

run	M.	cat.	$[PPA]_0/[PA]_0/[BO]_0/[TEA]$	time (h)	conv.PA (%) [b]	$M_{n,NMR}$ [b]	$M_{n,SEC}$ [c]	$Đ$ [c]
1	PA/BO	TEA	1/25/75/75	6.5	>99	5,200	1,910	1.39

[a] Polymerization conditions: temp., 80 °C; atmosphere, Ar; initiator, PPA; catalyst, TEA; monomer, PA and BO. [b] Determined via ^{1}H NMR in $CDCl_3$. [c] Determined via SEC in DMF containing 0.01 mol L^{-1} LiCl using PSt. standard.

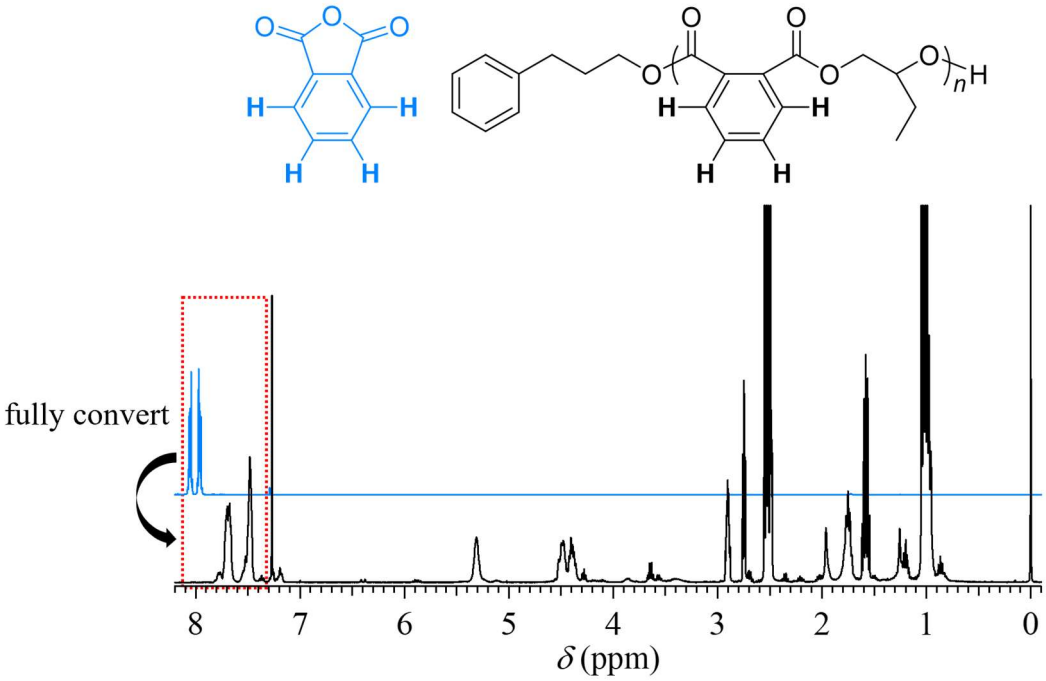

Figure 2.5. ^{1}H NMR spectra of PA (upper) and crude aliquot obtained via run 1 in Table 2.2 (in $CDCl_3$, 400 MHz).

To investigate the microstructure of the poly(PA-*alt*-DBGA) obtained by the optimized condition in more detail, the author employed ^{13}C NMR and matrix-assisted laser desorption ionization-time-of-flight (MALDI-TOF) mass spectrometry. In a typical ROAC of cyclic anhydrides and epoxides, ROP of epoxides, leading to polyether homopolymer formation or ether linkage formation in the resulting copolymer, can occur as a side reaction.[52,53] However, as shown in **Figure 2.6**, the MALDI-TOF mass spectrum of the product obtained from *t*-BuP_1-catalyzed ROAC exhibited two series of peaks with regular intervals of 400.8 Da corresponding to the unit molecular weight of the alternating copolymer (401.2 Da), confirming the perfectly alternating monomer sequence as well as no ether linkage. To further verify the absence of poly(glycidylamine) homopolymer and ether linkage, the author compared the ^{13}C NMR spectrum of the obtained poly(PA-*alt*-DBGA) with poly(DBGA) homopolymer. According to previous reports, a signal originating from the tertiary carbon of the poly(DBGA) main chain appears at 79 ppm,[13,17] which can be used as the signature for the unwanted ROP of DBGA. However, the ^{13}C NMR spectrum of poly(PA-*alt*-DBGA) (run 3 in **Table 2.1**) showed no signal around 79 ppm (**Figure 2.7**). Based on these results, the author concluded that the *t*-BuP_1-catalyzed polymerization solely proceeded by the alternating copolymerization mechanism, without continuous insertion of DBGA.

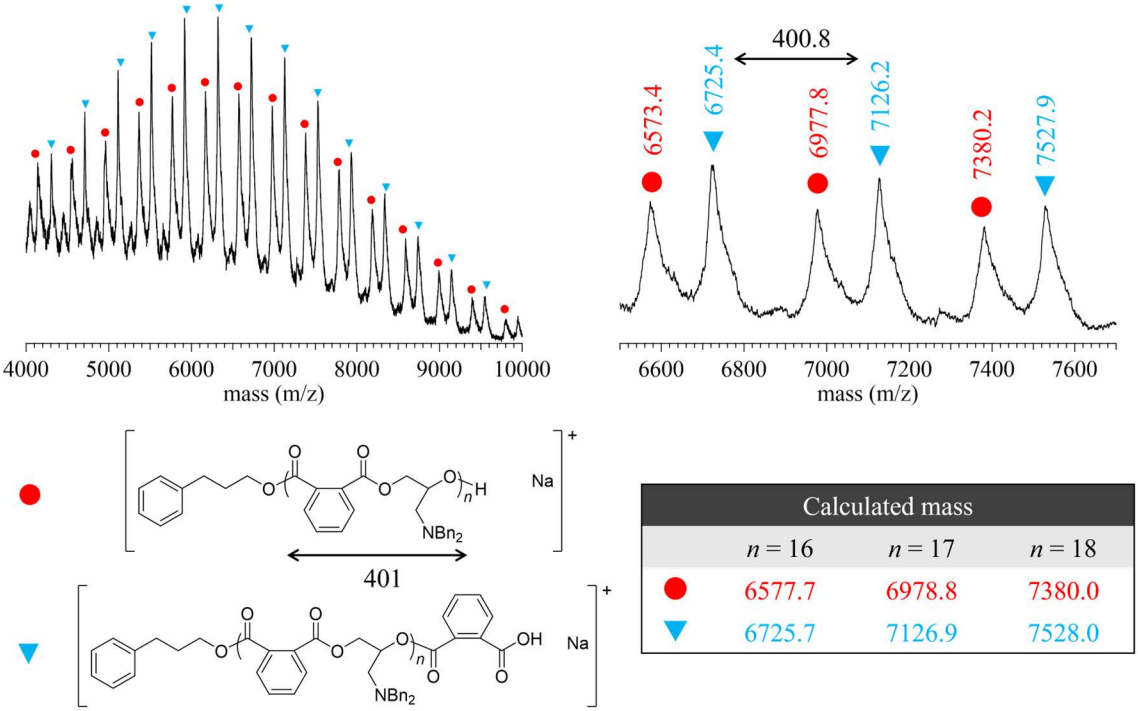

Figure 2.6. MALDI-TOF MS analysis of poly(PA-*alt*-DBGA) (run 3 in Table 2.1).

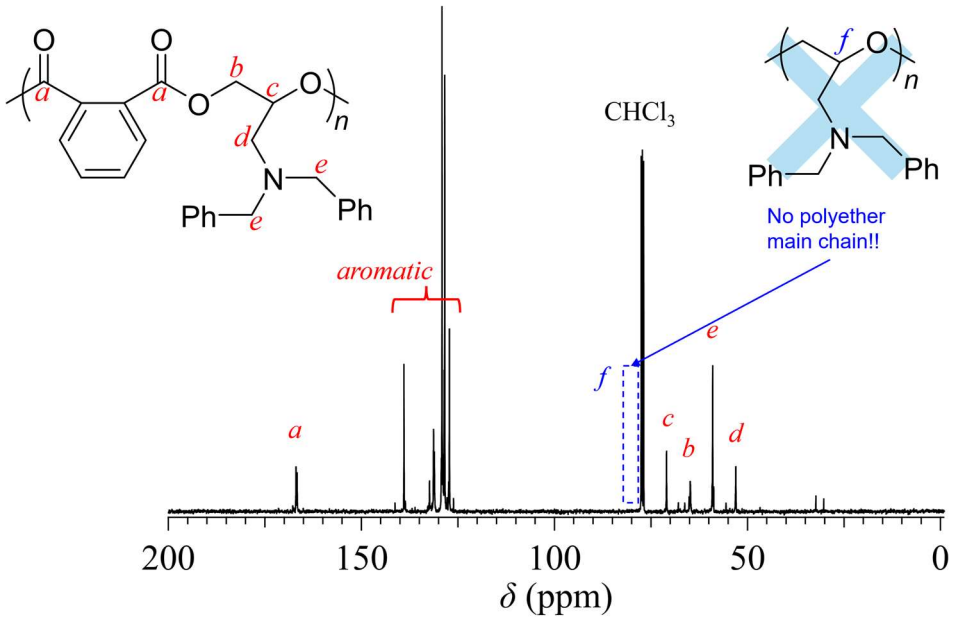

Figure 2.7. ^{13}C NMR spectrum ($CDCl_3$, 100 MHz) of poly(PA-*alt*-DBGA) (run 3 in Table 2.1).

After determining the optimized conditions, the author investigated the living nature of the copolymerization via a monomer addition study (**Figure 2.8**). The ROAC of PA and DBGA was performed under the same conditions as those of run 3 in **Table 2.1**. The $conv._{PA}$ increases with reaction time and reaches >99% at 4.5 h (**Figure 2.8a**). After confirming the complete conversion of PA, additional PA and DBGA (25 and 75 equiv. with respect to PPA, respectively, dissolved in a small amount of toluene) were added to the reaction mixture. Expectedly, $conv._{PA}$ increases further, even after monomer addition. Critically, upon monomer addition, the SEC elution peak shifts to a higher molecular weight region without broadening, indicating chain extension from the end of the living polymer chain (**Figure 2.8b**). Moreover, $M_{n,SEC}$ increases with increasing $conv._{PA}$, whereas the $Đ$ of approximately 1.5 is maintained (**Figure 2.8c**). These results confirm the controlled/living nature of this ROAC system.

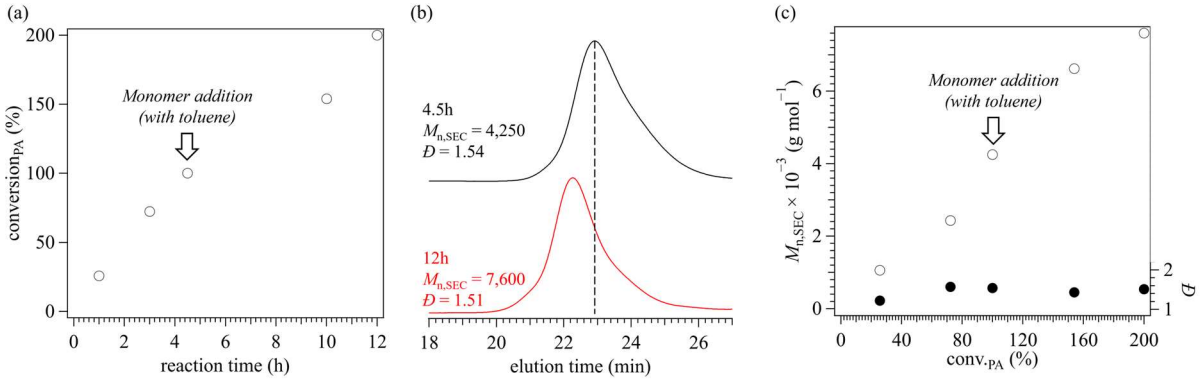

Figure 2.8. (a) Time to conv. plot in the first ROAC of PA and DBGA ([*t*-BuP$_1$]/[PPA]$_0$/[PA]$_0$/[DBGA]$_0$ = 1/1/25/75) and following monomer addition ([living poly(PA-*alt*-DBGA chain]$_0$/[PA]$_0$/[DBGA]$_0$ = 1/25/75). (b) SEC curves of poly(PA-*alt*-DBGA) obtained via the first copolymerization (black line; $M_{n,NMR}$ = 7,300 g mol^{-1}, $M_{n,SEC}$ = 4,250 g mol^{-1}, $Đ$ = 1.54) and following chain extension (red line; $M_{n,NMR}$ = 16,800 g mol^{-1}, $M_{n,SEC}$ = 7,600 g mol^{-1}, $Đ$ = 1.51). (c) Kinetic plots of chain extension experiment.

Exploiting its living nature, the author attempted to synthesize poly(PA-*alt*-DBGA) with different molecular weights by varying the [monomer]$_0$/[initiator]$_0$ ratio from 25 to 100 (runs 7–8 in **Table 2.1**). The polymerizations proceed quantitatively, and the SEC traces of the obtained products shift to the high molecular weight region as [monomer]$_0$/[initiator]$_0$ increases while narrow $Đ$ values are maintained (1.10–1.19, **Figure 2.9**). In addition, the $M_{n,NMR}$ values are fairly consistent with the $M_{n,theo}$ values, with the $M_{n,NMR}$ values of 8,000, 14,300, and 21,000 g mol^{-1} corresponding to the $M_{n,theo}$ values of 6,900, 12,000, and 24,000 g mol^{-1}, respectively.

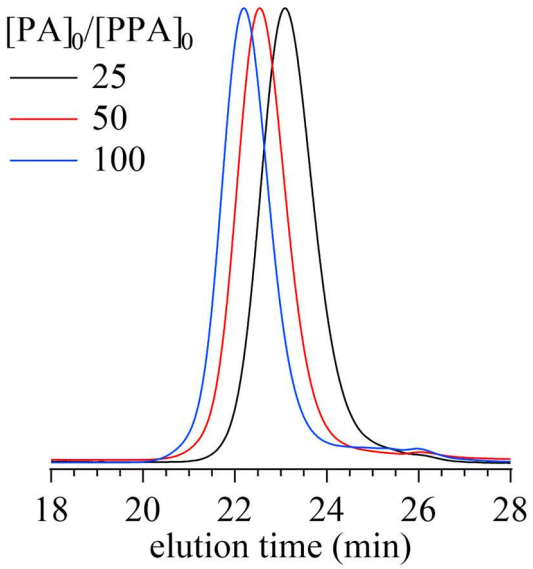

Figure 2.9. SEC traces of the poly(PA-*alt*-DBGA) polymers with different molecular weights prepared by varying the initial monomer-to-initiator ratio ($[PA]_0/[PPA]_0$ = 25, 50, and 100; runs 3, 7, and 8 in Table 2.1, respectively).

2.3.2 ROAC of PA and DBGA with functionalized initiators

To demonstrate the intrinsic advantages of this strategy, several functionalized initiators were used to synthesize poly(PA-*alt*-DBGA) polymers with various chain-end functionalities (**Table 2.3**). First, the author employed poly(ethylene glycol) with a hydroxyl group at one end (Me-PEG-OH; $M_{n,NMR}$ = 400 g mol^{-1}; $M_{n,SEC}$ = 1,070 g mol^{-1}) as a macroinitiator in synthesizing APE-based block copolymers. Even if the author uses Me-PEG-OH instead of PPA, the ROAC of PA and DBGA ([t-BuP$_1$]/[Me-PEG-OH]$_0$/[PA]$_0$/[DBGA]$_0$ = 1/1/25/75) proceeds smoothly, affording PEG-*b*-poly(PA-*alt*-DBGA) with a narrow dispersity ($Đ$ = 1.22; run 1 in **Table 2.3**). A clear shift in the SEC elution peak toward the higher molecular weight region compared to that of the Me-PEG-OH macroinitiator suggests chain extension from the hydroxyl group of the macroinitiator (**Figure 2.10**). The ^{1}H NMR spectrum of the product displays the proton signals representing the terminal methoxy (–OC*H*$_3$, (*A*), 3.4 ppm) and main chain methylene groups of the PEG chain (–C*H*$_2$C*H*$_2$O– (*B*), 3.5–3.7 ppm; (*C*), 4.3 ppm), in addition to the proton signals representing the poly(PA-*alt*-DBGA) backbone (**Figure 2.11**). Such PEG-containing APE block copolymers may be applied in the biomedical field, e.g. as a pH-responsive nanocarrier for drug delivery systems (DDS).[54] Subsequently, to synthesize end-functionalized poly(PA-*alt*-DBGA)s, alcohols with alkene and alkyne functional groups, i.e. 5-hexen-1-ol and propargyl alcohol, were used as initiators (runs 2 and

3 in **Table 2.3**). The ^{1}H NMR spectra of the obtained products display the characteristic signals representing the alkene (–CH=C*H*$_2$, (*A*), 4.9 ppm; –C*H*=CH$_2$, (*B*), 5.8 ppm) and alkyne protons (–C≡C*H*, (*A*), 3.1 ppm, **Figures 2.12** and **2.14**). The SEC traces of the alkene- and alkyne-functionalized poly(PA-*alt*-DBGA) polymers display monomodal elution peaks, suggesting the well-controlled natures of the polymerizations ($Đ$ = 1.16–1.20; **Figures 2.13–2.14**). These reactive end groups can be used for further functionalization. Furthermore, the diol initiator 1,4-benzenedimethanol (BDM) successfully provides the desired product (run 4 in **Table 2.3** and **Figure 2.15**). These results confirm the advantages of the ROAC approach in synthesizing functionalized, well-defined APEs.

Table 2.3. ROAC of PA and DBGA using different alcohol initiators [a]

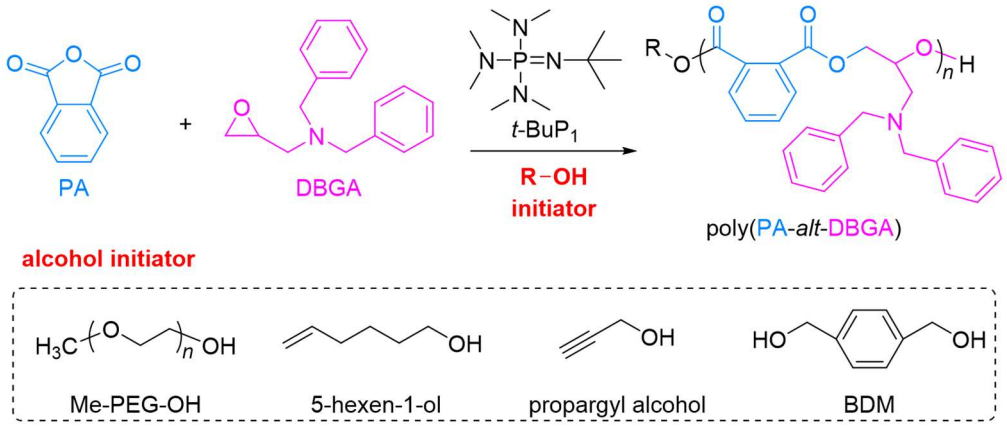

run	ini.	time (h)	conv.$_{PA}$ (%) [b]	$M_{n,theo.}$ (g mol^{-1}) [c]	$M_{n,NMR}$ (g mol^{-1}) [b]	$M_{n,SEC}$ (g mol^{-1}) [d]	$Đ$ [d]
1	Me-PEG-OH	6	69	7,300	6,700	4,830	1.22
2	5-hexen-1-ol	10	67	6,800	7,200	5,240	1.16
3	propargyl alcohol	6	90	9,000	9,000	5,240	1.20
4	BDM	3	79	8,000	7,900	4,150	1.21
5	none	154	66	*N.D.* [e]	*N.D.* [e]	44,500	1.43

[a] Polymerization conditions: temp., 80 °C; atmosphere, Ar; catalyst, *t*-BuP$_1$; monomers, PA and DBGA; [*t*-BuP$_1$]/[ini.]$_0$/[PA]$_0$/[DBGA]$_0$ = 1/1/25/75. [b] Determined via ^{1}H NMR spectroscopy in $CDCl_3$. [c] Calculated using (M.W. of ini.) + [PA]$_0$/[ini.]$_0$ × conv.$_{PA}$ × (M.W. of PA + M.W. of DBGA). [d] Determined via SEC in DMF containing 0.01 mol L^{-1} LiCl using a PSt. standard. [e] Not determined.

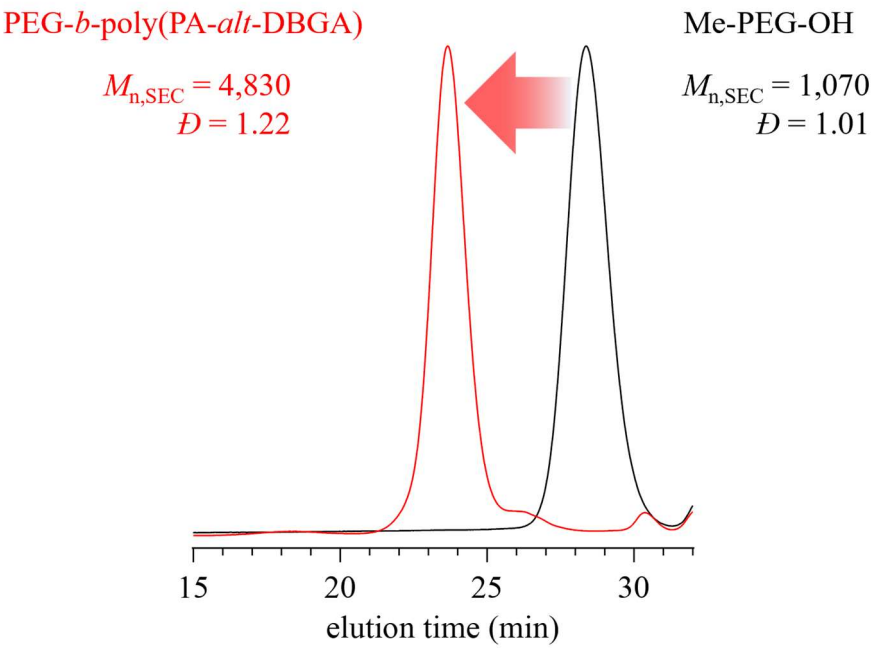

Figure 2.10. SEC traces of Me-PEG-OH (black line) and PEG-*b*-poly(PA-*alt*-DBGA) (red line) obtained via run 1 in Table 2.3 (eluent, DMF containing 0.01 mol L^{-1} LiCl; flow rate, 0.6 mL min^{-1}).

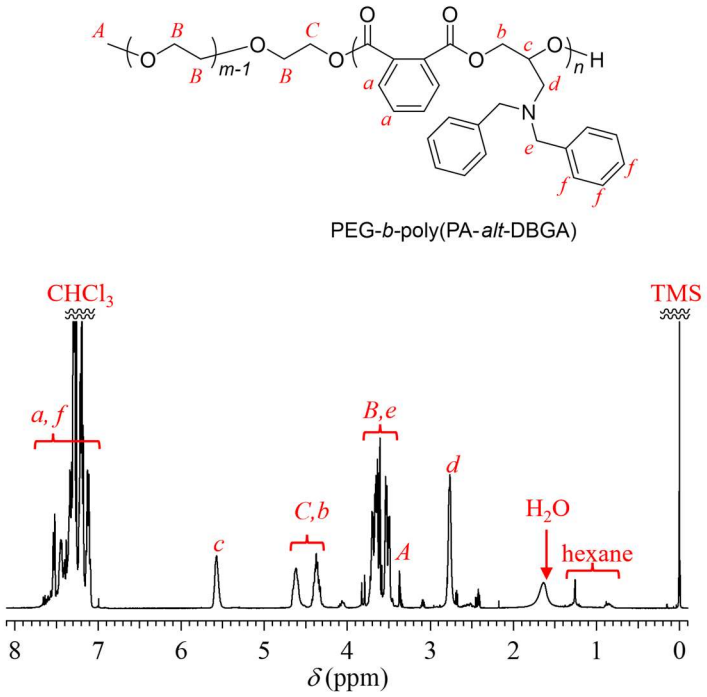

Figure 2.11. ^1H NMR spectrum ($CDCl_3$, 400 MHz) of PEG-*b*-poly(PA-*alt*-DBGA) (run 1 in Table 2.3).

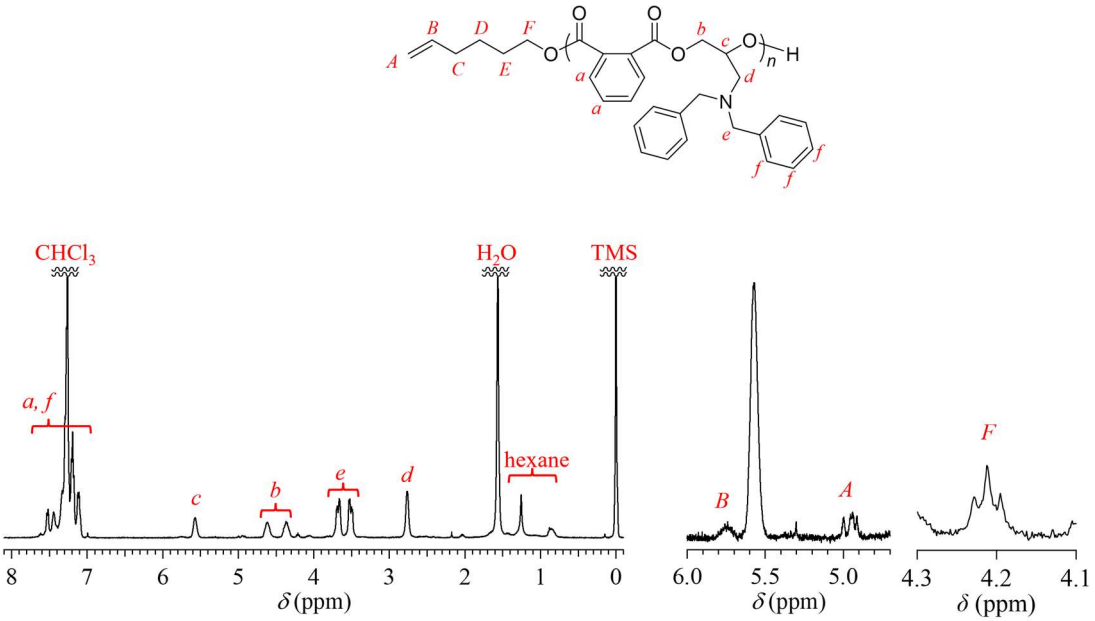

Figure 2.12. ^{1}H NMR spectrum ($CDCl_3$, 400 MHz) of poly(PA-*alt*-DBGA) using 5-hexen-1-ol as an initiator (run 2 in Table 2.3).

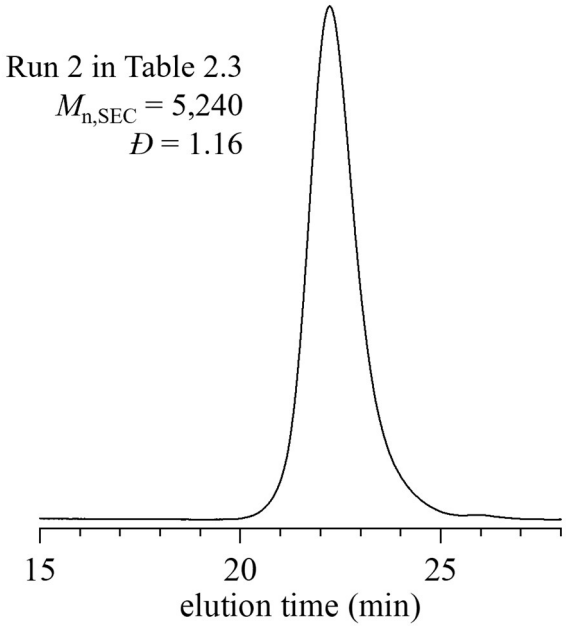

Figure 2.13. SEC trace (eluent, DMF containing 0.01 mol L^{-1} LiCl; flow rate, 0.6 mL min^{-1}) of poly(PA-*alt*-DBGA) using 5-hexen-1-ol as an initiator (run 2 in Table 2.3).

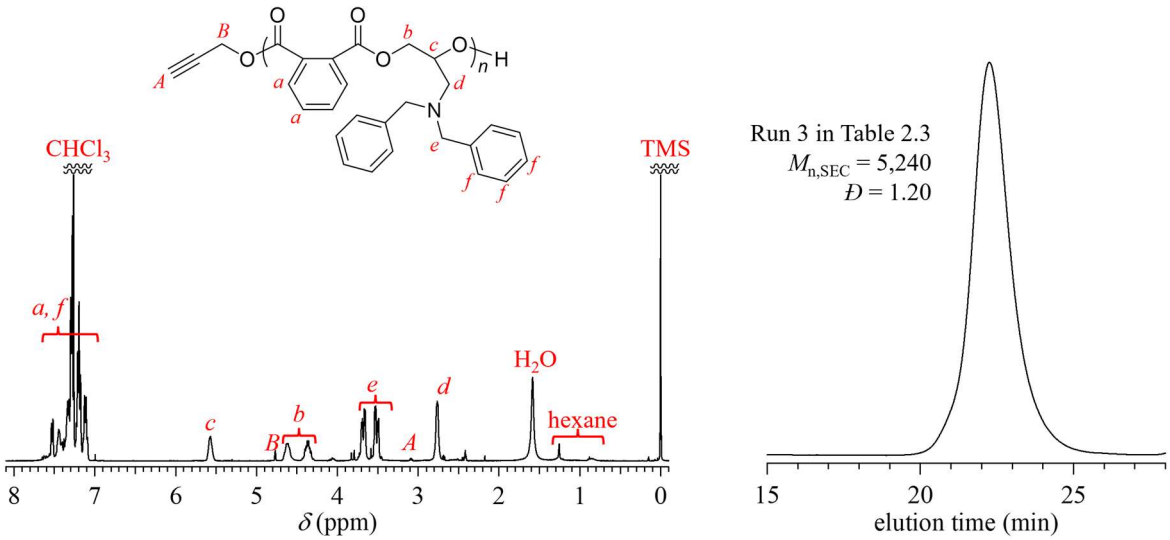

Figure 2.14. ^{1}H NMR spectrum ($CDCl_3$, 400 MHz; left panel) and SEC trace (eluent, DMF containing 0.01 mol L^{-1} LiCl; flow rate, 0.6 mL min^{-1}; right panel) of poly(PA-*alt*-DBGA) using propargyl alcohol as an initiator (run 3 in Table 2.3).

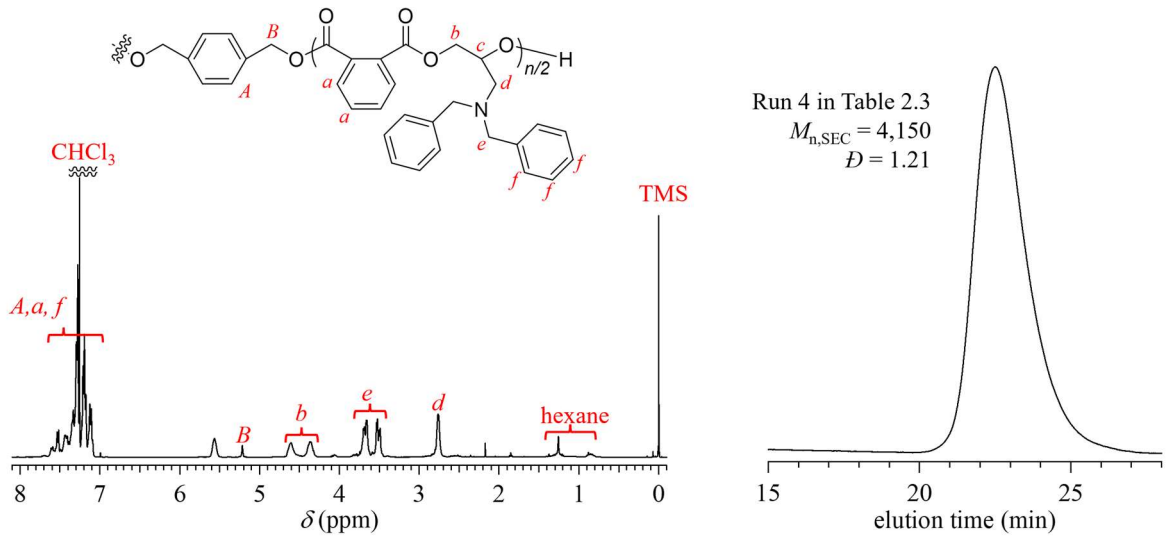

Figure 2.15. ^{1}H NMR spectrum ($CDCl_3$, 400 MHz; left panel) and SEC trace (eluent, DMF containing 0.01 mol L^{-1} LiCl; flow rate, 0.6 mL min^{-1}; right panel) of poly(PA-*alt*-DBGA) using BDM as an initiator (run 4 in Table 2.3).

To determine the role of the alcohol initiator in the ROAC system, the author conducted the ROAC of PA and DBGA without an initiator. Initially, it was expected that polymerization would not occur. However, polymerization proceeds slowly and a conv.$_{PA}$ of 66% is reached after 154 h, affording a high-molecular-weight poly(PA-*alt*-DBGA) ($M_{n,SEC}$ = 44,500 g mol^{-1}, $Đ$ = 1.43; run 5 in **Table 2.3** and **Figure 2.16**). This suggests that trace amounts of protic impurities, such as H_2O, a diol derived from DBGA, and a dicarboxylic acid derived from PA, act as initiators.

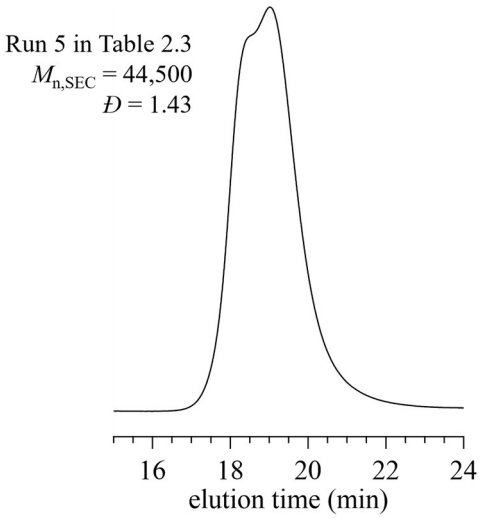

Figure 2.16. SEC trace (eluent, DMF containing 0.01 mol L^{-1} LiCl; flow rate, 0.6 mL min^{-1}) of poly(PA-*alt*-DBGA) synthesized without catalyst (run 5 in Table 2.3).

2.3.3 Monomer scope

The monomer scope of the ROAC system was then investigated using four cyclic anhydrides and three glycidylamines (**Scheme 2.2** and **Table 2.4**). First, ROACs with PA were conducted using *N*-benzyl-*N*-methylglycidylamine (BMGA) and *N*,*N*-diallylglycidylamine (DAGA) as glycidylamine monomers (runs 1 and 2 in **Table 2.4**). The ROAC of PA and BMGA successfully produces the desired polymer poly(PA-*alt*-BMGA), as confirmed via ^{1}H NMR spectroscopy and SEC (**Figure 2.17**). The ^{1}H NMR spectrum displays the characteristic signals representing the methyl (2.1–2.5 ppm (*g*)) and benzyl (–C*H*$_2$C$_6$H$_5$, (*e*), 3.4–3.6 ppm; –C$_6$*H*$_5$, (*f*), 7.1–7.3 ppm) moieties of the BMGA units. In copolymerizing PA and DAGA, the allyl groups isomerize to propenyl groups during the polymerization (–C*H*=CHCH$_3$, (*h*), 5.8 ppm; –CH=C*H*CH$_3$, (*i*), 4.3 ppm; –CH=CHC*H*$_3$, (*j*, *k*), 1.4 and 1.6 ppm), as confirmed by the ^{1}H NMR spectrum (**Figure 2.18**). Such isomerization in the anionic ROP of DAGA under harsh conditions has been reported by Frey *et al*.[13]

Scheme 2.2. ROAC of cyclic anhydride and glycidylamine

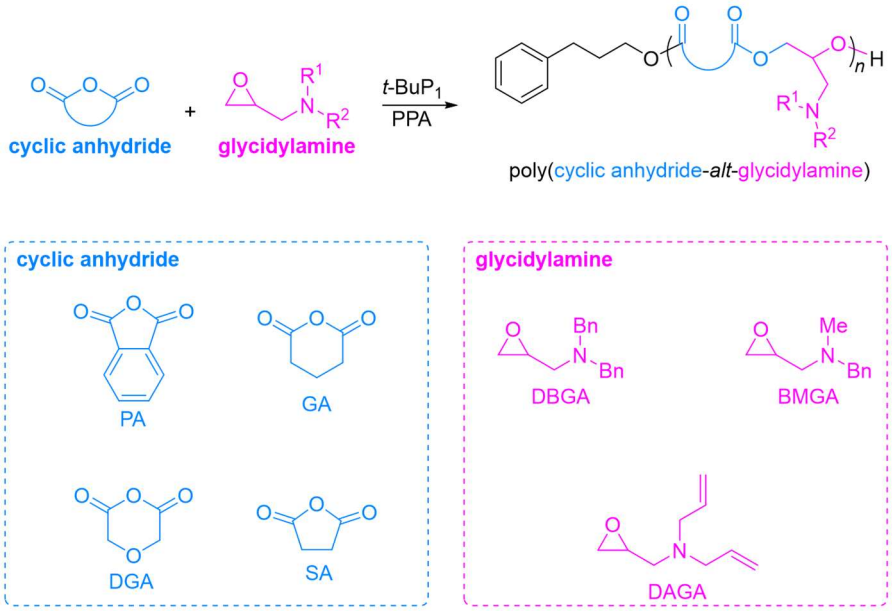

Table 2.4. ROAC of various cyclic anhydrides and glycidylamines using *t*-BuP$_1$ as the catalyst [a]

run	M1	M2	time (h)	conv.$_{M1}$ (%) [b]	$M_{n,theo.}$ (g mol^{-1}) [c]	$M_{n,NMR}$ (g mol^{-1}) [b]	$M_{n,SEC}$ (g mol^{-1}) [d]	$Đ$ [d]
1	PA	BMGA	2.5	74	6,100	4,600	2,350	1.41
2	PA	DAGA	1.0	>99	7,700	5,300	2,480	1.30
3	GA	DBGA	7.0	76	9,300	2,000	4,390	1.50
4	DGA	DBGA	3.0	74	9,400	N.D. [e]	5,000	1.86
5	SA	DBGA	7.0	67	9,000	4,900	6,800	2.22

[a] Polymerization conditions: temp., 80 °C; atmosphere, Ar; initiator, PPA; catalyst, *t*-BuP$_1$; [*t*-BuP$_1$]/[PPA]$_0$/[cyclic anhydride]$_0$/[glycidylamine]$_0$ = 1/1/25/75. [b] Determined via ^{1}H NMR spectroscopy in $CDCl_3$. [c] Calculated using (M.W. of PPA) + [cyclic anhydride]$_0$/[PPA]$_0$ × conv.$_{cyclic\ anhydride}$ × (M.W. of cyclic anhydride + M.W. of glycidylamine). [d] Determined via SEC in DMF containing 0.01 mol L^{-1} LiCl using a PSt. standard. [e] Not determined.

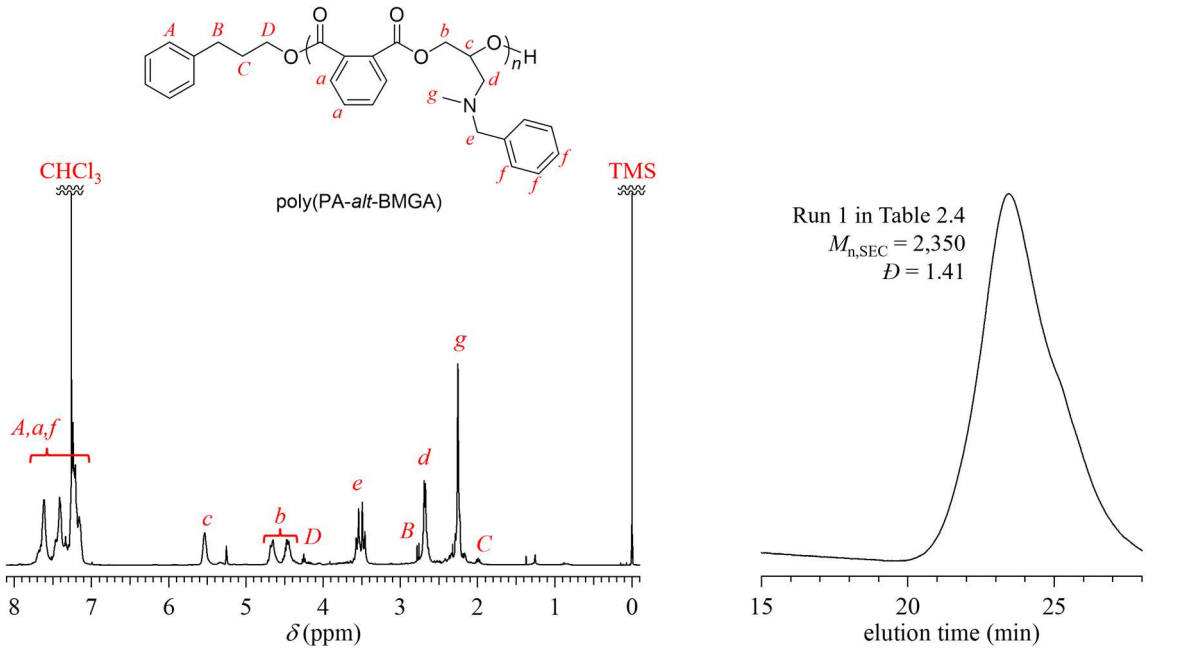

Figure 2.17. ^{1}H NMR spectrum ($CDCl_3$, 400 MHz; left panel) and SEC trace (eluent, DMF containing 0.01 mol L^{-1} LiCl; flow rate, 0.6 mL min^{-1}; right panel) of poly(PA-*alt*-BMGA) obtained via run 1 in Table 2.4.

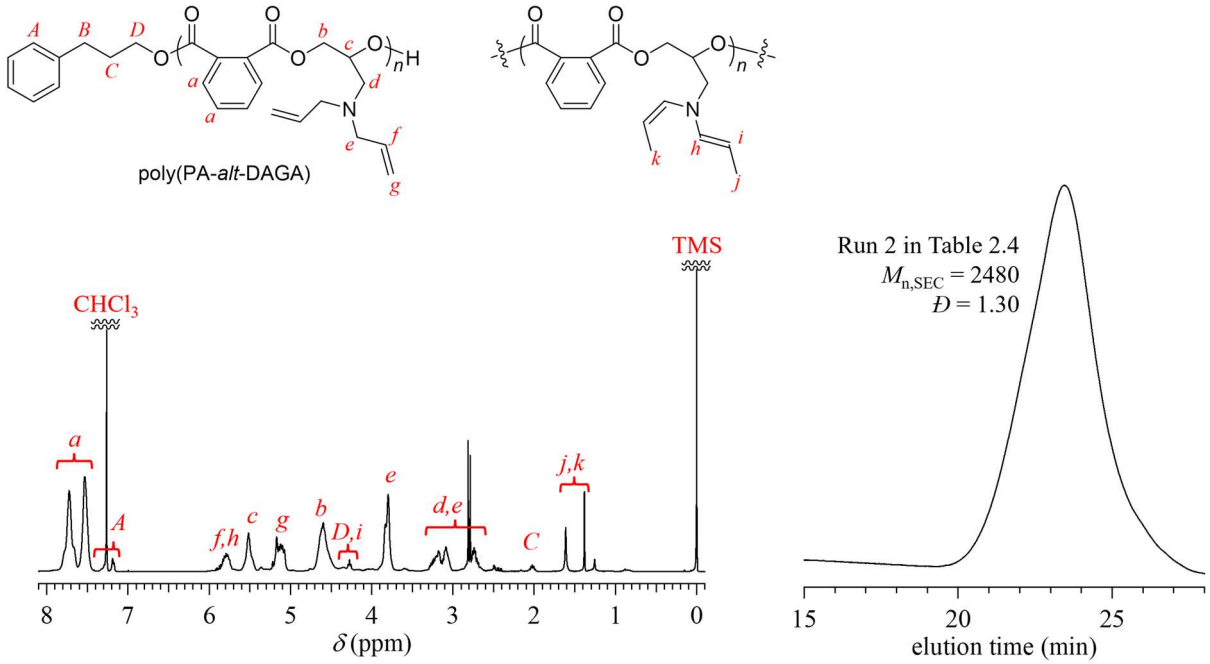

Figure 2.18. ^{1}H NMR spectrum ($CDCl_3$, 400 MHz; left panel) and SEC trace (eluent, DMF containing 0.01 mol L^{-1} LiCl; flow rate, 0.6 mL min^{-1}; right panel) of poly(PA-*alt*-DAGA) obtained via run 2 in Table 2.4.

The author evaluated the ROAC of DBGA with different cyclic anhydrides, including glutaric anhydride (GA), diglycolic anhydride (DGA), and succinic anhydride (SA) (runs 3–5 in **Table 2.4**). Although the polymerization rate varies depending on the cyclic anhydride used, the ROACs proceed with levels of cyclic anhydride conversion of >65%, affording the desired products: poly(GA-*alt*-DBGA), poly(DGA-*alt*-DBGA), and poly(SA-*alt*-DBGA) (**Figures 2.19–2.21**). The SEC trace of poly(SA-*alt*-DBGA) displays a bimodal elution peak, where the higher-molecular-weight byproduct may be due to the polymer chain that grows bidirectionally from a trace amount of succinic acid. It is notable that for all the obtained copolyesters, no evidence of the ether linkage formation via ROP of glycidylamine was detected from their ^{13}C NMR spectra (**Figures 2.22−2.26**). These results collectively confirm the broad monomer scope of the ROAC system.

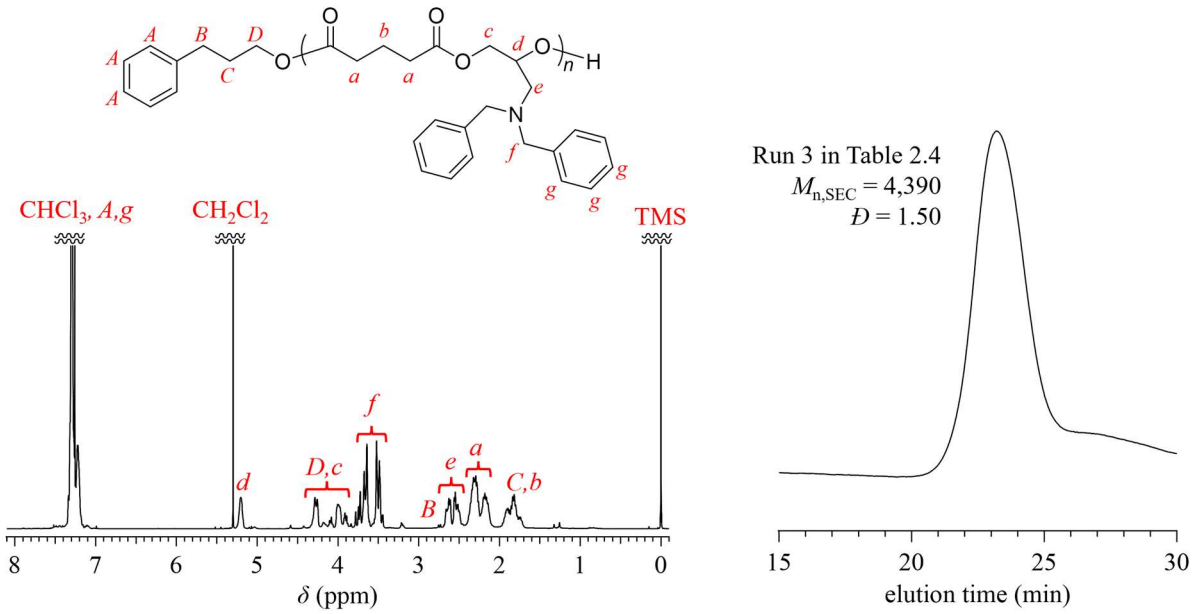

Figure 2.19. ^{1}H NMR spectrum ($CDCl_3$, 400 MHz; left panel) and SEC trace (eluent, DMF containing 0.01 mol L^{-1} LiCl; flow rate, 0.6 mL min^{-1}; right panel) of poly(GA-*alt*-DBGA) obtained via run 3 in Table 2.4.

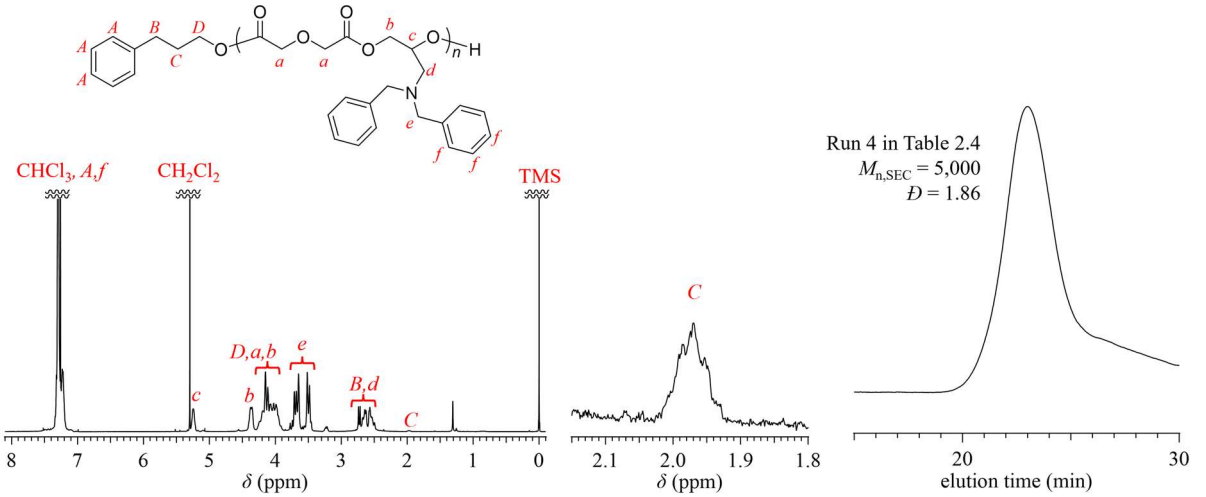

Figure 2.20. ^{1}H NMR spectrum ($CDCl_3$, 400 MHz; left panel) and SEC trace (eluent, DMF containing 0.01 mol L^{-1} LiCl; flow rate, 0.6 mL min^{-1}; right panel) of poly(DGA-*alt*-DBGA) obtained via run 4 in Table 2.4.

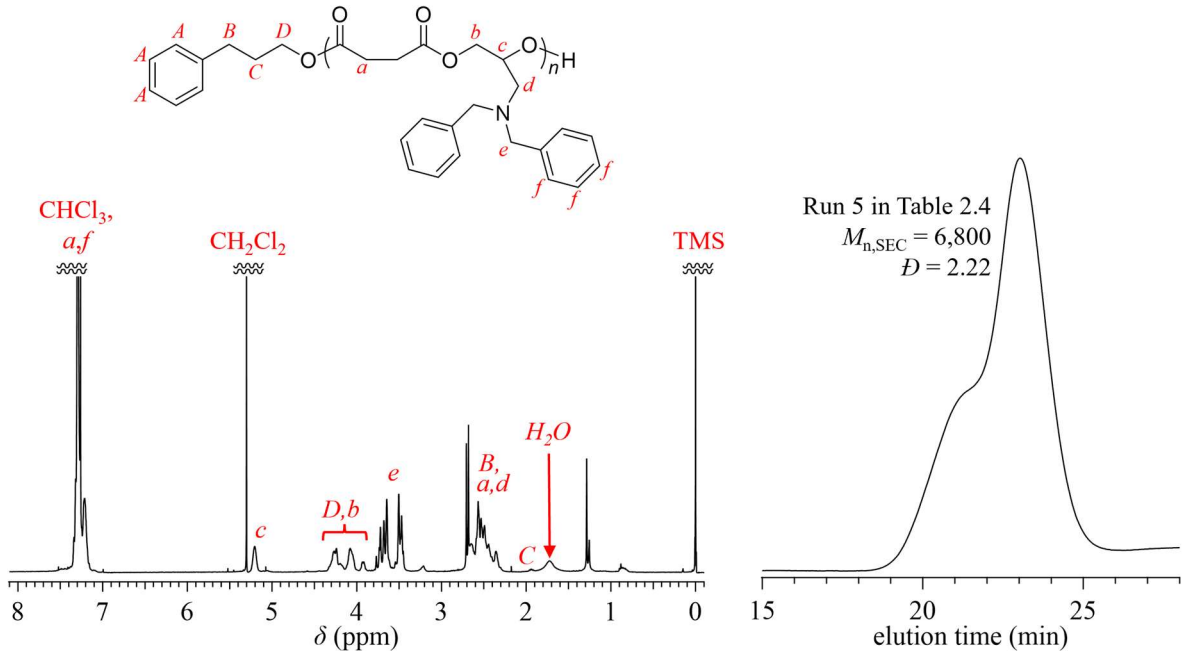

Figure 2.21. ^{1}H NMR spectrum ($CDCl_3$, 400 MHz; left panel) and SEC trace (eluent, DMF containing 0.01 mol L^{-1} LiCl; flow rate, 0.6 mL min^{-1}; right panel) of poly(SA-*alt*-DBGA) obtained via run 5 in Table 2.4.

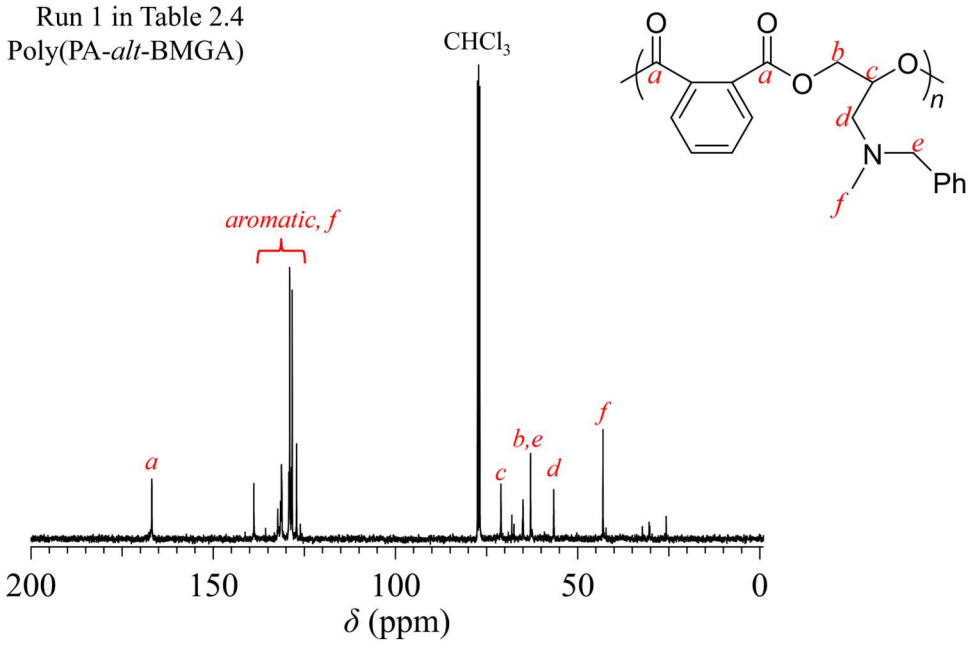

Figure 2.22. ^{13}C NMR spectrum ($CDCl_3$, 100 MHz) of poly(PA-*alt*-BMGA) (run 1 in Table 2.4).

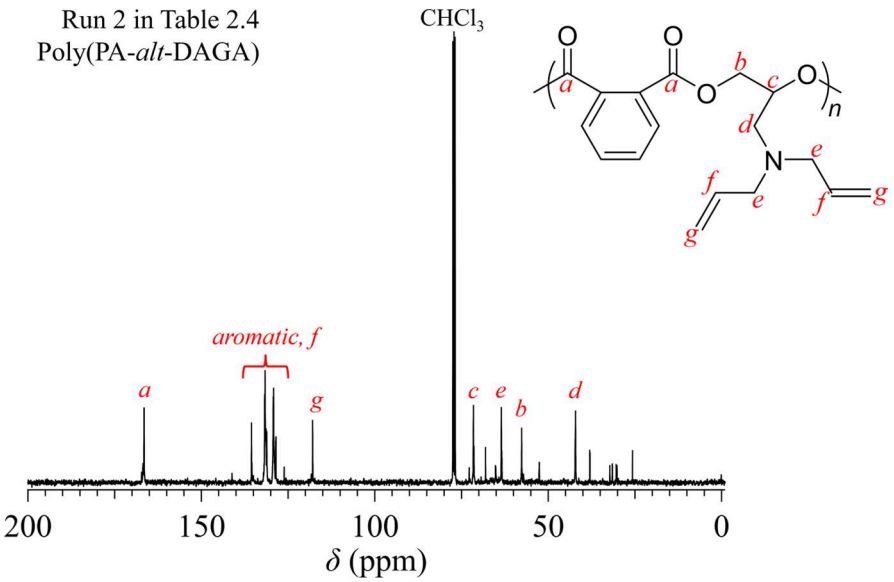

Figure 2.23. ^{13}C NMR spectrum ($CDCl_3$, 100 MHz) of poly(PA-*alt*-DAGA) (run 2 in Table 2.4).

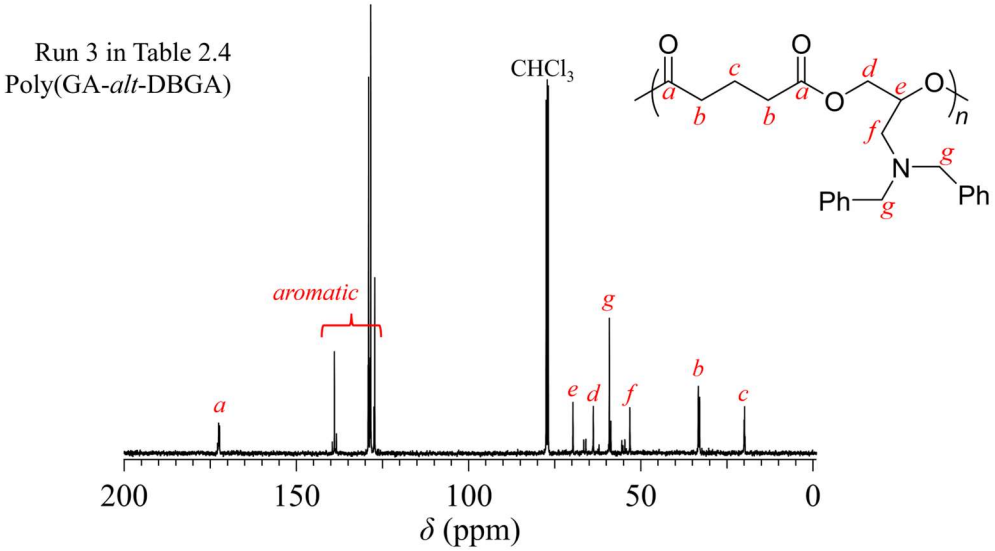

Figure 2.24. ^{13}C NMR spectrum ($CDCl_3$, 100 MHz) of poly(GA-*alt*-DBGA) (run 3 in Table 2.4).

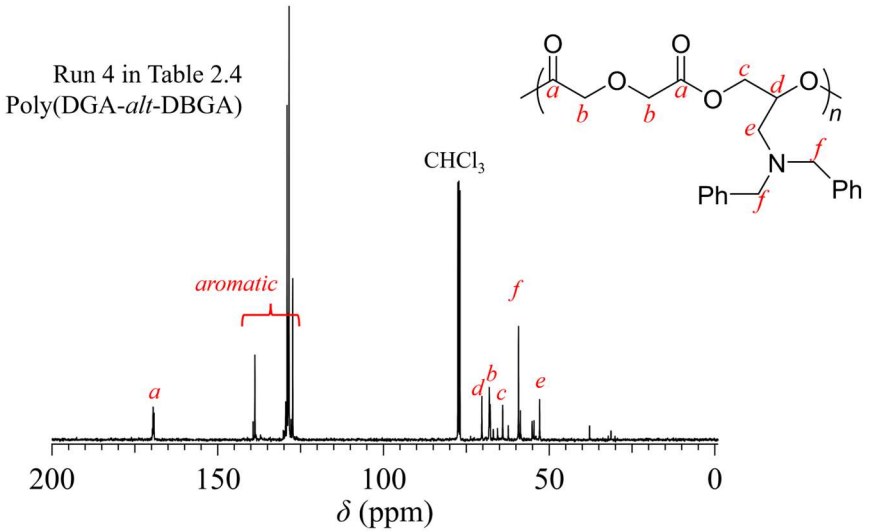

Figure 2.25. ^{13}C NMR spectrum ($CDCl_3$, 100 MHz) of poly(DGA-*alt*-DBGA) (run 4 in Table 2.4).

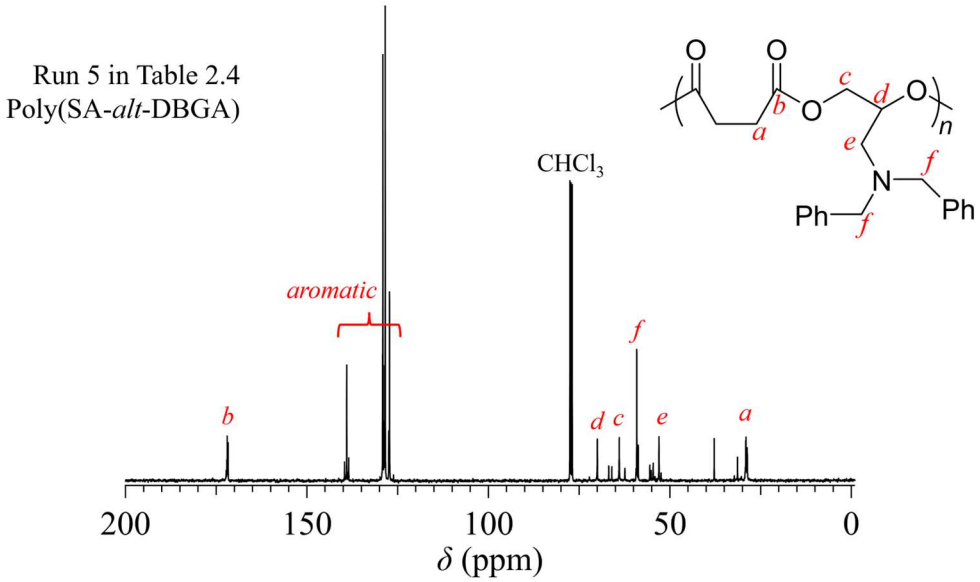

Figure 2.26. ^{13}C NMR spectrum ($CDCl_3$, 100 MHz) of poly(SA-*alt*-DBGA) (run 5 in Table 2.4).

The thermal properties of the APEs with different main-chain structures were evaluated using thermogravimetric analysis (TGA) and differential scanning calorimetry (DSC). Based on TGA, the 5% mass loss temperatures ($T_{d,5\%}$) are in the range 220–305 °C, indicating sufficient thermal stabilities (**Figure 2.27**). The DSC thermograms of all APEs display baseline shifts corresponding to the glass transition temperatures (T_g), whereas no other transitions, such as melting and crystallization, are detected, confirming their amorphous natures. The T_g is adjustable in the range 8.8–54.1 °C based on the choice of the two monomers (**Figure 2.28**). This indicates the versatility of the ROAC system in designing APE materials with adjustable properties.

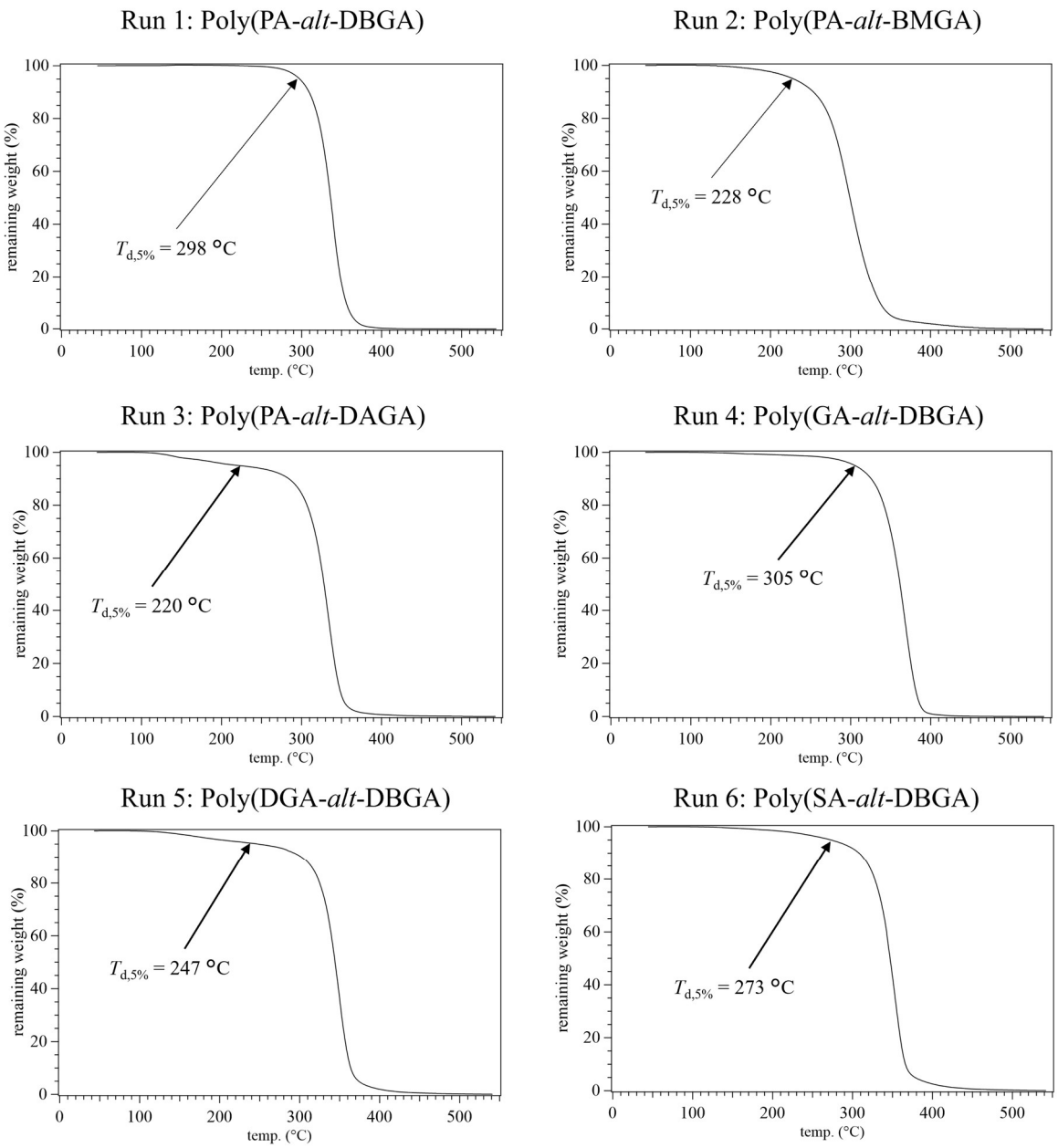

Figure 2.27. Thermogravimetric analysis of the poly(cyclic anhydride-*alt*-glycidylamine)s in Table 2.4.

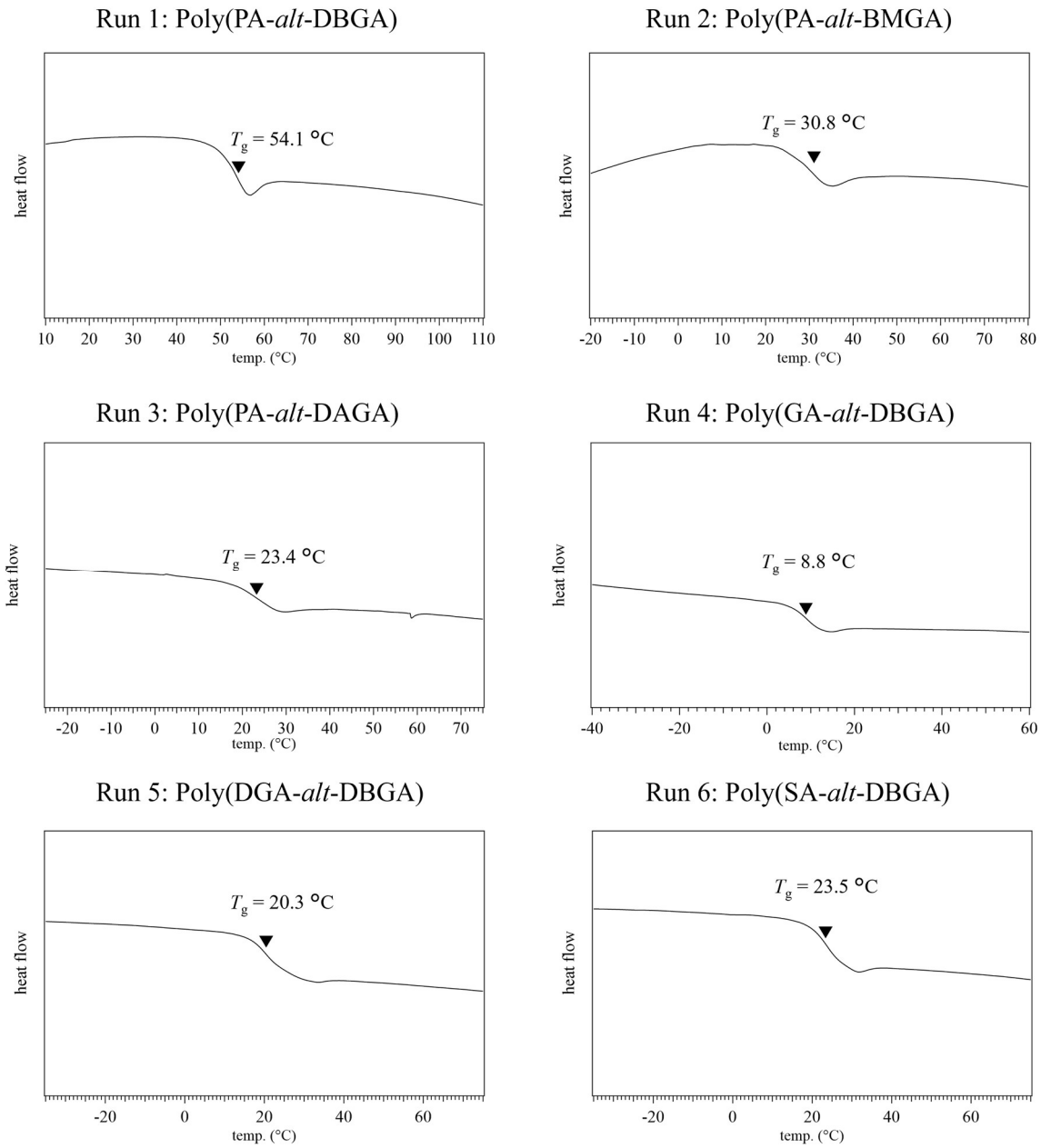

Figure 2.28. DSC thermograms of the poly(cyclic anhydride-*alt*-glycidylamine)s in Table 2.4.

2.3.4 Terpolymerization of a cyclic anhydride and glycidylamine and another cyclic ether

Finally, the author investigated terpolymerization of cyclic anhydrides, glycidylamines, and non-amino-functionalized epoxides to expand the range of accessible APE structures (**Scheme 2.3**). Terpolymerization was conducted using PA, BMGA, and BO as monomers, with *n*-butanol as the initiator, under the optimized conditions ([*t*-BuP_1]/[*n*-butanol]$_0$/[PA]$_0$/[BMGA]$_0$/[BO]$_0$ = 1/1/100/150/150, run 1 in **Table 2.5**). The initial mole fraction in the feed was f_{BMGA} = 0.5 (f_{BO} = 0.5). The simultaneous consumption of the three monomers is confirmed via ^{1}H NMR spectroscopy. The plots of the conv. values as functions of time reveal that BO consumption is faster than that of BMGA until the end of the reaction, suggesting that poly(PA-*alt*-BMGA)-*co*-poly(PA-*alt*-BO) is obtained as a statistical copolyester with excess poly(PA-*alt*-BO) units (**Figure 2.29**). The ^{1}H NMR spectra of the obtained polymer together with the corresponding homopolymers (i.e. poly(PA-*alt*-BMGA) and poly(PA-*alt*-BO), see **Table 2.6**) demonstrated the appearance of the signals representing both poly(PA-*alt*-BMGA) (*a*–*g*) and poly(PA-*alt*-BO) units (*a*, *h*–*k*), confirming successful terpolymerization (**Figure 2.30**, left-hand panel). Based on the signal intensities *c* and *h*, the estimated mole fractions of BMGA (F_{BMGA}) and BO (F_{BO}) within the terpolymer are 0.41 and 0.59, respectively, which closely match the theoretical mole fractions calculated based on monomer conv. ($F_{calc.BMGA}$ = 0.37 and $F_{calc.BO}$ = 0.63). Although $Đ$ is slightly large (2.23), the SEC trace displays

a unimodal elution peak (**Figure 2.30**, right-hand panel). Additionally, the covalent connection of the different blocks in the terpolyester was confirmed by the diffusion-ordered NMR (DOSY) analysis (**Figure 2.31**). Terpolymerization with an increased BO ratio ($[PA]_0/[BMGA]_0/[BO]_0$ = 100/60/240, f_{BMGA} = 0.2) also proceeds, yielding a terpolymer with F_{BMGA} = 0.15 (run 2 in **Table 2.5**). The ^{1}H NMR spectra of the terpolymers and the corresponding copolymers shown in **Figure 2.32** demonstrate the facile control based on f_{BMGA}.

Scheme 2.3. Ring-opening terpolymerization of cyclic anhydride and glycidylamine with another epoxide.

(a) Terpolymerization of PA, BMGA, and BO

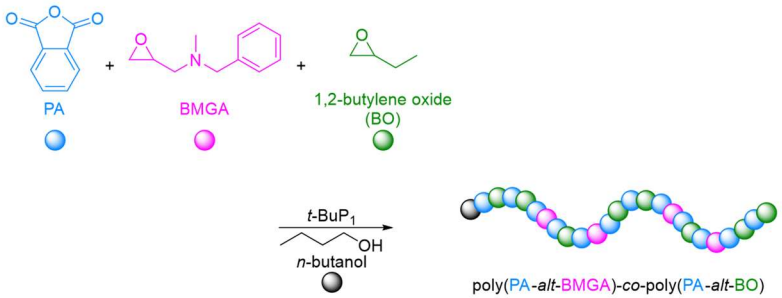

(b) Terpolymerization of PA, DBGA, and EGE

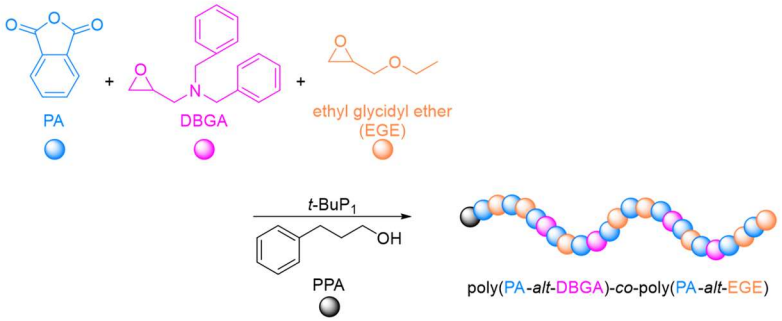

Table 2.5. Ring-opening terpolymerization of PA, BMGA or DBGA, and BO or EGE [a]

run	initiator (I)	$M_1/M_2/M_3$	$[t\text{-BuP}_1]/[I]_0/[M_1]_0/[M_2]_0/[M_3]_0$	time (h)	conv. (%) [b]	$M_{n,theo.}$ (g mol^{-1}) [c]	$M_{n,NMR}$ (g mol^{-1}) [b]	F_{M2} (mol.%) [b]	$M_{n,SEC}$ (g mol^{-1}) [d]	$Đ$ [d]
1	*n*-butanol	PA/BMGA /BO	1/1/100/150/150	2.0	PA = 92, BMGA = 28, BO = 46	24,000	6,200	0.41	3,120	2.23
2	*n*-butanol	PA/BMGA /BO	1/1/100/60/240	1.5	PA > 99, BMGA = 28, BO = 39	24,000	12,600	0.85	6,050	1.75
3	PPA	PA/DBGA /EGE	1/1/100/150/150	5.0	PA = 84, DBGA = 24, EGE = 31	26,000	14,700	0.64	6,350	1.39
4	PPA	PA/DBGA /EGE	1/1/100/60/240	3.0	PA > 99, DBGA = 8, EGE = 64	27,000	10,500	0.85	5,580	1.38

[a] Polymerization conditions: temp., 80 °C; atmosphere, Ar; catalyst, *t*-BuP_1. [b] Determined via ^{1}H NMR spectroscopy in $CDCl_3$. [c] Calculated using (M.W. of initiator) + $[PA]_0/[initiator]_0 \times conv._{PA} \times$ ((M.W. of PA + M.W. of glycidylamine) × (mol.% of glycidylamine) + (M.W. of PA + M.W. of epoxide) × (mol.% of epoxide)). [d] Determined via SEC in DMF containing 0.01 mol L^{-1} LiCl using a PSt. standard.

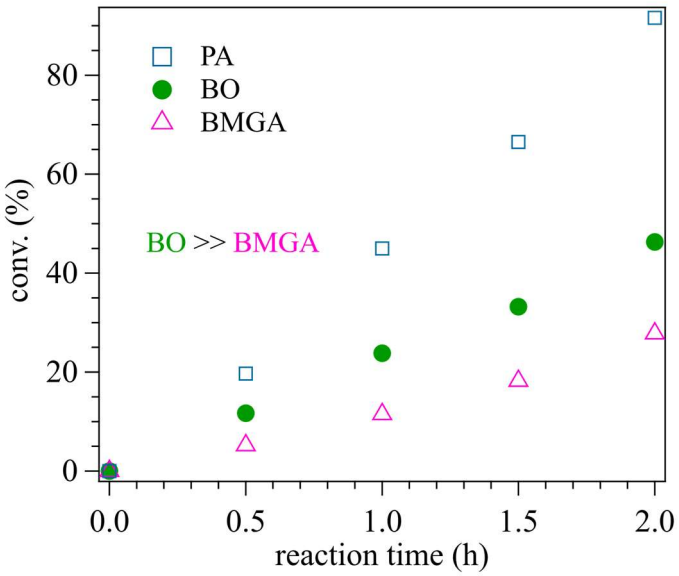

Figure 2.29. Time to conv. plots of PA (square), BO (filled circle), and BMGA (triangle) determined via ^{1}H NMR spectrum for run 1 in Table 2.5.

Table 2.6. ROAC of PA and cyclic ethers using *t*-BuP$_1$ as a catalyst [a]

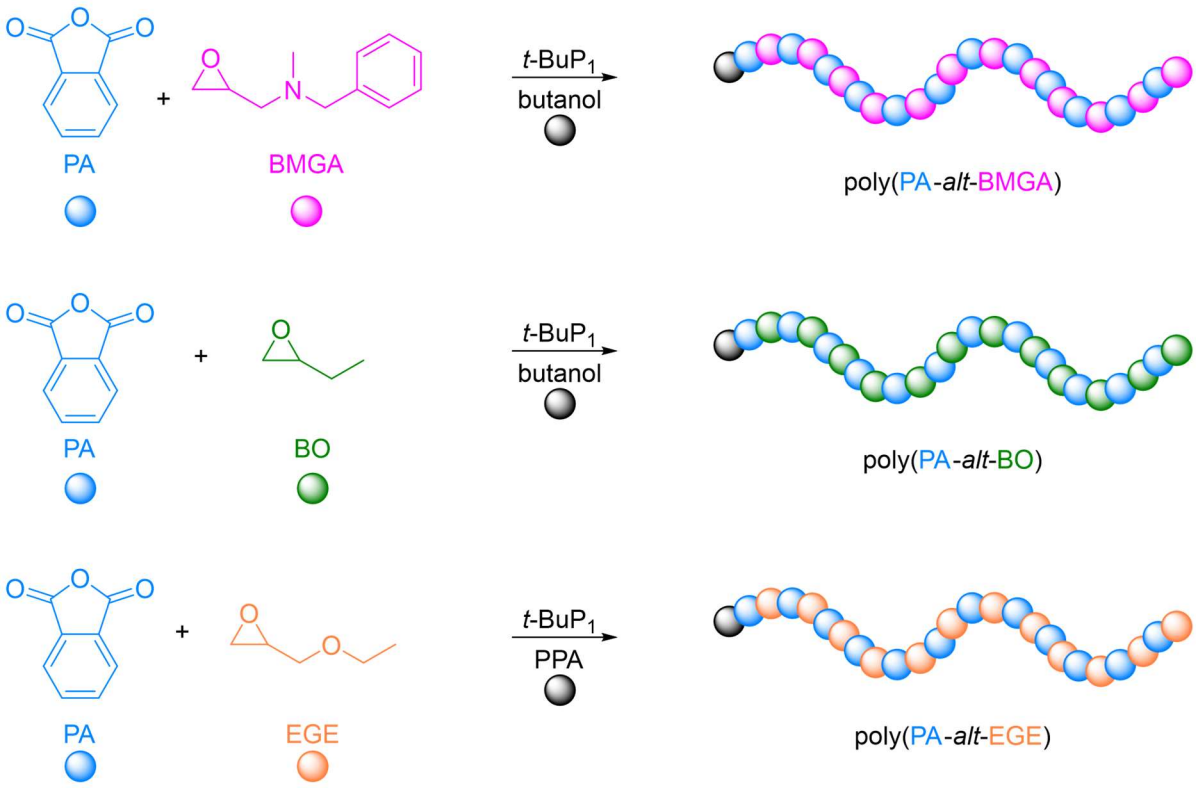

run	M	ini.	time (h)	conv.$_{PA}$ (%) [b]	$M_{n,theo.}$ [c]	$M_{n,NMR}$ [b]	$M_{n,SEC}$ [d]	$Đ$ [d]
1	PA/BMGA	*n*-butanol	3.0	>99	33 000	5800	3520	2.11
2	PA/BO	*n*-butanol	1.5	>99	22 000	18 000	11 000	1.22
3	PA/EGE	PPA	2.0	98	25 000	20 000	5680	1.31

[a] Polymerization conditions: temp., 80 °C; atmosphere, Ar; catalyst, *t*-BuP$_1$; monomer; [*t*-BuP$_1$]/[initiator]$_0$/[PA]$_0$/[glycidylamine or epoxide]$_0$ = 1/1/100/300. [b] Determined via ^{1}H NMR in $CDCl_3$. [c] Calculated from (M.W. of initiator) + [PA]$_0$/[initiator]$_0$ × conv.$_{PA}$ × (M.W. of PA + M.W. of glycidylamine or epoxide). [d] Determined via SEC in DMF containing 0.01 mol L^{-1} LiCl using PSt. standard.

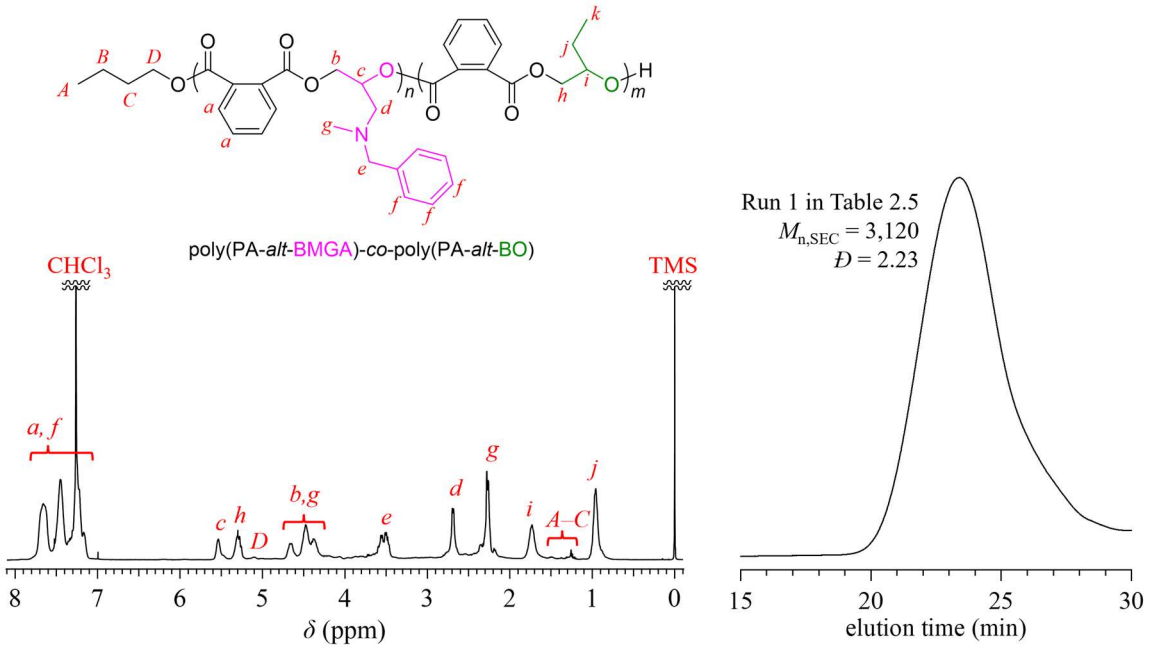

Figure 2.30. ^{1}H NMR ($CDCl_3$, 400 MHz; left panel) and SEC trace (eluent, DMF containing 0.01 mol L^{-1} LiCl; flow rate, 0.6 mL min^{-1}; right panel) of poly(PA-*alt*-BMGA)-*co*-poly(PA-*alt*-BO) obtained via run 1 in Table 2.5.

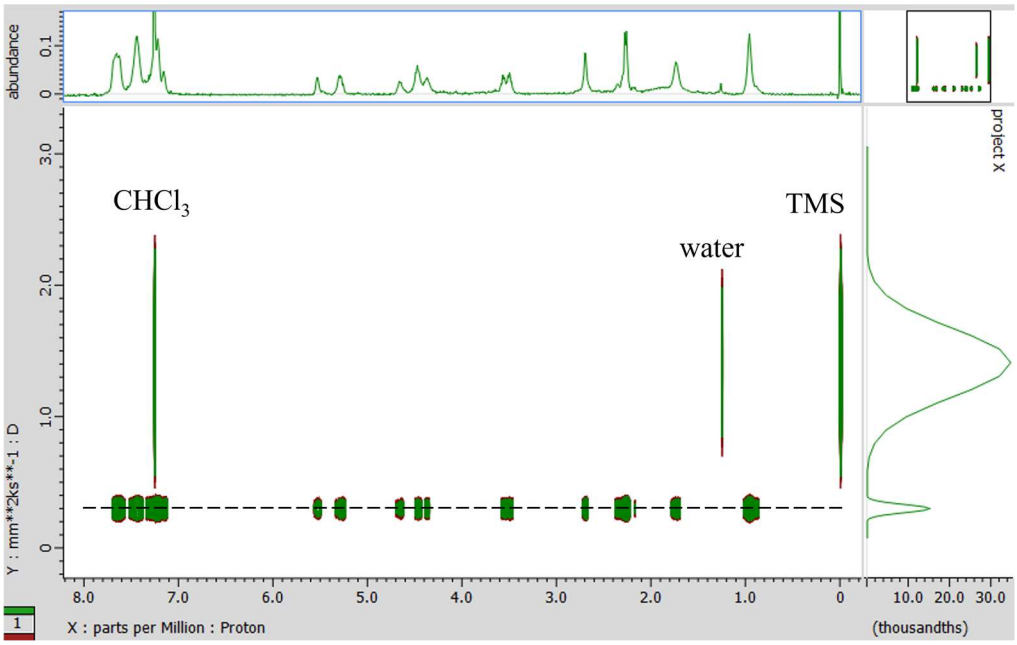

Figure 2.31. DOSY ($CDCl_3$, 600 MHz) spectrum of poly(PA-*alt*-BMGA)-*co*-poly(PA-*alt*-BO) obtained from run 1 in Table 2.5.

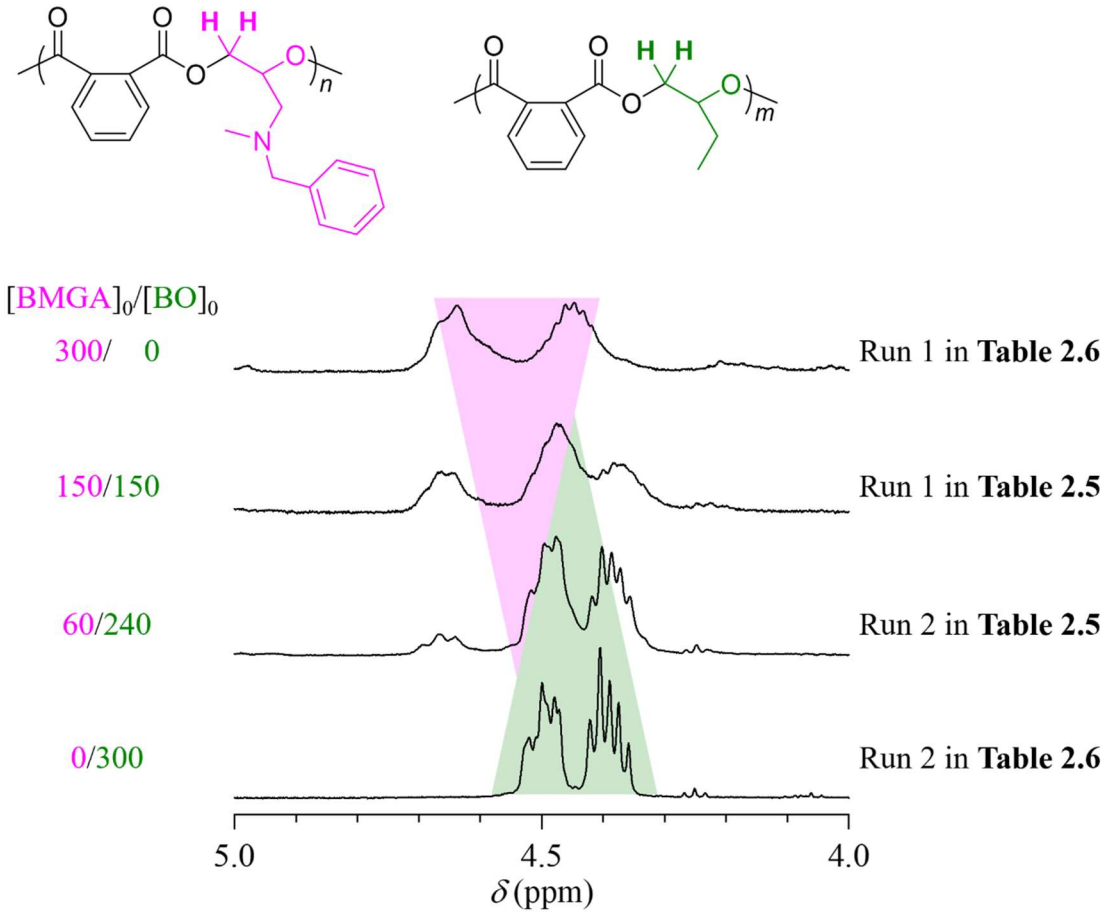

Figure 2.32. ^{1}H NMR spectra of poly(PA-*alt*-BMGA) (run 1 in Table 2.6), poly(PA-*alt*-BMGA)-*co*-poly(PA-*alt*-BO) ($[BMGA]_0/[BO]_0$ = 150/150, run 1 in Table 2.5; $[BMGA]_0/[BO]_0$ = 60/240, run 2 in Table 2.5), and poly(PA-*alt*-BO) (run 2 in Table 2.6) in $CDCl_3$ (400 MHz).

Similarly, the terpolymerization of PA, DBGA, and ethyl glycidyl ether (EGE) was conducted in the presence of PPA and *t*-BuP$_1$ as the initiator and catalyst, respectively, with [*t*-BuP$_1$]/[PPA]$_0$/[PA]$_0$/[DBGA]$_0$/[EGE]$_0$ = 1/1/50/75/75 (f_{DBGA} = 0.5) affording poly(PA-*alt*-DBGA)-*co*-poly(PA-*alt*-EGE) with F_{BMGA} = 0.36 (**Figures 2.33–2.35**). Moreover, F_{DBGA} can be adjusted by changing f_{DBGA} (**Figure 2.36**). Hence, the amino functional group contents of polyesters can be easily adjusted by incorporating an alkylene oxide or a glycidyl ether.

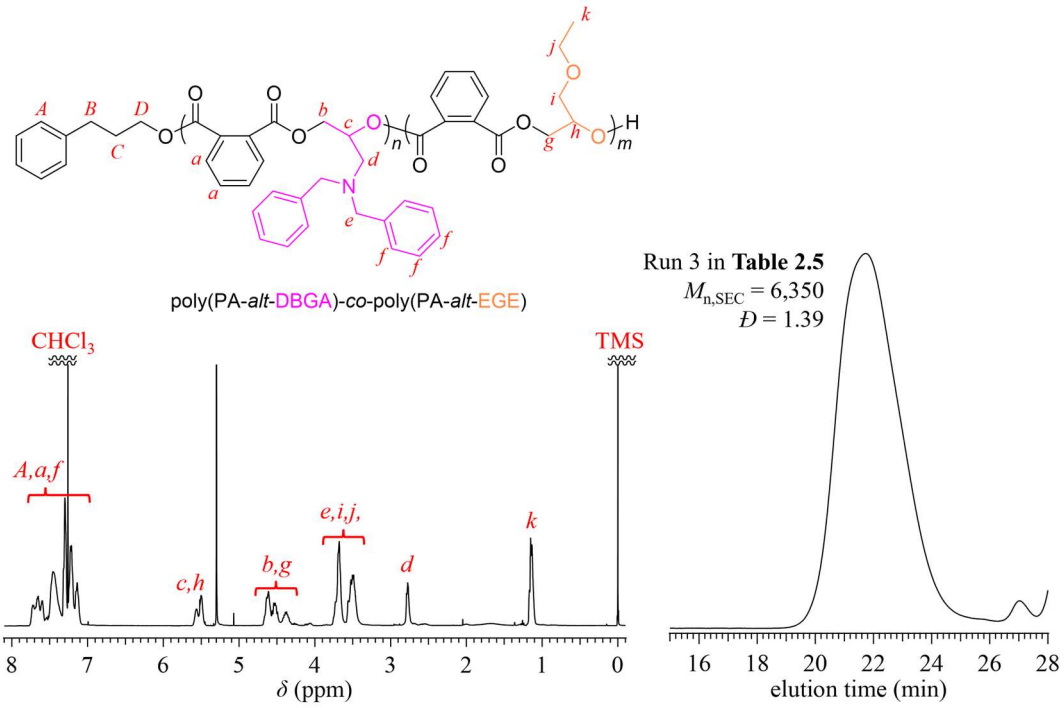

Figure 2.33. ^{1}H NMR ($CDCl_3$, 400 MHz; left panel) and SEC trace (eluent, DMF containing 0.01 mol L^{-1} LiCl; flow rate, 0.6 mL min^{-1}; right panel) of poly(PA-*alt*-DBGA)-*co*-poly(PA-*alt*-EGE) obtained from run 3 in Table 2.5.

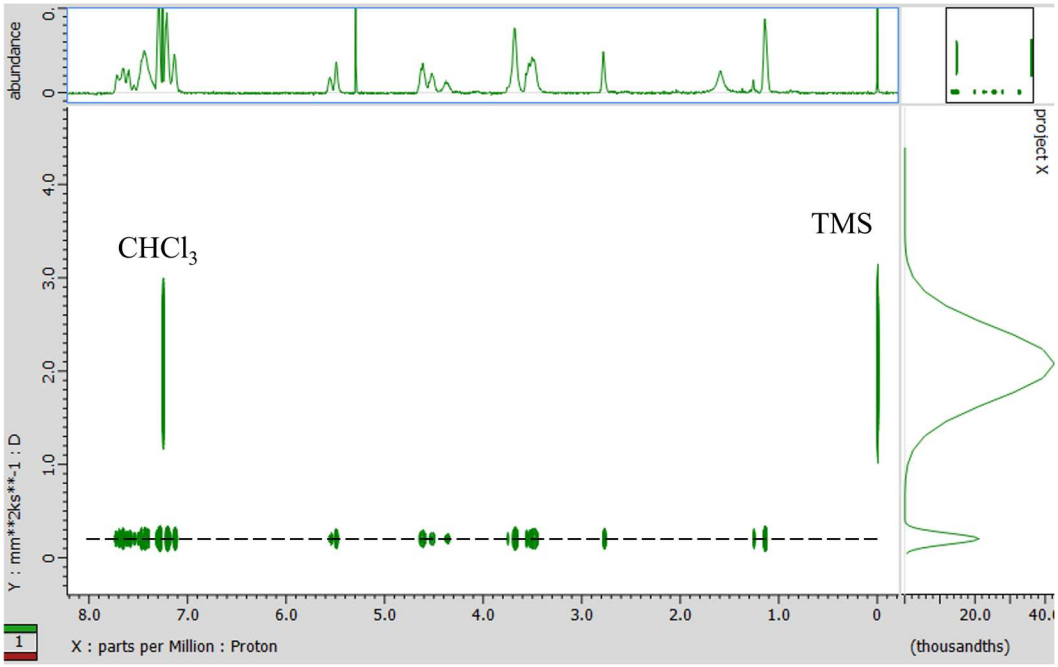

Figure 2.34. DOSY ($CDCl_3$, 600 MHz) spectrum of poly(PA-*alt*-DBGA)-*co*-poly(PA-*alt*-EGE) obtained from run 3 in Table 2.5.

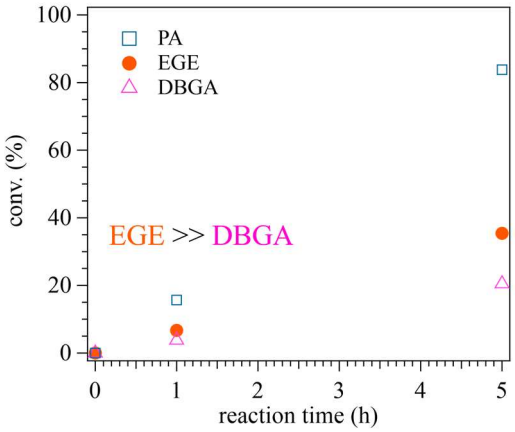

Figure 2.35. Time to conv. plots of PA (square), EGE (filled circle), and DBGA (triangle) determined via ^{1}H NMR spectrum for run 3 in Table 2.5.

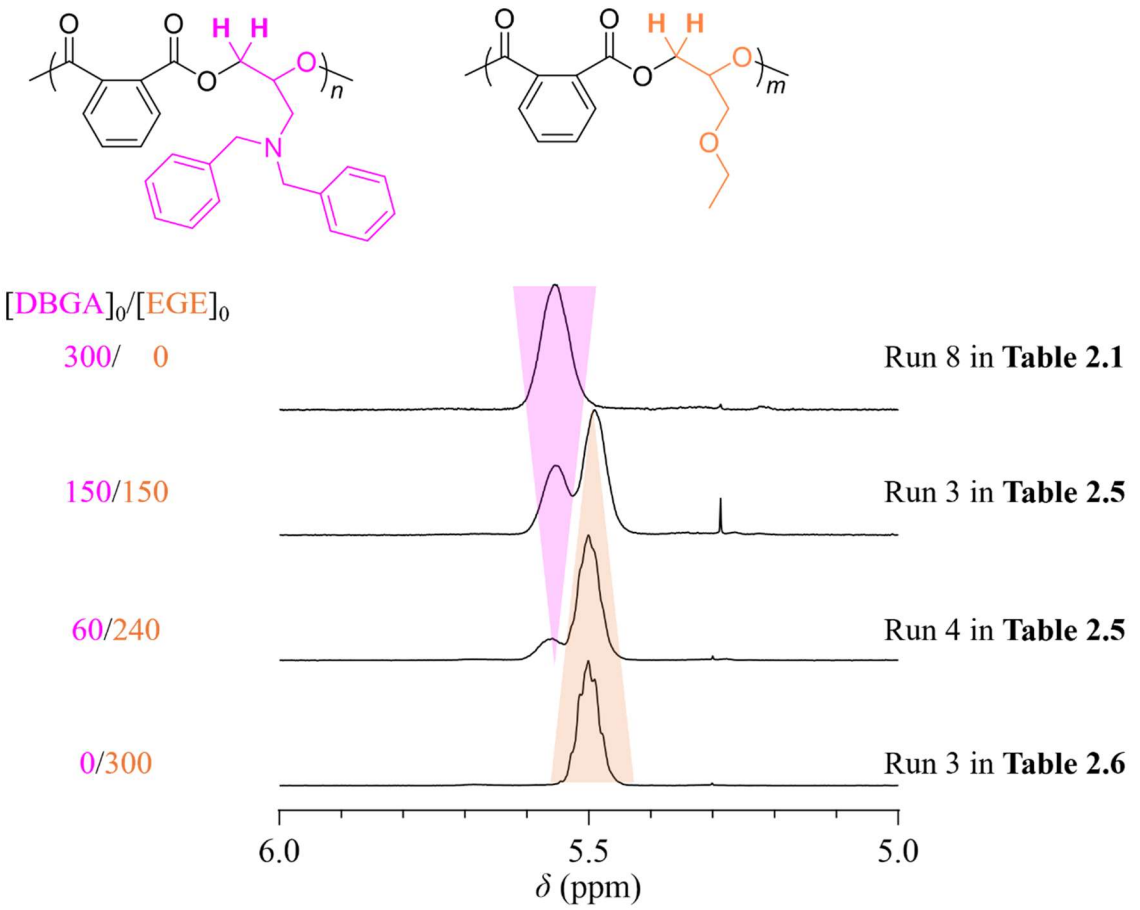

Figure 2.36. ^{1}H NMR spectra of poly(PA-*alt*-DBGA) (run 8 in Table 2.1), poly(PA-*alt*-DBGA)-*co*-poly(PA-*alt*-EGE) ($[DBGA]_0/[EGE]_0$ = 150/150, run 3 in Table 2.5; $[DBGA]_0/[EGE]_0$ = 60/240, run 4 in Table 2.5), and poly(PA-*alt*-EGE) (run 3 in Table 2.6) in $CDCl_3$ (400 MHz).

2.4 Conclusion

In this chapter, the author established a novel pathway for synthesizing APEs based on the ROAC of cyclic anhydrides and glycidylamines. ROAC proceeded smoothly with alkali metal carboxylates and phosphazene bases as catalysts, but it also proceeded without a catalyst. Because of the controlled nature of this ROAC system, APEs with adjustable molecular weights and functional end groups could be produced. Moreover, the ROAC system enabled the syntheses of APEs with different main-chain structures by simply changing the combination of the two monomers. Considering the advantages of chain-growth polymerization and the wide monomer scope, the established ROAC system may accelerate the exploration of a novel class of APEs.

2.5 References

1 Y. Nagasaki PEG-b-polyamine Stabilized Bionanoparticles for Nanodiagnostics and Nanotherapy. *Chem. Lett.* **2008**, *37*, 564–569.

2 J. Peng, F. Liu, F. Feng, X. Feng and J. Cui Enhancing Environmentally Friendly Tannin Adhesive for Plywood through Hyperbranched Polyamide. *ACS Sustainable Chem. Eng.* **2023**, *11*, 13805–13811.

3 M. Kim, J. Park, K. M. Lee, E. Shin, S. Park, J. Lee, C. Lim, S. K. Kwak, D. W. Lee and B.-S. Kim Peptidomimetic Wet-Adhesive PEGtides with Synergistic and Multimodal Hydrogen Bonding. *J. Am. Chem. Soc.* **2022**, *144*, 6261–6269.

4 C. Taplan, M. Guerre and F. E. D. Du Prez Covalent Adaptable Networks Using β-Amino Esters as Thermally Reversible Building Blocks. *J. Am. Chem. Soc.* **2021**, *143*, 9140–9150.

5 F. Schacher, M. Ulbricht, A. H. E. Müller Self-Supporting, Double Stimuli-Responsive Porous Membranes From Polystyrene-*block*-poly(*N,N*-dimethylaminoethyl methacrylate) Diblock Copolymers. *Adv. Funct. Mater.,* **2009**, *19*, 1040–1045.

6 P. Stenström, E. Hjorth, Y. Zhang, O. C. J. Andrén, S. Guette-Marquet, M. Schultzberg and M. Malkoch, M. Synthesis and in Vitro Evaluation of Monodisperse Amino-Functional Polyester Dendrimers with Rapid Degradability and Antibacterial Properties. *Biomacromolecules* **2017**, *18*, 4323–4330.

7 J. Ma, M. Shao, N. Ma, J. Liu, Y. Tang, W. Qu and W. Zhang Alkaline Amino Acid Alternating Copolymers with Potent Antibacterial Properties for the Treatment of Periodontitis. *ACS Appl. Polym. Mater.* **2023**, *5*, 3643–3652.

8 Y. Yan, H. Xiong, X. Zhang, Q. Cheng and D. J. Siegwart Systemic mRNA Delivery to the Lungs by Functional Polyester-based Carriers. *Biomacromolecules* **2017**, *18*, 4307–4315.

9 J. Hao, P. Kos, K. Zhou, J. B. Miller, L. Xue, Y. Yan, H. Xiong, S. Elkassih and D. J. Siegwart Rapid Synthesis of a Lipocationic Polyester Library via Ring-Opening

Polymerization of Functional Valerolactones for Efficacious siRNA Delivery. *J. Am. Chem. Soc.* **2015**, *137*, 9206–9209.

10 O. Lunov, T. Syrovets, C. Loos, G. U. Nienhaus, V. Mailänder, K. Landfester, M. Rouis and T. Simmet Amino-Functionalized Polystyrene Nanoparticles Activate the NLRP3 Inflammasome in Human Macrophages. *ACS Nano* **2011**, *5*, 9648–9657.

11 Z. Shi, F. Guo, Y. Li, Z. Hou Synthesis of Amino-Containing Syndiotactic Polystyrene as Efficient Polymer Support for Palladium Nanoparticles. *J. Polym. Sci. Part A: Polym. Chem.* **2015**, *53*, 5–9.

12 J. Blankenburg, M. Wagner and H. Frey Well-Defined Multi-Amino-Functional and Stimuli-Responsive Poly(propylene oxide) by Crown Ether Assisted Anionic Ring-Opening Polymerization. *Macromolecules* **2017**, *50*, 8885–8893.

13 V. S. Reuss, B. Obermeier, C. Dingels, H. Frey. *N*,*N*-Diallylglycidylamine: A Key Monomer for Amino-Functional Poly(ethylene glycol) Architectures. *Macromolecules* **2012**, *45*, 4581–4589.

14 J. Lee, A. J. McGrath, C. J. Hawker, B.-S. Kim. pH-Tunable Thermoresponsive PEO-Based Functional Polymers with Pendant Amine Groups. *ACS Macro Lett.* **2016**, *5*, 1391–1396.

15 P. Verkoyen, H. Frey. Amino-functional polyethers: versatile, stimuli-responsive polymers. *Polym. Chem.* **2020**, *11*, 3940–3950.

16 M. M. A. Abd Elwakil, R. Suzuki, A. M. Khalifa, R. M. Elshami, T. Isono, Y. H. A. Elewa, Y. Sato, T. Nakamura, T. Satoh, H. Harashima. Harnessing Topology and Stereochemistry of Glycidylamine-Derived Lipid Nanoparticles for in Vivo mRNA Delivery to Immune Cells in Spleen and Their Application for Cancer Vaccination. *Adv. Funct. Mater.* **2023**, *33*, 2303795.

17 T. Isono, S. Asai, Y. Satoh, T. Takaoka, K. Tajima, T. Kakuchi, T. Satoh. Controlled/Living Ring-Opening Polymerization of Glycidylamine Derivatives Using t-Bu-P4/Alcohol Initiating System Leading to Polyethers with Pendant Primary, Secondary, and Tertiary Amino Groups. *Macromolecules* **2015**, *48*, 3217–3229.

18 C.-Y. Won, C.-C. Chu, J. D. Lee. Novel biodegradable copolymers containing pendant amine functional groups based on aspartic acid and poly(ethylene glycol). *Polymer* **1998**, *39*, 6677–6681.

19 E. A. Chamsaz, S. Mankoci, H. A. Barton, A. Joy. Nontoxic Cationic Coumarin Polyester Coatings Prevent *Pseudomonas aeruginosa* Biofilm Formation. *ACS Appl. Mater. Interfaces* **2017**, *9*, 6704–6711.

20 M. O. Arıcan, S. Erdoğan, O. Mert. Amine-Functionalized Polylactide–PEG Copolymers. *Macromolecules* **2018**, *51*, 2817–2830.

21 M. Deng, J. Wu, C. A. Reinhart-King, C.-C. Chu. Synthesis and characterization of biodegradable poly(ester amide)s with pendant amine functional groups and in vitro cellular response. *Biomacromolecules* **2009**, *10*, 3037–3047.

22 Y. Bernhard, J. F. R. V. Van Guyse, M. Purino, R. Hoogenboom. Direct synthesis of poly(N-alkyl acrylamide) (co)polymers with pendant reactive amino groups by organocatalyzed amidation of polymethylacrylate. *Eur. Polym. J.* **2023**, *192*, 112077.

23 A. Bentolila, I. Vlodavsky, R. Ishai-Michaeli, O. Kovalchuk, C. Haloun, A. J. Domb. Poly(N-acryl amino acids): A New Class of Biologically Active Polyanions. *J. Med. Chem.* **2000**, *43*, 2591–2600.

24 A. K. Yamala, V. Nadella, Y. Mastai, H. Prakash, P. Paik. Poly-*N*-acryloyl-(L-phenylalanine methyl ester) hollow core nanocapsules facilitate sustained delivery of immunomodulatory drugs and exhibit adjuvant properties. *Nanoscale* **2017**, *9*, 14006–14014.

25 J. Hao, S. Elkassih, D. J. Siegwart. Progress towards the Synthesis of Amino Polyesters via RingOpening Polymerization (ROP) of Functional Lactones. *Synlett* **2016**, *27*, 2285–2292.

26 Y. Wei, X. Li, H. Yuan, Y. Qi, Y. Huang. Synthesis and characterization of amino-functional polyesters composed of lactic acids and serine amino acids. *Polymer* **2024**, *296*, 126820.

27 D. A. Barrera, E. Zylstra, P. T. Lansbury Jr, R. Langer. Synthesis and RGD peptide modification of a new biodegradable copolymer: poly(lactic acid-co-lysine). *J. Am. Chem. Soc.* **1993**, *115*, 11010–11011.

28 Y.-B. Lim, C.-H. Kim, K. Kim, S. W. Kim, J.-S. Park. Development of a Safe Gene Delivery System Using Biodegradable Polymer, Poly[α-(4-aminobutyl)-L-glycolic acid]. *J. Am. Chem. Soc.* **2000**, *122*, 6524–6525.

29 W. W. Gerhardt, D. E. Noga, K. I. Hardcastle, A. J. García, D. M. Collard, M. Weck. Functional Lactide Monomers: Methodology and Polymerization. *Biomacromolecules* **2006**, *7*, 1735–1742.

30 X. Chen, H. Lai, C. Xiao, H. Tian, X. Chen, Y. Tao, X. Wang. New bio-renewable polyester with rich side amino groups from l-lysine via controlled ring-opening polymerization. *Polym. Chem.* **2014**, *5*, 6495–6502.

31 T. R. Blake, R. M. Waymouth. Organocatalytic Ring-Opening Polymerization of Morpholinones: New Strategies to Functionalized Polyesters. *J. Am. Chem. Soc.* **2014**, *136*, 9252–9255.

32 C.-K. Chen, C. H. Jones, P. Mistriotis, Y. Yu, X. Ma, A. Ravikrishnan, M. Jiang, S. T. Andreadis, B. A. Pfeifer, C. Cheng. Poly(ethylene glycol)-*block*-cationic polylactide nanocomplexes of differing charge density for gene delivery. *Biomaterials* **2013**, *34*, 9688–9699.

33 Z. Zhang, L. Yin, Y. Xu, R. Tong, Y. Lu, J. Ren, J. Cheng. Facile Functionalization of Polyesters through Thiol-yne Chemistry for the Design of Degradable, Cell-Penetrating and Gene Delivery Dual-Functional Agents. *Biomacromolecules* **2012**, *13*, 3456–3462.

34 Z.-Y. Li, X. Zhang, Y.-L. Qian, F.-S. Du, Z.-C. Li. Synthesis and antibacterial properties of fluorinated biodegradable cationic polyesters. *J. Mater. Chem. B* **2024**, *12*, 1569–1578.

35 S. Blanquer, J. Tailhades, V. Darcos, M. Amblard, J. Martinez, B. Nottelet, J. Coudane. Easy synthesis and ring-opening polymerization of 5-Z-amino-δ-

valerolactone: New degradable amino-functionalized (Co)polyesters. *J. Polym. Sci. A Polym. Chem.* **2010**, *48*, 5891–5898.

36 H. Han, J. Zhu, F.-F. Zhang, F.-X. Li, X.-L. Wang, J.-Y. Yu, X.-H. Qin, D.-Q. Wu. Hydrophilic and degradable polyesters based on L-aspartic acid with antibacterial properties for potential application in hernia repair. *Biomater. Sci.* **2019**, *7*, 5404–5413.

37 Y. Liu, D. Wu, Y. Ma, G. Tang, S. Wang, C. He, T. Chung, S. Goh. Novel poly(amino ester)s obtained from Michael addition polymerizations of trifunctional amine monomers with diacrylates: safe and efficient DNA carriers. *Chem. Commun.* **2003**, *20*, 2630–2631.

38 J. C. Kaczmarek, A. K. Patel, K. J. Kauffman, O. S. Fenton, M. J. Webber, M. W. Heartlein, F. DeRosa, D. G. Anderson. Polymer–Lipid Nanoparticles for Systemic Delivery of mRNA to the Lungs. *Angew. Chem. Int. Ed.* **2016**, *55*, 13808–13812.

39 U. S. Gunay, M. Cetin, O. Daglar, G. Hizal, U. Tunca, H. Durmaz. Ultrafast and efficient aza- and thiol-Michael reactions on a polyester scaffold with internal electron deficient triple bonds. *Polym. Chem.* **2018**, *9*, 3037–3054.

40 T. Tang, A. Takasu. Facile synthesis of unsaturated polyester-based double-network gels via chemoselective cross-linking using Michael addition and subsequent UV-initiated radical polymerization. *RSC Adv.* **2015**, *5*, 819–829.

41 R. Xie, G.-W. Yang, Y.-Y. Zhang, C. Lu, W.Li, J. Wang, G.-P. Wu. A direct comparison between ring-opening copolymerization and polycondensation to produce polyesters using poly(ethylene succinate) as an example. *Polym. Chem.* **2024**, *15*, 412–421.

42 J. Herzberger, D. Kurzbach, M. Werre, K. Fischer, D. Hinderberger, H. Frey. Stimuli-Responsive Tertiary Amine Functional PEGs Based on *N*,*N*-Dialkylglycidylamines. *Macromolecules* **2014**, *47*, 7679–7690.

43 V. S. Reuss, M. were, H. Frey. Thermoresponsive Copolymers of Ethylene Oxide and N,N-Diethyl Glycidyl Amine: Polyether Polyelectrolytes and PEGylated Gold Nanoparticle Formation. *Macromol. Rapid Commun.* **2012**, *33*, 1556–1561.

44 B. Obermeier, F. Wurm, H. Frey. Amino Functional Poly(ethylene glycol) Copolymers via Protected Amino Glycidol. *Macromolecules* **2010**, *43*, 2244–2251.

45 R. Suzuki, X. Xia, T. Gao, T. Yamamoto, K. Tajima, T. Isono, T. Satoh. Synthesis of hyperbranched polyesters via the ring-opening alternating copolymerisation of epoxides with a cyclic anhydride having a carboxyl group. *Polym. Chem.* **2022**, *13*, 5469–5477.

46 X. Xia, R. Suzuki, K. Takojima, D.-H. Jiang, T. Isono, T. Satoh. Smart Access to Sequentially and Architecturally Controlled Block Polymers via a Simple Catalytic Polymerization System. *ACS Catal.* **2021**, *11*, 5999–6009.

47 X. Xia, R. Suzuki, T. Gao, T. Isono, T. Satoh. One-step synthesis of sequence-controlled multiblock polymers with up to 11 segments from monomer mixture. *Nat. Commun.* **2022**, *13*, 163.

48 X. Xia, T. Gao, F. Li, R. Suzuki, T. Isono, T. Satoh. Multidimensional Control of Repeating Unit/Sequence/Topology for One-Step Synthesis of Block Polymers from Monomer Mixtures. *J. Am. Chem. Soc.* **2022**, *144*, 17905–17915.

49 X. Xia, T. Gao, F. Li, R. Suzuki, T. Isono, T. Satoh. Self-Switchable Polymerization: A Smart Approach to Sequence-Controlled Degradable Copolymers. *Macromolecules* **2023**, *56*, 92–103.

50 F. Li, R. Suzuki, T. Gao, X. Xia, T. Isono, T. Satoh. Alkali Metal Carboxylates: Simple, Efficient, and Industrial Relevant Catalysts for Controlled Polymer Synthesis. *Bull. Chem. Soc. Jpn*. **2023**, *96*, 1003–1018.

51 I. Ota, R. Suzuki, Y. Mizukami, X. Xia, K. Tajima, T. Yamamoto, F. Li, T. Isono, T. Satoh. Organobase-Catalyzed Ring-Opening Copolymerization of Cyclic Anhydrides and Oxetanes: Establishment and Application in Block Copolymer Synthesis. *Macromolecules* **2024**, *57*, 3741–3750.

52 A. Kummari, S. Pappuru, D. Chakraborty. Fully alternating and regioselective ring-opening copolymerization of phthalic anhydride with epoxides using highly active metal-free Lewis pairs as a catalyst. *Polym. Chem.* **2018**, *9*, 4052–4062.

53 K. Bester, A. Bukowska, B. Myśliwiec, K. Hus, D. Tomczyk, P. Urbaniak, W. Bukowski. Alternating ring-opening copolymerization of phthalic anhydride with epoxides catalysed by salophen chromium(iii) complexes. An effect of substituents in salophen ligands. *Polym. Chem.* **2018**, *9*, 2147–2156.

54 D. Kurzbach, V. S. Wilms, H. Frey, D. Hinderberger. Impact of Amino-Functionalization on the Response of Poly(ethylene glycol) (PEG) to External Stimuli. *ACS Macro Lett.* **2013**, *2*, 128–131.

Chapter 3

Organobase-catalyzed ROAC of
Latent Trifunctional Anhydride with Epoxide for
Synthesizing Hyperbranched Polyester

3.1 Introduction

Hyperbranched polymers (HBPs) are highly branched macromolecules comprising a large number of dendritic and terminal units. They exhibit specific properties such as lower viscosity, higher solubility, and more highly dense terminal functionality than those of their linear counterparts.[1] Dendrimers are a type of branched polymers; however, the regular structure of dendrimers makes their synthesis highly complicated. Although HBPs are structurally less regular than dendrimers, the former have usually one-step synthesis methods.[2] In addition, their interesting properties originating from the highly branched architecture and easy synthesis make them greatly valuable in a wide variety of industrial applications such as coatings,[3,4] rheological modifiers,[5] and catalysts.[6] HBPs are particularly useful for fabricating high-strength sheets and films.[7] In addition, the application range of HBPs is expanding in biomedical fields as well such as drug delivery system (DDS) and tissue engineering.[8–10]

Hyperbranched polyesters (HBPEs) are of particular interest for biomedical applications because of their excellent biocompatibility and biodegradability. Wyatt *et al*. reported poly(glycerol succinate)-based HBPEs for application as surgical materials in orthopedic and ophthalmic operations,[11] while Gao *et al*. reported polyglycerol/poly(lactic acid) copolymer-based HBPEs for application in protein delivery.[12] Although a wide variety of HBPEs have been reported so far, further improvements in their molecular design capacity and synthesis methods

are still needed to fabricate novel functional materials that meet the needs of different industries.

In general, the synthesis methods of HBPE can be classified into two categories based on the polymerization mechanism: (1) step-growth polymerization and (2) chain-growth polymerization. Most HBPE syntheses rely on the step-growth polycondensation of a carboxylic acid (A) and an alcohol (B). The first HBPE synthesis was achieved before 1900 by polycondensation of tartaric acid (A_2B_2) and glycerol (B_3), in which ester bonds were formed between two tartaric acid molecules as well as between tartaric acid and glycerol.[13] Subsequently, a large number of monomer combinations of dicarboxylic acids (A_2) and polyols (B_x, $x > 2$) have been reported for constructing HBPEs. Zhang *et al*. reported the polycondensation of adipic acid (A_2) and glycerol (B_3),[14] while Kienle *et al*. reported the polycondensation of phthalic anhydride (A_2) and glycerol (B_3).[15] In addition, polycondensation of AB_x-type monomers (e.g., 3,5-diacetoxybenzoic acid) have been extensively used to synthesize various HBPEs.[16] Yan and Gao extended the monomer variety for polycondensation through the so-called couple-monomer methodology (CMM), in which a condensation reaction between A–A and B–B_2 monomers (e.g., succinic anhydride and trimethylolpropane) was first carried out to produce an AB_2 intermediate, followed by polycondensation to obtain HBP.[17] Although the polycondensation approach is widely used for HBPE synthesis because of the huge variety of available monomers, the step-growth character of this approach makes it

difficult to control the molecular weight and dispersity (*Đ*) of the resulting HBPEs. Moreover, the achievable molecular weight is often limited by gelation, by-product formation, and intramolecular cyclization.

The chain-growth polymerization approach is advantageous over the polycondensation approach as the former allows control over multibranching polymerization, thereby providing a precise way to synthesize HBPEs. More importantly, the chain-growth approach easily affords high-molecular-weight HBPEs as it suppresses side reactions and by-product formations. For example, an HBPE was successfully synthesized by multibranching ring-opening polymerization of a cyclic ester monomer having an alcohol moiety, such as 5-(2-hydroxyethyl)-2-oxepanone.[18] The resulting HBPEs had a high molecular weight (65,000–85,000 in weight-average molecular weight). Similarly, hydroxyl-functionalized cyclic esters such as bis(dihydroxymethyl)-*ε*-caprolactone[19,20] and 5-hydroxymethyl-1,4-dioxan-2-one[21] were also employed for HBPE synthesis via ring-opening multibranching polymerization. An additional advantage of this approach is the ability to control the initiation end group using a nucleophile as an initiator, which leads to functionalized HBPEs and linear-hyperbranched-block copolymers. Hence, the chain-growth polymerization approach involving ring-opening polymerization (ROP) is extremely useful for the synthesis of HBPEs. However, a major drawback of this approach is the narrow range of applicable monomers. Such specially designed

monomers often require a multi-step synthesis. Thus, it is highly desirable to establish a simple and versatile synthesis method for well-defined HBPEs via a chain-growth mechanism.

As noted in Chapter 1, ring-opening alternating copolymerization (ROAC) of cyclic anhydrides and epoxides has attracted much attention as a third method to access polyesters following polycondensation and ROP because of its key advantages lie in its accessible structural versatility and polymerization controllability.[22–31] In more details, polyesters with functional side chains can be easily synthesized using epoxides having functional side chains, as shown in Chapter 2. For example, optically active and isotactic polyesters can also be synthesized simply by employing optically pure epoxide monomers.[32,33] Thus, the author considered that the ROAC system can solve commonly synthetic problems about HBPEs. As mentioned above, a versatile synthesis method for HBPE based on chain-growth polymerization is required to further expand the application range of HBPEs. In this study, the author proposes a novel synthesis method for HBPEs using the concept of ROAC (**Figure 3.1**). ROAC gives rise to only linear polyesters because both the anhydride and epoxide monomers function as latent difunctional monomers. Thus, the author selected a cyclic anhydride possessing an extra carboxyl group as the latent A_3-type monomer to produce HBPEs through ROAC. Trimellitic anhydride (TA) is the best candidate of latent A_3-type cyclic anhydride monomers; indeed, one example of ROAC using TA have been reported in 2020 by Coates

group.[34] Coates *et al*. used TA as a chain-transfer agent to copolymerize propylene oxide and carbic anhydride and obtained an HBPE with a high dispersity ($Đ$ = 1.79). However, the scope of the epoxide monomer and the structural details and physical properties of the HBPEs obtained through ROAC with TA have not been investigated. Herein, the author reports a simple and versatile method for HBPE synthesis via ROAC using TA as a cyclic anhydride monomer (**Scheme 3.1**). The characterization of the resulting polymer revealed a hyperbranched structure, confirming the successful synthesis of the HBPE via ROAC. The versatility of this approach was further demonstrated by the synthesis of HBPEs using various epoxides and alcohol initiators.

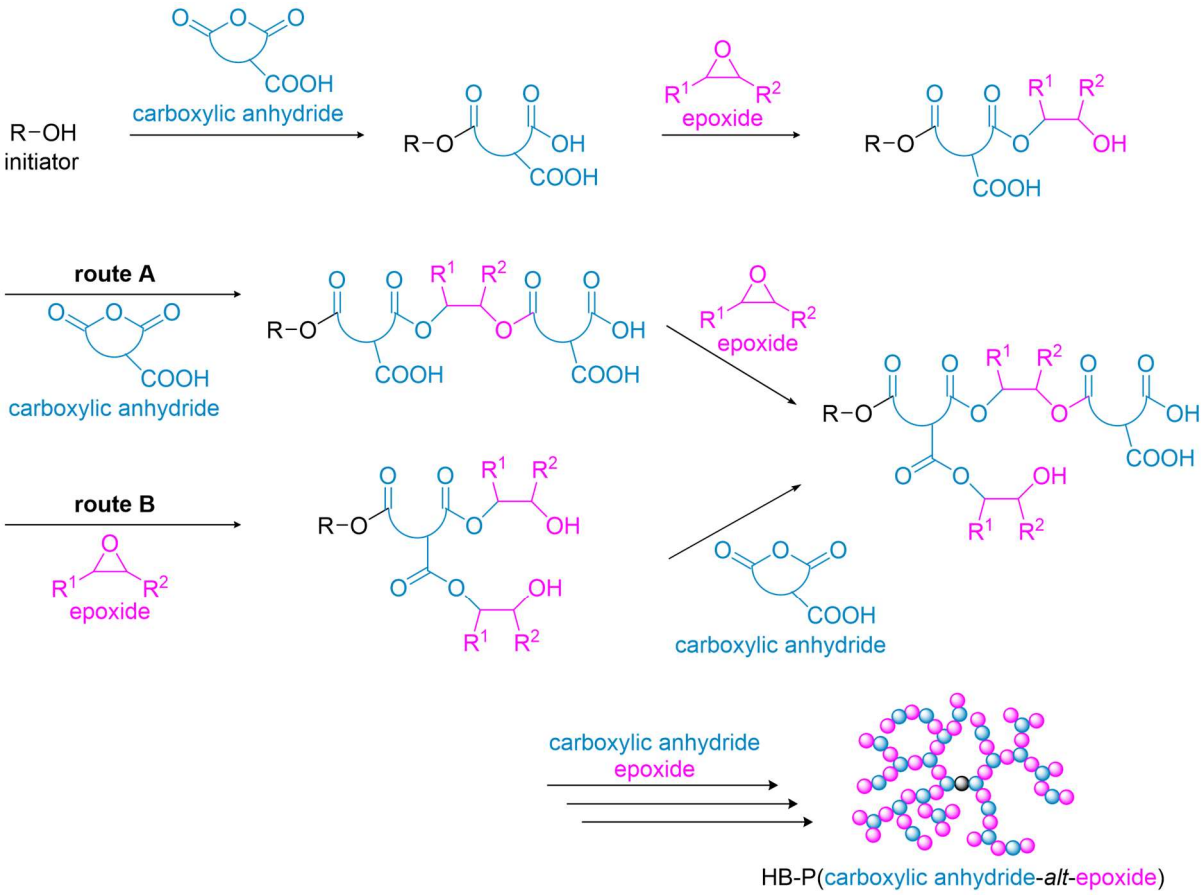

Figure 3.1. New pathway to HBPE via the ring-opening alternating copolymerization of carboxylic anhydride and epoxide.

Scheme 3.1. Syntheses of HBPEs via the ROAC of trimellitic anhydride and various epoxides

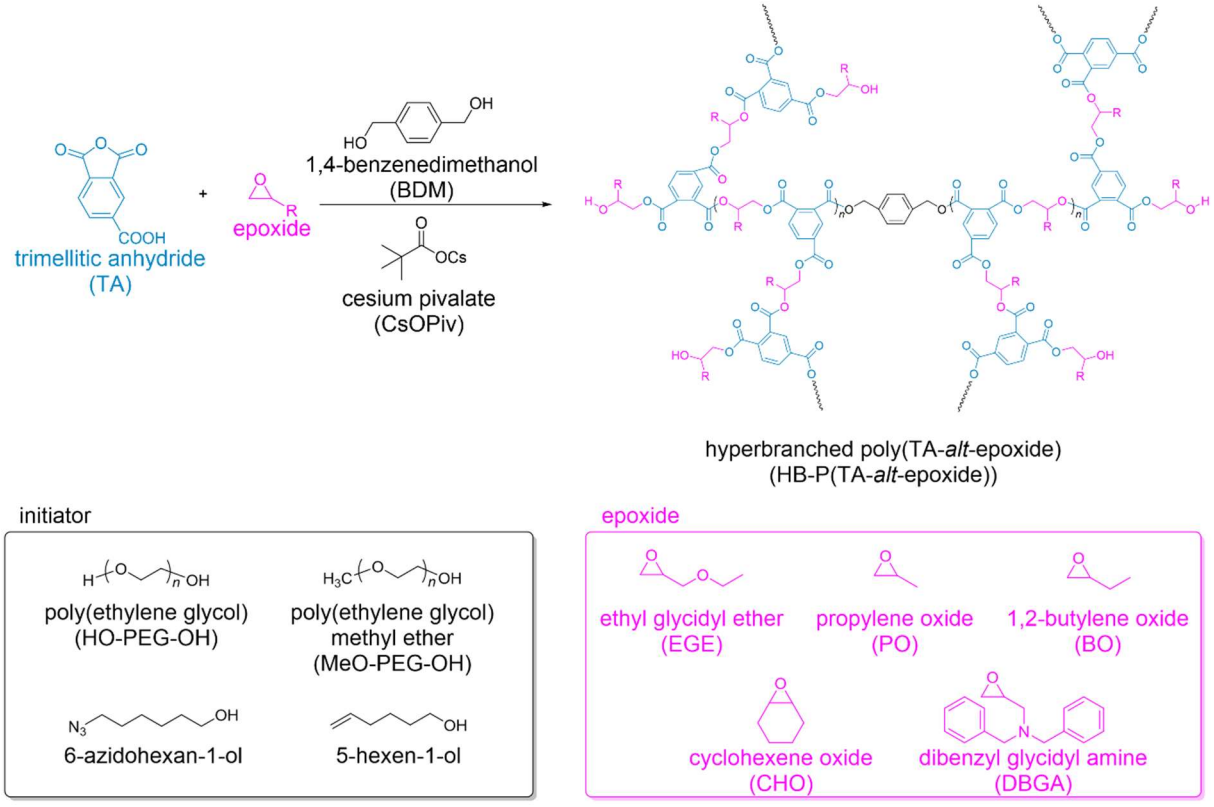

3.2 Experimental Section

3.2.1 Materials

Trimellitic anhydride (TA; >98.0%, TCI) and phthalic anhydride (PA; >98.0%, TCI) were recrystallized and then purified by sublimation before use. Ethyl glycidyl ether (EGE; >98.0%, TCI), propylene oxide (PO; >99.0%, TCI), 1,2-butylene oxide (BO; >99.0%, TCI), cyclohexene oxide (CHO; >98.0%, TCI), and 5-hexen-1-ol (>97.0%, TCI), were distilled over CaH_2 under reduced pressure and stored under argon atmosphere. 6-Azido-1-hexanol was synthesized according to a previous report[39] and purified by distillation over CaH_2 under reduced pressure. *N,N*-Dibenzylglycidylamine (DBGA) was prepared according to the reported methods[44] and purified by silica gel column chromatography followed by distillation over CaH_2 under vacuum (twice), which were then stored under an argon atmosphere. Cesium pivalate (CsOPiv; >97.0%, TCI) was dried by heating at 100 °C under high vacuum for at least 72 h prior to use. 1,4-Benzenedimethanol (BDM; >99.0%, TCI) was used as received. Poly(ethylene glycol) monomethyl ether (MeO-PEG-OH; typical M_n = 400, $M_{n,SEC}$ = 440, $Đ$ = 1.33, TCI) and poly(ethylene glycol) (HO-PEG-OH; typical M_n = 2000, $M_{n,SEC}$ = 4,020, $Đ$ = 1.07, Sigma−Aldrich) was dried by azeotropic distillation in benzene. Chloroform-*d* ($CDCl_3$; >99.8%), dimethyl sulfoxide-*d*6 (DMSO-d_6; >99.9%), benzoic acid (BA; >98.0%, TCI), and 2-propanol (>99.7%, Kanto Chemical) were used as received.

3.2.2 Instruments

The polymerization was carried out in an MBRAUN stainless steel glovebox equipped with a gas purification system (molecular sieves and copper catalyst) in a dry argon atmosphere (H_2O, O_2 <0.1 ppm). The moisture and oxygen contents in the glovebox were monitored by a MB-MO-SE 1 and MB-OX-SE 1, respectively. ^{1}H and ^{13}C NMR spectra were recorded at 25 °C on JEOL JNM-ECS400 (^{1}H: 400 MHz, ^{13}C: 100 MHz) or JNM-ECZ600R (^{13}C: 125 MHz) instruments.

The absolute number-averaged molecular weight ($M_{n,MALS}$), weight-averaged molecular weight ($M_{w,MALS}$) and dispersity ($Đ$) of the hyperbranched and linear polymer samples were determined by triple-detection size elusion chromatography (SEC-MALS-Visco) in $CHCl_3$ (flow rate, 1.0 mL min^{-1}) at 40 °C using a Jasco high-performance liquid chromatography system (PU-4180 HPLC pump, AS-4550 auto sampler, and CO-4060 column oven) equipped with a Shodex K-800D guard column (8.0 mm × 100 mm; particle size, 10 μm), K-806L column (linear, 8.0 mm × 100 mm; particle size, 10 μm), K-804L column (linear, 8.0 mm × 100 mm; particle size, 10 μm), a DAWN 8 multiangle laser light scattering detector (Wyatt Technology), a Viscostar viscosity detector (Wyatt Technology), and an RI-501 refractive index detector (Shodex).

Fourier-transform infrared (FT-IR) spectra were measured in an ATR mode with a PerkinElmer Frontier MIR spectrometer (PerkinElmer, Inc., Waltham, MA 02451, USA).

The preparative SEC was performed at 25 °C in $CHCl_3$ (flow rate, 10.0 mL min^{-1}) using a LaboACE LC-7080 liquid chromatography system (Japan Analytical Industry Co. Ltd., Tokyo, Japan) equipped with a JAIGEL-HR-P guard column (8 mm × 40 mm, Japan Analytical Industry Co. Ltd.), a JAIGEL 2HR column (linear, 20.0 mm × 600 mm; exclusion limit, 5.0 × 10^3, Japan Analytical Industry Co. Ltd.), and a JAIGEL 2.5HR column (linear, 20.0 mm × 600 mm; exclusion limit, 2.0 × 10^4, Japan Analytical Industry Co. Ltd.).

The thermal properties of the samples were measured by a Hitachi DSC 7000X. Sample was heated from 20 °C to 100 or 120 °C at a rate of 10 °C min^{-1} and held at 100 or 120 °C for 5 min to erase thermal history. Then, the sample was cooled to −100 °C at a rate of 10 °C min^{-1} and holed at −100 °C for 5 min. Finally, the sample was heated to 100 or 120 °C at a rate of 10 °C min^{-1}. The second heating DSC curve was used to evaluate the glass transition temperature.

Static water contact angle measurements were performed with a DropMaster (DMe-201, Kyowa Interface Science Co. Ltd., Saitama, Japan) under an ambient environment. The needle diameter was 0.47 mm, and the water droplet volume was set to ~5 μL. Each measurement was repeated 5 times for a better statistical significance. The error bars resulted from the standard deviation based on the measurement series.

3.2.3 Synthesis detail

3.2.3.1 The general synthesis of hyperbranched polyester via ROAC of latent A_3 type cyclic anhydride and epoxide

・Synthesis of HB-P(TA-*alt*-EGE)

A typical polymerization procedure is given as follows: In an argon-filled glovebox, 1,4-benzenedimethanol (BDM; 2.8 mg, 20 μmol), cesium pivalate (CsOPiv; 2.3 mg, 10 μmol), trimellitic anhydride (TA; 192 mg, 1.00 mmol), and ethyl glycidyl ether (EGE; 323 μL, 3.0 mmol) were added to the reaction vessel and stirred at 80 °C. After 5.5 h, crude aliquot was withdrawn from the system by pipette and monitored by ^{1}H NMR spectroscopy in $CDCl_3$ to determine the monomer conversions. The reaction mixture was diluted with small amount of dichloromethane to terminate the polymerization. The crude polymer was purified by preparative SEC to completely remove the unreacted EGE and catalyst, giving hyperbranched-poly(TA-*alt*-EGE) (HB-P(TA-*alt*-EGE)) as a colorless viscous liquid (84.3 mg). Yield: 21.1%

$M_{n,MALS}$ = 16,900 g mol^{-1} ($CHCl_3$), $Đ_{MALS}$ = 1.11 ($CHCl_3$)

・Synthesis of HB-P(TA-*alt*-EGE) without alcohol initiator

In an argon-filled glovebox, CsOPiv (11.7 mg, 50 μmol), TA (480 mg, 2.50 mmol),

and EGE (806 μL, 7.50 mmol) were added to the reaction vessel and stirred at 80 °C. After 5 h, crude aliquot was withdrawn from the system by pipette and monitored by ^{1}H NMR spectroscopy in DMSO-d_6 to determine the monomer conversions. The reaction mixture was purified by dialysis in Acetone/MeOH to completely remove the unreacted EGE and catalyst, giving HB-P(TA-*alt*-EGE) without the initiator residue as a colorless viscous liquid (680 mg). Yield: 68.6%

・Synthesis of HB-P(TA-*alt*-PO)

HB-P(TA-*alt*-PO) was synthesized in the same way, excepting the molar ratio of the reactants; BDM (5.5 mg, 40 μmol), CsOPiv (4.7 mg, 20 μmol), TA (192 mg, 1.00 mmol), and propylene oxide (PO; 210 μL, 3.00 mmol). After 4 h, the reaction mixture was diluted with small amount of dichloromethane and purified by preparative SEC to give HB-P(TA-*alt*-PO) as a colorless viscous liquid (41.6 mg). Yield: 16.4%

$M_{n,MALS}$ = 24,300 g mol^{-1} ($CHCl_3$), $Đ_{MALS}$ = 1.30 ($CHCl_3$)

・Synthesis of HB-P(TA-*alt*-BO)

HB-P(TA-*alt*-BO) was synthesized in the same way, excepting the molar ratio of the reactants; BDM (5.5 mg, 40 μmol), CsOPiv (4.7 mg, 20 μmol), TA (192 mg, 1.00 mmol), and

butylene oxide (BO; 261 μL, 3.00 mmol). After 4 h, the reaction mixture was diluted with small amount of dichloromethane and purified by preparative SEC to give HB-P(TA-*alt*-BO) as a colorless viscous liquid (248 mg). Yield: 72.5%

$M_{n,MALS}$ = 28,500 g mol^{-1} ($CHCl_3$), $Đ_{MALS}$ = 1.21 ($CHCl_3$)

・Synthesis of HB-P(TA-*alt*-CHO)

HB-P(TA-*alt*-CHO) was synthesized in the same way, excepting the molar ratio of the reactants; BDM (5.5 mg, 40 μmol), CsOPiv (4.7 mg, 20 μmol), TA (192 mg, 1.00 mmol), and cyclohexene oxide (CHO; 302 μL, 3.00 mmol). After 2 h, the reaction mixture was diluted with small amount of dichloromethane and purified by preparative chromatography to give HB-P(TA-*alt*-CHO) as a colorless viscous liquid (274 mg). Yield: 69.6%

$M_{n,MALS}$ = 98,600 g mol^{-1} ($CHCl_3$), $Đ_{MALS}$ = 1.58 ($CHCl_3$)

・Synthesis of HB-P(TA-*alt*-DBGA)

HB-P(TA-*alt*-DBGA) was synthesized in the same way, excepting the molar ratio of the reactants; BDM (5.5 mg, 40 μmol), CsOPiv (4.7 mg, 20 μmol), TA (192 mg, 1.00 mmol), and dibenzyl glycidyl amine (DBGA; 261 μL, 3.00 mmol). After 5.3 h, the reaction mixture was diluted with small amount of dichloromethane and purified by preparative SEC to give

HB-P(TA-*alt*-DBGA) as a colorless viscous liquid (127.5 mg). Yield: 89.8%

$M_{n,MALS}$ = 134,000 g mol^{-1} ($CHCl_3$), $Đ_{MALS}$ = 1.68 ($CHCl_3$)

3.2.3.2 The general synthesis of linear polyester via ROAC of cyclic anhydride and epoxide

・Synthesis of L-P(PA-*alt*-EGE)

Linear-poly(PA-*alt*-EGE) (L-P(PA-*alt*-EGE)) was synthesized in the same way, excepting the molar ratio of the reactants; BDM (5.5 mg, 40 μmol), CsOPiv (4.7 mg, 20 μmol), phthalic anhydride (PA; 148 mg, 1.00 mmol), and EGE (323 μL, 3 mmol). After 5 h, the reaction mixture was diluted with small amount of dichloromethane and purified by reprecipitation from a dichloromethane solution into cold methanol to give L-P(PA-*alt*-EGE) as a colorless viscous liquid (103.6 mg). Yield: 40.5%

$M_{n,MALS}$ = 8,000 g mol^{-1} ($CHCl_3$), $Đ_{MALS}$ = 1.06 ($CHCl_3$)

・Synthesis of L-P(PA-*alt*-PO)

L-P(PA-*alt*-PO) was synthesized in the same way, excepting the molar ratio of the reactants; BDM (6.9 mg, 50 μmol), CsOPiv (5.9 mg, 25 μmol), PA (185 mg, 1.25 mmol), and PO (525 μL, 7.50 mmol). After 2 h, the reaction mixture was diluted with small amount of dichloromethane and purified by reprecipitation from a dichloromethane solution into cold methanol to give L-P(PA-*alt*-PO) as a colorless viscous liquid (150 mg). Yield: 75.9%

$M_{n,MALS}$ = 7,900 g mol^{-1} ($CHCl_3$), $Đ_{MALS}$ = 1.02 ($CHCl_3$)

・Synthesis of L-P(PA-*alt*-BO)

L-P(PA-*alt*-BO) was synthesized in the same way, excepting the molar ratio of the reactants; BDM (6.9 mg, 50 μmol), CsOPiv (5.9 mg, 25 μmol), PA (185 mg, 1.25 mmol), and BO (652 μL, 7.50 mmol). After 2 h, the reaction mixture was diluted with small amount of dichloromethane and purified by reprecipitation from a dichloromethane solution into cold methanol to give L-P(PA-*alt*-BO) as a colorless viscous liquid (107 mg). Yield: 74.3%

$M_{n,MALS}$ = 5,700 g mol^{-1} ($CHCl_3$), $Đ_{MALS}$ = 1.01 ($CHCl_3$)

・Synthesis of L-P(PA-*alt*-CHO)

L-P(PA-*alt*-CHO) was synthesized in the same way, excepting the molar ratio of the reactants; BDM (5.5 mg, 40 μmol), CsOPiv (4.7 mg, 20 μmol), PA (148 mg, 1.00 mmol), and CHO (605 μL, 6.00 mmol). After 3 h, the reaction mixture was diluted with small amount of dichloromethane and purified by reprecipitation from a dichloromethane solution into cold methanol to give L-P(PA-*alt*-CHO) as a colorless viscous liquid (233 mg). Yield: 92.5%

$M_{n,MALS}$ = 8,300 g mol^{-1} ($CHCl_3$), $Đ_{MALS}$ = 1.03 ($CHCl_3$)

・Synthesis of L-P(PA-*alt*-DBGA)

L-P(PA-*alt*-DBGA) was synthesized in the same way, excepting the molar ratio of the

reactants; BDM (1.4 mg, 10 μmol), CsOPiv (1.2 mg, 5.0 μmol), PA (37.0 mg, 250 μmol), and DBGA (380 mg, 1.50 mmol). After 27 h, the reaction mixture was diluted with small amount of dichloromethane and purified by reprecipitation from a dichloromethane solution into cold methanol to give L-P(PA-*alt*-DBGA) as a colorless viscous liquid (63.0 mg). Yield: 61.9%

$M_{n,MALS}$ = 13,300 g mol^{-1} ($CHCl_3$), $Đ_{MALS}$ = 1.39 ($CHCl_3$)

3.2.3.3 The general synthesis of polyether via ROP of epoxide

・Synthesis of PEGE

In an argon-filled glovebox, BDM (12.0 mg, 87.0 μmol), CsOPiv (10.2 mg, 43.5 μmol) and EGE (488 mg, 4.78 mmol) were added to the reaction vessel and stirred at 100 °C. After 1.6 h, crude aliquot was withdrawn from the system by pipette and monitored by ^{1}H NMR spectroscopy in $CDCl_3$ to determine monomer conversion. The reaction mixture was diluted with small amount of dichloromethane and purified by reprecipitation from a dichloromethane solution into cold methanol to give PEGE as a colorless oil (236 mg). Yield: 48.4%

$M_{n,NMR}$ = 6,000 g mol^{-1} ($CDCl_3$)

3.2.3.4 Model reactions for investigation of TA's reactivity

・Reaction of TA and 2-propanol

CsOPiv (23.4 mg, 100 μmol), TA (96.1 mg, 500 μmol), and 2-propanol (115 μL, 1.50 mmol) were added to the reaction vessel and stirred at 80 °C. After 2 h, reaction mixture was evaporated to remove unreacted 2-propanol and measured by ^{1}H NMR spectroscopy in DMSO-*d6* to check the reaction products. Yield: 99.2%

・Reaction of PA and 2-propanol

CsOPiv (11.7 mg, 50.0 μmol), PA (74.1 mg, 500 μmol), and 2-propanol (195 μL, 1.50 mmol) were added to the reaction vessel and stirred at 80 °C. After 1.5 h, reaction mixture was evaporated to remove unreacted 2-propanol and measured by ^{1}H NMR spectroscopy in DMSO-*d6* to check the reaction products. Yield: 63.6%

・Reaction of BA and 2-propanol

CsOPiv (11.7 mg, 50.0 μmol), BA (61.1 mg, 500 μmol), and 2-propanol (195 μL, 1.50 mmol) were added to the reaction vessel and stirred at 80 °C. After 1.5 h, reaction mixture was evaporated to remove unreacted 2-propanol and measured by ^{1}H NMR spectroscopy in DMSO-*d6* to check the reaction products. Yield: 72.0%

・Reaction of BA and EGE

CsOPiv (11.7 mg, 50.0 μmol), BA (61.1 mg, 500 μmol), and EGE (161 μL, 1.50 mmol) were added to the reaction vessel and stirred at 80 °C. After 1.5 h, reaction mixture was evaporated to remove unreacted EGE and measured by ^{1}H NMR spectroscopy in $CDCl_3$ to check the reaction products. Yield: 83.6%

3.3 Results and Discussion

3.3.1 Ring-opening alternating copolymerization of trimellitic anhydride and ethyl glycidyl ether

First, the author investigated the ROAC of TA with ethyl glycidyl ether (EGE) under bulk conditions (run 1 in **Table 3.1**). The author employed cesium pivalate (CsOPiv) as a catalyst, as it shows sufficient catalytic ability for ROAC (see Chapter 2). The ROAC was conducted at 80 °C in the presence of 1,4-benzenedimethanol (BDM) as an initiator at a $[CsOPiv]/[BDM]_0/[TA]_0/[EGE]_0$ molar ratio of 0.5/1/25/75. After the reaction started, the conversion of TA ($conv._{TA}$) increased and finally reached 95%, as confirmed by ^1H NMR analysis of the crude aliquot. This result confirmed the progress of polymerization, even in the presence of the free carboxyl group. As the free carboxyl group on TA is also involved in the ROAC to generate a branching point, the consumption of EGE ($cons._{EGE}$) should be higher than that of $cons._{TA}$. More specifically, $cons._{EGE}$ should be twofold of $cons._{TA}$ when all the free carboxyl groups participate in ROAC. To test this hypothesis, the author monitored the consumption of two monomers during polymerization. Interestingly, $cons._{EGE}$ was always higher than that of TA, and it was eventually found to be approximately twice the amount of consumed TA (**Figure 3.2**). This result suggests that the obtained polymer had a hyperbranched structure, as expected, and most of the free carboxyl groups reacted with EGE to generate the

branching point (degree of branching ≈ 1). The absolute molecular weight ($M_{n,MALS}$) and dispersity ($Đ$) of the obtained hyperbranched poly(TA-*alt*-EGE) (HB-P(TA-*alt*-EGE)) were determined to be 16,900 g mol^{-1} and 1.11, respectively, using a triple-detection SEC equipped with refractive index, light scattering, and viscosity detectors (SEC-MALS-VISCO). Since the obtained products possess highly branched, the standard SEC analysis against linear polystyrene standards did not provide any meaningful information about the molecular weight. Note that the observed $M_{n,MALS}$ is much greater than the theoretical molecular weight ($M_{n,theo.}$) calculated based on the initial monomer-to-initiator ratio and $conv._{TA}$. This result implies that the intermolecular coupling should occur along with the propagation reaction.

Table 3.1. Syntheses of hyperbranched polyesters via ROAC of TA with various epoxides [a]

run	initiator	epoxide	time (h)	conv.$_{TA}$ (%) [b]	$M_{n,theo.}$ [c]	$M_{n,MALS}$ [d]	$M_{w,MALS}$ [d]	$Đ$ [d]	$[\eta]$ (mL min^{-1}) [d]	T_g (°C) [e]
1	BDM	EGE	5.5	95	9,600	16,900	18,700	1.11	3.07	−20.1
2	HO-PEG-OH	EGE	1.5	>99	9,300	36,010	37,600	1.05	2.99	- [f]
3	MeO-PEG-OH	EGE	2.0	77	9,200	46,500	49,200	1.06	1.17	- [f]
4	6-azido-hexan-1-ol	EGE	2.0	72	6,300	24,000	28,900	1.20	2.61	- [f]
5	5-hexen-1-ol	EGE	9.0	>99	11,000	10,900	14,000	1.28	1.91	- [f]
6	BDM	PO	4.0	87	6,800	24,300	31,600	1.30	4.42	30.3
7	BDM	BO	4.0	>99	8,500	28,500	34,500	1.21	3.54	−1.8
8	BDM	CHO	2.0	- [f]	- [f]	98,600	156,000	1.58	2.00	0.1
9	BDM	DBGA	5.3	>99	14,000	134,000	224,000	1.68	2.11	70.0

[a] Polymerisation conditions: [CsOPiv]/[initiator]$_0$/[TA]$_0$/[epoxide]$_0$ = 0.5/1/25/75; atmosphere, Ar; temperature, 80 °C. [b] Determined by ^{1}H NMR spectroscopy in $CDCl_3$. [c] Calculated from (M.W. of initiator) + [TA]$_0$/[initiator]$_0$ × (M.W. of TA) × (conv. of TA) + [epoxide]$_0$/[initiator]$_0$ × (M.W. of epoxide) × (conv. of epoxide). [d] Determined by SEC-MALS-VISCO measurements in $CHCl_3$. [e] Measured by DSC. [f] Not determined.

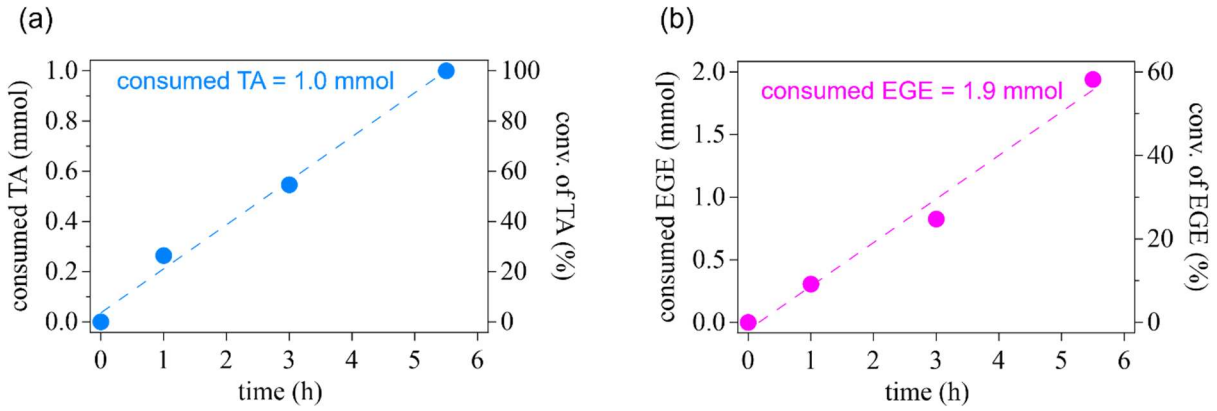

Figure 3.2. Plots of monomer consumption vs time for (a) TA and (b) EGE as monitored by ^{1}H NMR spectroscopy.

3.3.2 Ring-opening alternating copolymerization of phthalic anhydride and ethyl glycidyl ether for the synthesis linear counterpart

To characterize the polymer structure in detail, the author prepared the corresponding linear polyesters and homopolymers of EGE as reference for NMR analysis. According to a previous report,[35] the ROAC of phthalic anhydride (PA) and EGE using a BDM initiator and CsOPiv catalyst successfully produced the corresponding linear polyester, that is, linear-poly(PA-*alt*-EGE) (L-P(PA-*alt*-EGE); $M_{n,MALS}$ = 8,000, $Đ$ = 1.06; run 1 in **Table 3.2**). CsOPiv-catalyzed ROP of EGE was carried out at 100 °C to prepare the related homopolymer, poly(EGE) (PEGE; $M_{n,NMR}$ = 6,000), following the previous study by Satoh et al.[36] Overlay of ^{1}H and ^{13}C NMR spectra of these three polymers is shown in **Figure 3.3**.

Table 3.2. Syntheses of linear polyesters via ROAC of PA and epoxide [a]

run	epoxide	time (h)	conv.$_{TA}$ (%) [b]	$M_{n,theo.}$ [c]	$M_{n,MALS}$ [d]	$M_{w,MALS}$ [d]	$Đ$ [d]	[η] (mL min^{-1}) [d]	T_g (°C) [e]
1	EGE	5.0	>99	6,390	8,000	8,500	1.06	4.98	7.1
2	PO	2.0	73	4,000	7,900	8,100	1.02	3.23	11.0
3	BO	2.0	50	2,870	5,700	5,800	1.01	4.61	3.2
4	CHO	3.0	>99	6,300	8,300	8,500	1.03	5.40	64.4
5	DBGA	27.0	>99	10,200	13,300	18,400	1.39	3.65	38.7

[a] Polymerization conditions: [CsOPiv]/[BDM]$_0$/[PA]$_0$/[epoxide]$_0$ = 0.5/1/25/150; atmosphere, Ar; initiator, BDM; temp, 80 °C. [b] Determined by ^{1}H NMR in $CDCl_3$. [c] Calculated from (M.W. of BDM) + [PA]$_0$/[BDM]$_0$ × (M.W. of PA) × (conv. of PA) + [epoxide]$_0$/[BDM]$_0$ × (M.W. of epoxide) × (conv. of epoxide). [d] Determined by SEC-MALS-VISCO measurement in $CHCl_3$. [e] Measured by DSC.

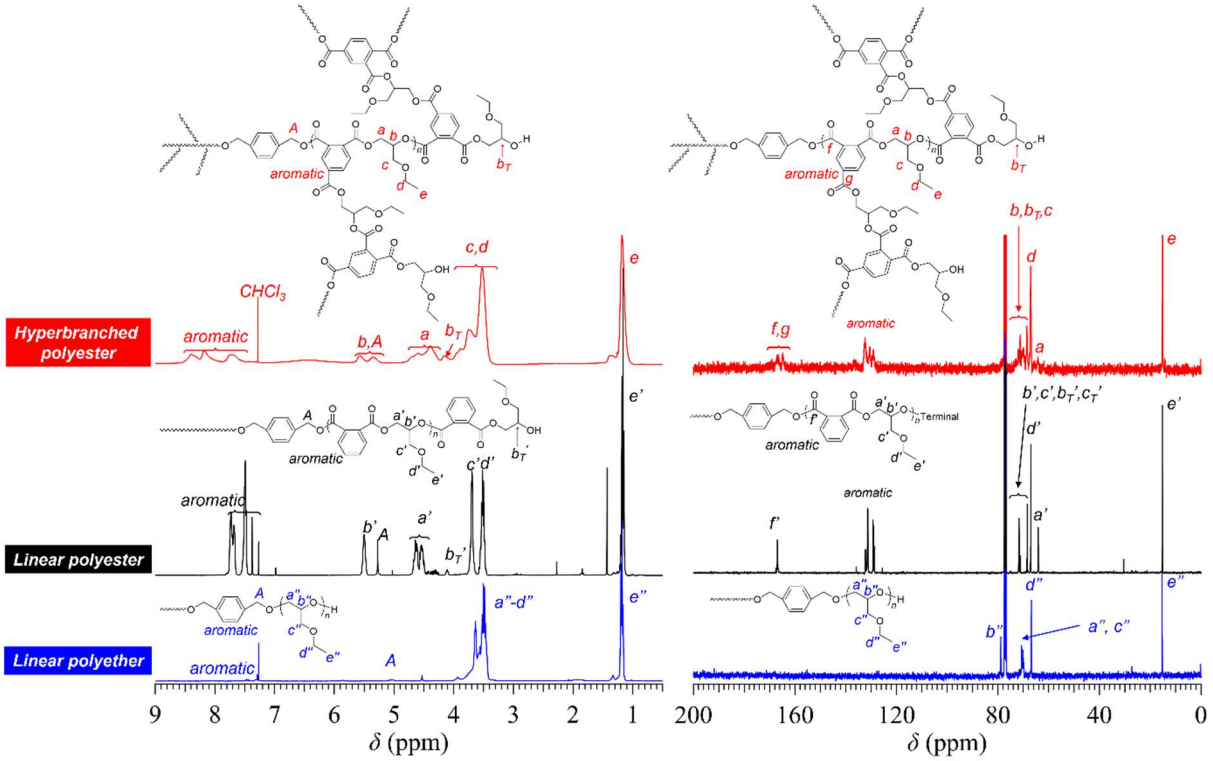

Figure 3.3. ^{1}H (400 MHz; left panel) and ^{13}C NMR (100 MHz; right panel) spectra of PEGE (blue), L-P(PA-*alt*-EGE) (black), and HB-P(TA-*alt*-EGE) (red) in $CDCl_3$.

The ^{1}H NMR spectrum of L-P(PA-*alt*-EGE) shows characteristic peaks owing to the benzene ring (7.42–7.85 ppm), polyester main chain (-CH_2CH- (*b'*), 5.37–5.73 ppm; -CH_2CH- (*a'*), 4.44–4.92 ppm), and EGE side chain (-$CH_2OCH_2CH_3$ (*c', d'*), 3.39–3.86 ppm; -$CH_2OCH_2CH_3$ (*e'*), 1.09–1.33 ppm), which agreed with the previously reported data.[35] According to previous reports, alternating polyesters synthesized by ROAC in the presence of excess epoxide over cyclic anhydride are known to possess hydroxyl terminal groups. Indeed, the methine proton adjacent to the terminal hydroxyl group was confirmed as a weak signal at 4.0 ppm (b_T'). Comparing this spectrum with that of HB-P(TA-*alt*-EGE), the signals at 5.15–

5.75 and 4.23–4.89 ppm observed in the latter could be reasonably assigned to the polyester main chain protons *b* and *a*, respectively. The aromatic signals in the HB-P(TA-*alt*-EGE) spectra appeared as three peaks on the downfield side (7.29–8.75 ppm) compared to that in the L-P(TA-*alt*-EGE) spectrum (7.42–7.85 ppm). The additional carbonyl group led to a downfield shift of the phenyl protons. In addition, it led to desymmetrization of the benzene ring, which explains the splitting of its peak into three different peaks. Similarly, the signals at approximately 3.30–4.02 and 0.99–1.26 ppm can be assigned to the side-chain protons (*c*–*e*). These results suggest that HB-P(TA-*alt*-EGE) and L-P(TA-*alt*-EGE) share the same repeating unit.

Notably, the NMR signals of HB-P(TA-*alt*-EGE) are much broader than those of L-P(TA-*alt*-EGE), owing to the lower structural regularity originating from the asymmetric nature of the TA unit.[1] Here, the author conducted a model reaction of TA with alcohol to investigate the regioselectivity in the cyclic anhydride ring-opening. 2-Propanol was selected as the substrate to simulate the secondary alcohol nature of the growing chain end derived from the epoxide. The model reaction was carried out in the presence of CsOPiv at 80 °C ($[CsOPiv]/[TA]_0/[2\text{-propanol}]_0 = 1/5/15$). After 2 h, TA was quantitatively consumed, and the ^{1}H NMR spectrum of the resulting mixture revealed the formation of two regioisomeric monoesters with 60:40 ratio. This result demonstrated the absence of any significant

regioselectivity in the ring-opening of the TA monomer (**Figure 3.4**). Additionally, the reactivity of the anhydride and carboxy moieties in TA was investigated. Thus, the author conducted the following two model reactions: (a) 2-propanol +PA and (b) 2-propanol + benzoic acid (BA) in the presence of CsOPiv with the feed ratio of [CsOPiv]/[PA or BA]$_0$/[2-propanol]$_0$ being 0.5/5/15. After 90 min, 30.4% of PA was reacted with 2-propanol in model reaction (a) to produce the corresponding monoester, whereas no reaction was observed in reaction (b) (**Figure 3.5**). This observation demonstrates that the alcohol initiator/growing hydroxy chain end first reacts with the anhydride moiety of TA and subsequently the carboxy groups react with the epoxide monomer. More importantly, a broad signal was confirmed at approximately 4 ppm (b_T), which was observed in the same range as the b_T' of L-P(PA-*alt*-EGE). Although it was difficult to quantify the signal intensity because of the overlap with the neighboring signals, the signal intensity of b_T was much higher than that expected for the product without branching. This observation proves the presence of multiple polymer chain ends resulting from the multibranching structure.

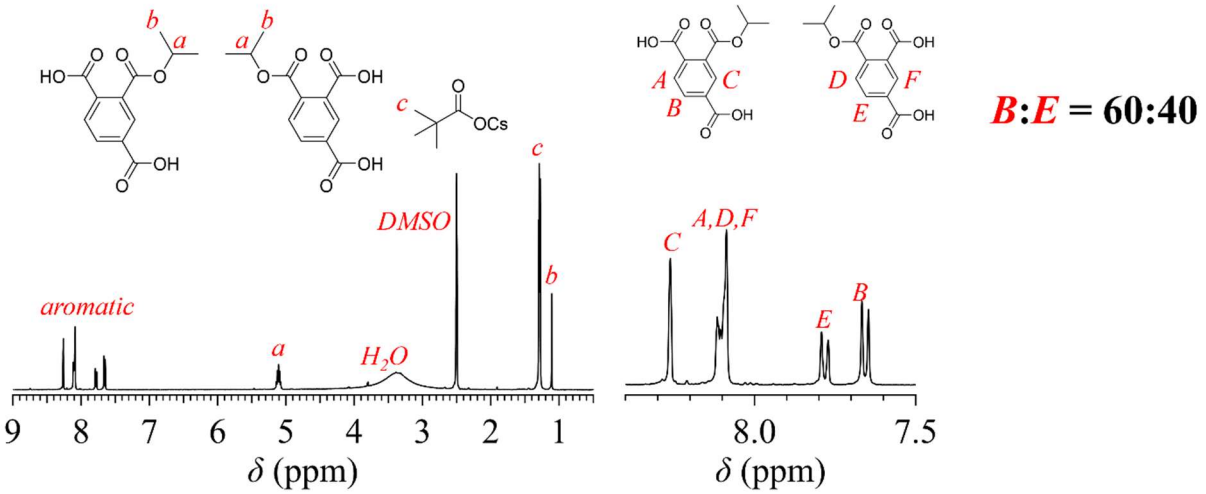

Figure 3.4. ^{1}H NMR spectrum of the products obtained from mixtures of 2-propanol, TA, and CsOPiv at 80 °C for 2 h with the feed ratio of [CsOPiv]/[TA]$_0$/[2-propanol]$_0$ being 1/5/15 (400 MHz, DMSO-*d6*).

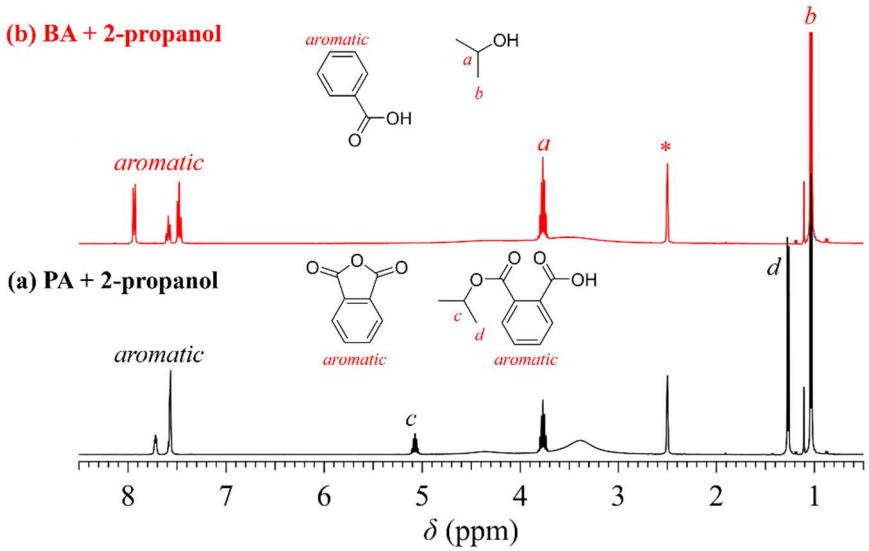

Figure 3.5. ^{1}H NMR spectra of the products obtained from mixtures of (a) 2-propanol + PA and (b) 2-propanol + BA in the presence of CsOPiv at 80 °C for 90 min with the feed ratio of [CsOPiv]/[PA or BA]$_0$/[2-propanol]$_0$ being 0.5/5/15 (400 MHz, DMSO-*d6*).

Similar to the ^{1}H NMR spectra, the ^{13}C NMR spectra of HB-P(PA-*alt*-EGE) was analogous to that of L-P(PA-*alt*-EGE), such as carbonyl signals (164–168 ppm, *f, g*), main chain

(benzene ring, 128–133 ppm; -C*H*$_2$CH- (*b, b$_T$*), 68.0–71.0 ppm; -C*H*$_2$CH- (a), 64.3 ppm), and side chain (-C*H*$_2$O- (*c*), 71.0–72.3 ppm; -OC*H*$_2$CH$_3$ (*d*), 67.5 ppm; -OCH$_2$C*H*$_3$ (*e*), 15.1 ppm) (**Figure 3.6**). It is worthwhile to compare the ^{13}C NMR spectra of HB-P(PA-*alt*-EGE) and PEGE to exclude the possibility of epoxide homopolymerization during ROAC. Therefore, one could expect that ROP may also proceed in addition to the ROAC of anhydride and epoxide in the current polymerization system. The ^{13}C NMR spectrum of PEGE shows a characteristic signal at 79.0 ppm because of the main-chain methine (*b"*), which can be used as a proof to determine whether ROP occurred concomitantly during ROAC. A closer look at approximately 80 ppm showed the absence of any signal for HB-P(PA-*alt*-EGE). This result unambiguously demonstrated that the ROP of EGE did not occur, and all the consumed EGE monomers were incorporated in the form of polyesters.

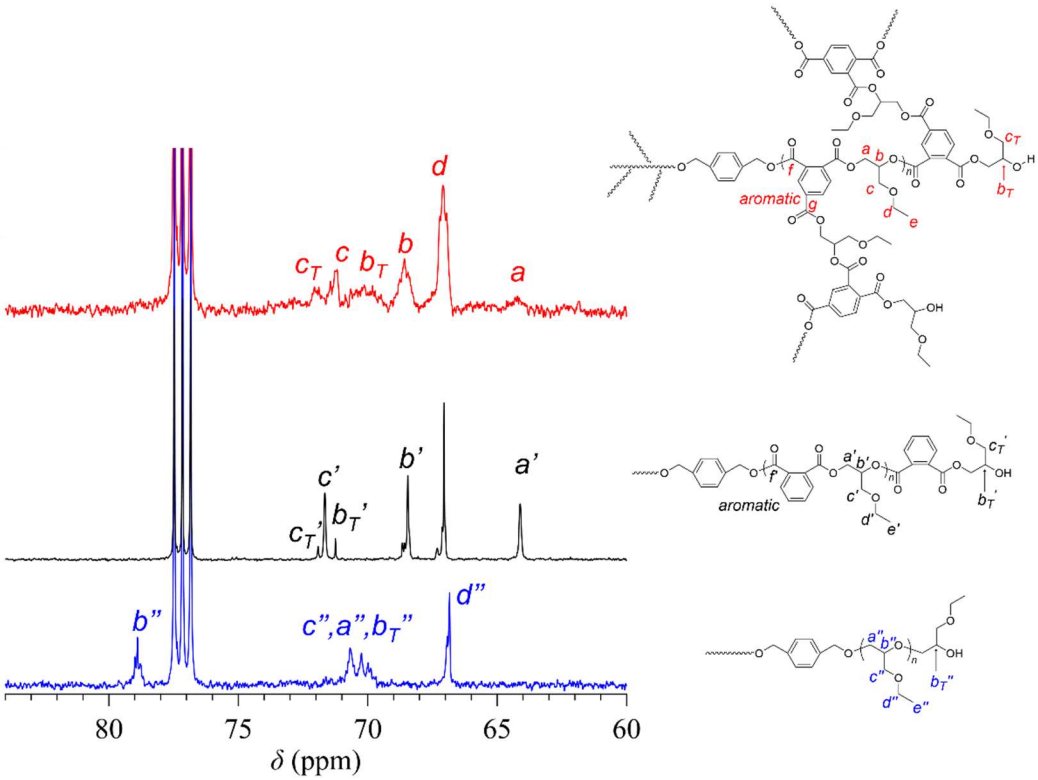

Figure 3.6. ^{13}C NMR spectra (100 MHz) of PEGE (blue), L-P(PA-*alt*-EGE) (run 1 in Table 3.2; black), and HB-P(TA-*alt*-EGE) (run 1 in Table 3.1; red) in $CDCl_3$.

In the present polymerization system, three routes are expected as the initiation pathway: the initiation from the alcohol initiator, initiation from pivalate, and initiation from the carboxyl group of TA. In the author's previous paper, the author has confirmed that the carboxylate does not initiate the ROAC of cyclic anhydride and epoxide in the presence of an alcohol initiator.[35] In contrast, Luo found that alkali metal carboxylates can work as a non-alcohol initiator for the ROAC.[37] If pivalate could also be used as an initiator in the present system, it may complicate the structure of the HBPEs. To intentionally synthesize HB-P(TA-*alt*-EGE) containing a pivalate end group, the author conducted the ROAC of TA and EGE

without an alcohol initiator and with the increased CsOPiv ratio. As expected, the ^{13}C NMR spectrum of the product showed a characteristic signal owing to the presence of the pivalate group (26.8 ppm, a; 32.2 ppm b; **Figure 3.7**). However, no such signal appeared in the spectrum of the HB-P(TA-*alt*-EGE) obtained from run 1 in **Table 3.1**. Therefore, the HBPEs synthesized by the author's optimized condition are virtually free from the pivalate moiety. Next, the author conducted the model reaction to check whether TA can also work as an initiator. The model reaction of BA with three equivalents of EGE in the presence of CsOPiv indeed proceeded (10.5% conversion of BA in 90 min at 80 °C), which supported the initiation from TA, producing TA-epoxide adduct (**2**) in **Figure 3.8**.

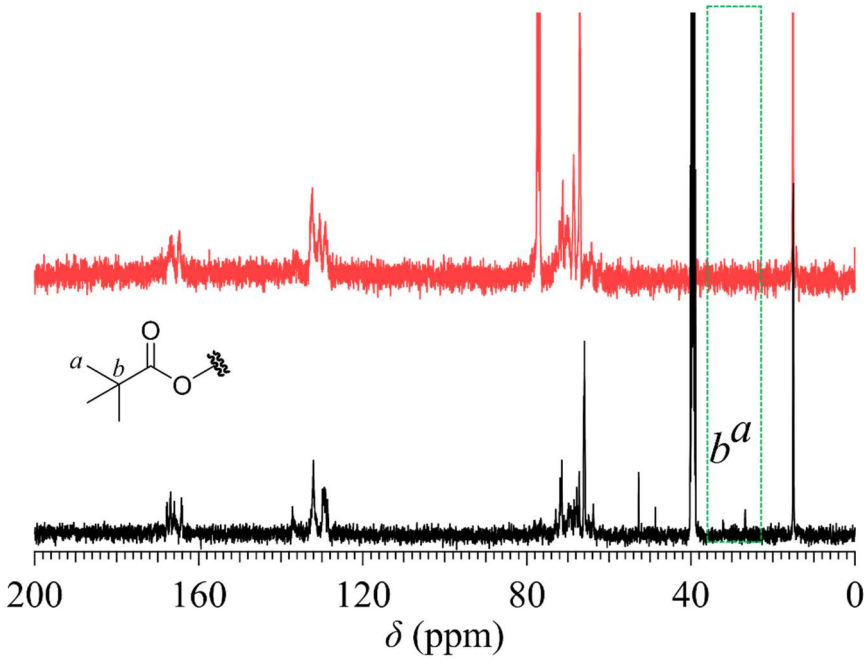

Figure 3.7. ^{13}C NMR spectra of HB-P(TA-*alt*-EGE) obtained from ROAC without alcohol initiator (black; 100 MHz) and with alcohol initiator (red; run 1 in Table 3.1; 125 MHz) in DMSO-*d6*.

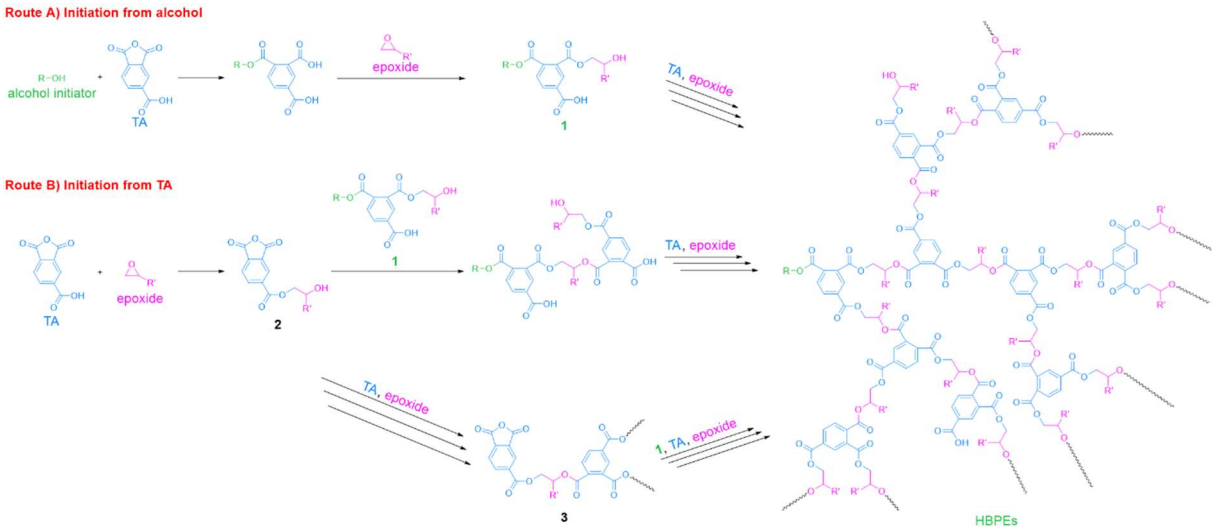

Figure 3.8. Reaction mechanism of ROAC using TA and epoxide.

Based on the above discussions, the author proposes the reaction mechanism to form HBPEs (**Figure 3.8**). The initiation reaction involves two routes. The first route involves the addition reaction of the alcohol initiator to TA and subsequent ring-opening reaction of epoxide, producing the initiator-TA-epoxide adduct (**1**). The second route is the ring-opening reaction of epoxide from the carboxyl group of TA to form TA-epoxide adduct (**2**). In the propagation reaction, the alkoxide species, such as **1** and **2**, react with TA and subsequently EGE, resulting in the formation of HBPEs (**3** and **4**). The unreacted anhydride moiety in **3** will be consumed when reacting with the alkoxide species, which finally produces the HBPEs with an initiator residue.

3.3.3 Physical properties comparison of hyperbranched poly(TA-*alt*-EGE) with linear counterpart

HBP is well known to exhibit lower viscosity, higher solubility, and a smaller hydrodynamic radius than those of their linear counterparts. To identify the specific properties originating from the hyperbranched structure, the author measured and compared the intrinsic viscosity ([η]) and hydrodynamic radius (R_h) of HB-P(TA-*alt*-EGE) and L-P(PA-*alt*-EGE) (**Figure 3.9**). The Mark–Houwink–Sakurada plots revealed that the [η] of HB-P(TA-*alt*-EGE) was apparently lower than that of L-P(PA-*alt*-EGE) within the same molecular weight range. The R_h conformation plots also revealed the smaller R_h of HB-P(TA-*alt*-EGE) than that of L-P(PA-*alt*-EGE). These results confirmed that HB-P(TA-*alt*-EGE) exhibits a smaller molecular dimension than that of L-P(PA-*alt*-EGE) with a comparable molecular weight. Based on NMR and solution property analyses, the author concluded that HB-P(TA-*alt*-EGE) possesses a truly hyperbranched structure. Thus, the ROAC of TA and epoxide is an efficient and convenient means of synthesizing HBPEs.

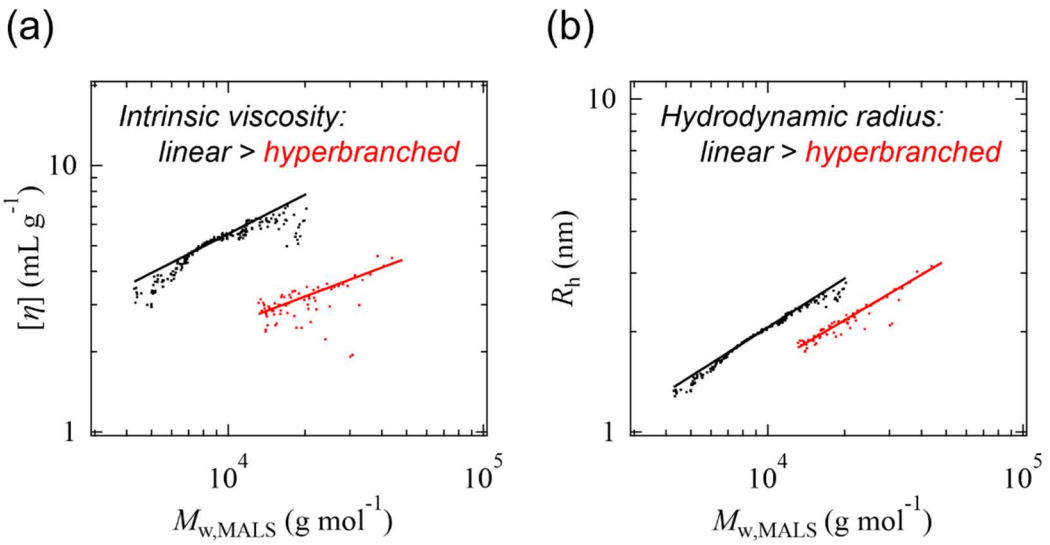

Figure 3.9. (a) Mark–Houwink–Sakurada plots and (b) conformation plots for HB-P(TA-*alt*-EGE) ($M_{n,MALS}$ = 16,900 g mol^{-1}, red) and L-P(PA-*alt*-EGE) ($M_{n,MALS}$ = 8,000 g mol^{-1}, black).

3.3.4 Investigation of initiator and monomer scope

To expand the synthetic utility of this method, ROACs of TA and EGE were carried out in the presence of various functional alcohol initiators such as bifunctional poly(ethylene glycol) (HO-PEG-OH), mono-functional PEG (MeO-PEG-OH), 6-azidohexan-1-ol, and 5-hexen-1-ol under established conditions ([CsOPiv]/[initiator]$_0$/[TA]$_0$/[EGE]$_0$ = 0.5/1/25/75 at 80 °C). When HO-PEG-OH and MeO-PEG-OH were used as the initiator, the obtained products clearly showed the signals owing to the methylene protons of the PEG backbone in their ^{1}H NMR spectra (runs 2 and 3 in **Table 3.1**; **Figures 3.10** and **3.11**). These initiators are useful for one-step reactions that synthesize block copolymers such as dendritic-*b*-linear-*b*-dendritic and linear-*b*-dendritic block copolymers consisting of HB-P(TA-*alt*-EGE) and PEG blocks. These block copolymers may find interesting biomedical applications owing to their amphiphilic nature.[38] Subsequently, alcohol initiators with azido and olefin groups were employed for the ROAC of TA and EGE (runs 4 and 5, **Table 3.1**). The ^{1}H NMR spectrum of the product obtained from run 4 showed the signals owing to the methylene protons of the initiator (1.60–2.00, 2.60, and 4.00 ppm; **Figure 3.12**). Moreover, the FT-IR spectrum showed a characteristic absorption peak at approximately 2100 cm^{-1}, confirming the presence of the azido group (**Figure 3.13**). In the ^{1}H NMR spectrum of the product obtained from run 5, the characteristic signals owing to the olefinic protons were observed at 1.40, 1,61, 1.77, 1.97, 2.63, and 3.95 ppm, supporting the

successful installation of the reactive functional groups (**Figure 3.14**). These functional groups are useful for further functionalization via azido-alkyne and thiol-ene click chemistry. These results demonstrated successful synthesis of functional HBPEs and HBPE-based block copolymers consisting of HBPE and PEG segments via ROAC with TA.

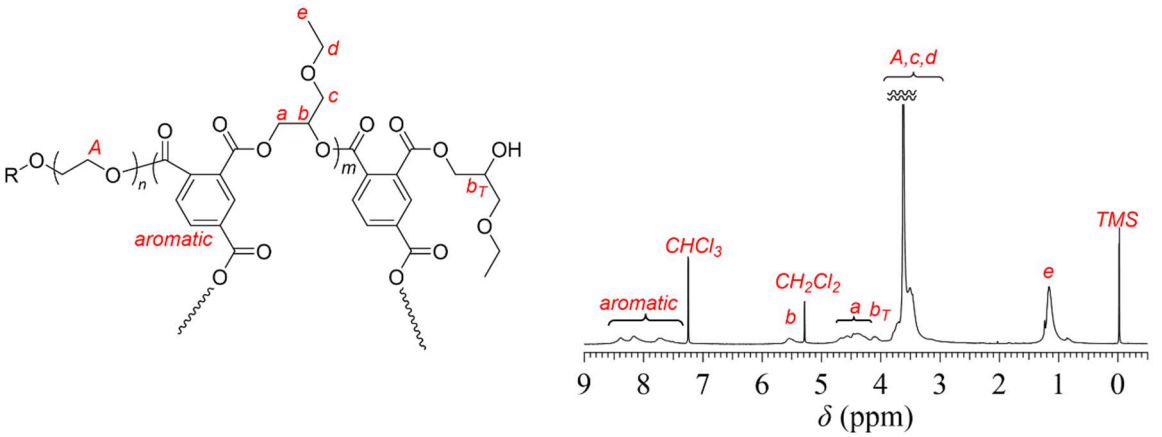

Figure 3.10. ^{1}H NMR of HB-P(TA-*alt*-EGE) initiated by HO-PEG-OH (run 2 in Table 3.1) in $CDCl_3$ (400 MHz).

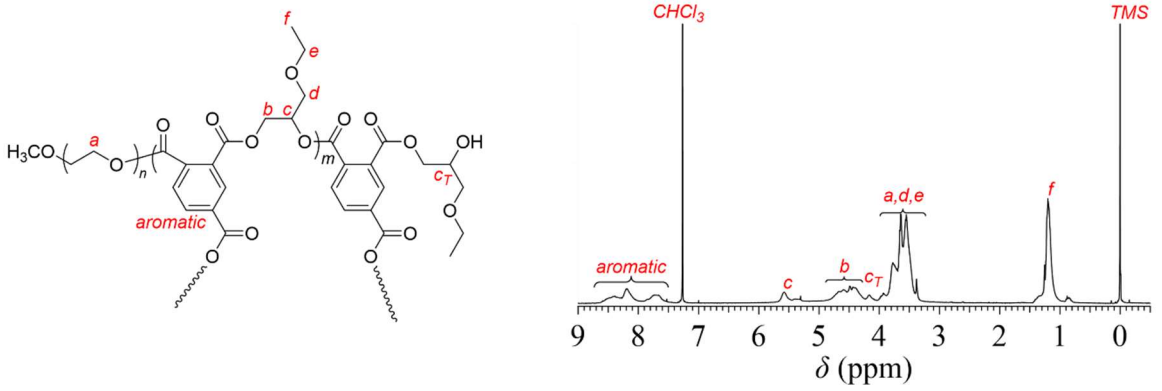

Figure 3.11. ^{1}H NMR of HB-P(TA-*alt*-EGE) initiated by MeO-PEG-OH (run 3 in Table 3.1) in $CDCl_3$ (400 MHz).

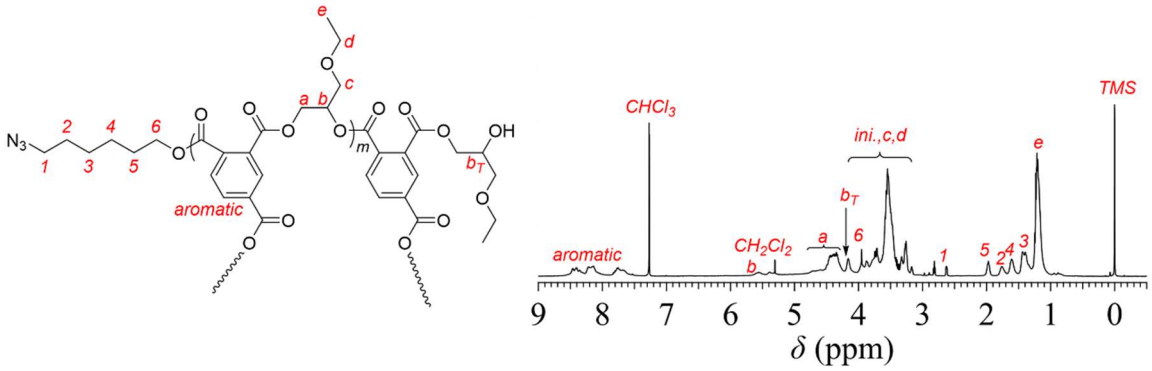

Figure 3.12. ^{1}H NMR of HB-P(TA-*alt*-EGE) initiated by 6-azidohexan-1-ol (run 4 in Table 3.1) in $CDCl_3$ (400 MHz).

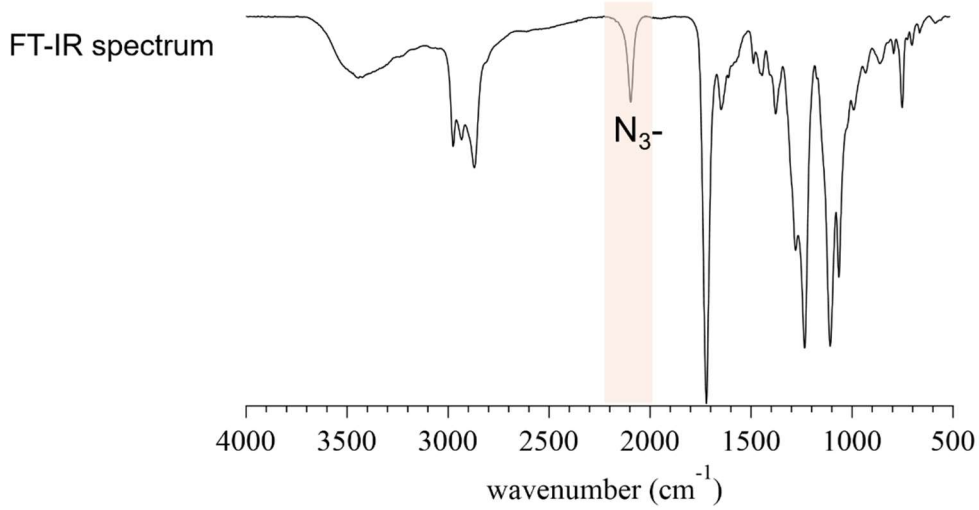

Figure 3.13. FT-IR spectrum of HB-P(TA-*alt*-EGE) initiated by 6-azidohexan-1-ol (run 4 in Table 3.1).

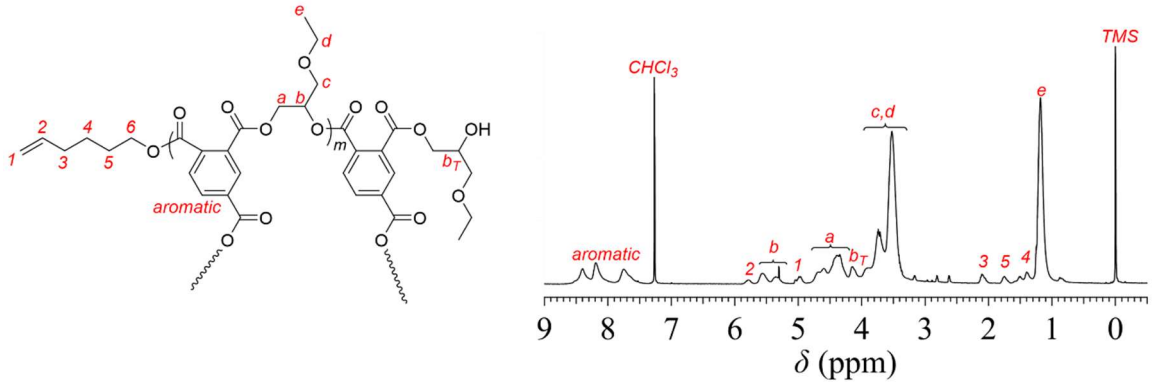

Figure 3.14. ^{1}H NMR of HB-P(TA-*alt*-EGE) initiated by 5-hexen-1-ol (run 5 in Table 3.1) in $CDCl_3$ (400 MHz).

Next, the author investigated the scope of applicable epoxide monomers. The monosubstituted epoxides propylene oxide (PO) and 1,2-butylene oxide (BO) were used under the optimized polymerization conditions, yielding HB-P(TA-*alt*-PO) and HB-P(TA-*alt*-BO), respectively (runs 6 and 7 in **Table 3.1**; **Figures 3.15–3.16**). The obtained HBPEs were characterized by ^{1}H NMR. These spectra showed the signals resulting from alkyl side chains (run 6, 0.68–1.53 (-C*H*$_3$); run 7, 1.36–1.96 (-C*H*$_2$CH$_3$) and 0.77–1.11 (-CH$_2$C*H*$_3$)). These polymers showed sufficient molecular weights ($M_{n,MALS}$ = 24,300 and 28,500) with relatively narrow *Đ* (*Đ* = 1.30 and 1.21). The author also employed cyclohexene oxide (CHO) as a representative example of disubstituted epoxides (run 8 in **Table 3.1**). The ^{1}H NMR spectrum showed the characteristic signals resulting from the cyclohexyl moiety at 0.80–2.50 ppm (*b* and *c* in **Figure 3.17**) and methine group adjacent to the terminal hydroxy group (a_T), which confirmed that the ROAC of TA and CHO also proceeded in a multibranching polymerization manner to produce HB-P(TA-*alt*-CHO). Based on the research in Chapter 2, the author tested *N,N*-dibenzyl glycidyl amine (DBGA) as a representative example of glycidylamines. The ROAC of TA and DBGA gives rise to HBPE with tertiary amino groups along the polymer backbone. These polymers are quite interesting for application as non-viral vectors for gene transfection.[39] After polymerization of DBGA and TA for 5.3 h, the ^{1}H NMR spectrum showed aromatic (6.71–7.39 ppm) and methylene signals (-C*H*$_2$Ph, 2.37–4.72 ppm; -C*H*$_2$NBn$_2$, 0.73–

1.55 ppm) owing to the DBGA unit, which confirmed that ROAC proceeded and formed HB-P(TA-*alt*-DBGA) with a high molecular weight ($M_{n,MALS}$ = 134,000 g mol^{-1}; run 9 in **Table 3.1**; **Figure 3.18**). To verify the hyperbranched structures for HB-P(PA-*alt*-PO), HB-P(PA-*alt*-BO), HB-P(PA-*alt*-CHO), and HB-P(PA-*alt*-DBGA), the author prepared the corresponding linear polyesters (i.e., L-P(PA-*alt*-PO), L-P(PA-*alt*-BO), L-P(PA-*alt*-CHO), and L-P(PA-*alt*-DBGA)) by the ROAC using PA instead of TA (runs 2–5 in **Table 3.2**; **Figures 3.19–3.22**) and compared their SEC-MALS-VISCO data against those of the corresponding HBPEs (**Figures 3.23–3.26**). The HBPEs showed smaller [η] and R_h values than those of their linear counterparts. These results demonstrate that a wide range of epoxide monomers can be used for ROAC with TA, supporting the versatility of this approach.

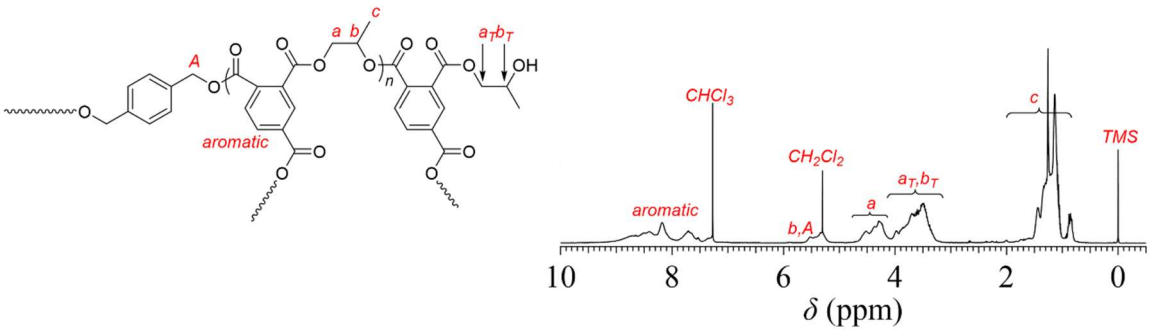

Figure 3.15. ^{1}H NMR of HB-P(TA-*alt*-PO) (run 6 in Table 3.1) in $CDCl_3$ (400 MHz).

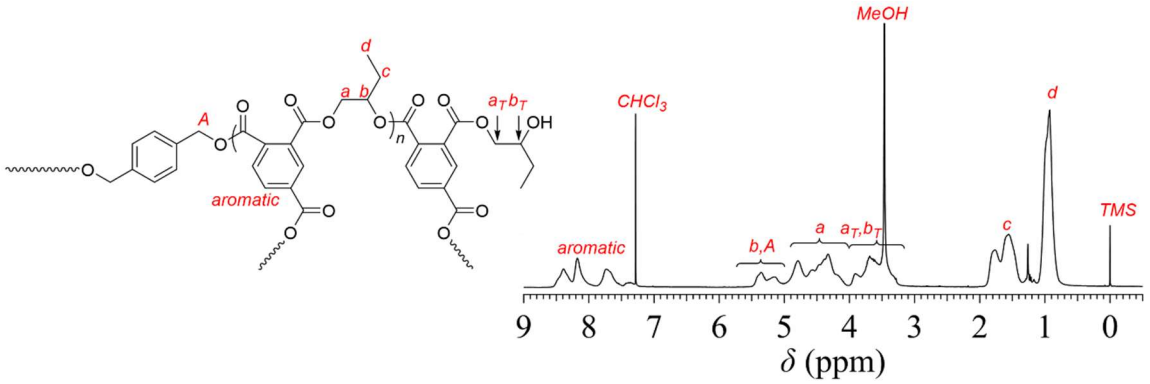

Figure 3.16. ^{1}H NMR of HB-P(TA-*alt*-BO) (run 7 in Table 3.1) in $CDCl_3$ (400 MHz).

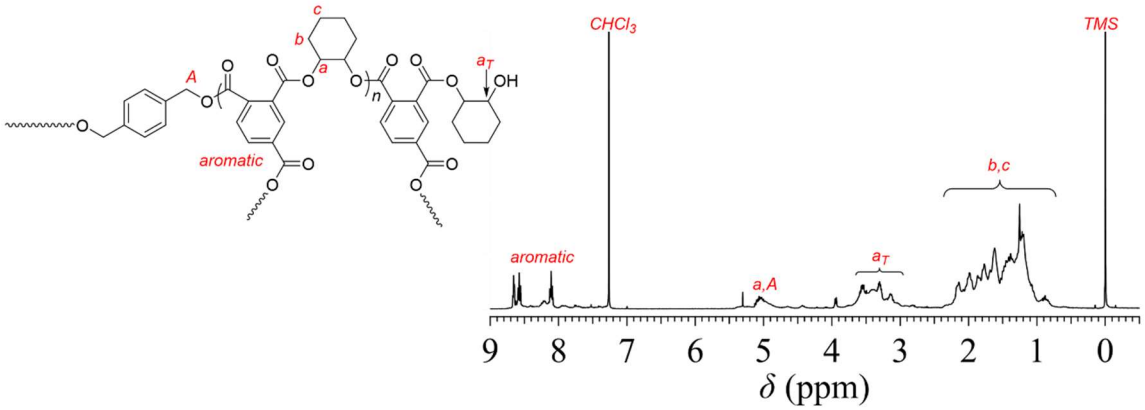

Figure 3.17. ^{1}H NMR of HB-P(TA-*alt*-CHO) (run 8 in Table 3.1) in $CDCl_3$ (400 MHz).

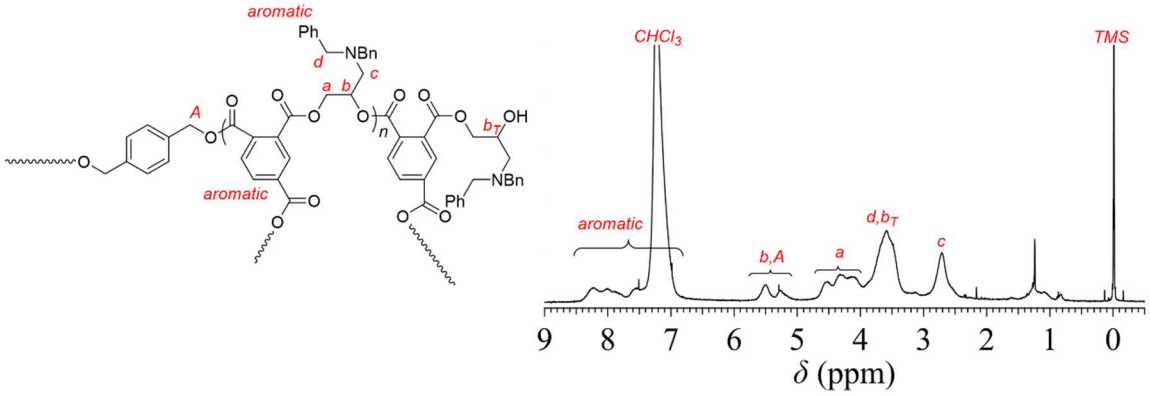

Figure 3.18. ^{1}H NMR of HB-P(TA-*alt*-DBGA) (run 9 in Table 3.1) in $CDCl_3$ (400 MHz).

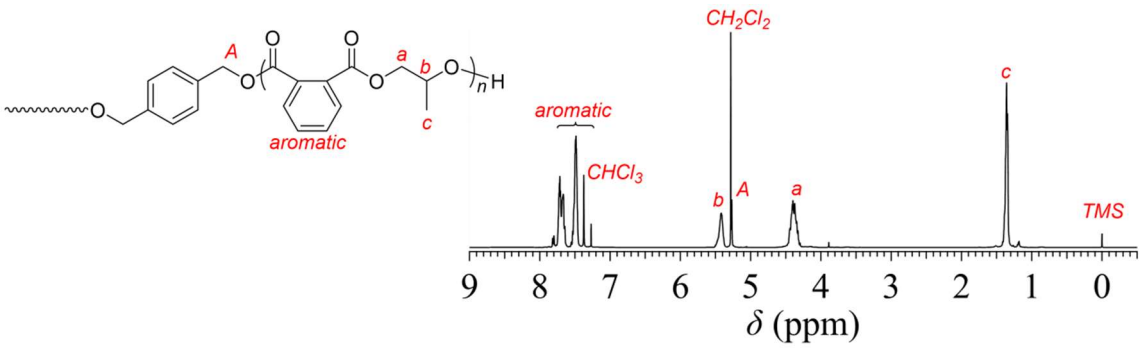

Figure 3.19. ^{1}H NMR of L-P(PA-*alt*-PO) (run 2 in Table 3.2) in $CDCl_3$ (400 MHz).

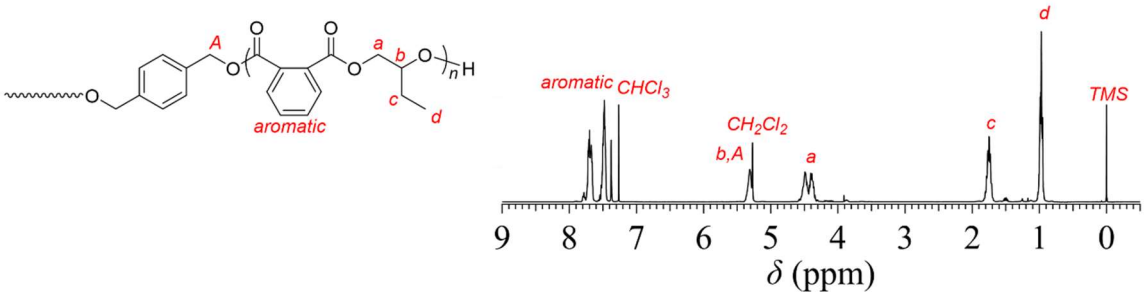

Figure 3.20. ^{1}H NMR of L-P(PA-*alt*-BO) (run 3 in Table 3.2) in $CDCl_3$ (400 MHz).

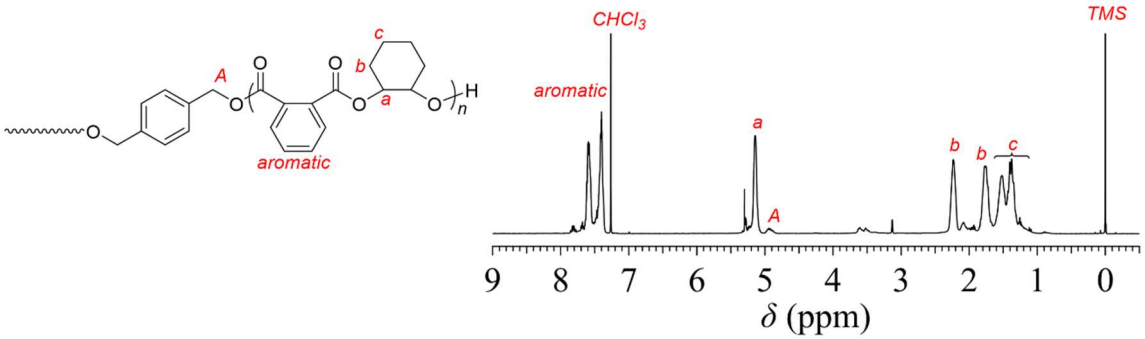

Figure 3.21. ^{1}H NMR of L-P(PA-*alt*-CHO) (run 4 in Table 3.2) in $CDCl_3$ (400 MHz).

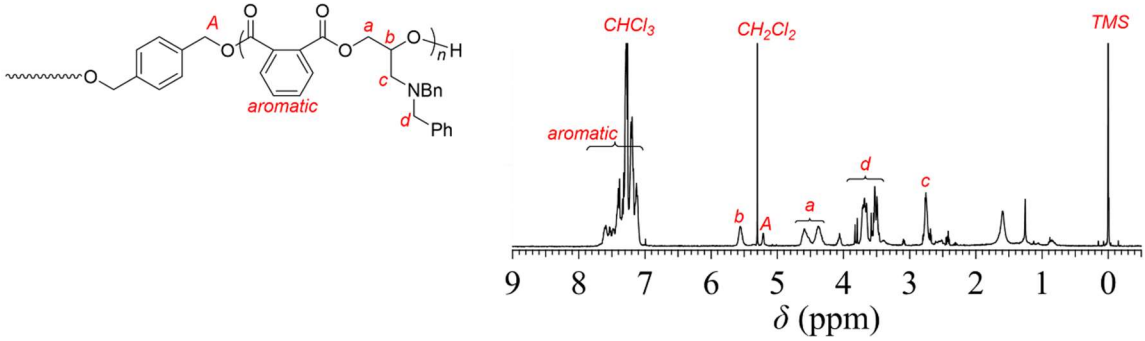

Figure 3.22. ^{1}H NMR of L-P(PA-*alt*-DBGA) (run 5 in Table 3.2) in $CDCl_3$ (400 MHz).

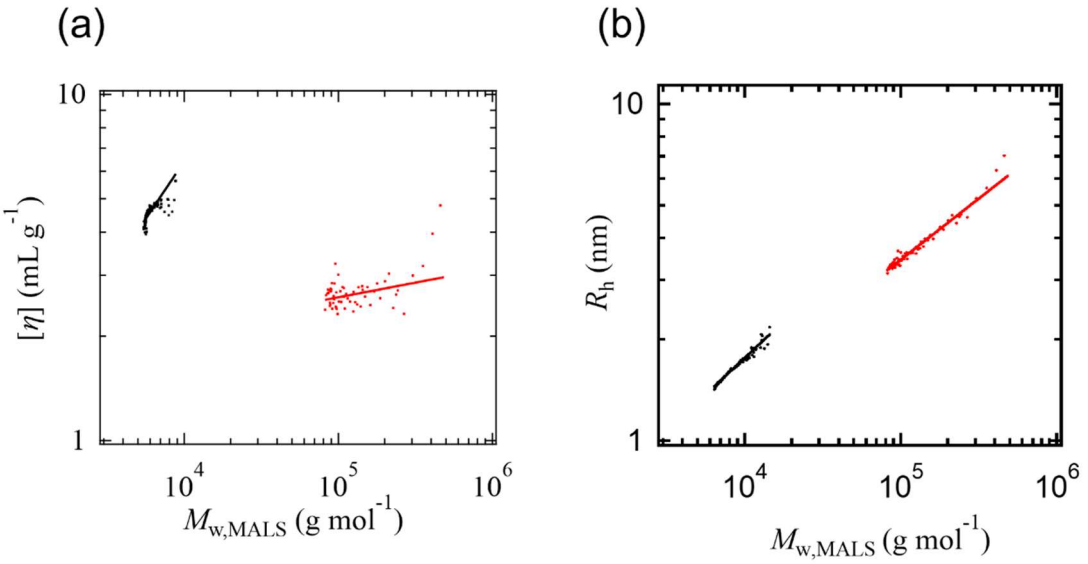

Figure 3.23. (a) Mark-Houwink-Sakurada plots and (b) conformation plots for HB-P(TA-*alt*-PO) ($M_{n,MALS}$ = 24,300 g mol^{-1}, red) and L-P(PA-*alt*-PO) ($M_{n,MALS}$ = 7,900 g mol^{-1}, black).

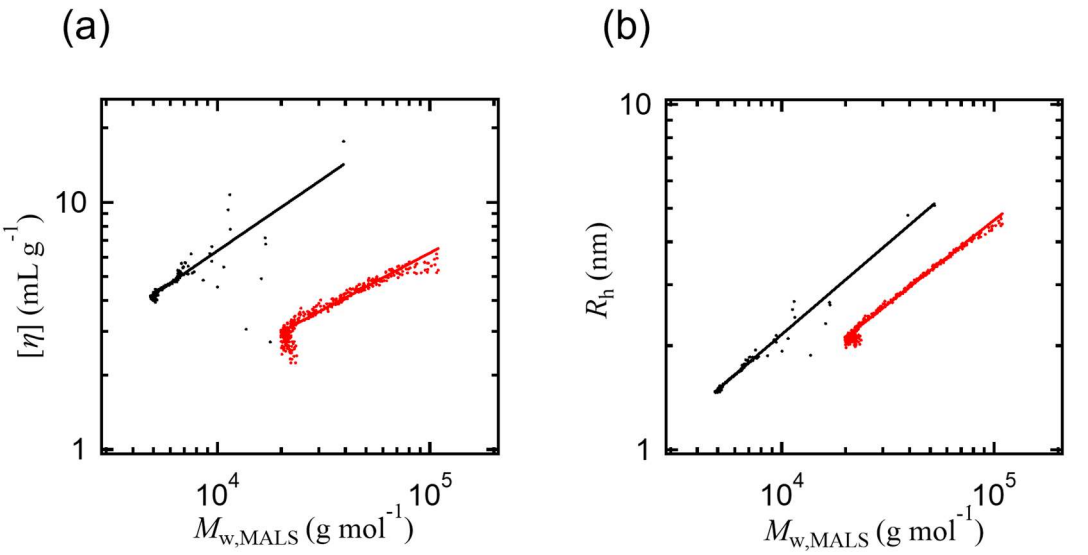

Figure 3.24. (a) Mark-Houwink-Sakurada plots and (b) conformation plots for HB-P(TA-*alt*-BO) ($M_{n,MALS}$ = 28,500 g mol^{-1}, red) and L-P(PA-*alt*-BO) ($M_{n,MALS}$ = 5,700 g mol^{-1}, black).

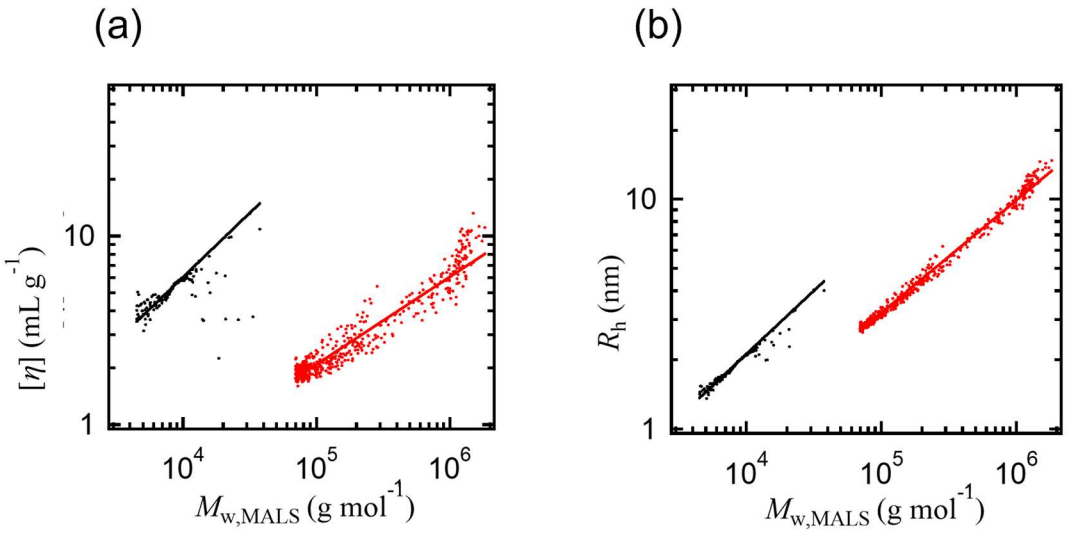

Figure 3.25. (a) Mark-Houwink-Sakurada plots and (b) conformation plots for HB-P(TA-*alt*-CHO) ($M_{n,MALS}$ = 98,600 g mol^{-1}, red) and L-P(PA-*alt*-CHO) ($M_{n,MALS}$ = 8,300 g mol^{-1}, black).

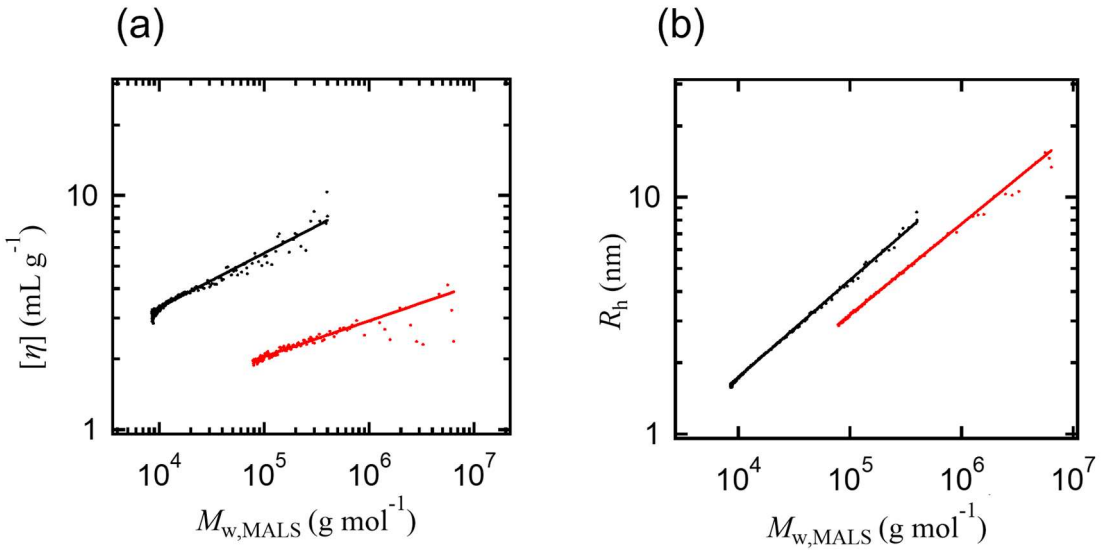

Figure 3.26. (a) Mark-Hauwink-Sakurada plots and (b) conformation plots for HB-P(TA-*alt*-DBGA) ($M_{n,MALS}$ = 134,000 g mol^{-1}, red) and L-P(PA-*alt*-DBGA) ($M_{n,MALS}$ = 13,300 g mol^{-1}, black).

3.3.5 Investigation of physical properties of linear and hyperbranched poly(cyclic anhydride-*alt*-epoxide)

Next, the thermal properties of the HBPEs were evaluated using differential scanning calorimetry (DSC). The HBPEs showed no transition because of crystallization and melting; only a glass transition temperature (T_g) was observed (**Table 3.1**; **Figures 3.27a** and **3.28–3.31**). The T_g value varied from −20.1 to 70.0 °C, depending on the structure of the epoxide monomer. Notably, HB-P(TA-*alt*-DBGA) showed the highest T_g among the HBPEs because of the presence of two benzene side chains on the polyester side chain. Generally, the T_g of HBPs is known to be lower than that of their corresponding linear counterparts owing to the increased number of highly mobile chain ends in the former.[40] Indeed, a comparison of the T_g values of HBPEs and their corresponding linear counterparts showed that HB-P(PA-*alt*-EGE), HB-P(PA-*alt*-BO), and HB-P(PA-*alt*-CHO) followed this rule. However, HB-P(TA-*alt*-PO) and HB-P(TA-*alt*-DBGA) exhibited higher T_g than those of the corresponding linear polyesters. To explain the higher T_g of these HBPEs, other factors such as molecular weight, end group, and intrinsic chemical composition need to be taken into account. Indeed, previous literatures found that these factors also affect the T_g of HBPs. The increased T_g of HB-P(TA-*alt*-PO) compared to that of its linear counterpart can be explained by the contribution from the end group; polar end group is known to increase the T_g of HBPs.[41] It is known that the end group of the polyester

obtained via ROAC mainly consists of carboxyl group when the anhydride is not fully consumed.[42] When synthesizing HB-P(TA-*alt*-PO), the conv.$_{TA}$ was 87%. Therefore, the end group is supposed to be mainly consisted of the carboxyl group, which is the main reason for the increased T_g. This result can also explain the large difference in the T_g values of HB-P(TA-*alt*-PO) and HB-P(TA-*alt*-BO). In contrast, the increased T_g of HB-P(TA-*alt*-DBGA) could be explained by its higher molecular weight compared to that of the liner counterpart. In addition, the densely attached benzene ring around the branching unit presumably restricts the chain motion, which might also contribute to increased T_g.

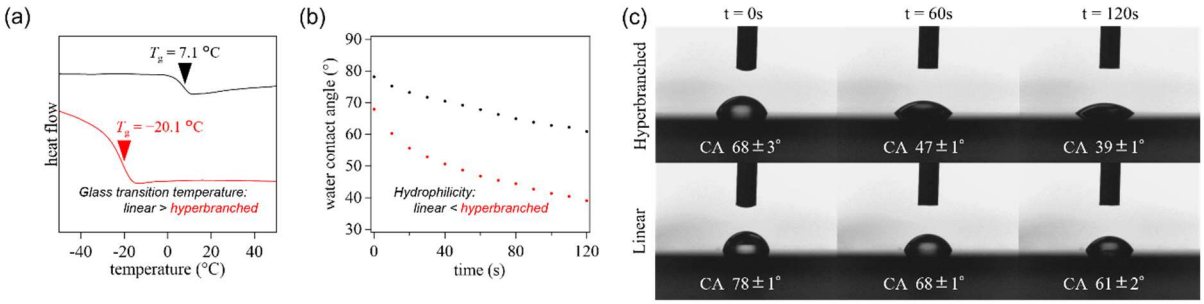

Figure 3.27. (a) DSC curve of HB-P(TA-*alt*-EGE) (red) and L-P(PA-*alt*-EGE) (black). (b) Contact angle versus time measurements of HB-P(TA-*alt*-EGE) (red) and L-P(PA-*alt*-EGE) (black). (c) Images used in the contact-angle analysis of HB-P(TA-*alt*-EGE) (upper) and L-P(PA-*alt*-EGE) (lower).

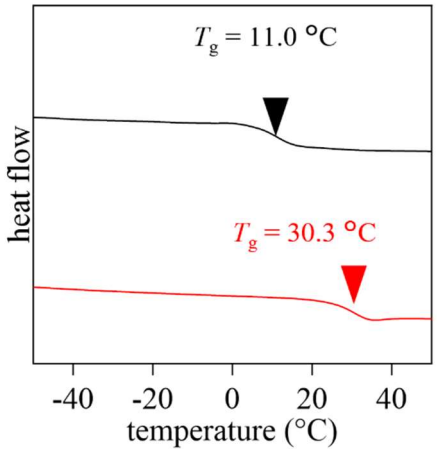

Figure 3.28. DSC curve of HB-P(TA-*alt*-PO) (red) and L-P(PA-*alt*-PO) (black).

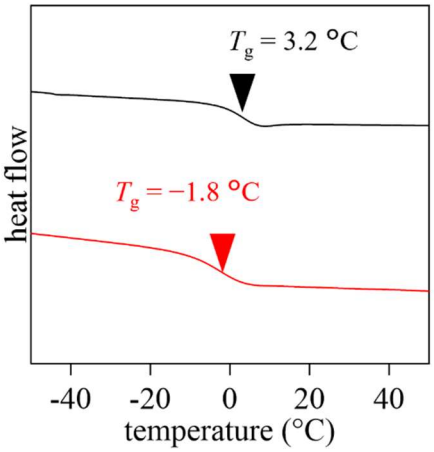

Figure 3.29. DSC curve of HB-P(TA-*alt*-BO) (red) and L-P(PA-*alt*-BO) (black).

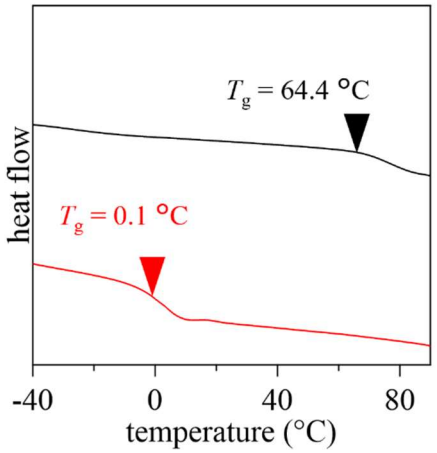

Figure 3.30. DSC curve of HB-P(TA-*alt*-CHO) (red) and L-P(PA-*alt*-CHO) (black).

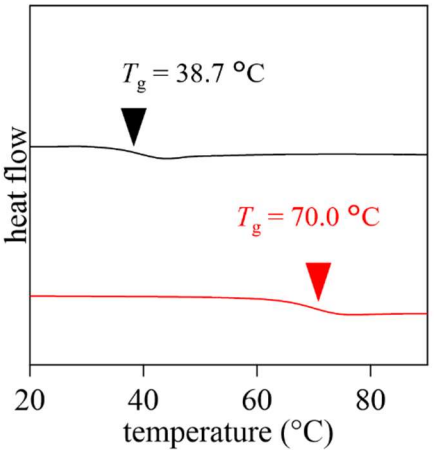

Figure 3.31. DSC curve of HB-P(TA-*alt*-DBGA) (red) and L-P(PA-*alt*-DBGA) (black).

Hence, based on these results, it can be suggested that the proposed method is an excellent strategy for synthesizing HBPEs with various thermal properties by simply changing the epoxide monomer.

Water contact angle (WCA) measurements were performed on the thin films of HBPE and its linear counterpart to further explore the characteristic properties stemming from the hyperbranched structure. Thin films were prepared by spin-coating the polymer solution in $CHCl_3$ onto a silicone substrate. The film thickness was in the range of 26–110 nm, as determined by reflectometry. As shown in **Figures 3.27b, c,** and **3.32–3.35**, the WCA of the HBPEs was always smaller than that of their linear counterparts, indicating that the hydrophilicity of the HBPEs was higher than that of their linear counterparts because of the presence of a large number of hydroxyl terminal groups. Additionally, these HBPEs are intrinsically much more hydrophilic than their linear counterparts because of the repeating units of the former contain tricarboxylate moieties. Such higher hydrophilicity of the HBPEs is interesting for their application as a coating material.

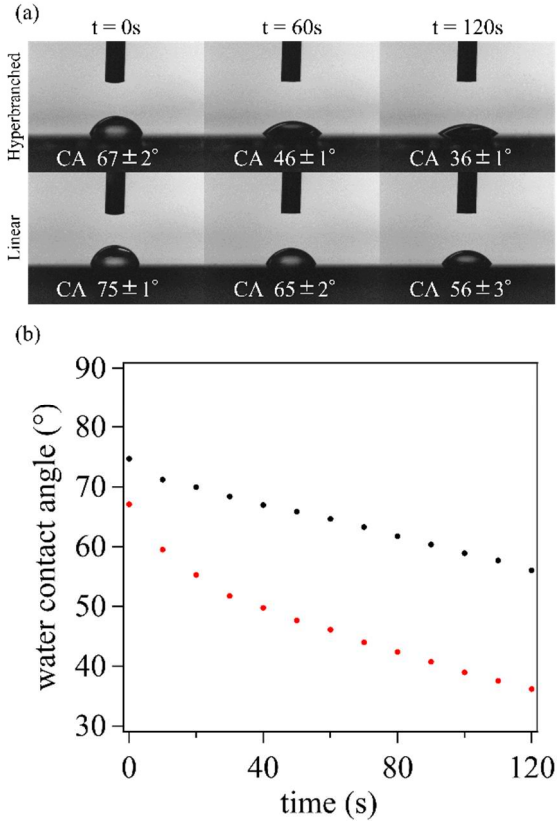

Figure 3.32. (a) contact angles versus time measurements of HB-P(TA-*alt*-PO) (red) and L-P(PA-*alt*-PO) (black). (b) Images used in the contact angle analysis of HB-P(TA-*alt*-PO) (upper) and L-P(PA-*alt*-PO) (lower).

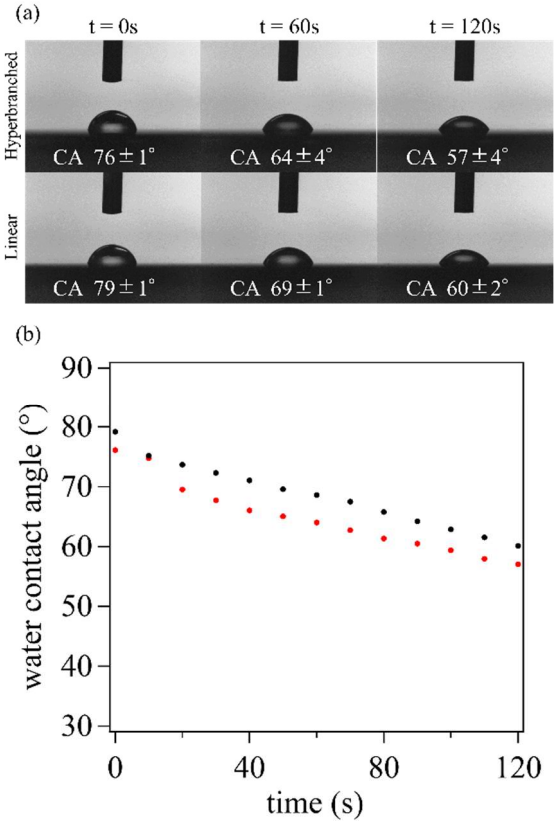

Figure 3.33. (a) contact angles versus time measurements of HB-P(TA-*alt*-BO) (red) and L-P(PA-*alt*-BO) (black). (b) Images used in the contact angle analysis of HB-P(TA-*alt*-BO) (upper) and L-P(PA-*alt*-BO) (lower).

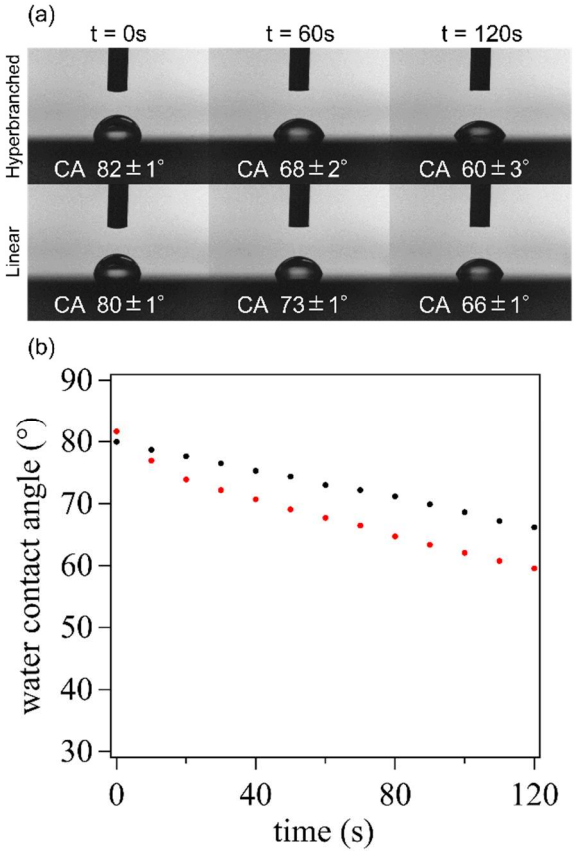

Figure 3.34. (a) contact angles versus time measurements of HB-P(TA-*alt*-CHO) (red) and L-P(PA-*alt*-CHO) (black). (b) Images used in the contact angle analysis of HB-P(TA-*alt*-CHO) (upper) and L-P(PA-*alt*-CHO) (lower).

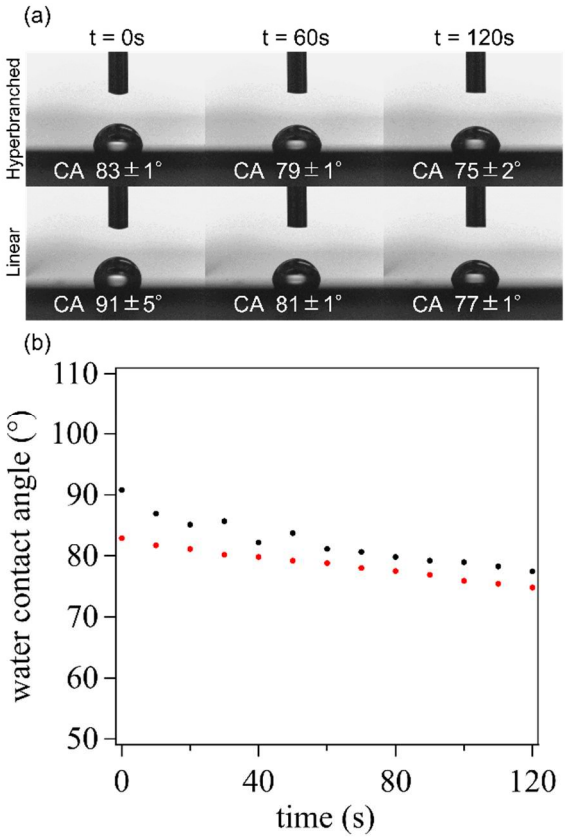

Figure 3.35. (a) contact angles versus time measurements of HB-P(TA-*alt*-DBGA) (red) and L-P(PA-*alt*-DBGA) (black). (b) Images used in the contact angle analysis of HB-P(TA-*alt*-DBGA) (upper) and L-P(PA-*alt*-DBGA) (lower).

3.3.6 Self-switchable polymerization of trimellitic anhydride, epoxide, and L-lactide

To expand on the synthesis of hyperbranched polyesters via ROAC, the author performed the terpolymerization of TA, EGE, and L-lactide (LLA), aiming at producing a core-shell type block copolymer. According to previous works, terpolymerization of cyclic anhydride, epoxide, and cyclic ester is proceeded ROAC, followed by ROP of cyclic ester, due to the reactivity differences between cyclic ester and cyclic anhydride.[35]

The terpolymerization of TA, EGE and LLA was performed in the presence of BDM and CsOPiv as an initiator and catalyst, respectively. As expected, when polymerization began, only conversion of TA was observed, suggesting that ROAC was proceeding first (**Figure 3.36**). After the complete consumption of TA, the conversion of LLA started, indicating a self-switching from ROAC to ROP. This resulted in the product being a core-shell type block copolymer, consisting of a hyperbranched P(TA-*alt*-EGE) [degree of branching (DB) of ~0.70] core and a PLLA outer shell. The ^{1}H NMR of the product showed signals derived from PLLA in addition to poly(TA-*alt*-EGE), confirming the formation of the target product (**Figure 3.37**). The SEC trace of the product showed a unimodal peak, confirming relatively controlled polymerization with $Đ$ of 1.36 (**Figure 3.38**). Thus, compared with conventional stepwise syntheses, the catalytic system provided an efficient and simple one-step procedure for the preparation of core−shell-type block copolymers.

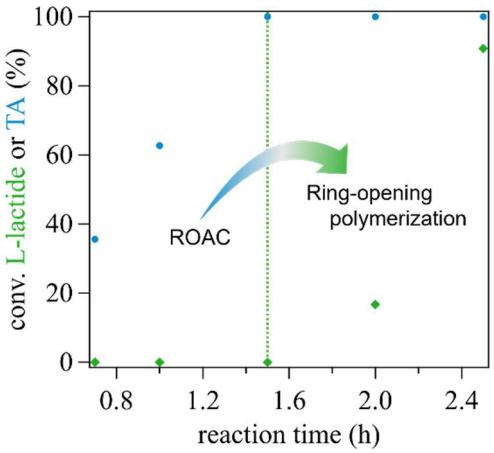

Figure 3.36. The time to conv. plots for the terpolymerization of TA, EGE, and LLA performed at 100 °C.

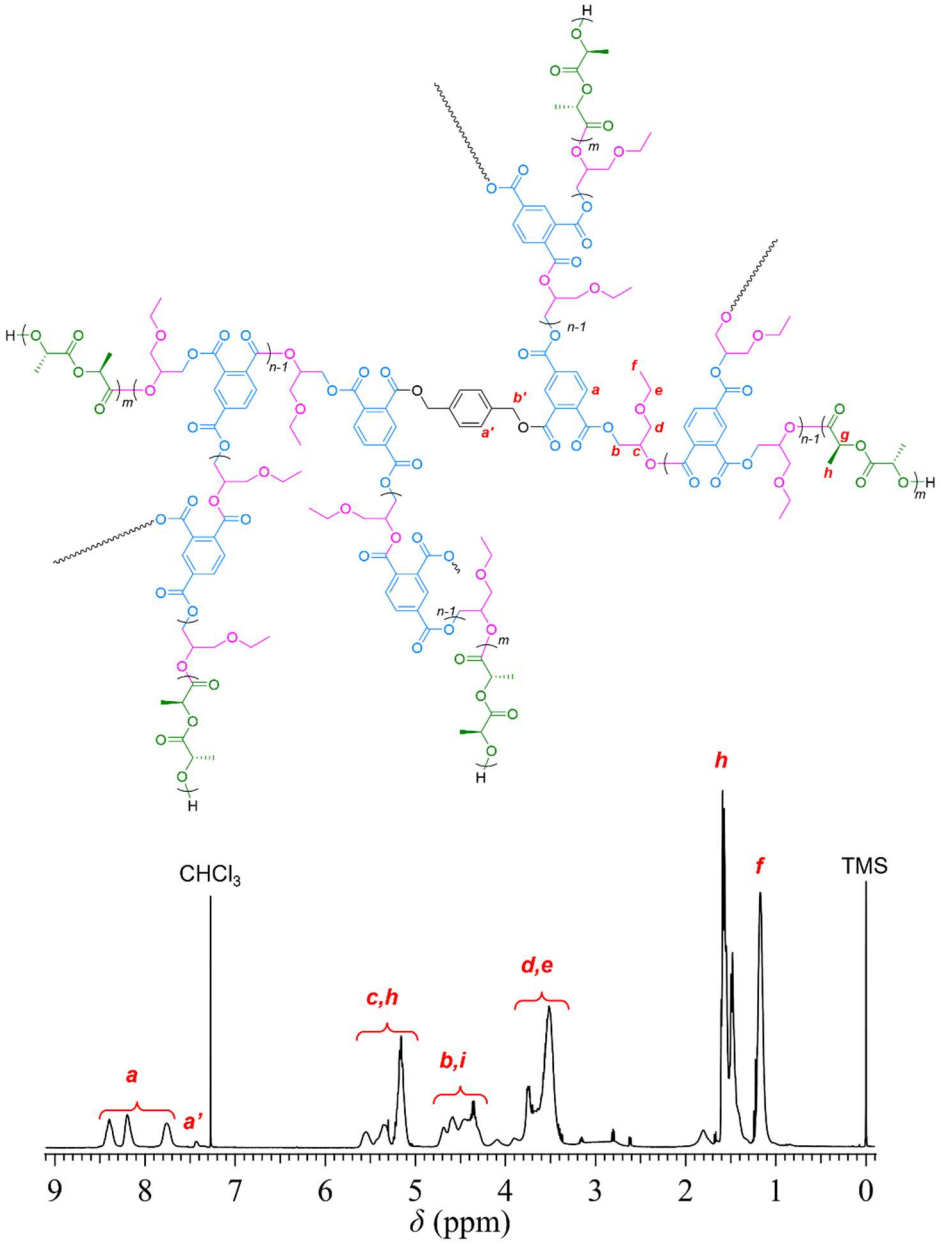

Figure 3.37. ^{1}H NMR spectrum of the core-shell type block copolymer (poly(TA-*alt*-EGE)-*b*-PLLA).

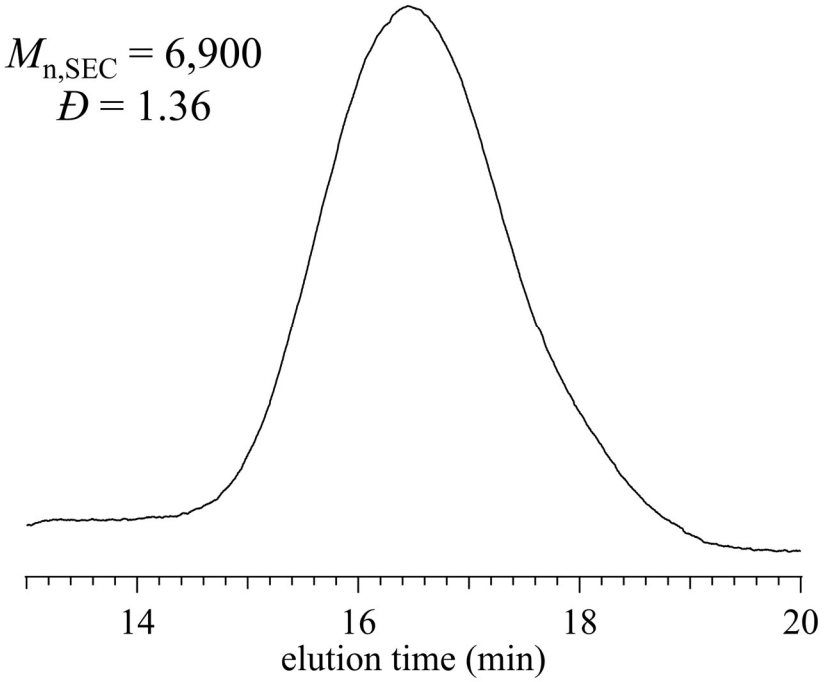

Figure 3.38. SEC trace of the core-shell type block copolymer (poly(TA-*alt*-EGE)-*b*-PLLA).

3.4 Conclusions

The author successfully demonstrated the cesium pivalate-catalyzed ROAC of TA with various epoxides in the presence of an alcohol initiator, leading to the formation of HBPEs. This is the first systematic study of the synthesis of HBPE based on ROAC. The HBPEs obtained via ROAC showed lower viscosity, smaller hydrodynamic radius, and higher hydrophobicity than those of their linear counterparts. By judiciously choosing anhydride and epoxide monomers and the alcohol initiator, the present approach can afford a variety of HBPEs with different backbone structures and architects, which will eventually allow the design of HBPEs with the desired properties and functions. This polymerization system is used for synthesizing core-shell type block polyester in a one-pot, one-step via terpolymerization of TA, epoxide, and LLA.

3.5 Reference

1 C. Gao and D. Yan. Hyperbranched polymers: from synthesis to applications. *Prog. Polym. Sci.* 2004, **29**, 183–275.

2 M. Jikei and M. Kakimoto. Hyperbranched polymers: a promising new class of materials. *Prog. Polym. Sci.* 2001, **26**,1233–1285.

3 P. Zhao, F. Mecozzi, S. Wessel, B. Fieten, M. Driesse, W. Woudstra, H. J. Busscher, H. C. van der Mei and T. J. A. Loontjens. Preparation and Evaluation of Antimicrobial Hyperbranched Emulsifiers for Waterborne Coatings. *Langmuir* 2019, **35**, 5779–5786.

4 E. Murillo and B. López. Waterborne hyperbranched alkyd-acrylic resin obtained by miniemulsion polymerization. *Polimeros* 2016, **26**, 343–351.

5 R. Hobzová, J. Peter and P. Sysel, *J. Macromol. Sci. C,* 2006, **102**, 906–913.

6 L. Xu and Z. Ye, *Chem. Commun. (Camb)*, 2013, **49**, 8800–8802.

7 L. J. Ma, H. Q. Wang, L. F. He and X. Y. Li. Hypervetvene polymery. *Chem Listy* 2008, 906–913.

8 J. Pan, L. Mei, H. Zhou, C. Zhang, Q. Xie and C. Ma. Self-regenerating zwitterionic hyperbranched polymer with tunable degradation for anti-biofouling coatings. *Prog. Org. Coat.* 2022, **163**, 106674.

9 S. E. Stiriba, H. Frey and R. Haag. Dendritic Polymers in Biomedical Applications: From Potential to Clinical Use in Diagnostics and Therapy. *Angew. Chem. Int. Ed.* 2002, **41**, 1329–1334.

10 S. Son, E. Shin and B.-S. Kim. Redox-Degradable Biocompatible Hyperbranched Polyglycerols: Synthesis, Copolymerization Kinetics, Degradation, and Biocompatibility. *Macromolecules* 2015, **48**, 600–609.

11 V. T. Wyatt, A. Nuñez, T. A. Foglia and W. N. Marmer. Synthesis of Hyperbranched Poly(glycerol-diacid) Oligomers. *J. Am. Oil Chem. Soc.* 2006, **83**, 1033–1039.

12 X. Gao, X. Zhang, Z. Wu, X. Zhang, Z. Wang and C. Li. Synthesis and physicochemical characterization of a novel amphiphilic polylactic acid-hyperbranched polyglycerol conjugate for protein delivery. *J. Control. Release* 2009, **140**, 141–147.

13 R. H. Kienle and A. G. Hovey. THE POLYHYDRIC ALCOHOL-POLYBASIC ACID REACTION. I. GLYCEROL-PHTHALIC ANHYDRIDE. *J. Am. Chem. Soc.* 1929, **51**, 509–519.

14 X. Zhang. Synthesis and Characterization of Hyperbranched Polyesters Based on Isophthalic Acid and Trimethylolpropane. *Journal of Macromolecular Science Part A*, 2010, **48**, 128–134.

15 R. H. Kienle, P.A. van der. Meulen and F. E. Petke. The polyhydric alcohol-polybasic acid reaction. III. Further studies of the glycerol-phthalic anhydride reaction. *J. Am. Chem. Soc.* 1939, **61**, 2258–2268.

16 S. R. Turner, B. I. Voit and T. H. Mourey. All-aromatic hyperbranched polyesters with phenol and acetate end groups: synthesis and characterization. *Macromolecules* 1993, **26**, 4617–4623.

17 D. Yan and C. Gao. Hyperbranched Polymers Made from A_2 and BB'_2 Type Monomers. 1. Polyaddition of 1-(2-Aminoethyl)piperazine to Divinyl Sulfone. *Macromolecules* 2000, **33**, 7693–7699.

18 M. Liu, N. Vladimirov and J. M. J. Fréchet. A new approach to hyperbranched polymers by ring-opening polymerization of an AB monomer: 4-(2-hydroxyethyl)-epsilon-caprolactone. *Macromolecules* 1999, **32**, 6881–6884.

19 M. Trollsås, P. Löwenhielm, V. Y. Lee, M. Möller, R. D. Miller and J. L. Hedrick. New Approach to Hyperbranched Polyesters: Self-Condensing Cyclic Ester Polymerization of Bis(hydroxymethyl)-Substituted ε-Caprolactone. *Macromolecules* 1999, **32**, 9062–9066.

20 X. H. Yu, J. Feng and R. X. Zhuo. Preparation of Hyperbranched Aliphatic Polyester Derived from Functionalized 1,4-Dioxan-2-one. *Macromolecules* 2005, **38**, 6244–6247.

21 P. G. Parzuchowski, M. Grabowska, M. Tryznowski and G. Rokicki. Synthesis of Glycerol Based Hyperbranched Polyesters with Primary Hydroxyl Groups. *Macromolecules* 2006, **39**, 7181–7186.

22 J. M. Longo, M. J. Sanford and G. W. Coates. Ring-Opening Copolymerization of Epoxides and Cyclic Anhydrides with Discrete Metal Complexes: Structure–Property Relationships. *Chem. Rev.* 2016, **116**, 15167–15197.

23 S. Paul, Y. Zhu, C. Romain, R. Brooks, P. K. Saini and C. K. Williams. Ring-opening copolymerization (ROCOP): synthesis and properties of polyesters and polycarbonates. *Chem. Commun.* 2015, **51**, 6459–6479.

24 B. Han, L. Zhang, B. Liu, X. Dong, I. Kim, Z. Duan and P. Theato. Controllable Synthesis of Stereoregular Polyesters by Organocatalytic Alternating Copolymerizations of Cyclohexene Oxide and Norbornene Anhydrides. *Macromolecules* 2015, **48**, 3431–3437.

25 R. C. Jeske, A. M. DiCiccio, and G. W. Coates. Alternating Copolymerization of Epoxides and Cyclic Anhydrides: An Improved Route to Aliphatic Polyesters. *J. Am. Chem. Soc.* 2007, **129**, 11330–11331.

26 H.-Y. Ji, X.-L. Chen, B. Wang, L. Pan, and Y. S. Li. Metal-free, regioselective and stereoregular alternating copolymerization of monosubstituted epoxides and tricyclic anhydrides. *Green Chem.* 2018, **20**, 3963–3973.

27 J. Xu, X. Wang and N. Hadjichristidis. Diblock dialternating terpolymers by one-step/one-pot highly selective organocatalytic multimonomer polymerization. *Nat. Commun.* 2021, **12**, 7124.

28 L. Hu, X. Zhang, X. Cao, D. Chen, Y. Sun, C. Zhang, and X. Zhang. Alternating Copolymerization of Isobutylene Oxide and Cyclic Anhydrides: A New Route to Semicrystalline Polyesters. *Macromolecules* 2021, **54**, 6182–6190.

29 W. T. Diment, G. L. Gregory, R. W. F. Kerr, A. Phanopoulos, A. Buchard, and C. K. Williams. Catalytic Synergy Using Al(III) and Group 1 Metals to Accelerate Epoxide and Anhydride Ring-Opening Copolymerizations. *ACS Catal*., 2021, **11**, 12532–12542.

30 X. Liang, F. Tan, and Y. Zhu. Recent Developments in Ring-Opening Copolymerization of Epoxides With CO_2 and Cyclic Anhydrides for Biomedical Applications. *Front. Chem.* 2021, **9**, 647245.

31 G.-H. He, B.-H. Ren, S.-Y. Chen, Y. Liu, X.-B. Lu. Enantioselective, Stereoconvergent Resolution Copolymerization of Racemic *cis*-Internal Epoxides and Anhydrides. *Angew. Chem. Int. Ed.* 2021, **60**, 5994–6002.

32 J. Li, Y. Liu, W.-M. Ren, and X.-B. Lu. Asymmetric Alternating Copolymerization of Meso-epoxides and Cyclic Anhydrides: Efficient Access to Enantiopure Polyesters. *J. Am. Chem. Soc.* 2016, **138**, 11493–11496.

33 J. M. Longo, A. M. DiCiccio and G. W. Coates. Poly(propylene succinate): A New Polymer Stereocomplex. *J. Am. Chem. Soc.* 2014, **136**, 15897–15900

34 C. A. L. Lidston, B. A. Abel and G. W. Coates. Bifunctional Catalysis Prevents Inhibition in Reversible-Deactivation Ring-Opening Copolymerizations of Epoxides and Cyclic Anhydrides. *J. Am. Chem. Soc.* 2020, **142**, 20161–20169.

35 X. Xia, R. Suzuki, K. Takojima, D. H. Jiang, T. Isono and T. Satoh. Smart Access to Sequentially and Architecturally Controlled Block Polymers via a Simple Catalytic Polymerization System. *ACS Catal.* 2021, **11**, 5999–6009.

36 T. Gao, X. Xia, K. Tajima, T. Yamamoto, T. Isono and T. Satoh. Polyether/Polythioether Synthesis via Ring-Opening Polymerization of Epoxides and Episulfides Catalyzed by Alkali Metal Carboxylates. *Macromolecules* 2022, **55**, 9373–9383.

37 C.-M. Chen, X. Xu, H.-Y. Ji, B. Wang, L. Pan, Y. Luo, and Y.-S. Li. Alkali Metal Carboxylates: Simple and Versatile Initiators for Ring-Opening Alternating Copolymerization of Cyclic Anhydrides/Epoxides. *Macromolecules* **54**, 713–724.

38 J. K. Oh. Polylactide (PLA)-based amphiphilic block copolymers: synthesis, self-assembly, and biomedical applications. *Soft Matter* 2011, **7**, 5096–5108.

39 T. Isono, S. Asai, Y. Satoh, T. Takaoka, K. Tajima, T. Kakuchi and T. Satoh. Controlled/Living Ring-Opening Polymerization of Glycidylamine Derivatives

Using *t*-Bu-P_4/Alcohol Initiating System Leading to Polyethers with Pendant Primary, Secondary, and Tertiary Amino Groups. *Macromolecules* 2015, **48**, 3217–3229.

40 G. C. Behera, A. Saha and S. Ramakrishnan. Hyperbranched Copolymers versus Linear Copolymers: A Comparative Study of Thermal Properties. *Macromolecules* 2005, **38**, 7695–7701.

41 A. Hult, M. Johansson and E. Malmström. Hyperbranched Polymers. *Branched Polym.* 1999, **II**, 1–34.

42 H. Li, J. Zhao, and G. Zhang. Self-Buffering Organocatalysis Tailoring Alternating Polyester. *ACS Macro Lett.* 2017, **6**, 1094–1098.

43 A. E. Speers, G. C. Adam, B. F. Cravatt. Activity-based protein profiling in vivo using a copper(i)-catalyzed azide-alkyne [3 + 2] cycloaddition. *J. Am. Chem. Soc.* **2003**, *125* (16), 4686–4687.

Chapter 4

One-step Synthesis of
Polyester-based Hot-melt Adhesives
using Self-switching System
Consisting of ROAC and ROP

4.1 Introduction

Polymer products such as plastics, elastomers, and fibers are essential for daily life. However, most of these polymer materials are derived from petroleum-based monomers such as styrene, ethylene, and propylene. Because mitigating the dependence on petroleum resources is essential for creating a sustainable society, interest in sustainable plastics as a solution to this pervasive global problem has been increasing in recent years, with polyester (PE) emerging as one of the most sustainable polymers. Poly(lactide) (PLA) is a well-known sustainable polymer material because it is derived from renewable resources and is biodegradable. However, a significant drawback of PLA is its brittleness, which limits its industrial application as a sustainable alternative to conventional petroleum-based polymers. Therefore, the development of a new strategy for improving the physical properties of PLA is urgently needed to expand its possible application range.

Block copolymerization is an attractive approach for enhancing the properties and functionalities of polymers. For example, block copolymers consisting of PLA and poly(ε-caprolactone) (PCL) have been studied for aiming at using as thermoplastic elastomers, compatibilizers, and shape memory materials.[1–6] Additionally, combining PLA with the other bio-based PEs, e.g. polymenthide and poly(γ-methyl-ε-caprolactone), have also been investigated for various applications, including pressure-sensitive adhesives and tough

plastics.[7,8]

To further expand the potential of PLA through block copolymerization, the author used ring-opening alternating copolymerization (ROAC) to synthesize counter PE blocks. As mentioned previously, the ROAC of cyclic anhydrides and epoxides has attracted attention as a useful method for the precise synthesis of PEs.[9–15] As ROAC arranges the two types of monomers in an alternating sequence, it readily produces PEs with diverse repeating structures, realizing tunable properties depending on the combination of the two monomers. Because of this advantage, ROAC has recently been applied to the design of novel PE-based materials. For example, Williams et al. reported the synthesis of BAB-type triblock copolymers composed of poly(ε-decalactone) (PDL; A soft segment) and poly(anhydride-*alt*-epoxide) (B hard segment), i.e., poly(anhydride-*alt*-epoxide)-*b*-PDL-*b*-poly(anhydride-*alt*-epoxide), through a one-pot, two-step monomer addition method and demonstrated their use as pressure-sensitive adhesives.[16] Similarly, the same group successfully developed thermoplastic elastomers using the ROAC approach.[17,18] Therefore, linking diverse PE syntheses via ROAC with the development of PLA-based block copolyesters can lead to the creation of novel functional sustainable polymer materials.

Self-switchable polymerization is an emerging method for synthesizing block copolymers in a one-pot, one-step process involving the reaction of multiple monomers with significantly

different reactivities, which allows the polymerization reactions to switch automatically according to differences in reactivity.[19–24] For example, Williams and co-workers, pioneers in self-switchable polymerization, have synthesized poly(maleic anhydride-*alt*-propylene oxide)-*b*-poly(L-lactide) through the self-switchable polymerization of maleic anhydride, propylene oxide, and L-lactide (LLA), demonstrating its potential as an additive to enhance the properties of poly(L-lactide) (PLLA).[25] In Chapter 3, the author has demonstrated a one-pot, one-step block copolymer synthesis from a mixture of cyclic anhydride, epoxide, and LLA using an alkali metal carboxylate as a catalyst.[20] By optimizing the soft segment properties by the judicious choice of cyclic anhydride and epoxide, the author obtained PLLA-containing block copolymers that exhibited thermoplastic elastomer-like properties owing to the microphase separation between the soft segment and PLLA blocks. Thus, self-switchable polymerization based on ROAC has great potential in the design and development of novel sustainable polymer materials.

Hot-melt adhesives are widely used in industrial fields, and many rely on petroleum-based polymers such as vinyl polymers, necessitating a shift toward sustainable PEs. In this study, the author aimed to develop a sustainable alternative to conventional hot-melt adhesives using a self-switchable polymerization approach. Thermoplastic elastomers with a “hard-soft-hard” type triblock architecture, such as polystyrene-*b*-polyisoprene-*b*-polystyrene, have been widely

used as hot-melt adhesives. Based on similar concepts, hard PLLA segments attached to both ends of a ROAC-derived soft segment can function as an adhesive.

In this chapter, the author utilized the self-switchable polymerization of cyclic anhydride, epoxide, and LLA to develop hot-melt adhesives with a high biomass content (**Scheme 4.1**). By changing the initiator, cyclic anhydride, and epoxide, the author successfully synthesized a variety of copolyesters consisting of PLLA segments with various repeating structures, molecular weights, compositions, and architectures. Lap shear tests revealed that some of the synthesized copolyesters exhibited sufficient adhesive performance to a wooden substrate, which could potentially substitute commercial products such as PE-based and poly(vinyl acetate) (PVAc)-based hot-melt adhesives.

Scheme 4.1. One-pot, one-step synthesis of polyester adhesives via self-switchable polymerization

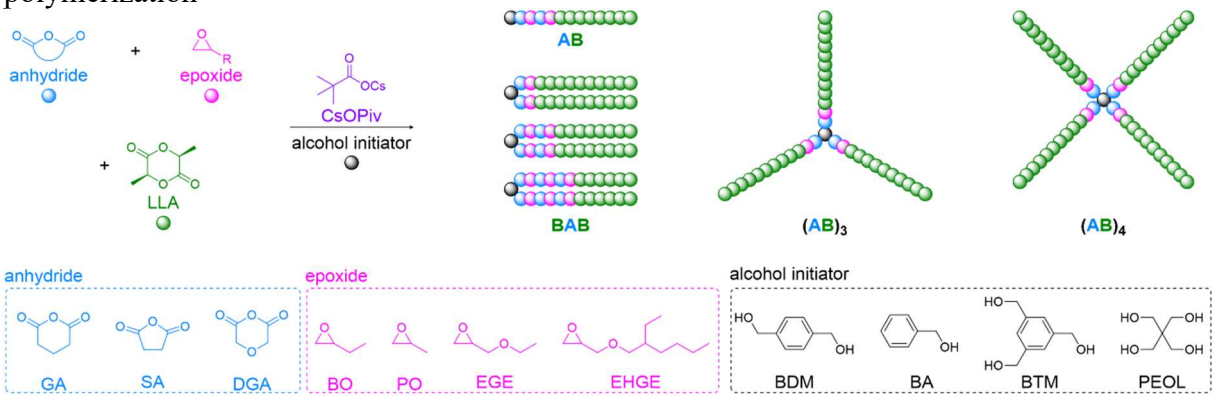

4.2 Experimental section

4.2.1 Materials

L-Lactide (LLA; >98.0%, Tokyo Kasei Kogyo Co., Ltd. (TCI)) was purified by recrystallization from dry toluene twice. 1,2-Butylene oxide (BO; >99.0%, TCI), 2-ethylhexyl glycidyl ether (EHGE; >98.0%, TCI), and ethyl glycidyl ether (EGE; >98.0%, TCI) were distilled over CaH_2 under reduced pressure and stored under argon atmosphere. Propylene oxide (PO; >99.0%, TCI) was distilled over CaH_2 and stored under argon atmosphere. Succinic anhydride (SA; >95.0%, TCI), diglycolic anhydride (DGA; >98.0%, TCI), and glutaric anhydride (GA; >98.0%, TCI) were purified by sublimation under reduced pressure. Cesium pivalate (CsOPiv; >97.0%, TCI) was dried by heating at 100 °C under high vacuum for at least 72 h before use. Benzyl alcohol (BA; >99.0%, TCI), 1,4-benzenedimethanol (BDM; >99.0%, TCI), 1,3,5-benzenetrimethanol (BTM; >95.0%, TCI), and pentaerythritol (PEOL; >98.0%, TCI) were used as received.

4.2.2 Instruments

Polymerization mixture was prepared in an MBRAUN stainless steel glovebox equipped with a gas purification system (molecular sieves and copper catalyst) in a dry argon atmosphere (H_2O, O_2 <0.1 ppm). The moisture and oxygen contents in the glovebox were monitored by MB-MO-SE-1 and MB-OX-SE-1, respectively.

^1H, ^{13}C, and DOSY NMR. The ^1H (400 MHz) and ^{13}C (100 MHz) NMR spectra were recorded using a JEOL JNM-ECS400 instrument. The diffusion-ordered NMR (DOSY) spectrum was recorded using a JEOL JNM-ECZ600R (600 MHz) instrument. DOSY analysis was carried out at 30 °C using the ledbpgp2s sequence with at least 15 gradient increments.

Size elution chromatography (SEC). The size exclusion chromatography (SEC) was performed at 40 °C in THF (flow rate, 1.0 mL min^{-1}) using a Jasco high-performance liquid chromatography system (PU-4180 HPLC pump, AS-4550 auto sampler, and CO-4060 column oven) equipped with a Shodex K-800D guard column (8.0 mm × 100 mm; particle size, 10 μm), two Shodex columns (K-806L and K-804L; linear, 8.0 mm × 100 mm; particle size, 10 μm).

Differential scanning calorimetry (DSC). The DSC experiments were performed using a Hitachi High-Tech Science DSC 7000X under a nitrogen atmosphere. The samples were pre-heated by hot-pressing at 100 °C, following the same preparation as for the lap shear tensile test, and then agedat 10 °C for 7 days. After aging, the thin films were subjected to the DSC

measument, where the sample was firstly cooled to −100 °C and heated to 180 °C at the cooling and heating rate of 10 °C min^{-1}.

Thermogravimetric analysis (TGA). The TGA experiments were performed using a Hitachi High-Tech Science STA200RV under nitrogen atmosphere. The samples were heated from 30 °C to 600 °C at the heating rate of 10 °C min^{-1}.

Lap shear adhesive test. The adhesive property was evaluated by lap shear adhesive tests. Four different kinds of adherents were used including wood (Beech; 25 mm × 50mm × 4 mm), aluminum (Al; 25 mm × 50mm × 2 mm), iron (Fe; 25 mm × 50mm × 1.6 mm), glass (25 mm × 50mm × 2 mm), and poly(ethylene terephthalate) (25 mm × 50mm × 0.1 mm). The samples for the lap shear test were obtained as follows: the polymer was hot-pressed at 100 °C to produce 300 μm thick film, which was then cut into 12.5 mm × 25.0 mm. The cut films were sandwiched between the two adherents of the same kind, which were swiped using methanol to remove impurities before used, and pressed at 100 °C again. The sandwiched plates were kept at room temperature for seven days before tests. Lap shear adhesive test was carried out following JIS K 6850:1999 using an Instron 34SC-1 at room temperature. At least three samples were tested for each polymer.

4.2.3 Synthesis detail

4.2.3.1 Typical synthesis of the block copolyesters via self-switchable polymerization

・Synthesis of PLLA-*tb*-poly(GA-*alt*-BO)-*tb*-PLLA (P1)

A typical polymerization procedure is given as follows: In an argon-filled glovebox, BDM (41.4mg, 300 μmol), CsOPiv (70.2 mg, 300 μmol), GA (685 mg, 6.00 mmol), LLA (4.76 g, 33.0 mmol), and BO (1.73 g, 24.0 mmol) were added to the reaction vessel and sealed with a greaseless valve. After removing the vessel from the glovebox, the reaction mixture was stirred at 100 °C in an oil bath. After 5.5 h, crude aliquot was withdrawn from the system by pipette and monitored by ^{1}H NMR spectroscopy in $CDCl_3$ to determine the monomer conversions. The reaction mixture was diluted with small amount of dichloromethane to terminate the polymerization. The crude polymer was purified by reprecipitation in cold methanol to give poly(L-lactide)-*tapered block*-poly(glutaric anhydride-*alternating*-butylene oxide)-*tapered block*-poly(L-lactide) (PLLA-*tb*-poly(GA-*alt*-BO)-*tb*-PLLA) as a colorless solid. Yield: 4.94 g, 83.5%.

$M_{n,NMR}$ = 17,800 g mol^{-1} ($CDCl_3$), $M_{n,SEC}$ = 3,990 g mol^{-1} (THF), $Đ$ = 1.72 (THF)

・**Synthesis of PLLA-*b*-poly(SA-*alt*-BO)-*b*-PLLA (P6)**

PLLA-*block*-poly(SA-*alt*-BO)-*block*-PLLA (PLLA-*b*-poly(SA-*alt*-BO)-*b*-PLLA) was synthesized in the same way, excepting the cyclic anhydride monomer and the molar ratio of the reactants; BDM (41.4 mg, 300 μmol), CsOPiv (70.2 mg, 300 μmol), SA (691 mg, 6.90 mmol), LLA (4.76 g, 33.0 mmol), and BO (1.99 g, 27.6 mmol). After 6 h, the reaction mixture was diluted with small amount of dichloromethane and purified by reprecipitation in cold methanol to PLLA-*b*-poly(SA-*alt*-BO)-*b*-PLLA as a black powder. Yield: 5.77 g, 96.4%.

$M_{n,NMR}$ = 20,000 g mol^{-1} ($CDCl_3$), $M_{n,SEC}$ = 8,610 g mol^{-1} (THF), $Đ$ = 1.46 (THF)

・**Synthesis of PLLA-*b*-poly(DGA-*alt*-BO)-*b*-PLLA (P7)**

PLLA-*b*-poly(DGA-*alt*-BO)-*b*-PLLA was synthesized in the same way, excepting the cyclic anhydride monomer and the molar ratio of the reactants; BDM (20.7 mg, 150 μmol), CsOPiv (35.1 mg, 150 μmol), DGA (348 mg, 3.00 mmol), LLA (2.38 g, 16.5 mmol), and BO (865 mg, 12.0 mmol). After 3.5 h, the reaction mixture was diluted with small amount of dichloromethane and purified by reprecipitation in cold methanol to PLLA-*b*-poly(DGA-*alt*-BO)-*b*-PLLA as a colorless solid. Yield: 2.80 g, 94.6%.

$M_{n,NMR}$ = 23,700 g mol^{-1} ($CDCl_3$), $M_{n,SEC}$ = 11,200 g mol^{-1} (THF), $Đ$ = 1.18 (THF)

・Synthesis of PLLA-*b*-poly(GA-*alt*-PO)-*b*-PLLA (P8)

PLLA-*tb*-poly(GA-*alt*-PO)-*tb*-PLLA was synthesized in the same way, excepting the cyclic anhydride monomer and the molar ratio of the reactants; BDM (27.6 mg, 200 μmol), CsOPiv (46.8 mg, 200 μmol), GA (571 mg, 5.00 mmol), LLA (3.17 g, 22.0 mmol), and PO (1.16 g, 20.0 mmol). After 5 h, the reaction mixture was diluted with small amount of dichloromethane and purified by reprecipitation in cold methanol to PLLA-*tb*-poly(GA-*alt*-PO)-*tb*-PLLA as a colorless solid. Yield: 3.72 g, 91.6%.

$M_{n,NMR}$ = 22,800 g mol^{-1} ($CDCl_3$), $M_{n,SEC}$ = 5,380 g mol^{-1} (THF), $Đ$ = 1.51 (THF)

・Synthesis of PLLA-*b*-poly(GA-*alt*-EGE)-*b*-PLLA (P9)

PLLA-*tb*-poly(GA-*alt*-EGE)-*tb*-PLLA was synthesized in the same way, excepting the epoxide monomer and the molar ratio of the reactants; BDM (27.6 mg, 200 μmol), CsOPiv (46.8 mg, 200 μmol), GA (456 mg, 4.00 mmol), LLA (3.17 g, 22.0 mmol), and EGE (1.63 g, 16.0 mmol). After 4 h, the reaction mixture was diluted with small amount of dichloromethane and purified by reprecipitation in cold methanol to PLLA-*tb*-poly(GA-*alt*-EGE)-*tb*-PLLA as a colorless solid. Yield: 4.20 g, 98.2%.

$M_{n,NMR}$ = 24,700 g mol^{-1} ($CDCl_3$), $M_{n,SEC}$ = 4,160 g mol^{-1} (THF), $Đ$ = 1.84 (THF)

・**Synthesis of PLLA-*b*-poly(GA-*alt*-EHGE)-*b*-PLLA (P10)**

PLLA-*tb*-poly(GA-*alt*-EHGE)-*tb*-PLLA was synthesized in the same way, excepting the epoxide monomer and the molar ratio of the reactants; BDM (27.6 mg, 200 μmol), CsOPiv (46.8 mg, 200 μmol), GA (342 mg, 3.00 mmol), LLA (3.46 g, 24.0 mmol), and EHGE (2.24 g, 24.0 mmol). After 6.5 h, the reaction mixture was diluted with small amount of dichloromethane and purified by reprecipitation in cold methanol to PLLA-*tb*-poly(GA-*alt*-EHGE)-*tb*-PLLA as a colorless solid. Yield: 3.80 g, 86.6%.

$M_{n,NMR}$ = 23,000 g mol^{-1} ($CDCl_3$), $M_{n,SEC}$ = 8,260 g mol^{-1} (THF), $Đ$ = 1.39 (THF)

・**Synthesis of AB-type poly(GA-*alt*-BO)-*tb*-PLLA (P11)**

Poly(GA-*alt*-BO)-*tb*-PLLA was synthesized in the same way, excepting the initiator and the molar ratio of the reactants; BA (32.4 mg, 300 μmol), CsOPiv (70.2 mg, 300 μmol), GA (411 mg, 3.60 mmol), LLA (2.59 g, 18.0 mmol), and BO (1.04 g, 14.4 mmol). After 5.5 h, the reaction mixture was diluted with small amount of dichloromethane and purified by reprecipitation in cold methanol to poly(GA-*alt*-BO)-*tb*-PLLA as a colorless solid. Yield: 2.23 g, 67.6%.

$M_{n,NMR}$ = 10,800 g mol^{-1} ($CDCl_3$), $M_{n,SEC}$ = 5,060 g mol^{-1} (THF), $Đ$ = 1.59 (THF)

・Synthesis of (poly(GA-*alt*-BO)-*tb*-PLLA)$_3$ (P12)

(poly(GA-*alt*-BO)-*tb*-PLLA)$_3$ was synthesized in the same way, excepting the initiator and the molar ratio of the reactants; BTM (16.8 mg, 100 μmol), CsOPiv (23.4 mg, 100 μmol), GA (399 mg, 3.50 mmol), LLA (2.45 g, 17.0 mmol), and BO (1.01 g, 14.0 mmol). After 8.0 h, the reaction mixture was diluted with small amount of dichloromethane and purified by reprecipitation in cold methanol to (poly(GA-*alt*-BO)-*tb*-PLLA)$_3$ as a colorless solid. Yield: 2.61 g, 83.8%.

$M_{n,NMR}$ = 32,600 ($CDCl_3$), $M_{n,SEC}$ = 8,110 g mol^{-1} (THF), $Đ$ = 1.22 (THF)

・Synthesis of PLLA-*tb*-poly(GA-*alt*-BO)-*tb*-PLLA (10k) (P13)

PLLA-*tb*-poly(GA-*alt*-BO)-*tb*-PLLA (10k) was synthesized in the same way, excepting the molar ratio of the reactants; BDM (69.1 mg, 500 μmol), CsOPiv (117 mg, 500 μmol), GA (571 mg, 5.00 mmol), LLA (3.96 g, 27.5 mmol), and BO (1.44 g, 20.0 mmol). After 4 h, the reaction mixture was diluted with small amount of dichloromethane and purified by reprecipitation in cold methanol to PLLA-*tb*-poly(GA-*alt*-BO)-*tb*-PLLA (10k) as a colorless solid. Yield: 4.96 g, 99.8%.

$M_{n,NMR}$ = 11,800 g mol^{-1} ($CDCl_3$), $M_{n,SEC}$ = 2,180 g mol^{-1} (THF), $Đ$ = 2.12 (THF)

・**Synthesis of PLLA-*tb*-poly(GA-*alt*-BO)-*tb*-PLLA (40k) (P14)**

PLLA-*tb*-poly(GA-*alt*-BO)-*tb*-PLLA (40k) was synthesized in the same way, excepting the molar ratio of the reactants; BDM (27.6 mg, 200 μmol), CsOPiv (46.8 mg, 200 μmol), GA (958 mg, 8.40 mmol), LLA (6.34 g, 44.0 mmol), and BO (2.42 g, 33.6 mmol). After 9 h, the reaction mixture was diluted with small amount of dichloromethane and purified by reprecipitation in cold methanol to PLLA-*tb*-poly(GA-*alt*-BO)-*tb*-PLLA (40k) as a colorless solid. Yield: 7.52 g, 94.7%.

$M_{n,NMR}$ = 38,100 g mol^{-1} ($CDCl_3$), $M_{n,SEC}$ = 6,510 g mol^{-1} (THF), $Đ$ = 1.53 (THF)

・**Synthesis of (poly(GA-*alt*-BO)-*tb*-PLLA)$_4$ (80k) (P15)**

(poly(GA-*alt*-BO)-*tb*-PLLA)$_4$ (80k) was synthesized in the same way, excepting the initiator and the molar ratio of the reactant; PET (9.5 mg, 70 μmol), CsOPiv (16.4 mg, 70 μmol), GA (671 mg, 5.88 mmol), LLA (4.44 g, 30.8 mmol), and BO (1.70 g, 23.5 mmol). After 23 h, the reaction mixture was diluted with small amount of dichloromethane and purified by reprecipitation in cold methanol to (poly(GA-*alt*-BO)-*tb*-PLLA)$_4$ (80k) as a colorless solid. Yield: 4.96 g, 89.4%.

$M_{n,NMR}$ = *N.D.*, $M_{n,SEC}$ = 9,170 g mol^{-1} (THF), $Đ$ = 1.62 (THF)

4.2.3.2 Synthesis of poly(GA-*alt*-BO) and PLLA

・Synthesis of poly(GA-*alt*-BO)

Poly(GA-*alt*-BO) was synthesized in the same way, excepting the monomer and the molar ratio of the reactants; benzyl alcohol (54.1 mg, 500 μmol), CsOPiv (117 mg, 500 μmol), GA (1.14 g, 10.0 mmol), and BO (2.88 g, 40.0 mmol). After 19 h, the reaction mixture was diluted with small amount of dichloromethane and purified by reprecipitation in cold methanol to poly(GA-*alt*-BO) as a colorless solid. Yield: 1.06 g, 55.1%.

$M_{n,NMR}$ = 4,640 g mol^{-1} ($CDCl_3$), $M_{n,SEC}$ = 2,560 g mol^{-1} (THF), $Đ$ = 1.61 (THF)

・Synthesis of PLLA

PLLA was synthesized in the same way, excepting the monomer and the molar ratio of the reactants; benzyl alcohol (64.9 mg, 600 μmol), CsOPiv (140 mg, 600 μmol), and LLA (4.76 g, 33.0 mmol). After 1.5 h, the reaction mixture was diluted with small amount of dichloromethane and purified by reprecipitation in cold methanol to PLLA as a colorless solid. Yield: 4.46 g, 92.6%.

$M_{n,NMR}$ = 9,410 g mol^{-1} ($CDCl_3$), $M_{n,SEC}$ = 7,360 g mol^{-1} (THF), $Đ$ = 1.27 (THF)

4.3 Results and Discussion

4.3.1 Self-switchable polymerization using GA, BO, and LLA

The author initially selected glutaric anhydride (GA), 1,2-butylene oxide (BO), and LLA to explore the optimized condition to one-pot, one-step synthesize "hard-soft-hard" type triblock copolymers via the self-switchable polymerization. In addition to LLA, GA and BO can potentially be produced from bio-based raw materials; therefore, they are considered as potential bio-based monomers.[26,27] In previous study, the author found that the ROAC of cyclic anhydride and epoxide was more reactive than the ring-opening polymerization (ROP) of LLA in cesium pivalate-catalyzed self-switchable polymerization using cyclic anhydride, epoxide, and LLA.[20] Consequently, the terpolymerization of the cyclic anhydride, epoxide, and LLA in the presence of a diol is expected to yield a hard-soft-hard triblock copolymer, that is, PLLA-*b*-poly(GA-*alt*-BO)-*b*-PLLA. First, polymerization was attempted with an initial feed ratio [CsOPiv]/$[BDM]_0$/$[GA]_0$/$[BO]_0$/$[LLA]_0$ of 1/1/20/80/110 to obtain a copolyester consisting of an LLA weight fraction of 0.80 (**P1** in **Table 4.1**). The time course of the copolymerization was monitored via ^{1}H NMR to gain insight into the monomer sequence of the obtained copolyester. The time-to-conversion plots of GA and LLA revealed that the ROAC of GA and BO proceeded preferentially, while the ROP of LLA also proceeded very slowly at the same time, owing to the similar reactivity of GA and LLA. (**Figure 4.1a**). Thus, the obtained copolyester was found

to possess a large tapered region with a poly(GA-*alt*-BO)-rich structure in the middle and a PLLA-rich structure in the outer parts, that is, PLLA-*tapered block*-poly(GA-*alt*-BO)-*tapered block*-PLLA (PLLA-*tb*-poly(GA-*alt*-BO)-*tb*-PLLA). **P1** was characterized using ^{1}H NMR and size-exclusion chromatography (SEC) measurements. The ^{1}H NMR spectrum of **P1** revealed signals corresponding to the initiator residue (-$CH_2C_6H_4CH_2$- (*A*), 7.34 ppm), poly(GA-*alt*-BO) repeating unit (-OCOC$H_2$$CH_2CH_2$COO- (*a*), 2.24–2.56 ppm; -OCOCH_2C$H_2$$CH_2$COO- (*b*), 1.83–2.06 ppm; -OCH_2CH(CH_2CH_3)O- (*c*), 3.91–4.49 ppm; -OCH_2C*H*(CH_2CH_3)O- (*d*), 4.90–5.05 ppm; -C$H_2$$CH_3$ (*e*), 1.34–1.81 ppm; -CH_2CH_3 (*f*), 0.70–0.99 ppm), and PLLA repeating unit (–C*H*CH_3 (*g*), 5.05–5.28 ppm; –CHCH_3 (*h*), 1.34–1.81 ppm), as expected (**Figure 4.1b**). Additionally, the LLA weight fraction determined from ^{1}H NMR spectrum (F_{LLA} = 0.83) closely matches that calculated from the monomer feed ratio (f_{LLA} = 0.81). The author noted the signal *a*' originating from the GA unit proton adjacent to LLA unit was observed at 2.4 ppm, supporting the presence of the tapered region (**Figure 4.2**). In addition, the ^{13}C NMR spectrum showed signal *a'*, indicating a tapered region (**Figure 4.3**). The diffusion-ordered NMR (DOSY) spectra provided only one diffusion coefficient for the observed signals of both poly(GA-*alt*-BO) and PLLA, providing strong evidence that these segments were covalently linked (**Figure 4.1c**). The SEC traces maintained an unimodal shape while shifting toward higher molecular weights over time, confirming that both segments were interconnected

(**Figure 4.1d**). The calculated polystyrene-equivalent number-average molecular weight ($M_{n,SEC}$) and polydispersity ($Đ$) were 3,990 and 1.72, respectively. These results demonstrate the one-pot and one-step synthesis of BAB-type tapered-block copolyester with A and B blocks of poly(GA-*alt*-BO) and PLLA, respectively. In the same manner, the copolyesters **P2**–**P5**, which consist of F_{LLA} ranging from 0.25 to 0.87 were synthesized by changing f_{LLA} (**Table 4.1**, **Figures 4.4**–**4.8**).

Table 4.1. Molecular characteristics of copolyesters consisting of PLLA and different poly(cyclic anhydride-*alt*-epoxide) [a]

sample	M1/M2/M3	[CsOPiv]/[BDM]$_0$/ [M1]$_0$/[M2]$_0$/[M3]$_0$	f_{LLA} [b]	time (h)	$M_{n,theo.}$ [c]	$M_{n,NMR}$ [d]	$M_{n,sec}$ [$Đ$][e]	F_{LLA} [f]	T_g [g] (°C)	$T_{d,5\%}$ [h] (°C)
P1	GA/BO/LLA	1/1/20/80/110	0.81	5.5	19,700	17,800	3,990 [1.72]	0.83	19.0	218
P2	GA/BO/LLA	1/1/65/260/55	0.40	13.5	20,200	14,800	9,550 [1.20]	0.25	−15.6	244
P3	GA/BO/LLA	1/1/45/180/85	0.59	7.0	20,800	18,300	8,090 [1.30]	0.45	−6.1	189
P4	GA/BO/LLA	1/1/36/144/110	0.70	6.0	22,700	28,200	5,200 [1.57]	0.69	13.7	196
P5	GA/BO/LLA	1/1/11/44/130	0.90	4.5	20,900	23,500	6,420 [1.36]	0.87	32.5	184
P6	SA/BO/LLA	1/1/23/92/110	0.80	6.0	20,000	20,000	8,610 [1.46]	0.81	31.4	207
P7	DGA/BO/LLA	1/1/20/80/110	0.81	3.5	19,800	23,700	11,200 [1.18]	0.80	34.9	216
P8	GA/PO/LLA	1/1/25/100/110	0.79	5.0	20,300	22,800	5,380 [1.51]	0.74	15.7	194
P9	GA/EGE/LLA	1/1/20/80/110	0.79	4.0	20,300	24,700	4,160 [1.84]	0.77	1.4	188
P10	GA/EHGE/LLA	1/1/15/60/120	0.79	6.5	21,900	23,000	8,260 [1.39]	0.77	1.3	210

[a] Polymerization conditions: temp., 100 °C; atmosphere, Ar; initiator, BDM; catalyst, CsOPiv. [b] LLA weight fraction calculated from the monomer feed ratio. [c] Calculated from (M.W. of BDM) + [anhydride]$_0$/[BDM]$_0$ × (M.W. of anhydride + M.W. of epoxide) + [LLA]$_0$/[BDM]$_0$ × (M.W. of LLA). [d] Determined by ^{1}H NMR spectroscopy in $CDCl_3$. [e] Determined by SEC in THF using polystyrene standards. [f] LLA weight fraction calculated from ^{1}H NMR spectrum. [g] Determined by DSC (first heating run, 10 °C min^{-1}, nitrogen atmosphere). [h] Determined using TGA (10 °C min^{-1}, nitrogen atmosphere).

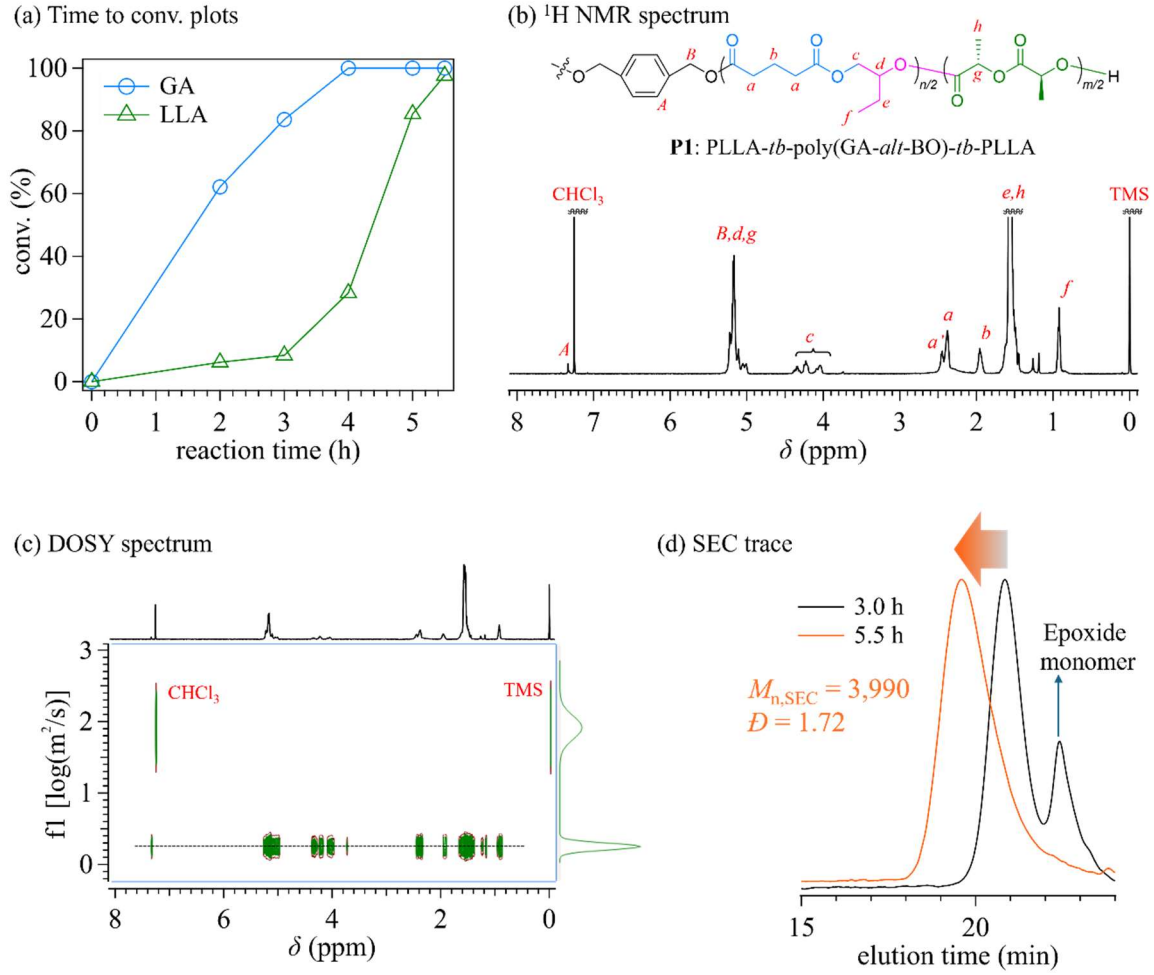

Figure 4.1. Characterization of **P1**. (a) Time to conv. plots monitored by ^{1}H NMR. (b) ^{1}H NMR and (c) DOSY spectrum in $CDCl_3$. (d) SEC traces of the product withdrawn at 3.0 h and the final product (5.5 h) (eluent, THF; flow rate, 1.0 mL min^{-1}). *Signal *a'* of ^{1}H NMR corresponding to the proton signal from the GA unit adjacent to the LLA unit.

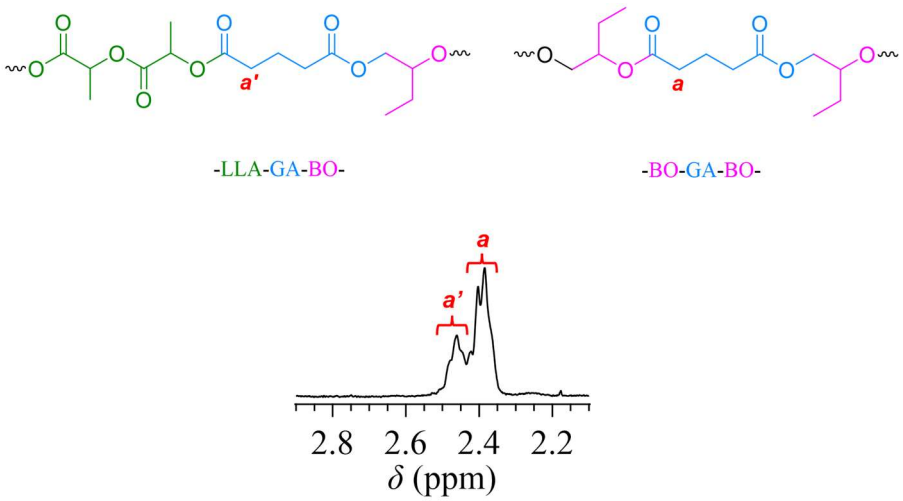

Figure 4.2. ^{1}H NMR spectrum of **P1** in $CDCl_3$ (400 MHz).

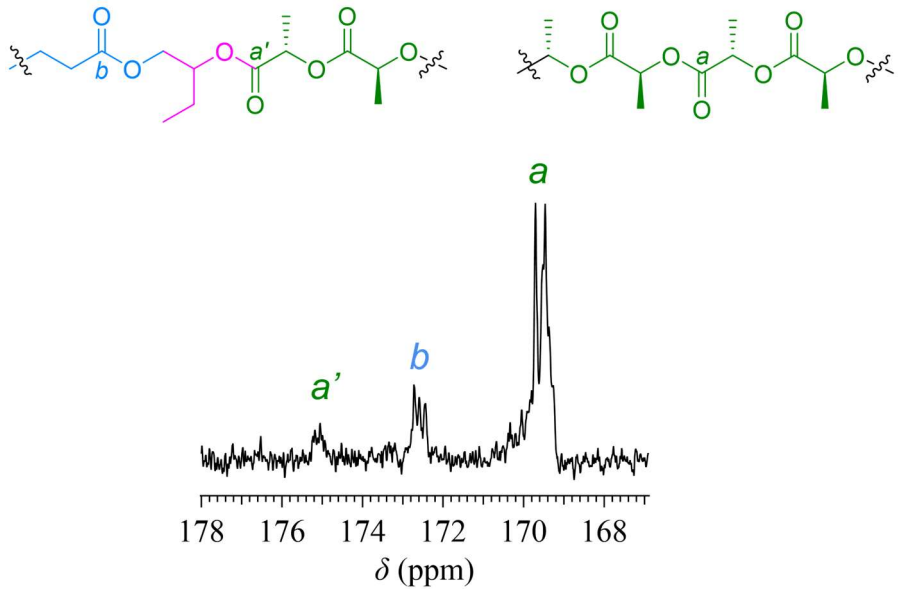

Figure 4.3. ^{13}C NMR spectrum of **P1** in $CDCl_3$ (100 MHz).

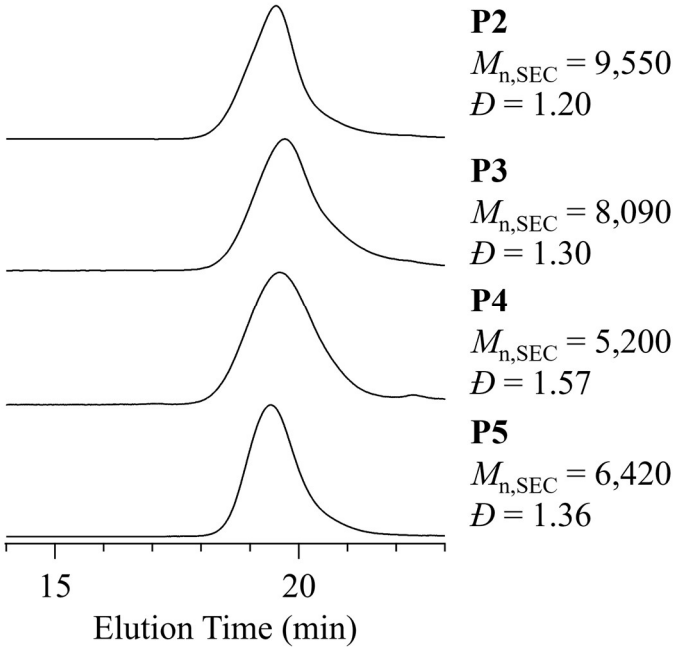

Figure 4.4. SEC traces of **P2**–**P5** (solvent, THF; flow rate, 1.0 mL min^{-1}).

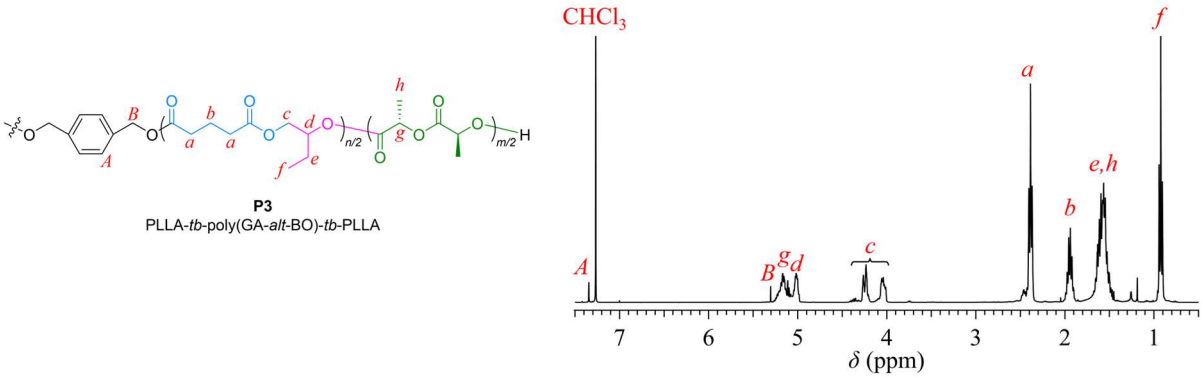

Figure 4.5. ^{1}H NMR spectrum of **P2** in $CDCl_3$ (400 MHz).

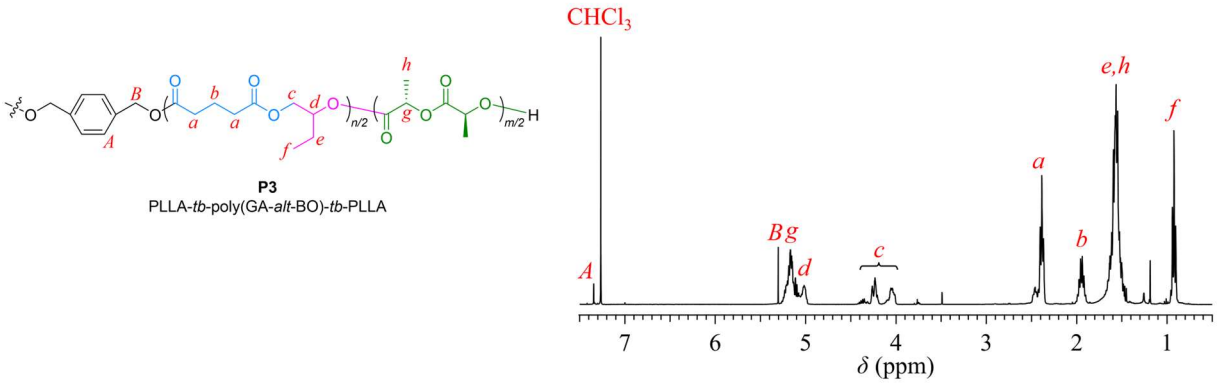

Figure 4.6. ^{1}H NMR spectrum of **P3** in $CDCl_3$ (400 MHz).

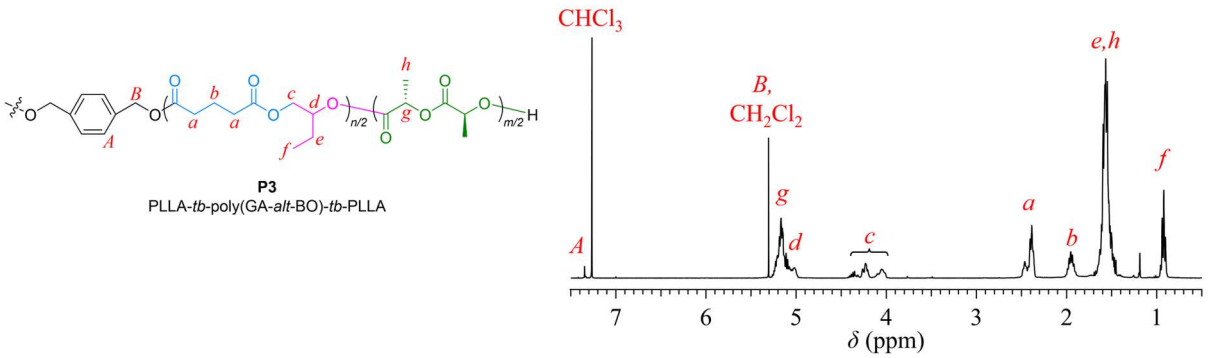

Figure 4.7. ^{1}H NMR spectrum of **P4** in $CDCl_3$ (400 MHz).

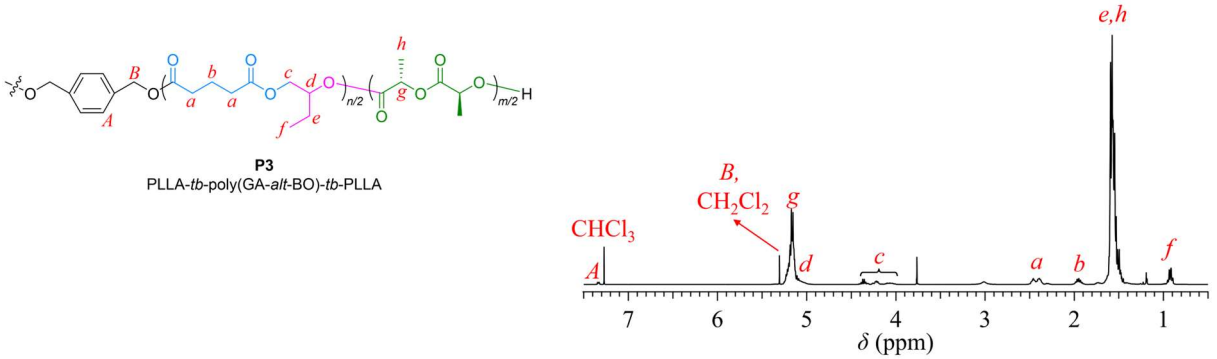

Figure 4.8. ^{1}H NMR spectrum of **P5** in $CDCl_3$ (400 MHz).

4.3.2 Thermal properties of PLLA-*tb*-poly(GA-*alt*-BO)-*tb*-PLLA

The thermal properties of **P1**–**P5** were investigated via thermogravimetric analysis (TGA) and differential scanning calorimetry (DSC) under a N_2 atmosphere. TGA revealed a 5% weight-loss temperature ($T_{d,5\%}$) of 189–244 °C, implying that these copolyesters were useful below 180 °C (**Figures 4.9a** and **4.10**).

DSC measurements of **P1** were performed at a heating and cooling rate of 10 °C (**Figure 4.9b**). Neither crystallization nor melting transitions were observed even during the 1st heating process, implying that the crystallization of PLLA was inhibited by the presence of the poly(GA-*alt*-BO) repeating units in the PLLA segment. Another reason for poor crystallization in the PLLA segment could be partial epimerization (see **Figure 4.3**). In the ^{13}C NMR spectrum of **P1**, the signal corresponding to the carbonyl carbons (signal *a*) around 169.5 ppm shows splitting, indicating that epimerization occurred. **P1** exhibited a glass transition temperature (T_g) at 29.0 °C, which is in between the T_g of PLLA (60 °C)[28] and poly(GA-*alt*-BO) (−43.1 °C), suggesting that the two segments are miscible. T_g was calculated using the Fox equation ($T_{g,calc.}$ = 35.7 °C) is in good agreement with the measurement T_g of 29.0 °C, supporting the miscibility of the two segments. Similarly, only one T_g was observed for **P2**–**P5**, and their T_g values agreed with $T_{g,calc.}$ (**Figure 4.11**, **Table 4.2**). Based on the DSC results, the author confirmed that

PLLA-*tb*-poly(GA-*alt*-BO)-*tb*-PLLAs were amorphous and exhibited T_g values ranging from −15.6–32.5 °C depending on F_{LLA}.

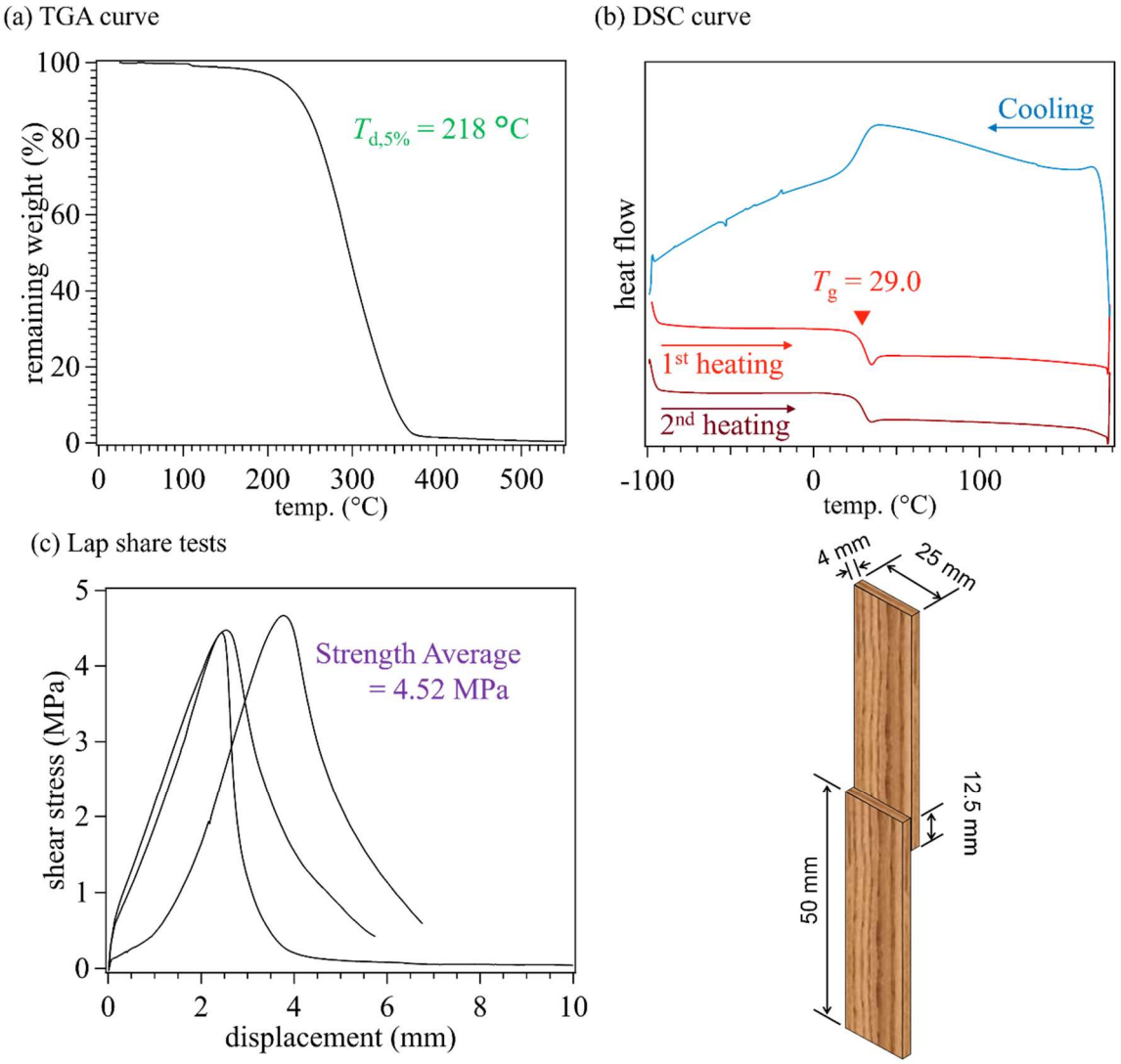

Figure 4.9. Physical properties of **P1**: (a) TGA curve (heating ratio, 10 °C min^{-1}; nitrogen atmosphere). (b) DSC thermogram detected during heating/cooling/heating scan (1st heating: −100–180 °C, 1st cooling: −100–180 °C, 2nd heating: −100–180 °C; 10 °C min^{-1}; N_2 atmosphere). (c) Lap share tests using wood pieces (adherent, wood; tensile speed = 10 mm min^{-1}; n = 3).

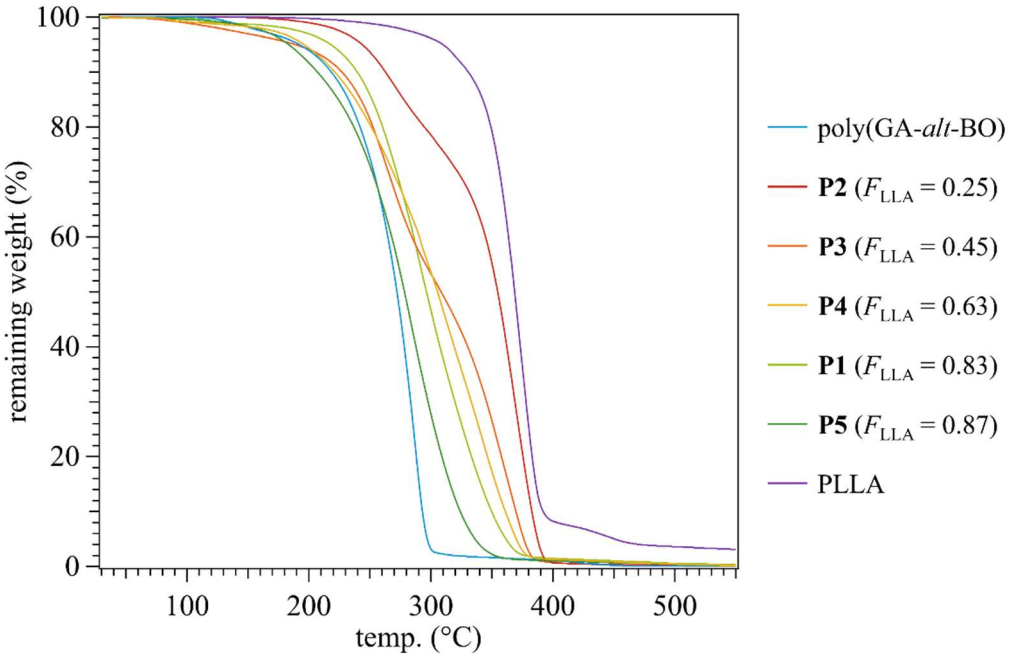

Figure 4.10. TGA thermograms of poly(GA-*alt*-BO) homopolymer ($M_{n,NMR}$ = 4,640), PLLA homopolymer ($M_{n,NMR}$ = 9,410), and the obtained PLLA-*tb*-poly(GA-*alt*-BO)-*tb*-PLLA (**P1**–**P5**; $M_{n,NMR}$ = 14,800–28,200, f_{LLA} = 0.25, 0.45, 0.63, 0.83, and 0.87).

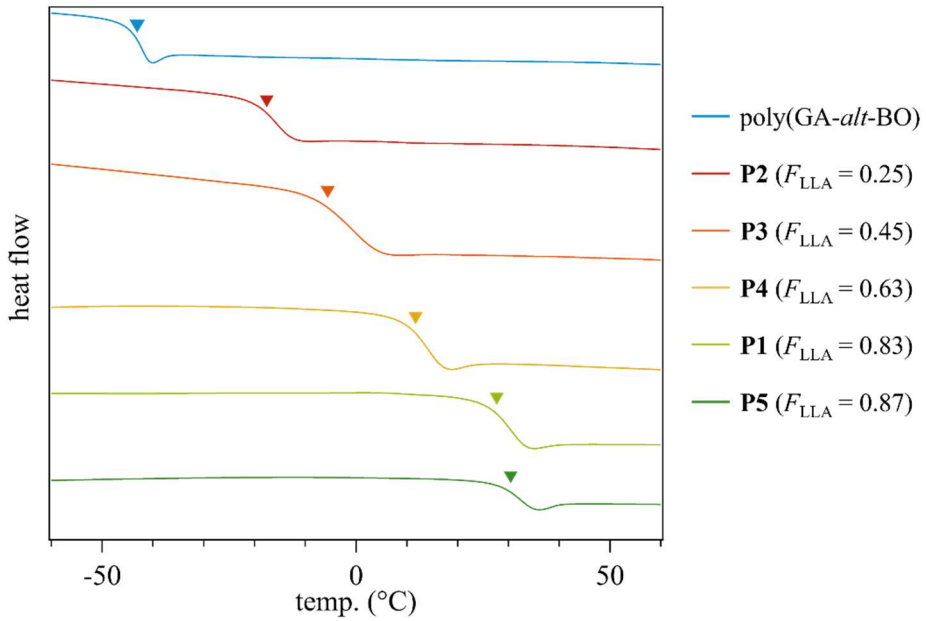

Figure 4.11. 1st heating DSC curves of poly(GA-*alt*-BO) homopolymer and **P1**–**P5** (heating rate, 10 °C min^{-1}; N_2 atomosphere).

Table 4.2. Measured and theoretical T_g for the miscible blocks

Polymer	$T_{g,measured}$ (°C) [a]	$wt\%_{hard}$ [b]	$wt\%_{soft}$ [b]	$T_{g,calculated}$ (°C) [c]
P1	29.0	83	17	35.7
P2	−15.6	25	75	−24.0
P3	−6.1	45	55	−6.2
P4	13.7	69	31	18.8
P5	32.5	87	13	40.9

[a] Measured by DSC. [b] calculated by ^{1}H NMR spectrum. [c] T_g for the sample miscribe (as calculated using the Fox equation: $1/T_{g,calculated} = wt\%_{hard}/T_{g,hard} + wt\%_{soft}/T_{g,soft}$; $T_{g,hard}$ and $T_{g,soft}$ were used 60 and −43.1 °C, respectively).

4.3.3 Evaluation of adhesive property by lap shear test

Next, the author investigated the adhesive properties of the obtained PLLA-*tb*-poly(GA-*alt*-BO)-*tb*-PLLAs by lap shear tests using wood test pieces at room temperature (JIS K 6850:1999; right side in **Figure 4.2c** and **4.12**). Test samples were prepared by pressing polymer thin film between two wooden substrates at 100 °C.

The author was unable to prepare the test samples from **P2**, **P3**, and **P5** (F_{LLA} = 0.25, 0.45, and 0.87, respectively) as well as poly(GA-*alt*-BO) and PLLA homopolymers because of the following reasons (**Figure 4.13**): For **P2**, **P3**, and poly(GA-*alt*-BO), the author could not get a self-standing film for the hot-melt adhesive application due to their low T_g as well as their liquid nature (their appearance was viscous liquid even at 10 °C). In contrast, **P5** and PLLA are brittle solids; therefore, effective adhesion cannot be achieved. In contrast, the author successfully prepared a self-standing film from **P1** and **P4** that functioned as a hot-melt adhesive. A lap shear test on **P1** sample (**Figure 4.2c**) revealed an adhesive strength of 4.52 MPa, indicating cohesion failure. While **P1** demonstrated high adhesive strength to the wooden substrate, **P4** with an F_{LLA} of 0.69, showed a much lower strength (0.24 MPa, **Figure 4.14** and **4.15**). Although the adhesive strength appears to increase with the increasing F_{LLA}, pure PLLA is too brittle to function as an adhesive. This indicates the importance of combining the PLLA and poly(GA-*alt*-BO) blocks in a balanced composition to achieve sufficient adhesive performance.

To confirm the importance of chemically linking PLLA and poly(GA-*alt*-BO) blocks for adhesive performance, a polymer blend with a composition corresponding to **P1** was prepared by mixing the two homopolymers (PLLA/poly(GA-*alt*-BO) = 83/17 (weight fraction)) at 100 °C for 2 min, following the hot-pressing at 100 °C for 1 min (**Table 4.3**). As shown in **Figure 4.16**, the DSC curve of the PLLA/poly(GA-*alt*-BO) blend sample shows only one T_g, suggesting that these two polymers have high miscibility. The adhesive strength of the blended sample to the wooden substrate was only one-third that of **P1** (1.20 MPa, **Figures 4.17** and **4.18**). Thus, the author successfully demonstrated that copolymerization, rather than two-homopolymer blending, is a significant contributor to the adhesive performance.

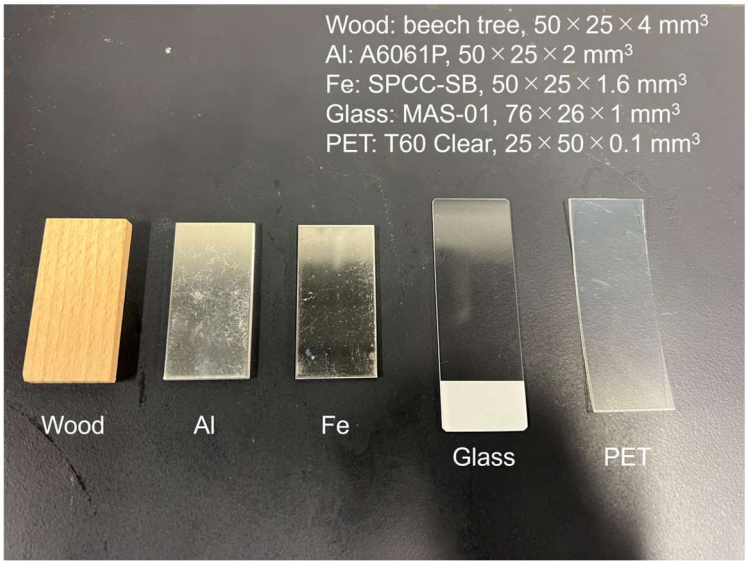

Figure 4.12. Digital photographs and information about adherents.

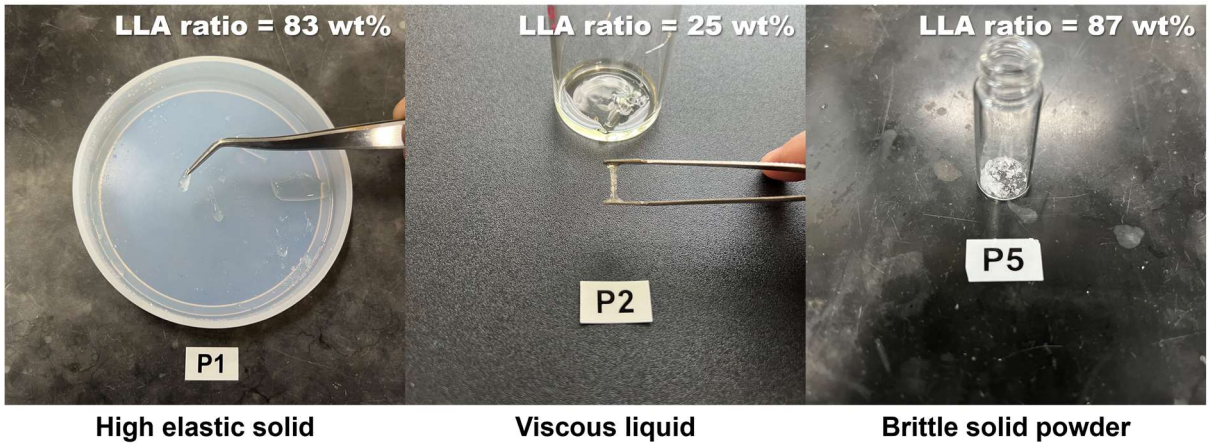

Figure 4.13. Digital photographs of **P1**, **P2**, and **P5**.

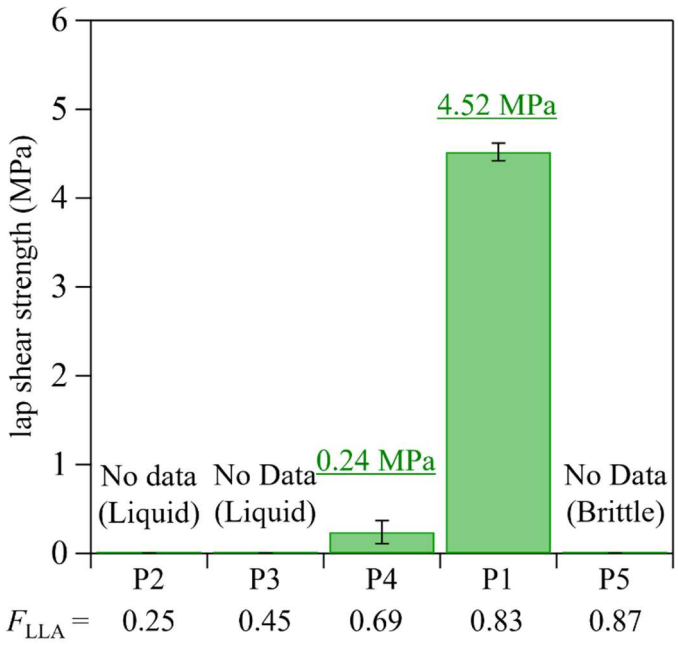

Figure 4.14. Lap shear strengths of PLLA-*tb*-poly(GA-*alt*-BO)-*tb*-PLLA with varying compositions in F_{LLA} (adherent, wood; tensile speed = 10 mm min^{-1}; n = 3).

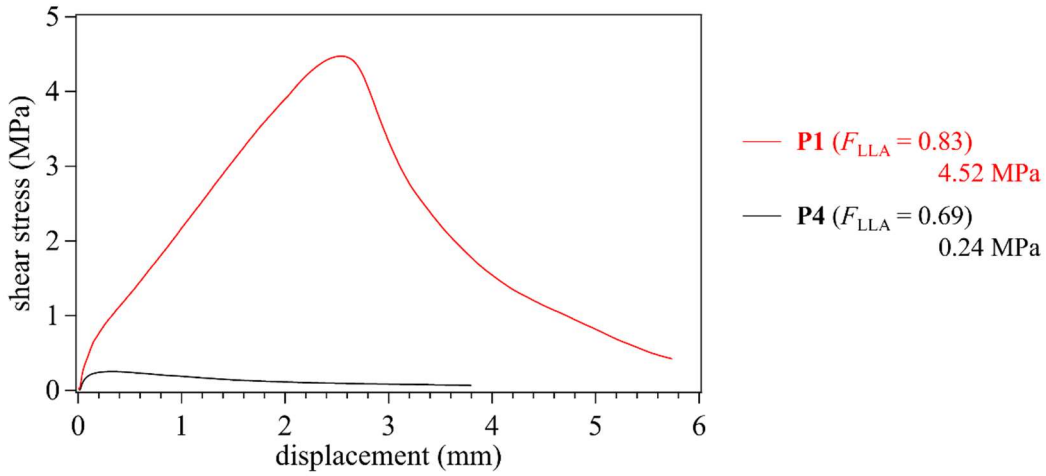

Figure 4.15. Lap shear tests of **P1** and **P4** using wood pieces (adherent, wood; tensile speed = 10 mm min^{-1}).

Table 4.3. Synthesis of PLLA and poly(GA-*alt*-BO) homopolymers [a]

sample	monomer	time (h)	conv. (%) [b]	$M_{n,theo.}$ [c]	$M_{n,NMR}$ [b]	$M_{n,SEC}$ [d]	$Đ$ [d]
PLLA [e]	LLA	1.5	80.3	6,470	9,410	7,360	1.27
Poly(GA-*alt*-BO) [f]	GA and BO	19	>99.9	3,830	4,640	2,560	1.61

[a] Polymerization conditions: temp., 100 °C; atmosphere, Ar; initiator, benzyl alcohol; catalyst, CsOPiv. [b] Calculated from (M.W. of initiator) + $[monomer]_0/[initiator]_0$ × (M.W. of monomer). [c] Determined by ^1H NMR in $CDCl_3$. [d] Determined by SEC in THF using polystyrene standards. [e] $[CsOPiv]/[initiator]_0/[LLA]_0$ = 1/1/55. [f] $[CsOPiv]/[initiator]_0/[GA]_0/[BO]_0$ = 1/1/20/80.

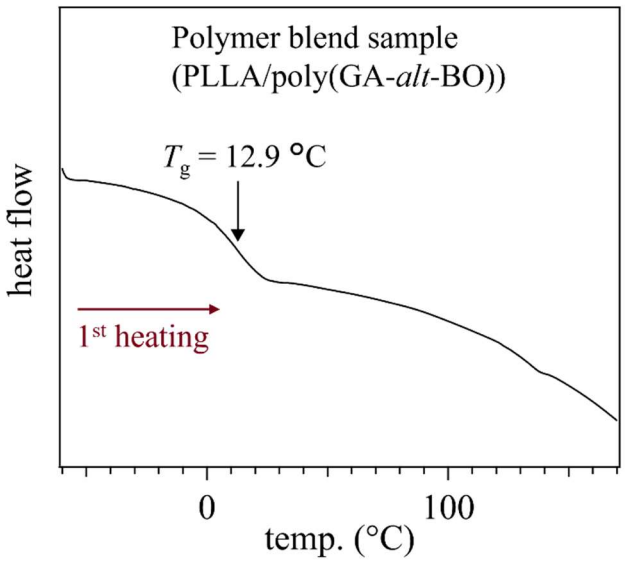

Figure 4.16. 1st heating DSC curves of polymer blend (PLLA/poly(GA-*alt*-BO) = 83/17 (weight ratio); 1st heating, 10 °C/min, N_2 atmosphere).

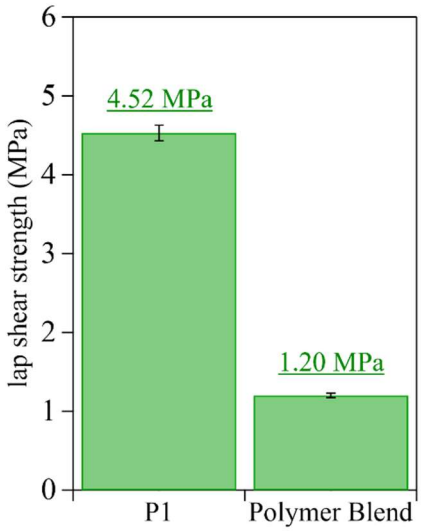

Figure 4.17. Lap shear strengths of **P1** and polymer blend (PLLA/poly(GA-*alt*-BO) = 83/17 (weight fraction)).

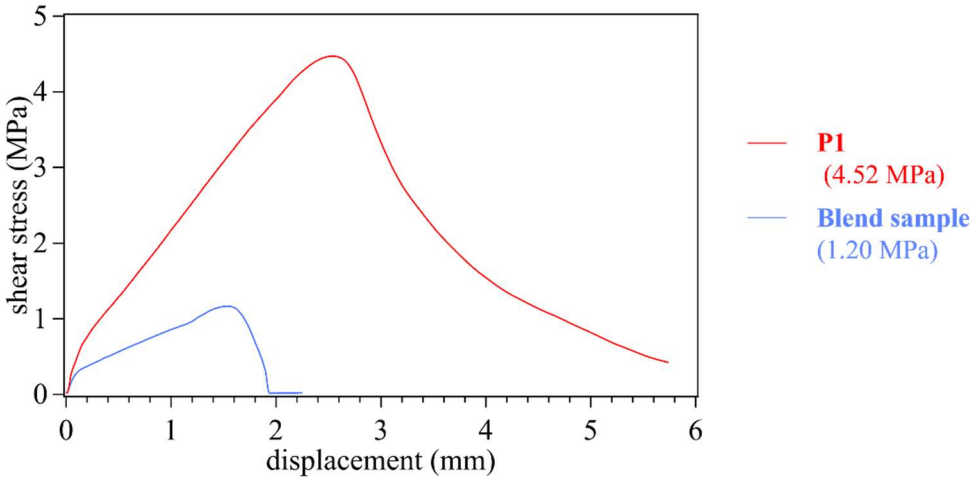

Figure 4.18. Lap shear tests of **P1** and polymer blend sample of PLLA and poly(GA-*alt*-BO) (PLLA/poly(GA-*alt*-BO) = 83/17 (weight ratio)) using wood pieces (adherent, wood; tensile speed = 10 mm min^{-1}).

4.3.4 Effect of monomer combinations

To evaluate the effect of the repeating structure of the poly(cyclic anhydride-*alt*-epoxide) segment, the author then prepared **P6**–**P10** using several anhydrides and epoxides (**Table 4.1**). First, the author carried out self-switchable polymerization under optimized conditions with a BDM initiator using succinic anhydride (SA) and diglycolic anhydride (DGA) as the anhydride monomers, while fixing BO as the epoxide monomer (**P6**–**P7** in **Table 4.1**). Here, the author set f_{LLA} to approximately 0.80 because the lap shear results in the previous section indicate that an F_{LLA} of 0.83 exhibits excellent adhesive properties. The SEC traces of the final products showed an unimodal peak, confirming successful copolymerization (**Figure 4.19**). Monitoring the progress of the polymerization by ^{1}H NMR revealed the switching of the polymerization from the ROAC of anhydrides and BO to the ROP of LLA, suggesting the formation of a BAB-type sequence with PLLA as the B block (**Figure 4.20**). Owing to the insufficient sampling frequency, the exact switching timing could not be determined. However, the signals assignable to the LLA-(anhydride-*alt*-BO) and (anhydride-*alt*-BO)-LLA units were almost undetectable in the ^{13}C NMR spectra of **P6** and **P7**, suggesting a real block copolymer structure rather than a tapered structure, that is PLLA-*b*-poly(SA-*alt*-BO)-*b*-PLLA and PLLA-*b*-poly(DGA-*alt*-BO)-*b*-PLLA (**Figures 4.21**–**4.24**). This is due to the much higher reactivities of SA and DGA compared to that of LLA, which enabled sharper switching from ROAC to

ROP. The DSC curves of **P6** and **P7** show no crystallization or melting peaks, suggesting their amorphous nature (**Figure 4.25**). Although the observed T_g is almost the same as **P1** consisting of GA, **P6** and **P7** samples were too brittle, and the preparation of adhesive test samples was unsuccessful.

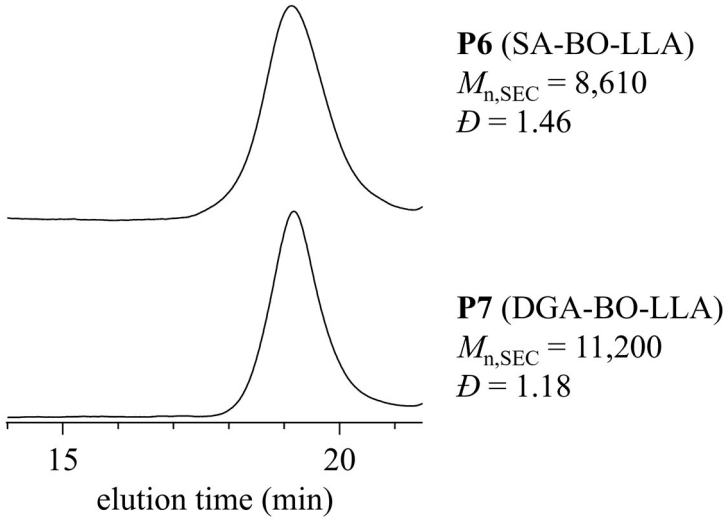

Figure 4.19. SEC traces of **P6**–**P7** (solvent, THF; flow rate, 1.0 mL min^{-1}).

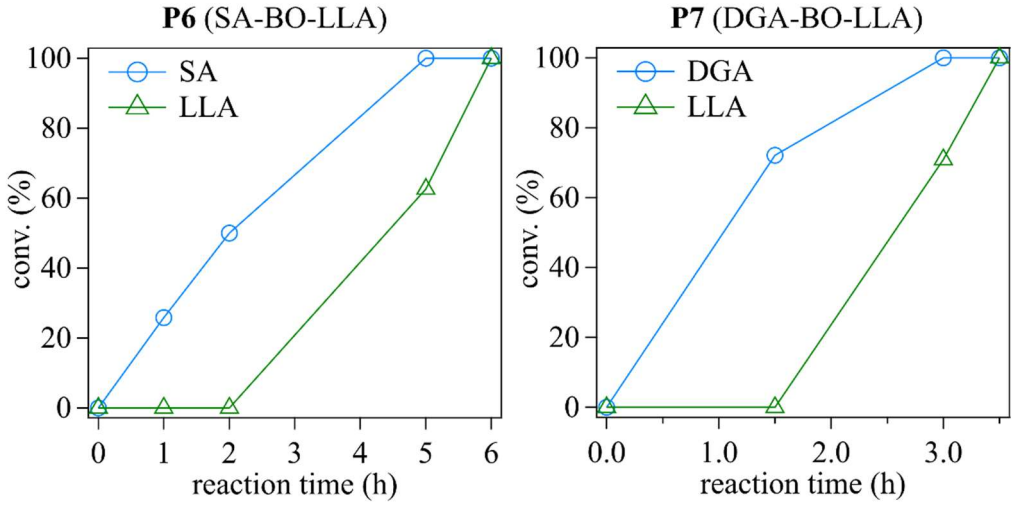

Figure 4.20. Time to conv. plots for the synthesis of **P6**–**P7** monitored by ^{1}H NMR.

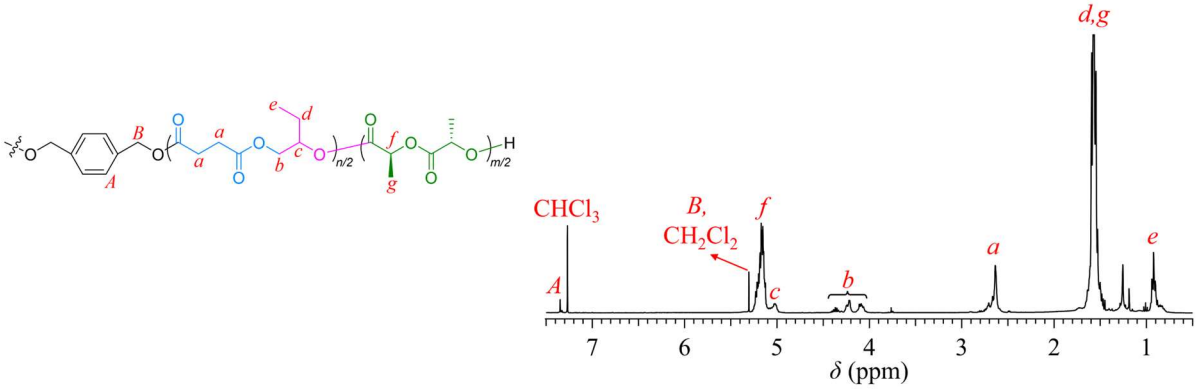

Figure 4.21. ^{1}H NMR spectrum of **P6** in $CDCl_3$ (400 MHz).

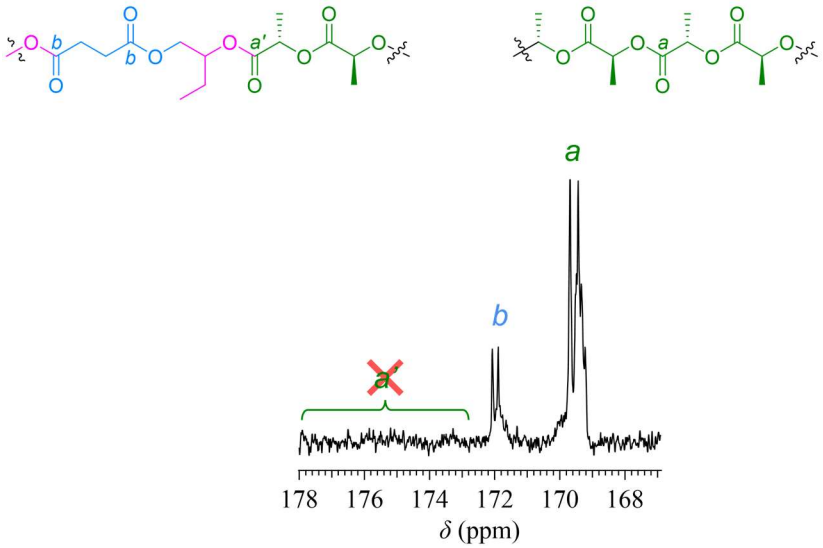

Figure 4.22. ^{13}C NMR spectrum of **P6** in $CDCl_3$ (100 MHz).

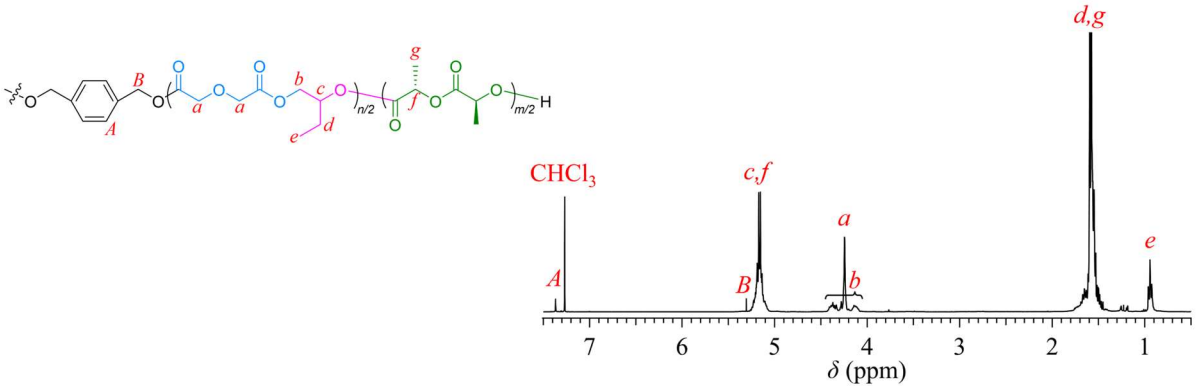

Figure 4.23. ^{1}H NMR spectrum of **P7** in $CDCl_3$ (400 MHz).

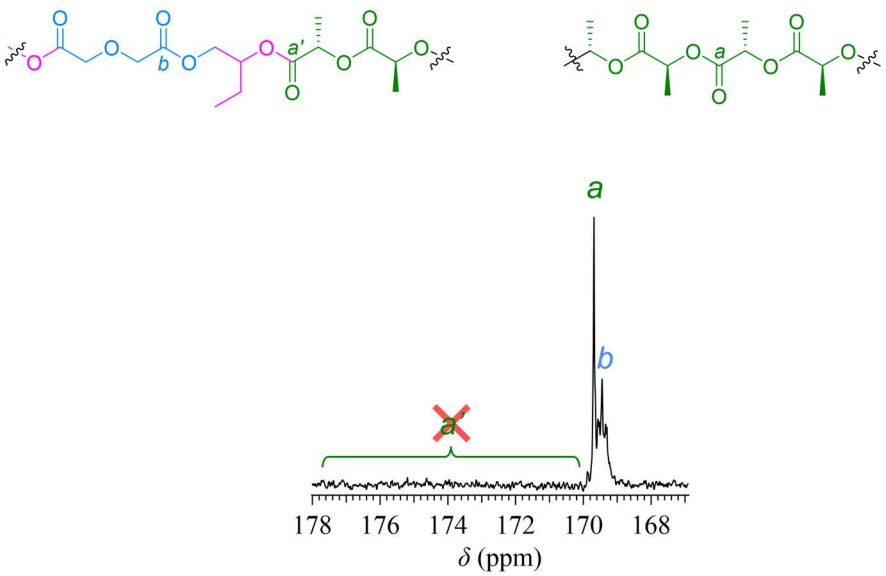

Figure 4.24. ^{13}C NMR spectrum of **P7** in $CDCl_3$ (100 MHz).

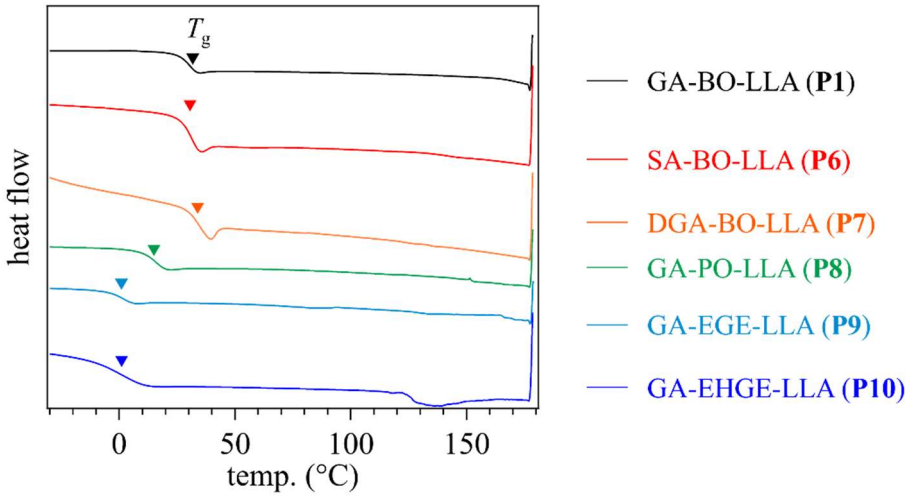

Figure 4.25. 1st heating DSC curves of **P1**, **P6**–**P10** (1st heating, 10 °C min^{-1}, N_2 atmosphere).

Next, to synthesize copolyesters with different epoxide moieties, the author carried out self-switchable copolymerization of GA and LLA with several different epoxides, *i.e.*, propylene oxide (PO), ethyl glycidyl ether (EGE), and 2-ethylhexyl glycidyl ether (EHGE) (**P8**–**P10** in **Table 4.1**). The ROP of LLA proceeded slowly, while the ROAC of GA and

epoxides proceeded, as evidenced by reaction monitoring by ^{1}H NMR, indicating that the obtained copolymers possessed a significantly tapered region (**Figure 4.26**). The ^{1}H NMR and SEC analyses revealed the F_{LLA} of 0.78–0.88 and narrow to moderate $Đ$ of 1.39–1.84, respectively (**Figures 4.27**–**4.32**). The T_g of **P8**–**P10** were observed at 1.3–15.1 °C from the DSC curves (**Figure 4.25**). The copolyesters synthesized using glycidyl ethers (**P9** and **P10**) were found to show particularly low T_g (ca. 1 °C), which could be due to the flexibility of glycidyl ether side chain. Lap shear samples are difficult to prepare because of their low T_g. The adhesive strengths of **P8**–**P10** are shown in **Figure 4.33**. Compared to the adhesive strengths of **P9** and **P10** (0.05 MPa and 0.56 MPa), **P1** and **P8** showed much higher adhesive strength (4.52 MPa and 2.49 MPa; **Figure 4.34**). This trend seems to correlate with the T_g of the copolyesters, where alkylene oxide monomers lead to higher T_g rather than glycidyl ethers. Overall, the author found that altering the epoxide monomer was an effective means of adjusting the adhesion performance. Because altering the cyclic anhydride significantly affects the main-chain structure as well as the monomer sequence, this results in substantial effects on the adhesive properties. In contrast, altering the epoxide monomer only affected the side chains. Because the side chain structure allows for the precise control of T_g, modifying the epoxide monomer is effective in tuning the adhesive properties.

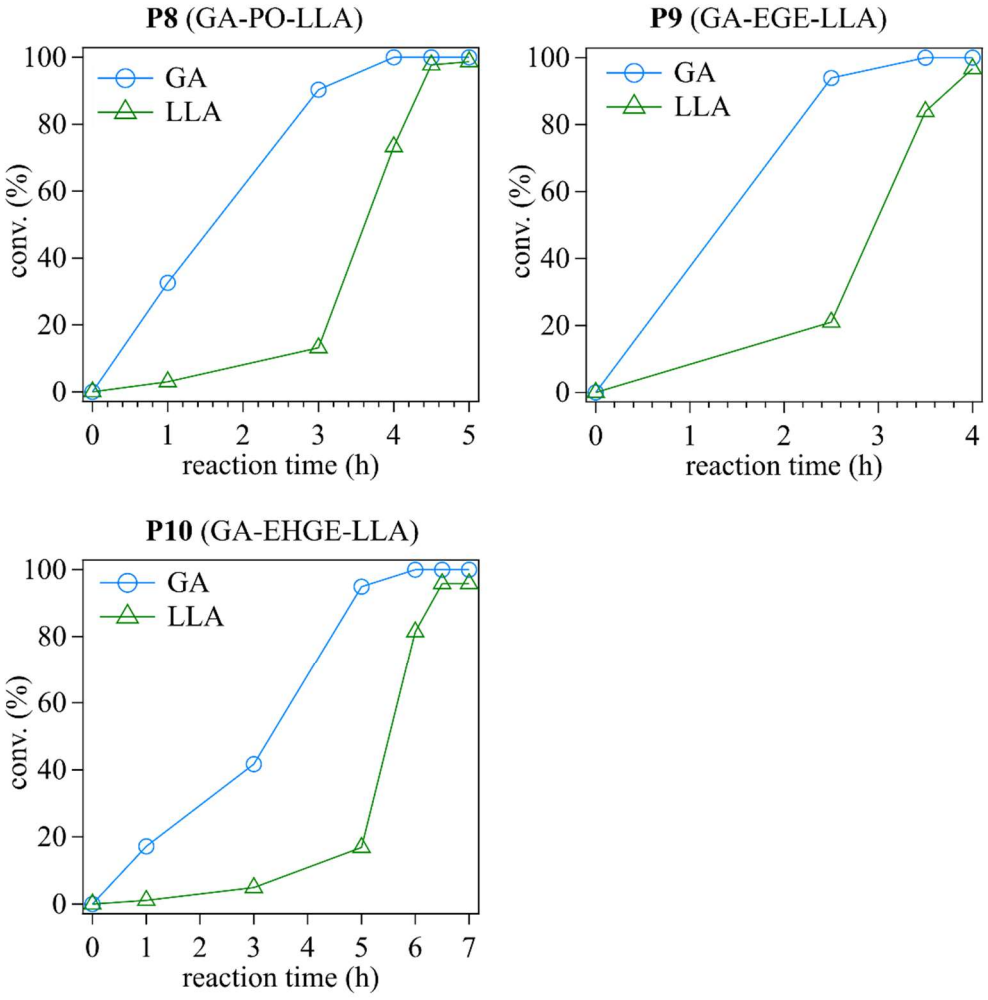

Figure 4.26. Time to conv. plots for the synthesis of **P8**–**P10** monitored by ^{1}H NMR.

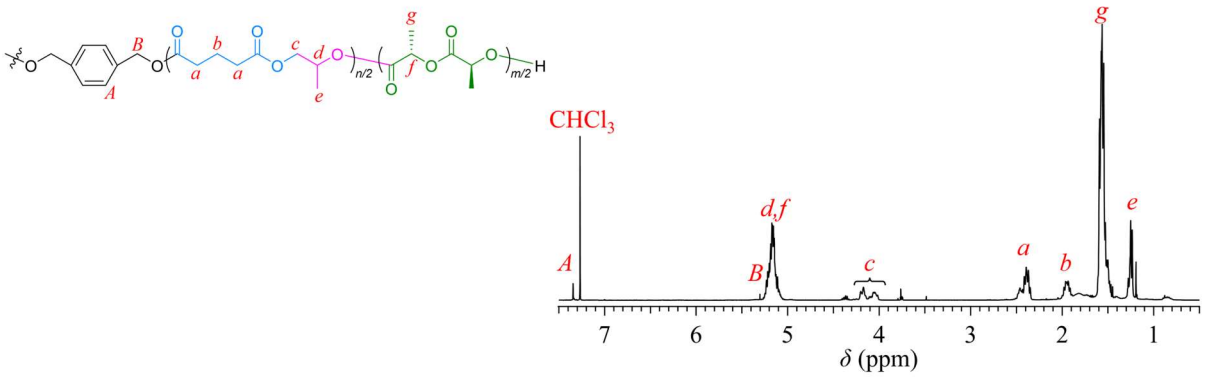

Figure 4.27. ^{1}H NMR spectrum of PLLA-*tb*-poly(GA-*alt*-PO)-*tb*-PLLA in $CDCl_3$ (**P8** in **Table 1**; 400 MHz).

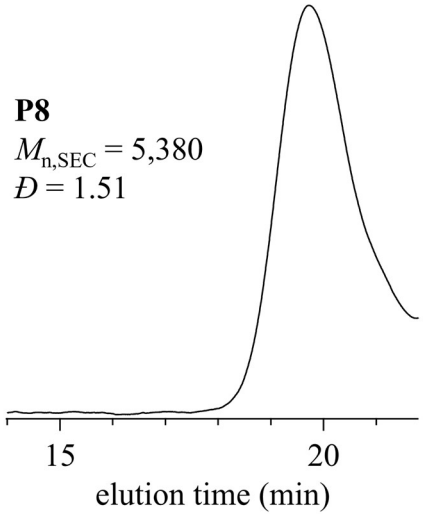

Figure 4.28. SEC trace of PLLA-*b*-poly(GA-*alt*-PO)-*b*-PLLA (**P8** in **Table 1**; eluent, THF; flow rate, 1.0 mL min^{-1}).

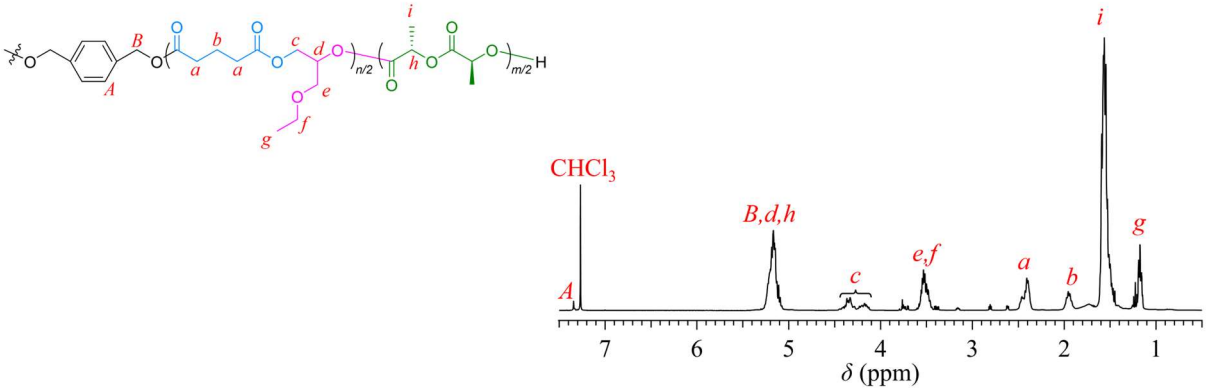

Figure 4.29. ^{1}H NMR spectrum of PLLA-*tb*-poly(GA-*alt*-EGE)-*tb*-PLLA in $CDCl_3$ (**P9** in **Table 1**; 400 MHz).

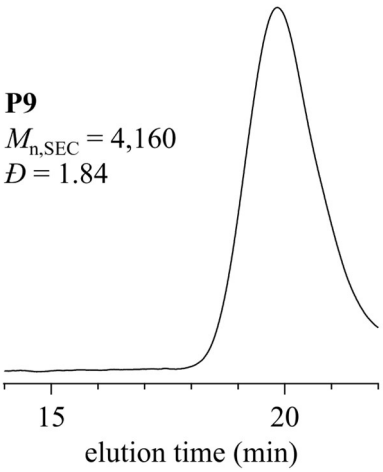

Figure 4.30. SEC trace of PLLA-*b*-poly(GA-*alt*-EGE)-*b*-PLLA (**P9** in **Table 1**; THF; flow rate, 1.0 mL min^{-1}).

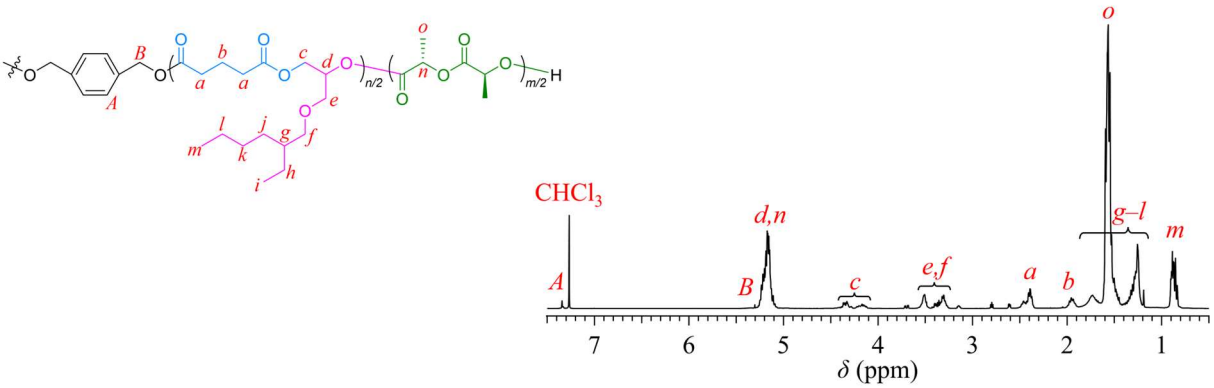

Figure 4.31. ^{1}H NMR spectrum of PLLA-*b*-poly(GA-*alt*-EHGE)-*b*-PLLA in $CDCl_3$ (**P10** in **Table 1**; 400 MHz).

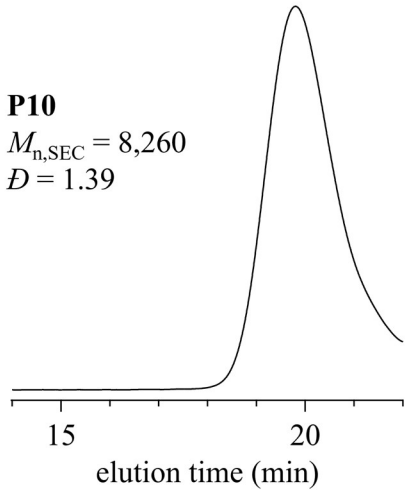

Figure 4.32. SEC trace of PLLA-*b*-poly(GA-*alt*-EHGE)-*b*-PLLA (**P10** in **Table 1**; eluent, THF; flow rate, 1.0 mL min^{-1}).

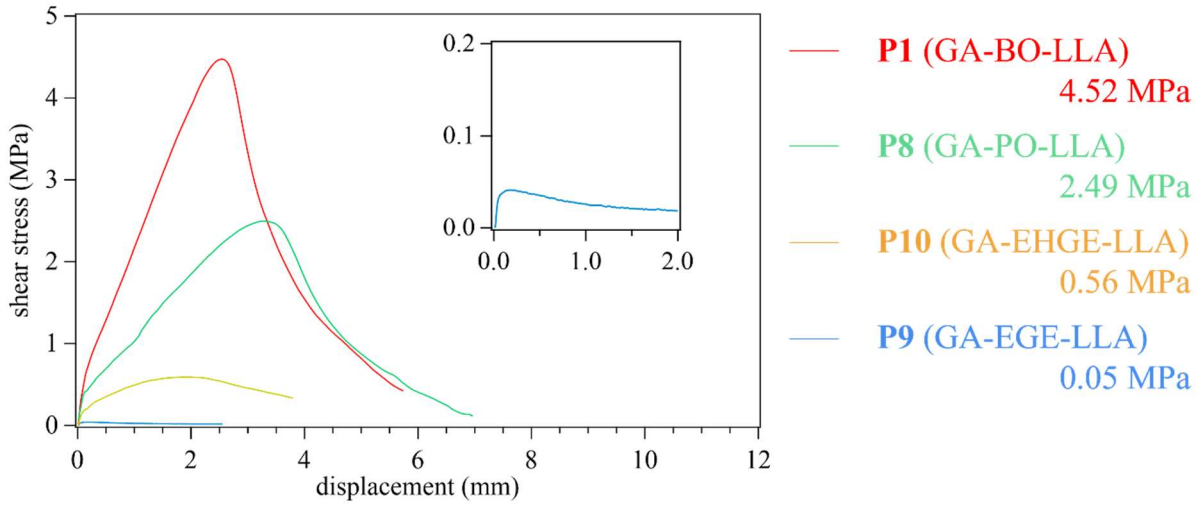

Figure 4.33. Lap shear tests of PLLA-*tb*-poly(anhydride-*alt*-epoxide)-*tb*-PLLA using wood test pieces (**P1**, **P8**–**P10** in **Table 1**; adherent, wood; tensile speed = 10 mm min^{-1}).

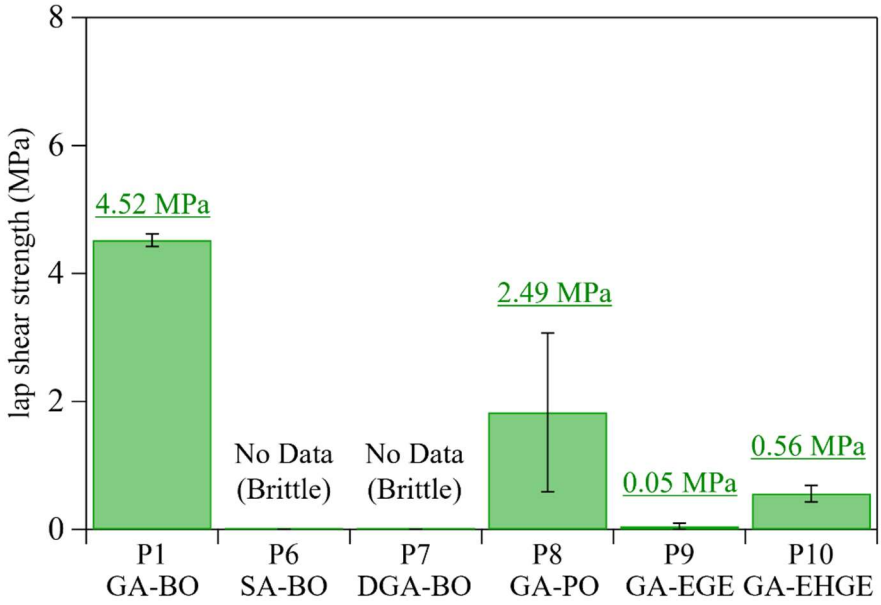

Figure 4.34. Lap shear strengths of BCPs with various repeating unit structures (adherent, wood; tensile speed = 10 mm min^{-1}; n = 3).

4.3.5 Effect of branched structure and molecular weight on adhesive property

To further improve the adhesive properties, the author investigated the effects of the polymer chain architecture and molecular weight. To reveal these relationships, the author synthesized poly(GA-*alt*-BO)-*tb*-PLLA with different branching structures and total molecular weights (**P11**–**P15** in **Table 4.4**). Linear AB diblock and three-armed $(AB)_3$ star block type copolyesters were synthesized by the self-switchable polymerization of GA, BO, and LLA under established conditions while altering the initiator from BDM to benzyl alcohol (BA) and 1,3,5-benzenetrimethanol (BTM) (**P11** and **P12**). In the ^{1}H NMR spectrum of **P11**, signal *A* corresponding to the initiator moiety was clearly observed at 7.35 ppm (**Figure 4.35**). The ^{1}H NMR spectrum of **P12** also displayed the proton signals representing the initiator residue ((*A*), 7.25 ppm; (*B*), 5.16 ppm in **Figure 4.36**). SEC traces of **P11** and **P12** showed a unimodal elution peak (**P11**: $M_{n,SEC}$ = 5,060, $Đ$ = 1.59; **P13**: $M_{n,SEC}$ = 8,110, $Đ$ = 1.22; **Figures 4.28** and **4.29**), and the ^{1}H NMR revealed the F_{LLA} of 0.80 and 0.76, respectively. The adhesive strength of the obtained **P11** and **P12** were 3.41 and 5.20 MPa (**Figure 4.37**), where **P1** with the BAB architecture locates in between **P11** and **P12**. These results suggest that the adhesive strength increased with an increasing number of arms.

Table 4.4. Molecular characteristics of copolyesters with different branched structure and molecular weight [a]

sample	arm	ini.	[CsOPiv]/ [initiator]$_0$/[GA]$_0$/ [BO]$_0$/[LLA]$_0$	f_{LLA} [b]	time (h)	$M_{n,theo.}$ [c]	$M_{n,NMR}$ [d]	$M_{n,sec}$ [$Đ$] [e]	F_{LLA} [f]	T_g (°C) [g]	$T_{d,5\%}$ (°C) [h]
P11	1	BA	1/1/12/48/60	0.80	5.5	11,000	10,800	5,060 [1.59]	0.80	23.2	254
P12	3	BTM	1/1/35/140/170	0.79	8.0	31,200	32,600	8,110 [1.22]	0.76	23.2	226
P13	2	BDM	1/1/10/40/55	0.81	4.0	9,930	11,800	2,180 [2.12]	0.78	21.0	190
P14	2	BDM	1/1/42/168/220	0.80	9.0	39,700	38,100	6,510 [1.69]	0.80	25.0	224
P15	4	PEOL	1/1/84/336/440	0.80	23.0	79,200	N.D.	9,170 [1.62]	0.79	21.2	235

[a] Polymerization conditions: temp., 100 °C; atmosphere, Ar; initiator, BDM; catalyst, CsOPiv. [b] LLA weight fraction calculated from the monomer feed ratio. [c] Calculated as (M.W. of initiator) + [GA]$_0$/[initiator]$_0$ × (M.W. of GA + M.W. of BO) + [LLA]$_0$/[initiator]$_0$ × (M.W. of LLA). [d] Determined by ^{1}H NMR spectroscopy in $CDCl_3$. [e] Determined by SEC in THF using polystyrene standards. [f] LLA weight fraction calculated from ^{1}H NMR spectrum. [g] Determined by DSC (first heating run, 10 °C min^{-1}, nitrogen atmosphere). [h] Determined using TGA (10 °C min^{-1}, nitrogen atmosphere).

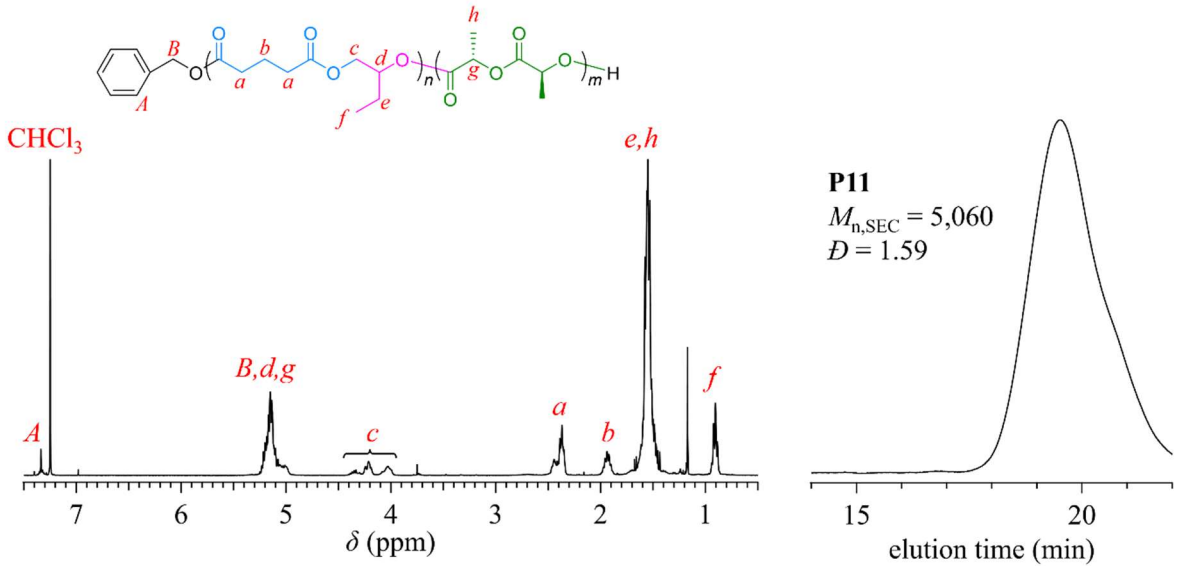

Figure 4.35. ^{1}H NMR spectrum ($CDCl_3$, 400 MHz; left panel) and SEC trace (eluent, THF; flow rate, 1.0 mL min^{-1}; right panel) of poly(GA-*alt*-BO)-*tb*-PLLA (**P11** in **Table 2**).

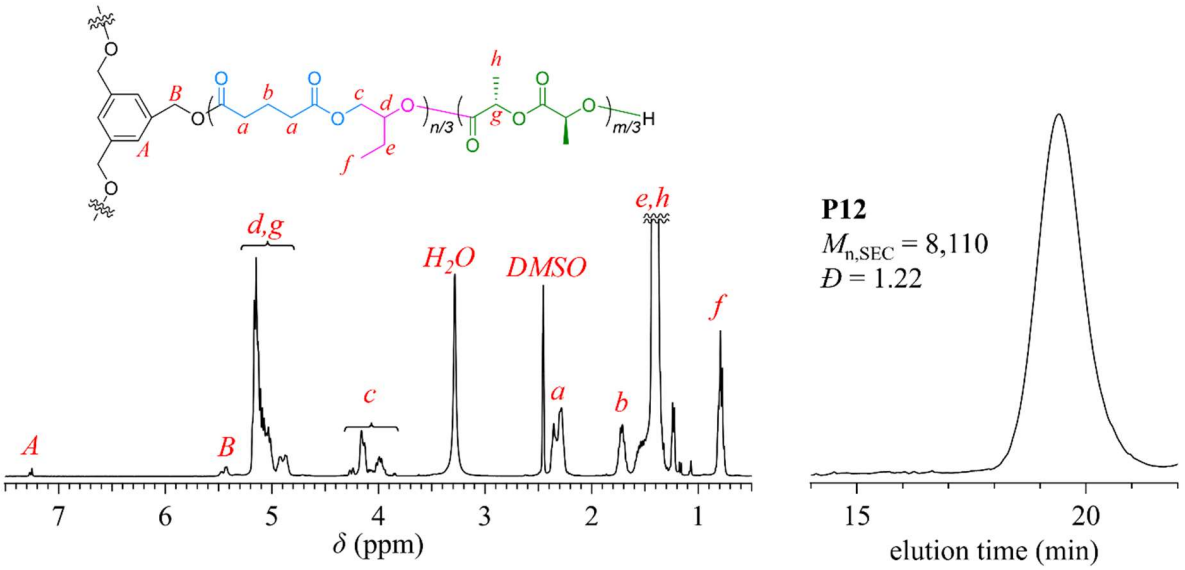

Figure 4.36. ^{1}H NMR spectrum (DMSO-d_6, 400 MHz; left panel) and SEC trace (eluent, THF; flow rate, 1.0 mL min^{-1}; right panel) of (poly(GA-*alt*-BO)-*tb*-PLLA)$_3$ (**P12** in **Table 2**).

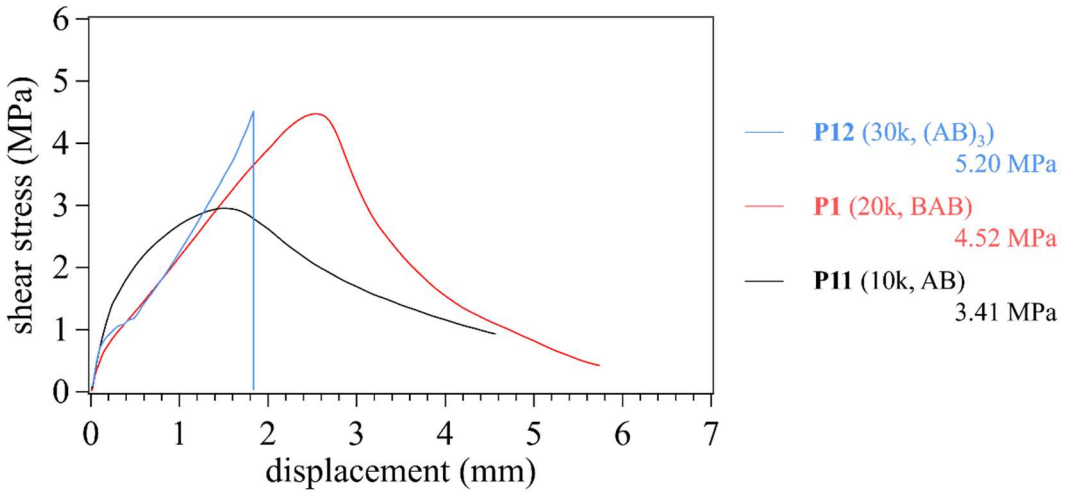

Figure 4.37. Lap shear tests of **P1**, **P11**, and **P12** using wood pieces (adherent, wood; tensile speed = 10 mm min^{-1}).

Next, to evaluate the effect of the total molecular weight on the adhesive properties, copolyesters with a comparable f_{LLA} to **P1** but with smaller and larger molecular weights, were synthesized by changing the initial $[monomer]_0/[initiator]_0$ ratios (**P13** and **P14** in **Table 4.4**). The $M_{n,NMR}$ spectra of the obtained products are similar to those $M_{n,theo.}$ (**P13**: $M_{n,theo.}$ = 9,930, $M_{n,NMR}$ = 11,800; **P14**: $M_{n,theo.}$ = 39,700; $M_{n,NMR}$ = 38,100), and the F_{LLA} ratio was determined to be 0.78–0.80. In addition, T_g of **P13** and **P14** was evaluated to be 21.0 and 25.0 °C, which are comparable to that of **P1** (T_g = 19.0 °C). The adhesive strength of **P13** and **P14** were determined to be 0.06 and 6.31 MPa, respectively (**Figure 4.38**). When compared with the results of **P1** with a compatible F_{LLA}, it was demonstrated that the adhesive strength could be improved by increasing the molecular weight. This is likely due to the increased molecular weight, which leads to greater entanglement of the polymer chains. From these investigations,

increasing the molecular weight and number of branches while fixing the F_{LLA} at approximately 0.80 was found to be an effective strategy for improving the adhesive properties.

Based on these results, a four-armed $(AB)_4$ type copolyester with the highest molecular weight ($M_{n,theo.}$ of 79,200) and F_{LLA} of 0.79 was synthesized using a tetraol, *i.e.* pentaerythritol (PEOL), as an initiator with the initial feed ratio of $[CsOPiv]/[PEOL]_0/[GA]_0/[BO]_0/[LLA]_0$ = 1/1/84/336/440 (**P15** in **Table 4.4**). As expected, the adhesive strength of **P15** (6.74 MPa) was the highest among all tested samples (**Figure 4.39a**). Importantly, the adhesive strength of **P15** was comparable to that of commercially available PE and PVAc adhesives[29] (**Figure 4.39b**).

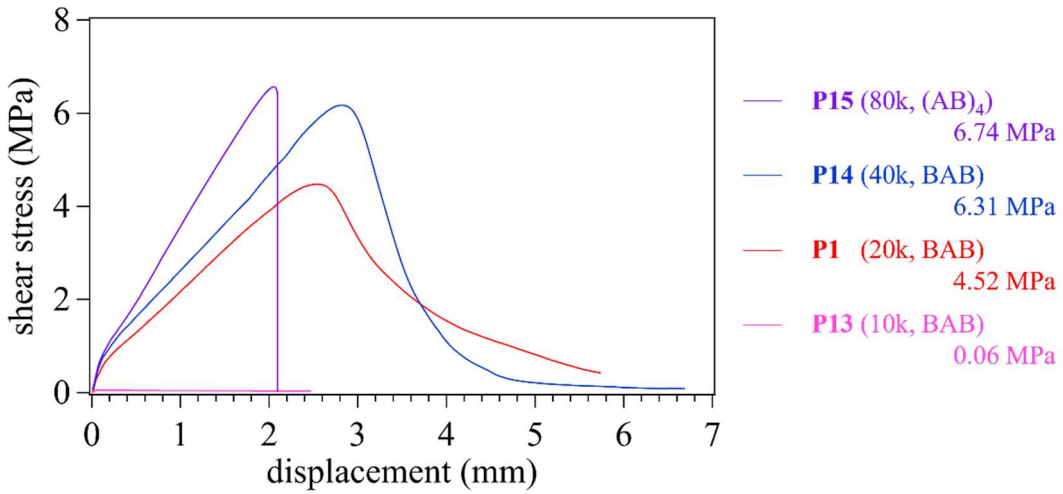

Figure 4.38. Lap shear tests of **P1** and **P13**–**P15** using wood pieces (adherent, wood; tensile speed = 10 mm min^{-1}).

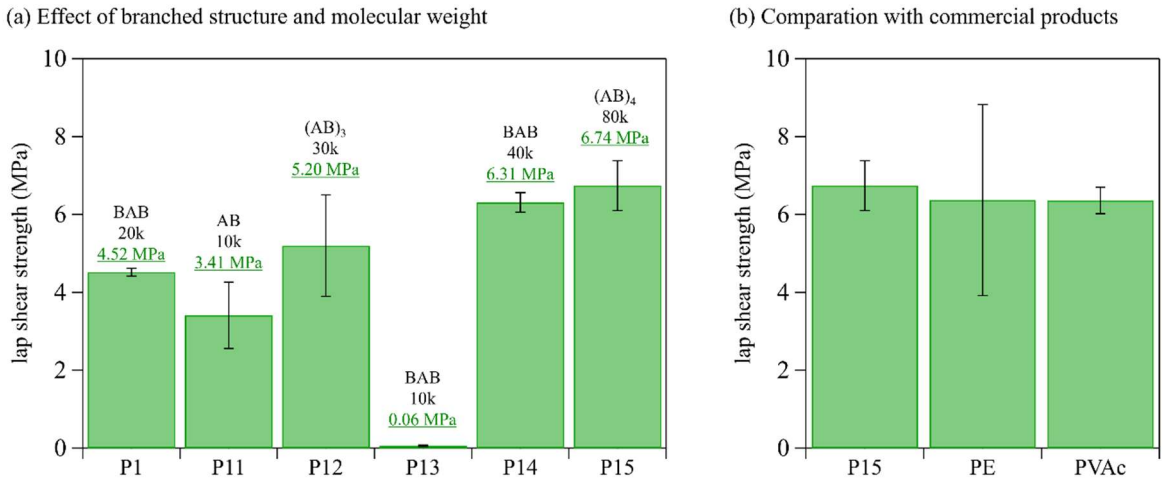

Figure 4.39. Lap shear strength results: (a) poly(GA-*alt*-BO)-*tb*-PLLA copolyesters with different molecular weight and branched structure, and (b) **P15** compared to commercial polyester (PE; PES-111, Toagosei) and poly(vinyl acetate) (PVAc; ref. 29) adhesives (adhesion, wood; tensile speed = 10 mm min^{-1}; n = 3).

Using **P15**, the author investigated the substrate versatility and recyclability of the copolyester adhesives. In addition to the wooden substrate, aluminum plate (Al), iron plate (Fe), glass plate (glass), and poly(ethylene terephthalate) (PET) film were used as adherents (**Figure 4.40a**). **P15** was found to function as a good adhesive for these substrates, except for PET. Finally, the author conducted a recycling test on the **P15** adhesive (**Figures 4.40b** and **4.41**–**S4.43**). Following the lap shear adhesive test, the fractured samples were subjected to hot pressing at 100 °C for 1 min and cured for 1 week to generate recycled samples. Adhesive tests of the recycled samples revealed adhesive resilience values of 86%, 95%, and 86% for the wood, aluminum, and iron substrates, respectively, demonstrating sufficient recyclability.

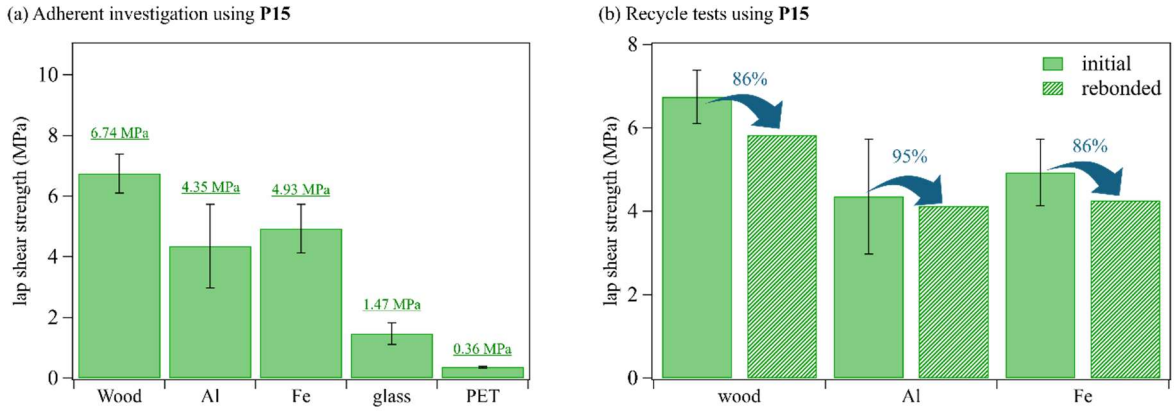

Figure 4.40. Lap shear strength results: (a) **P15** on different adherents (tensile speed = 10 mm min^{-1}; n = 3), (b) **P15** adhered wood, Al, and Fe pieces for both initial (n = 3) and rebounded (n = 1) samples.

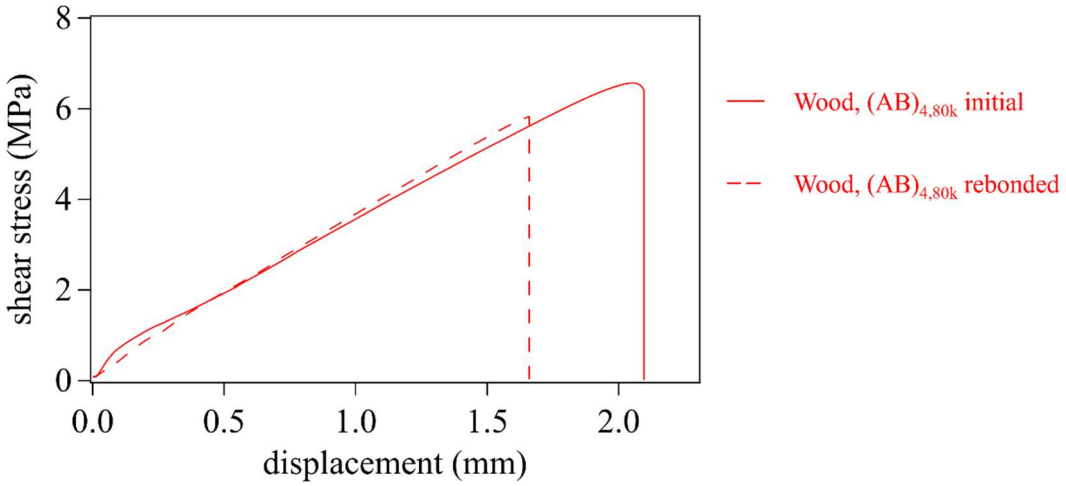

Figure 4.41. Lap shear strength of **P15** on Wood adherent during recycling.

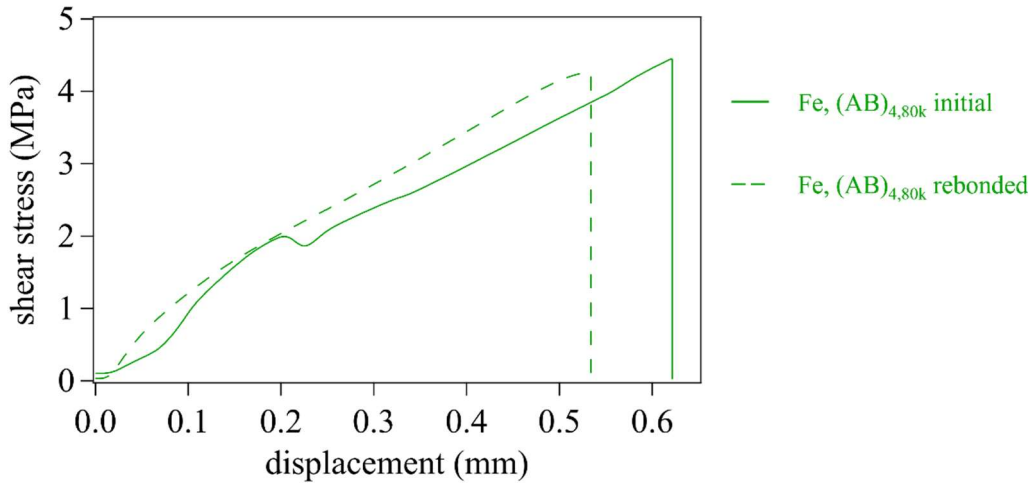

Figure 4.42. Lap shear strength of **P15** on Fe adherent during recycling.

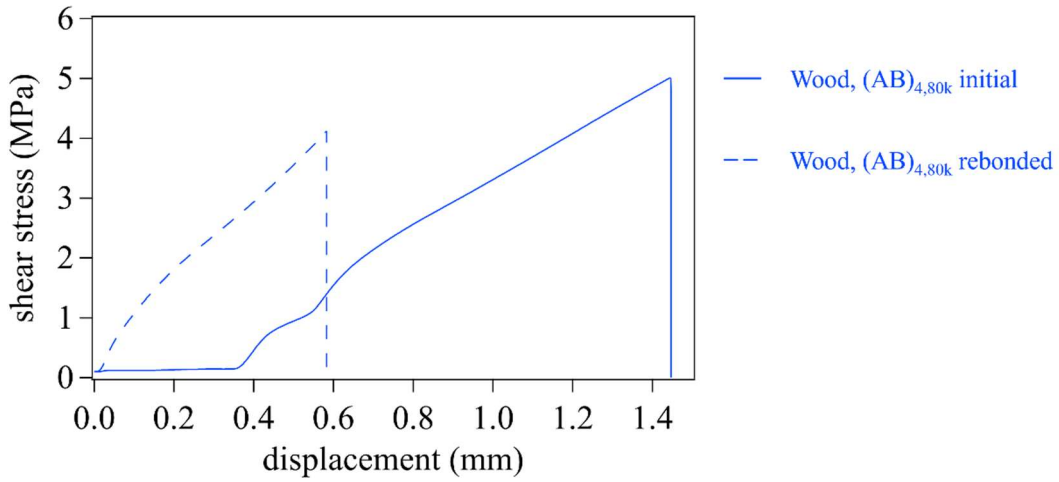

Figure 4.43. Lap shear strength of **P15** on Al adherent during recycling.

4.4 Conclusion

In this study, the author succeeded in the one-pot, one-step synthesis of PE-based hot-melt adhesives with high bio-based content using a self-switchable polymerization approach. The copolyesters consisting of poly(cyclic anhydride-*alt*-epoxide) and PLLA functioned as hot-melt adhesives. Taking advantage of the easy handling of self-switchable polymerization, a series of copolyesters with different molecular weights, PLLA weight fractions, repeating unit structures, and branched structures were readily prepared and subjected to lap shear tests, providing molecular design guidance for high-performance adhesives. Because these adhesives can adhere not only to wood, but also to glass, Fe, and Al substrates, they can be applied in a wide range of industrial fields. In this study, self-switchable polymerization was demonstrated as a powerful tool for the efficient exploration of new sustainable polymer materials. This strategy would be useful not only for hot-melt adhesives but also for the future development of tough plastics and elastomers with high bio-based contents and excellent biodegradability.

4.5 Reference

1. Cohn, D.; Salomon, A.H. Designing biodegradable multiblock PCL/PLA thermoplastic elastomers. *Biomaterials* **2005**, *26*, 2297–2305.

2. Vilay, V.; Mariatti, M.; Ahmad, Z.; Pasomsouk, K.; Todo, M. Improvement of microstructures and properties of biodegradable PLLA and PCL blends compatibilized with a triblock copolymer. *Mater. Sci. Eng. A* **2010**, *527*, 6930–6937.

3. Peponi, L.; Navarro-Baena, I.; Sonseca, A.; Gimenez, E.; Marcos-Fernandez, A.; Kenny, J.M. Synthesis and characterization of PCL–PLLA polyurethane with shape memory behavior. *Eur. Polym. J.* **2013**, *49*, 893–903.

4. Navarro-Baena, I.; Marcos-Fernández, A.; Fernández-Torres, A.; Kenny, J.M.; Peponi, L. Synthesis of PLLA-b-PCL-b-PLLA linear tri-block copolymers and their corresponding poly(ester-urethane)s: Effect of the molecular weight on their crystallisation and mechanical properties. *RSC Adv.* **2014**, *4*, 8510–8524.

5. Xiang, S.; Feng, L.; Bian, X.; Zhang, B.; Sun, B.; Liu, Y.; Li, G.; Chen, X. Toughening modification of PLLA with PCL in the presence of PCL- b -PLLA diblock copolymers as compatibilizer. *Polymers for Advanced Techs* 2019**,** 30, 963–972.

6. Jeon, O.; Lee, S.-H.; Kim, S.H.; Lee, Y.M.; Kim, Y.H. Synthesis and characterization of poly(L-lactide)−poly(ε-caprolactone) multiblock copolymers. *Macromolecules* **2003**, *36*, 5585–5592.

7. Shin, J.; Martello, M.T.; Shrestha, M.; Wissinger, J.E.; Tolman, W.B.; Hillmyer, M.A. Pressure-sensitive adhesives from renewable triblock copolymers. *Macromolecules* **2011**, *44*, 87–94.

8. Krajovic, D.M.; Haugstad, G.; Hillmyer, M.A. Crystallinity-independent toughness in renewable poly(L-lactide) triblock plastics. *Macromolecules* **2024**, *57*, 2818–2834.

9. Longo, J.M.; Sanford, M.J.; Coates, G.W. Ring-opening copolymerization of epoxides and cyclic anhydrides with discrete metal complexes: Structure–property relationships. *Chem. Rev.* **2016**, *116*, 15167–15197.

10. Pappuru, S.; Chakraborty, D. Progress in metal-free cooperative catalysis for the ring-opening copolymerization of cyclic anhydrides and epoxides. *Eur. Polym. J.* **2019**, *121*, 109276.

11. Buchaca, M.M.de S.; Martinez, C.; Martinez, J.; A.-Moreno, C; F.-Baeza, J.; Tejeda, J.; Niza, E.; C.-Osma, J. A.; Otero, A.; L.-Sanchez, A. Alternating Copolymerization of Epoxides and Anhydrides Catalyzed by Aluminum Complexes. *ACS Omega*, **2018**, *3*, 17581–17589.

12. Hirschmann, M.; Andriani, F.; Fuoco, T. Functional and degradable copolyesters by ring-opening copolymerization of epoxides and anhydrides. *Eur. Polym. J.* **2023**, *183*, 111766.

13. Xie, X.; Huo, Z.; Jang, E.; Tong, R. Recent advances in enantioselective ring-opening polymerization and copolymerization. *Commun. Chem.* **2023**, *6*, 202.

14. Paul, S.; Zhu, Y.; Romain, C.; Brooks, R.; Saini, P.K.; Williams, C.K. Ring-opening copolymerization (ROCOP): Synthesis and properties of polyesters and polycarbonates. *Chem. Commun. (Camb)* **2015**, *51*, 6459–6479.

15. Zhang, J.; Wang, L.; Liu, S.; Li, Z. Phosphazene/lewis acids as highly efficient cooperative catalyst for synthesis of high-molecular-weight polyesters by ring-opening alternating copolymerization of epoxide and anhydride. *J. Polym. Sci.* **2020**, *58*, 803–810.

16. Lee, S.; Lee, K.; Kim, Y.-W.; Shin, J. Preparation and characterization of a renewable pressure-sensitive adhesive system derived from ε-decalactone, L-Lactide, epoxidized soybean oil, and rosin ester. *ACS Sustainable Chem. Eng.* **2015**, *3*, 2309–2320.

17. Gregory, G.L.; Sulley, G.S.; Carrodeguas, L.P.; Chen, T.T.D. T.T.D.; Santamarti, A.; Terrill: NJ; Lee, K.-Y.; CK: Williams. Triblock polyester thermoplastic elastomers with semi-aromatic polymer end blocks by ring-opening copolymerization. *Chem. Sci.* **2020**, *11*, 6567–6581.

18. Gregory, G.L.; Williams, C.K. Exploiting sodium coordination in alternating monomer sequences to toughen degradable block polyester thermoplastic elastomers. *Macromolecules* **2022**, *55*, 2290–2299.

19. Hu, C.; Pang, X.; Chen, X. Self-switchable polymerization: A smart approach to sequence-controlled degradable copolymers. *Macromolecules* **2022**, *55*, 1879–1893.

20. Xia, X.; Suzuki, R.; Takojima, K.; Jiang, D.-H.; Isono, T.; Satoh, T. Smart access to sequentially and architecturally controlled block polymers via a simple catalytic polymerization system. *ACS Catal.* **2021**, *11*, 5999–6009.

21. Xia, X.; Suzuki, R.; Gao, T.; Isono, T.; Satoh, T. One-step synthesis of sequence-controlled multiblock polymers with up to 11 segments from monomer mixture. *Nat. Commun.* **2022**, *13*, 163.

22. Xia, X.; Gao, T.; Li, F.; Suzuki, R.; Isono, T.; Satoh, T. Multidimensional control of repeating unit/sequence/topology for one-step synthesis of block polymers from monomer mixtures. *J. Am. Chem. Soc.* **2022**, *144*, 17905–17915.

23. Xia, X.; Gao, T.; Li, F.; Suzuki, R.; Isono, T.; Satoh, T. Sequential polymerization from complex monomer mixtures: Access to multiblock copolymers with adjustable sequence, topology, and gradient strength. *Macromolecules* **2023**, *56*, 92–103.

24. Ota, I.; Suzuki, R.; Mizukami, Y.; Xia, X.; Tajima, K.; Yamamoto, T.; Li, F.; Isono, T.; Satoh, T. Organobase-catalyzed ring-opening copolymerization of cyclic anhydrides and Oxetanes: Establishment and application in block copolymer synthesis. *Macromolecules* **2024**, *57*, 3741–3750.

25. Yuntawattana, N.; Gregory, G.L.; Carrodeguas, L.P.; Williams, C.K. Switchable polymerization catalysis using a tin(II) catalyst and commercial monomers to toughen poly(l-lactide). *ACS Macro Lett.* **2021**, *10*, 774–779.

26. Arbenz, A.; Avérous, L. Synthesis and characterization of fully biobased aromatic polyols–oxybutylation of condensed tannins towards new macromolecular architectures. *RSC Adv.* **2014**, *4*, 61564–61572.Rohles, C.M.; Gläser, L.; Kohlstedt, M.; Gießelmann, G.; Pearson, S.; del Campo, A.; Becker, J.; Wittmann, C. A bio-based route to the carbon-5 chemical glutaric acid and to bionylon-6,5 using metabolically engineered *Corynebacterium glutamicum*. *Green Chem.* **2018***, 20,* 4662–4674.

27. Capuana, E.; Lopresti, F.; Ceraulo, M.; La Carrubba, V.L. Poly-L-lactic acid (PLLA)-based biomaterials for regenerative medicine: A review on processing and applications. *Polymers* **2022**, *14*, 1153.

28. Todorovic, T.; Norström, E.; Khabbaz, F.; Brücher, J.; Malmström, E.; Fogelström, L. A fully bio-based wood adhesive valorising hemicellulose-rich sidestreams from the pulp industry. *Green Chem.* **2021**, *23*, 3322–3333.

Chapter 5

Conclusions

This dissertation describes a simple, efficient, and controlled method for synthesizing functional polyesters, including side-chain/chain-end functionalized polyesters, polyesters with highly branched architectures, and block polyesters, using organocatalyzed ring-opening alternating copolymerizations (ROACs) of cyclic anhydrides and epoxides. Chapter 2 established a synthetic approach toward amino-functionalized polyesters (APEs) using ROACs involving glycidylamines, epoxides bearing tertiary amine functional groups, and cyclic anhydrides. Chapter 3 describes the synthesis of hyperbranched polyesters (HBPEs) via ROACs involving trimellitic anhydride and various epoxides, while Chapter 4 describes the use of self-switchable polymerization that combines ROAC and ring-opening polymerization (ROP) to develop hot-melt adhesives. The system established in this thesis for synthesizing functional polyesters facilitates precise control of critical parameters, including main-chain/side-chain/chain-end structures, molecular weight, branching structure, monomer sequence, and material properties, which is achieved by varying initiator/monomer combinations, adjusting the initial monomer feed ratio, and incorporating a third monomer. Furthermore, all syntheses in this study were carried out under solvent-free conditions promoted by organocatalysts, thereby minimizing the reliance on organic solvents and organometallic catalysts, which are detrimental to both the environment and human health. This comprehensive approach is expected to lead to advanced applications of functional polyesters. The important

achievements and findings in the present study is as follows.

Chapter 2 established the ROACs of cyclic anhydrides and glycidylamines using organocatalysts to precisely synthesize APEs. A wide range of APEs with narrow polydispersity were synthesized by varying the cyclic anhydride/glycidylamine combination. Among the samples tested, the $(AB)_4$-type copolyester (i.e., poly(GA-*alt*-BO)-*tb*-PLLA)$_4$) exhibited the best adhesive strength, with the value of 6.74 ± 0.64 MPa comparable to those of commercial products such as polyester-based and poly(vinyl acetate)-based hot-melt adhesives.

Chapter 3 described successful syntheses involving cesium-pivalate-catalyzed ROACs with latent trifunctional cyclic anhydrides. This method paves the way for the development of polyesters with unique physical properties that arise from their branching topologies. Additionally, core–shell polyesters were synthesized in a one-pot, one-step manner by employing self-switchable polymerization. This established HBPE synthetic system may find broader use in the development of novel HBPE materials, such as additives and coatings, as well as in biomedical applications.

Chapter 4 reported the successful development of a one-step terpolymerization-based

method for the synthesis of ABA triblock copolymers, namely, the self-switchable polymerization of a cyclic anhydride, an epoxide, and LLA using an alcohol initiator. The adhesive properties of the synthesized polyesters were adjusted according to the structures of the main and side chains. This strategy is anticipated to be useful not only for the development of hot-melt adhesives, but also for creating tough highly biodegradable plastics and elastomers with high bio-based contents.

Overall, a novel ROAC-based method for the synthesis of functional polyesters with advanced structural characteristics was developed that uses simple organocatalysts, including phosphazene bases and alkali metal carboxylates. In addition, foundations that provide valuable insight into the designs of polyester materials were established by evaluating correlations between various structural parameters and material properties. The findings of this study are expected to contribute significantly to the development of a broad range of polyester-based materials as degradable alternatives to polyolefin plastics, adhesives, tough elastomers, and biomedical polymers.